Assessment of Landscape Processes, Forms and Features in the Lake Manyara Region, East African Rift Valley

Dissertation

der Mathematisch-Naturwissenschaftlichen Fakultät

der Eberhard Karls Universität Tübingen

zur Erlangung des Grades eines

Doktors der Naturwissenschaften

(Dr. rer. nat.)

vorgelegt von

Geraldine Suzanne Quénéhervé

aus Sigmaringen

Tübingen

2018

Gedruckt mit Genehmigung der Mathematisch-Naturwissenschaftlichen Fakultät der Eberhard Karls Universität Tübingen.

Tag der mündlichen Qualifikation:	27.11.2018
Dekan:	Prof. Dr. Wolfgang Rosenstiel
1. Berichterstatter:	Prof. Dr. Volker Hochschild
2. Berichterstatter:	Ass.-Prof. Dr. Michael Märker

Table of Contents

Abstract

The rift valleys of the East African Rift Systems form two branches (Eastern and Western rift). Within the Eastern rift, there is a southward propagation in the onset of volcanism, and hence rifting that has led to the formation of a narrow graben commonly referred to as the Gregory rift (in Tanzania). The endorheic basin at its southern end where the present saline Lake Manyara was formed. The lakes largest tributary is the Makuyuni River that is providing fresh water from northwest volcanic highlands. Along the Makuyuni River, where first and second tributaries cut deep into the sediments, the landscape is dominated by erosion features. These sediments reveal exposed and outcropping artefacts and fossils, which have been found starting in the 1930s in archaeological and paleontological expeditions. In the close vicinity of Makuyuni town, two hominin bearing sites were discovered in 2008. As few is known about the landscape itself, this study has set its focus on the surrounding landscapes of Makuyuni and its geomorphic implications.

Key drivers of landscape development in Northern Tanzania are the tectonics and tectonically induced processes. The thus disrupt drainage networks and analyses thereof can reveal the effects on the morphology of stream longitudinal profiles. These transformations in turn, have an impact on driving river incision, in general on linear erosion phenomena. The triggered rill and gully erosion features will eventually lead to soil loss. Gully erosion is a major threat concerning landscape degradation in semiarid ecosystems, as they remove fertile topsoil and as such prevent agricultural use. The study showed, that most of the gully systems are there for decades and in stable conditions. There are, however, areas of exposed risk for erosion. A detailed examination of soil loss areas, innovative automatic surface runoff detector (SRD) devices have been installed. They measure runoff height and duration. This data contribute to a better understanding of the water cycle as well as to soil functions in semiarid environments.

The specific research questions have been considered in five different publications that describe the applied methodologies and results in detail. In order to understand the different geomorphic processes, different methods and scales have been used. Field sur-

veying was an important factor and surface runoff, soil characteristics and erosion phenomena have been sampled and measured. Specifically, this study examined rill and gully erosion features and underwent a detailed mapping around Makuyuni in order to describe and understand the occurring landscape systems. Laboratory procedures involved soil parameter analysing and digital data analysis involved digital elevation model analysis, remote sensing imagery, sophisticated statistical models and in the end a detailed geomorphic map compiling of the greater area.

Many studies have focused on partial aspects of geomorphic processes. The framework of this doctoral thesis seeks to answer a holistic approach, in order to understand, interpret and discuss related geomorphic processes, their spatial extents and locations. This work contributes to the knowledge of present geomorphic processes and features and the landscape evolution within the Lake Manyara area in Northern Tanzania. The above mentioned methods and analyses may be applicable to similar areas in the African rift.

Zusammenfassung

Der große Ostafrikanische Grabenbruch teilt sich im südlichen Äthiopien in zwei Hauptsysteme, den östlichen und den westlichen Graben. Im östlichen Graben nehmen die vulkanischen Aktivitäten und daher auch die aktive Grabenbildung nach Süden zu, was zu der heutigen Bildung einer engen Grabenschlucht geführt hat, das sogenannte Gregory Rift in Tansania. An dessen südlichem Ende hat sich ein endorheisches Becken gebildet, wo sich heute der flache Salzsee Manyara befindet. Sein größter Zubringer ist der Fluss Makuyuni, welcher Frischwasser aus den vulkanischen Hochlanden nordwestlich des Beckens mit sich führt. Entlang diesen Flusses haben sich weitere Verzweigungen tief in die Sedimente gegraben; die Landschaft wird von Erosionsformen dominiert. In diesen Sedimenten zeigen sich nun freigelegte Artefakte und Fossilien, welche seit den 1930er Jahren bei archäologischen wie paläontologischen Expeditionen entdeckt wurden. In der Nähe der Siedlung Makuyuni wurden 2008 zwei Knochenreste von frühen Hominiden gefunden. Wenig Forschung gibt es über die Landschaft selber, die vorliegende Arbeit beschäftigt sich daher mit der Umgebung Makuyunis und seinen geomorphologischen Eigenschaften.

Wesentlich für die Formung der Landschaft Nordtansanias sind die tektonischen und tektonisch-getriebenen Prozesse. Die dadurch gestörten Abflussnetzwerke und deren Analysen können die Auswirkungen auf die Morphologie der Abflusslängsprofile aufzeigen. Diese Veränderungen wiederum wirken sich auf die Einschneidungsdynamiken der Flüsse und Bäche aus, generell also auf lineare Abflussprozesse. Die so entstehenden Rillen- und Gullyerosionsformen führen zu Bodenverlusten. Die Gullyerosion ist eine der größten Naturgefahren in semiariden Ökosystemen, da sie große Teile des Oberbodens abtragen und so die Landschaft einer agrarischen Nutzung entziehen. Die Arbeit konnte aufzeigen, dass viele der Gullysysteme seit mehreren Jahrzehnten bestehen und stabil sind. E gibt jedoch Bereiche, die von potentiellen Abtragungsrisiken betroffen sind. Um diese Bodenabtragungen genauer zu untersuchen, wurde mit innovativen Oberflächenabflussdetektoren gearbeitet. Diese messen den Oberflächenabfluss in seiner Höhe und Dauer. Diese Daten tragen zu einem besseren Verständnis des Wasserkreislaufes sowie allgemein zu Bodenfunktionen semiarider Ökosysteme bei.

Die jeweiligen Forschungsfragen wurden in fünf Artikeln abgehandelt, diese beschreiben die angewandten Methoden und Resultate im Detail. Um die verschiedenen geomorphologischen Prozesse zu untersuchen, wurde mit verschiedenen Methoden und verschiedenen Skalen gearbeitet. Die Feldarbeit nahm einen wichtigen Teil ein und es wurden u.a. Oberflächenabfluss, Bodenwerte und Erosionsformen beprobt und vermessen. Im Speziellen wurden auf die Rillen- und Gullyerosion eingegangen sowie auf eine detaillierte Kartierung der Umgebung Makuyunis um die verschiedenen Landschaftssysteme zu beschreiben und zu verstehen. Im Labor wurden die Bodenproben analysiert und mit den digitalen Geländemodellen, den Fernerkundungsdaten und statistischen Methoden wurden einzelne Studien durchgeführt und am Ende eine geomorphologische Karte des Gebiets erarbeitet.

Viele Studien untersuchten Teilbereiche geomorphologischer Prozesse. Im Rahmen dieser Doktorarbeit wurde daher ein ganzheitlicher Ansatz verfolgt, um die geomorphologischen Prozesse, ihre räumliche Ausdehnung und Verortung zu verstehen, zu interpretieren und die wissenschaftlichen Erkenntnisse als Ganzes zu diskutieren. Diese Arbeit trägt daher zu neuem Wissen aktueller geomorphologischer Prozesse und Formen sowie der Landschaftsentwicklung als solche in der Umgebung des Manyarasees in Nordtansania bei. Die dabei verwandten Methoden und Analysen sind in ähnlichen Ökosystemen entlang des Ostafrikanischen Grabens anwendbar.

List of Publications

This cumulative doctoral thesis is based on the following papers, which are referred to in the text by their Roman numerals. My contribution is highlighted.

Publication I

Flores-Prieto, E.; **Quénéhervé, G.**; Bachofer, F.; Shahzad, F.; and Maerker, M. (2015). Morphotectonic Interpretation of the Makuyuni Catchment in Northern Tanzania using DEM and SAR data. *Geomorphology* **248**, 427–439.
DOI: 10.1016/j.geomorph.2015.07.049

Own contribution: study design, structure of the paper, contribution to data preparation, completion to figures and substantial writing.

Publication II

Bachofer, F.; **Quénéhervé, G.**; Hochschild, V.; and Maerker, M. (2015). Multisensoral Topsoil Mapping in the Semiarid Lake Manyara Region, Northern Tanzania. *Remote Sensing,* **7(8)**, 9563–9586.
DOI: 10.3390/rs70809563.

Own contribution: contribution to study design, field work, contribution to structure of the paper, soil profile analysis, contribution to figures, interpretation and writing.

Publication III

Quénéhervé, G.; Bachofer, F.; and Maerker, M. (2015). Experimental Assessment of Runoff Generation Processes on Hillslope Scale in a Semiarid Region in Northern Tanzania. *Geografia Fisica e Dinamica Quaternaria*, **38(1)**, 55–66.
DOI: 10.4461/GFDQ.2015.38.06.

Own contribution: study design, structure of the paper, data preparation, data analyses, figures, interpretation and writing.

Publication IV

Maerker, M.; **Quénéhervé, G.**; Bachofer, F.; and Mori, S. (2015). A simple DEM assessment procedure for gully system analysis in the Lake Manyara area, northern Tanzania. *Natural Hazards,* **79(1)**, 235–253.
DOI: 10.1007/s11069-015-1855-y

Own contribution: supported study design and structure of the paper, data preparation and analyses and provided figures, substantial manuscript writing as well as proofreading.

Manuscript V

Quénéhervé G.; Bachofer F.; and Maerker, M.: Geomorphology Makuyuni Area, Northern Tanzania. *Submitted to Journal of Maps*.

Own contribution: structure of the paper, geomorphic and geologic feature digitizing, maps, figures, photos, interpretation and writing.

List of Figures

List of Tables

Acknowledgments

So many people have supported me during my PhD time. Thank you all!

I would like to express my deep and sincere gratitude to my supervisors Prof. Dr. Volker Hochschild and Prof. Dr. Michael Märker who always supported me throughout my PhD studies.

This thesis would not have been accomplished without the encouragement of Michael Märker and his support via ROCEEH. Thank you so much for the lengthy discussions on all kind of topics in these years. Also for your guidance to pursue a holistic geomorphic view whilst being in the field and the introduction to pedo-hydrologic measurements.

Felix, my sincere thanks to you, without you accompanying me to all kind of field stages in all the countries we have been together and encouraging me during my PhD time with most fruitful scientific discussions, I would have not achieved the same.

Elena, Silvia, Natha, Rike: thank you so much for your time and discussions, thankfully not only based on scientific issues.

My thank goes to my colleagues and the great time we spent together: Hans, Andy, Gebbo, Markus, Elmar, Joel, Jeannine, Christian S., Elio, Reza, Christian C., Luigi, Edoardo, Jan, Bernd, Mansour, Saman, and Christian B.

I also thank the ROCEEH team for the time being together and the opportunity to conduct my PhD thesis in East Africa: Michael M., Christine, Mimi, Angela, Andrew, Michael B., Zara and the way-back-Hiwi-group: Rebekka, Chidi, Patrick and Martin.

I specially thank Dr. Christine Hertler for the introduction and the discussions about the palaeontology of Makuyuni and her support throughout my time with ROCEEH. I thank Dr. Liane Giemsch for the fruitful discussion about the archaeology of Makuyuni and its place within the landscape. I thank Jun.-Prof. Dr. Annett Junginger and Dr. Lydia Olaka for the discussions about the EARS evolution and lake dynamics.

My special thanks goes to Lameck Marick, who drove me wherever and organised whatever I wanted, and who kept the locals happy (he still has this sheep growing up in Makuyuni…).

I thank Prof. Dr.-Ing. Felix Mtalo and Dr. Preksedis Ndomba, Department of Water Resources Engineering, University of Dar es Salaam, for their support to get the COSTECH clearance and to be able to export my soil and rock samples via the Ministry of Energy and Minerals, Tanzania. I thank Yustina Kiwango, Park Ecologist, Lake Manyara National Park (TANAPA), for the discussions in the field and the stroll through Lake Manyara. I thank the African Wildlife Foundation for the access and work permission on the Manyara Ranch Conversation Area. I thank the Tanzania Commission for Science and Technology (COSTECH) for the research permits.

My special thanks go to all the students that went with me to sit around long-lasting infiltration measurements under the African sun: Atrianus Mutungi, Elio Flores-Prieto, Simone Mori, Rike Becker, Giulia Cianchi, Francesco Chiosi and Reza Zakerinejad. Additionally, I thank following persons that helped me with the data: Karina Traub, Tahira Ullah.

I thank following institutions for the financial support of my field stages and for congress grants: 'The Role of culture in Early Expansions of Humans (ROCEEH)' project, Heidelberg Academy of Sciences and Humanities; German Academic Exchange Service (DAAD); Tübingen University Club; Prof. Dr. Volker Hochschild – Chair of Physical Geography and GIS, University of Tübingen.

Last but not least:

I thank my parents Marianne and Michael Quénéhervé, my twin sister Chantal with her husband Markus and my brother Pascal for their unconditional support, trust and faith in me. You all know what I owe you.

This is for Linus and Jan – the next generation.

1 Introduction

This chapter provides an introduction to the background of this work, the state of the art in relation to the individual research questions and it presents the structure of this thesis.

1.1 Background and Motivation

The main objective of this dissertation work is to study geomorphic processes, forms and features on different scales in order to gain a deeper understanding of landscape related processes and the landscape evolution itself. The focus area lies within the Lake Manyara basin in Northern Tanzania that is part of the East African rift system (Figure 1).

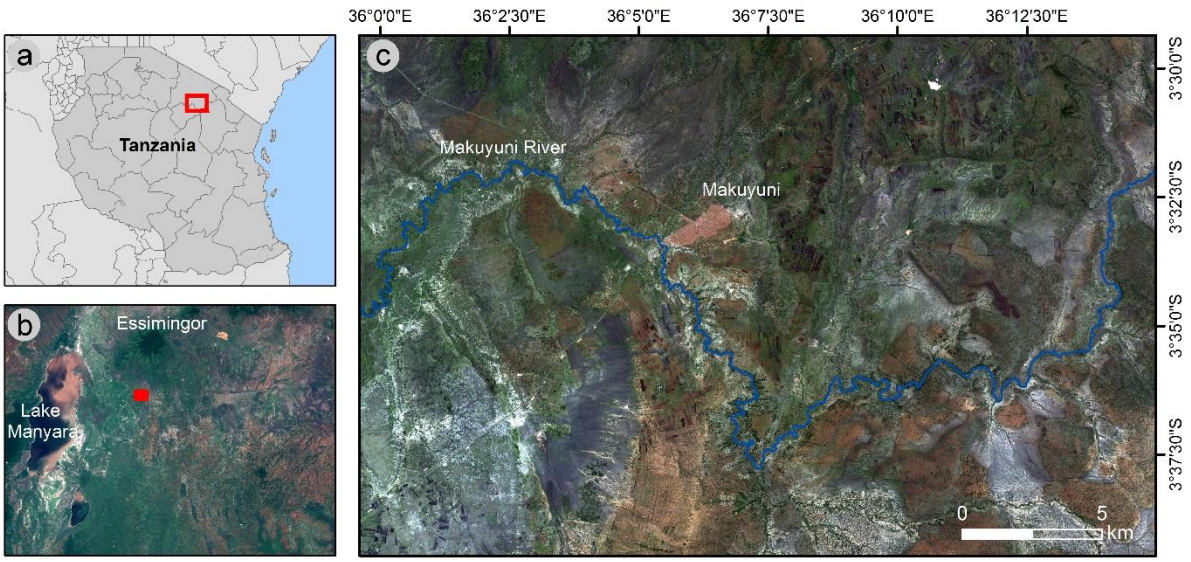

Figure 1. Study area located in Northern Tanzania. a) Tanzania with district boundaries, red box shows extend of b. b) SENTINEL-2 scene (2016-02-04) of the greater Lake Manyara area, volcano Essimingor in the North. Rec box shows extend of c. c) WorldView2- scene (2011-02-21). Close up of the Makuyuni area, Makuyuni River with blue line, Makuyuni town in light red.

Since 2007, the area of Makuyuni town has been studied archaeologically by the University of Dar es Salaam in cooperation with the University of Tübingen, among others (Kaiser et al. 2010). Work was done on the geology and stratigraphy of the area (e.g. Frost et al. 2012; Schwartz et al. 2012), but there was a lack of information on the surrounding landscape and its geomorphology. In 2010, geographic, geomorphic and remote sensing

fieldwork of the Heidelberg Academy of Sciences' Research Center ROCEEH (Haidle et al. 2010), under the supervision of Michael Maerker, started to work on this research gap. This thesis is written within this framework.

Beginning in the 1860s, many discovery expeditions in northern Tanzania reported about the rift valley and their volcanoes (cf. Chorowicz 2005; Dawson 2008). During the times of the "German East Africa" colony, there had been an increasing number of German expeditions for detailed local geological and geographical studies (Baumann 1894; Meyer 1909; Jäger 1911). In the early 20th Century, German and later British researchers investigated East Africa in search for human origin: At Olduvai, first expedition 1931–32 lead by Louis Leakey (Reck 1933; Leakey, Reck 1951; Leakey 1979); at Mumba Cave Kohl-Larsen expedition 1934–36 (Kohl-Larsen 1943); at Laetoli, first investigation 1935 by Louis Leakey (Leakey 1987).

Richard Leaky suggested in 1973 that the East African Rift System is the "Origin of Mans" (Leakey 1973: 450), because most early hominid fossils have been found in those rift sediments. Ring (2014: 142) stated that rifting processes drive dynamic topography that "may have been the most important cause for climate change in equatorial Africa, thereby influencing the development and evolution of mankind". Rift basins with their rivers and lakes are ideal sites for faunal and floral development. Widespread lake formation let to more diversified environments that have potentially influenced the evolution of hominids by altering their habitat.

En route to Olduvai on the 1934–35 expedition, Kent recognized and later described a section of lacustrine deposits near Makuyuni town and suggested a Middle Pleistocene age for them (Kent 1942). These fossiliferous deposits were re-investigated in 1969–70 (Keller et al. 1975), in 1994–95 by the Hominid Corridor Project (Kaiser et al. 1995; Kaiser et al. 2005; Ring et al. 2005) and in 2007–11 (Frost et al. 2010; Frost et al. 2012; Schwartz et al. 2012; Märker et al. 2013; Giemsch et al. 2018).

At the Makuyuni location, greyish lacustrine, fossil-rich deposits are overlaid by brownish-red terrestrial sediments. These 30 m-thick sections were named Manyara Beds by Ring et al. (2005). The field season in 2008 revealed two hominin-bearing sites, namely MK2 and MK4, described by Kaiser *et al.* (Kaiser et al. 2010). Both fragments – from a parietal bone and a tooth – have been collected from the lacustrine, Lower Manyara Bed deposits (Kaiser et al. 2010). These two different sites demonstrate that hominins were

more or less frequent visitors at the shoreline of the paleolake Manyara. Within her doctoral thesis, Liane Giemsch (2015) conducted additional archaeological surveys from 2007–2009 around Makuyuni and added 52 new find localities to the fieldwork of Kaiser (1997). On a comparative study on Palaeolithic artefacts on test excavations, she could identify the majority of the artefacts to be Acheulean, mainly from 630–400 thousand years (ka) (Giemsch et al. 2018). She postulates that during the early Middle Pleistocene, hominins have used the lacustrine fresh water environment of the paleolake Manyara. The paleolake and paleolandscape analyses were conducted as well by the ROCEEH geography group from 2009–2014; see the dissertation work of Felix Bachofer (Bachofer 2015). The focus of this thesis is laid on the surrounding landscapes of Makuyuni and its geomorphic implications.

"Geomorphology is a highly complex science that involves elements of geography and geology," and studies landforms at different temporal and spatial scales (García-Ruiz 2015: 87). Understanding the geomorphic evolution of the landscape as it is present nowadays, means to understand a combination of landforms, vegetation, climate, bedrock as well as human activities reacting on the landscape. This holistic perspective enables the analysis of geomorphic processes to explain dynamic aspects of the present landscape. Many studies have focused on partial aspects of geomorphic processes; the interrelation of this information providing a holistic view on the landscape can provide deeper insights into landscape functions.

This doctoral work combines analyses of geomorphic forms and features, morphotectonics, geomorphic and erosional processes (esp. gully, rill and sheetwash processes), as well as soil characteristics in the semiarid environment of Northern Tanzania. The aim is to understand the influence of tectonics, climate and geology on current geomorphic forms such as erosion phenomena, surface transport conditions and the distribution of landscape features.

1.2 State of the Art and Research Questions

The present publication-based doctoral thesis is composed of a framework body and five publications. This section provides a brief introduction into the state of the art of the

relevant methodologies and analyses presented in each publication and states research question as well as the main objective of the present thesis.

The East African rift system (EARS) is an intra-continental ridge system with a series of several thousand kilometres long successions of rift valleys generally bordered by uplifted shoulders (Chorowicz 2005). The rift valley forms two main lines, the eastern branch runs over a distance of 2200 km from the Afar triangle in the north to the Northern Tanzania Divergence Zone in the south. The western branch runs over a distance of 2100 km from Lake Albert in the north to Lake Malawi in the south. Cenozoic volcanoes in the EARS occurred first in the Lake Tana region, Ethiopia, during the Oligocene and migrated southwards up to the Northern Tanzania Divergence Zone where volcanic activities are still ongoing (Chorowicz 2005). The EARS is structurally controlled creating topographically complex relief and drainage conditions (Baker et al. 1972).

Tectonic geomorphology studies, that have their origin in earthquake studies, reveal complexities of tectonic landscapes associated with active faulting (Bailey et al. 2011). Morphotectonic is considered synonymous with tectonic geomorphology and extracts information of active deformation directly from landscape topography (Kirby, Whipple 2001; Scheidegger 2004). In tectonically active regions, drainage network analysis reveals relationships between relief, elevation, and denudation rates (Howard 1994; Kirby, Whipple 2001). Tectonic activity disrupts drainage networks; studying the nature of these disruptions can give clues about the ongoing tectonic activity (Howard 1994). Identifiable geomorphic features, so called geomorphic markers or morphometric features, measure the amount of deformation (Burbank, Anderson 2001).

Morphotectonic analyses using digital elevation models (DEMs) for active tectonic regions show their possibilities for tectonic interpretations (Shahzad, Gloaguen 2011a, 2011b; Rahnama, Gloaguen 2014). In the catchment of the Makuyuni River, not only stream lines but also linear erosion features are characteristic landscape elements. Therefore, both were the focus of the morphotectonic analysis and validation. Out of the research deficits, following research question (RGQ) has been developed:

RQ1 How strong is the influence of active tectonics within the Makuyuni River basin and which geomorphic markers are suitable for their delineation?

The spatial distribution of soils and lithologies provide additional information for different landscape studies, including digital soil mapping (McBratney et al. 2003; Sanchez et al. 2009; Viscarra Rossel et al. 2010), soil production (Minasny, McBratney 1999; Minasny et al. 2008), and landscape reconstruction (Berking et al. 2011). The definition of topsoil varies in different soil taxonomies (Soil Survey Staff 1999; FAO 2014) but is regarded as the most relevant part of the 3-dimensional soil column considering food production, degradation and soil management (Broll et al. 2006; FAO 1998).

In geostastistical approaches for spatial soil distributions, various parameters are incorporated: (i) topographic features providing information on soil formation processes (Conacher, Dalrymple 1977), (ii) remotely sensed data and derivatives (Mulder et al. 2011) and (iii) geologic, soil and climatic parameters (Viscarra Rossel, Chen 2011).

Remote sensing imagery, especially suitable in sparsely vegetated areas, support the spatial interpolation of sampled soil property data. Remote sensing data can be analysed using physically-based methods to derive soil properties and to segment the landscape in homogeneous soil-landscape units (Mulder et al. 2011). The lack of existing information on soil types and distribution leaded to two campaigns focussing on soil survey and sampling regarding following research question:

RQ2 What soil types are available and how are the soils distributed over the study area?

The rate at which water enters the soil is called infiltration rate or infiltration capacity, typically measured in mm/h. When rainfall exceeds the rate at which water can infiltrate the ground, surface runoff will be produced (see 2, p. 6), called Hortonian overland flow (Bull, Kirkby 1997). Overland flow in semiarid areas, that are only sparsely and patchy vegetated, occurs on stretched slopes as laminar sheet flow. The term is somewhat misleading since the water flow is never of uniform depth because of the microtopography of hillslope surfaces (Summerfield 1991).

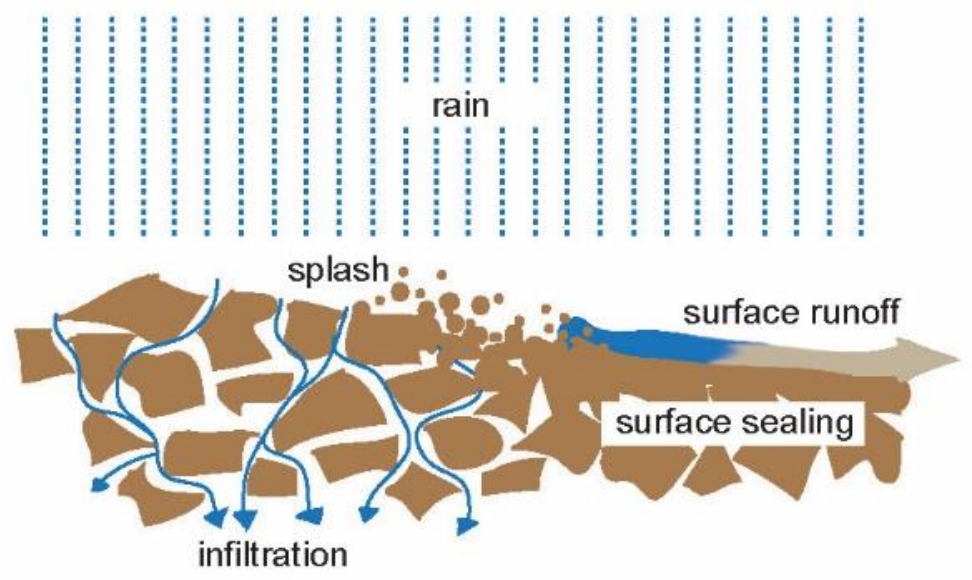

Figure 2. Soil infiltration and surface runoff processes. When rainfall exceeds the rate at which water can infiltrate the ground or when sediment detachment leads to a sealing of the soil surface, surface runoff will be produced.

Lauenroth & Bradford (2006) stated, that the runoff part of the water balance in semi-arid regions is close to zero, and hence often ignored. In general, runoff after small precipitation events can only be short distance runoff. On the other hand, Jensen et al. (1990) reported that runoff depends on the characteristics of precipitation and can only be neglected for a particular type of soils, i.e. coarse textured (sand and loamy sand) and moderately coarse textured soils (sandy loams). However, at the event scale there can occur remarkable amounts of surface runoff on top of all kinds of soil texture types (Zema et al. 2012), especially after dry periods.

To look in detail into infiltration and runoff processes at the hillslope scale, it is necessary to gain knowledge about soil types, especially soil texture distributions and infiltration, as well as (pedo-)hydrological parameters such as rainfall and surface runoff data. To measure latter, we used an innovative automatic surface runoff detector (SRD) device, measuring runoff height (from soil surface) and duration. Following research questions have arisen out of this research gap:

RQ3 How can surface runoff be quantified in semiarid savannah type environments?

When surface runoff concentrates further down the slope it becomes turbulent and promotes sediment detachment that leads to linear depressions. Rills and gullies are different morphological stages of incised channels. Gully erosion is a major threat concerning landscape degradation in large areas along the Northern Tanzanian Rift valley. It is the dominant erosion process producing large parts of the sediments that are effectively conducted into the river network. The "off-site damages" of gully erosion processes are related to the transported sediments that are mainly affecting water quality and are causing reservoir sedimentation (Sidorchuk et al. 2003).

Gully morphometric attributes (such as gully length, depth, catchment area and volume), are coupled to different gully evolution phases (according to Kosov et al. 1978; compare with Figure 3). The authors divided the gully's lifetime in a dynamic phase covering just the first 5% and a static phase covering the remaining 95% of the gully's lifetime. The dynamic phase is characterized by i) gully length up to 90% of the entire length development, ii) gully depth that reaches up to 80% of its final depth, iii) gully catchment or contributing area of less than 60% of the entire contributing area and iv) less than 45% of the final gully volume.

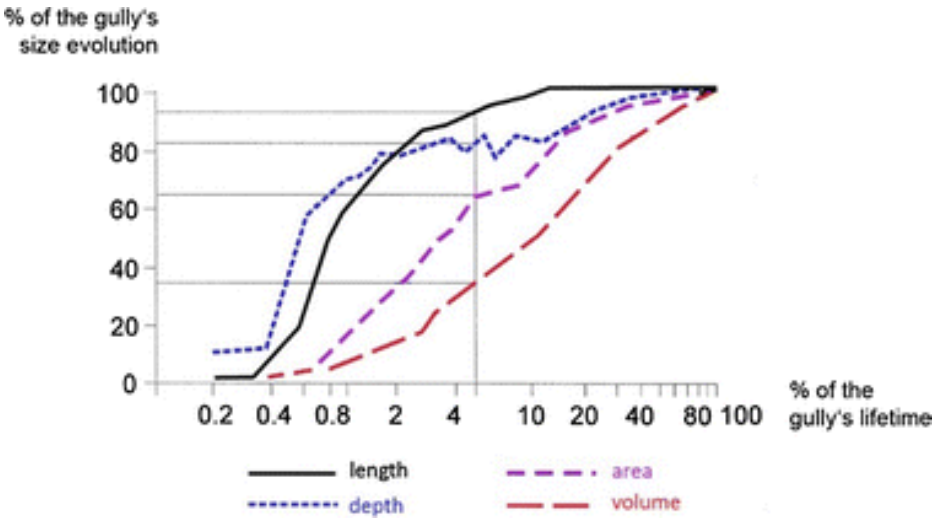

Figure 3. Gully evolution phases. Gully evolution phases according to morphometric characteristics (from Sidorchuk 1999, after Kosov et al. 1978).

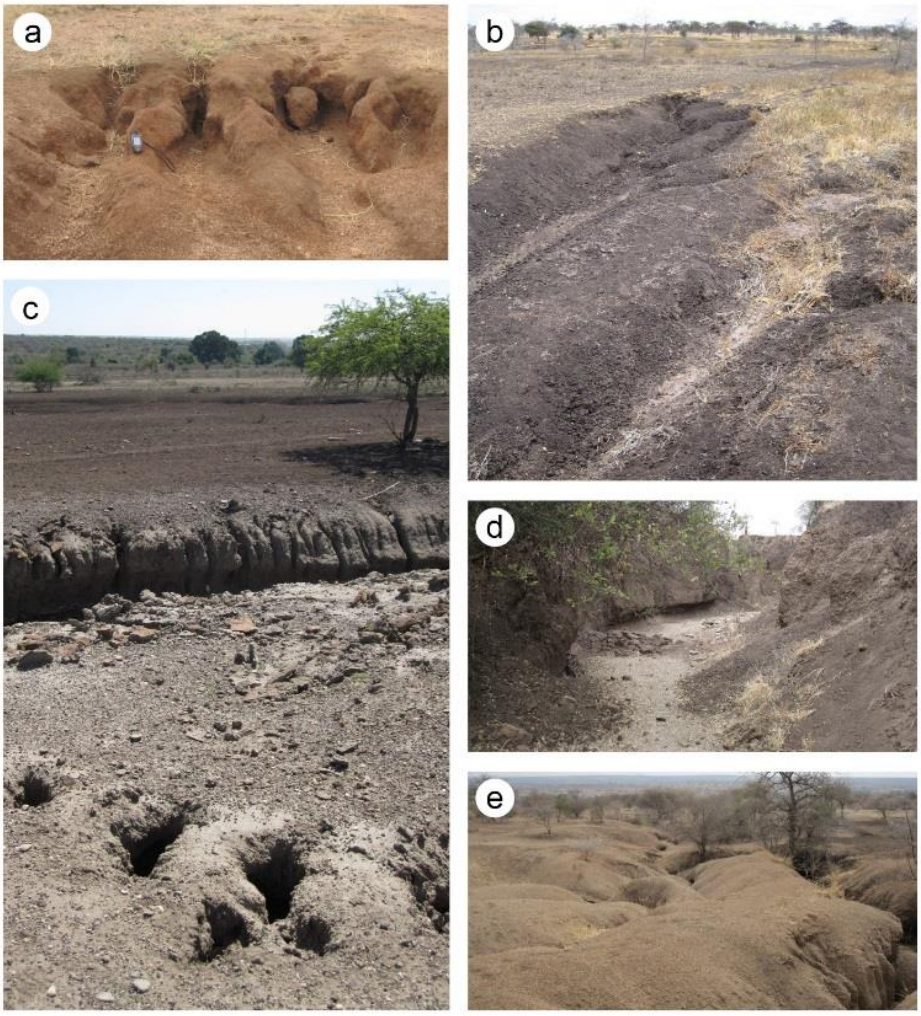

Figure 4. Gully morphology and processes. a) Gully headcut (Photo: 06/2013). b) Ephemeral gully with headcut (09/2010). c) Gully (background) and piping (fore-ground) (03/2014). d) Permanent gully with mass failure (08/2011). e) Badland formation (08/2011). Photos: G. Quénéhervé.

Gullies are typically more than 0.3 m wide and range from 0.5 to 30 m in depth (Poesen et al. 2002). They differ from stable river channels in having steep sides, step/pool profiles, characteristically with a headcut (Figure 4a) at the upslope end (Knighton 1998). Two main processes initiate permanent gully formation: surface flow and piping. Piping (Figure 4c) is an erosional process caused by subsurface flow within the bulk soil. Poesen et al. (2002) distinguish gullies on a physically based classification in ephemeral (Figure 4b) and permanent systems. Permanent gullies (Figure 4d) are larger systems that typically develop on abandoned fields or rangeland. When gullies grow into each other, they result in badland formation. Badlands are intensively dissected high relief areas unusable for agriculture (Figure 4e).

A detailed assessment of gullying processes yield valuable information on the landscape and landscape functions such as sediment load, water quality, landscape stability, soil- and groundwater storage as well as soil fertility and soil depth (Hancock, Evans 2010). In sub-Saharan Africa, a proper assessment of gully erosion is difficult as most of the affected areas are not accessible for comprehensive fieldwork (missing permits; dangerous areas because of conflicts, diseases, etc.). Enhancing existing elevation data with additional topographic information was already successfully deployed to assess soil erosion processes (Costanzo et al. 2012; Conoscenti et al. 2013; Frankl et al. 2013). Consequently, to understand the local gully erosion processes and features, detailed field measurements have been combined with digital data to answer following research questions:

RQ3 Are the local gullies in stable or in dynamic conditions? How can these analyses contribute to a better understanding of landscape developments?

Geomorphic studies in Eastern Africa, after the discovery expeditions beginning in the 1860s, had a renewal period from the 1960s to the 1980s. Langlands (1964) offers a short review of geomorphic studies and maps for eastern Africa, mostly Uganda and Kenya. Grove (Grove 1986) provided a description of the geomorphology of the EARS. Toya and colleagues conducted geomorphic field studies in southeaster Kenya from 1969–1971 (Toya et al. 1973). Tricart (1972) and Morgan (1972) worked on landscape descriptions.

Geomorphic maps are fundamental components of geographic investigations (Rădoane et al. 2011). Geomorphic mapping plays an essential role in understanding surface processes, spatial distribution of landforms, geo-chronology, natural resources, natural hazards and landscape evolution (Blaszczynski 1997; Bishop, Shroder 2004; Finkl et al. 2008). Modern comprehensive geomorphic map construction started in the early 20th century, while detailed geomorphic maps have been published from the late 1950s up to the 1970s (Klimaszeski 1990). In the late 1980s, the use of Geographic Information Systems (GIS) became widespread in geomorphology and GIS technologies have become important tools for landform analysis, data management and construction of geomorphic databases (Gustavsson et al. 2006; Demek et al. 2011).

Nevertheless, geomorphic mapping approaches in East Africa are few, detailed maps (<1:50,000) are scarce. The only available geomorphic mapping work near the focus area was done at the eastern shorelines of Lake Manyara (Vaidyanadhan et al. 1993). Doornkamp (1971) emphasizes that the potential value of geomorphic studies in East Africa "has not yet been fully realized and geomorphology has not yet developed beyond its most elementary stage" in East Africa. Nowadays, more than 40 years later, there is no significant change in that statement. To overcome this lack of information, an extensive mapping in the focus area was undertaken.

Out of this research deficits and the research questions stated, the main objective (MO) of this thesis is therefore to better understand the landscape processes, forms and features of the Makuyuni River system around Makuyuni town:

MO Understanding geomorphic processes, their spatial extent and location.

1.3 Structure of this Doctoral Thesis

The present framework of my doctoral thesis unites the five different research approaches to answer the main objective of this thesis as well as to provide background information on the study area.

Chapter 1 provides the state of the art of the thematic topics tackled within this thesis. It also states the research questions of singular thematic topics (represented by the individual publications) and the main objective.

The study area is presented in **Chapter 2**. An introduction in the geology and tectonics of the East African Rift Valley constitutes the basis for understanding the formation of the landscape and its influences on the present-day forms and features. The present geomorphology and soils are outlined as well as a brief overview of the climatic and hydrologic conditions as well as the dominant vegetation is provided.

Chapter 3 presents an overview of important methods used throughout the study; an emphasize was set on the conducted fieldwork and exploited devices as well as on field data collections and modelling thereof.

The important findings and outcomes in regard to the research questions are presented and discussed in **Chapter 4**.

Chapter 5 is dedicated to the main objective of this thesis on understanding geomorphic processes, their spatial extent and location. The section highlights a synthesis of the landscape processes, forms and features.

Finally, **Chapter 6** draws the conclusions of the study and states recommendations for future research.

Appendices: All four peer-reviewed publications as well as the submitted manuscript, that are related to this PhD cumulative thesis, are attached (I – V).

A supplemental geomorphic map completes the thesis.

2 Study Area

This chapter provide a brief introduction into the geologic situation, the active tectonics, main geomorphic features, soil type occurrences and distribution as well as the climatic and hydrologic conditions.

2.1 Geology and Tectonics

The Precambrian basement of East Africa consists of the Archean Tanzania craton (4–2.5 billion years) that is a stable part of the continental lithosphere. The Archaean Tanzania craton extends from central Tanzania to western Kenya and southeast Uganda (~350,000 km^2) and to a depth of 140–170 km (Chesley et al. 1999; Weeraratne et al. 2003; Manya et al. 2006) and is composed of greenstone belts and granitoids (Weeraratne et al. 2003).

There is profound evidence that the asthenospheric mantle beneath the Archaean Tanzanian craton has isotopic characteristics of a mantle plume (Weeraratne et al. 2003; Chesley et al. 1999). Although this region has been well studied, there has been no consensus on the number of plumes and associated mantle flow beneath East Africa and Arabia (Chang, Van der Lee 2011). While Cenozoic rifting at the craton fringe has eroded the edge of the original craton boundary, the Archean lithosphere behave stable in the presence of the proposed upwelling plume activity (Weeraratne et al. 2003; Chesley et al. 1999).

The northward drift of Africa causes extensive volcanism and distinct evolution from initial rifting stages in Tanzania via mature stages in northern Kenya to a continental break-up in the Ethiopian/Afar section (Ring et al. 2005; Ring 2014). The EARS (Figure 5, p. 14) and its structurally and magmatically controlled processes have created complex relief and drainage conditions, beginning in the Eocene at about 45 million years (Ma) and continuing into the present (Trauth et al. 2005).

The Cenozoic rift valleys of the EARS form two branches (Eastern and Western rift), within the Eastern rift, there is an obvious southward propagation in the onset of volcanism, and hence rifting. In the Ethiopian Rift, volcanism started between 45–33 Ma. I in northern Kenya it started at about 33 Ma and continued to about 25 Ma, the magmatic activity of the central and southern segments of the rifts in Kenya started around 15 Ma,

and in northern Tanzania at about 8 Ma (Ebinger et al. 2000; Trauth et al. 2005; Nyblade, Brazier 2002). Extension within the Eastern rift starting in Kenya has led to the formation of a narrow graben commonly referred to as the Kenya rift (in Kenya) or Gregory rift (in Tanzania) (Weeraratne et al. 2003).

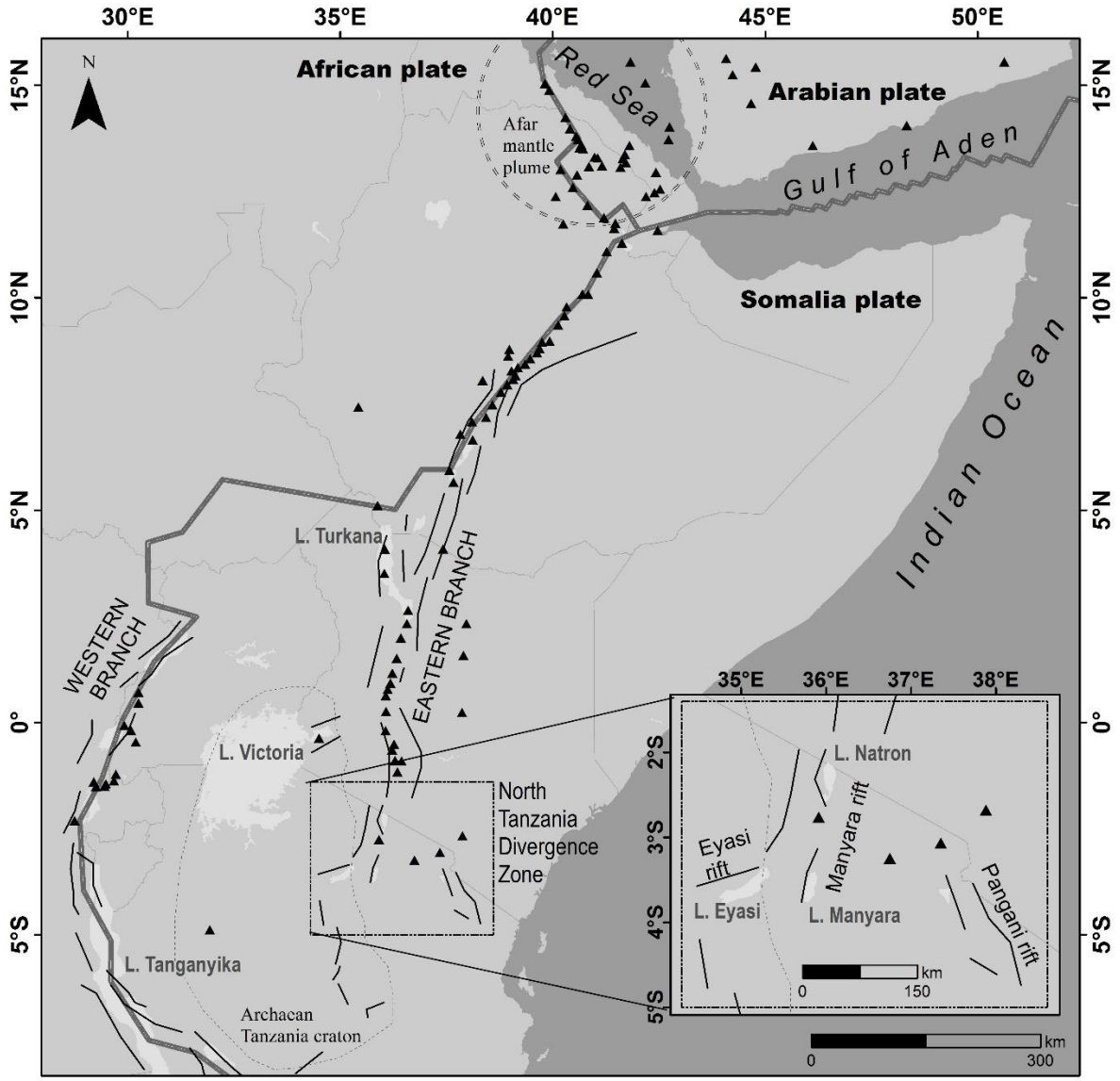

Figure 5. Tectonic map of Eastern Africa. East African Rift System (black line segments); plate boundaries (thick grey line) (Bird 2003); Afar mantle plume (dotted circle) (Chang, Van der Lee 2011); Archaean Tanzania craton (dashed dark grey outline); volcanoes (solid triangles) (Venzke 2013); close up of the North Tanzania Divergence Zone (black rectangular).

The southward progression of the Gregory rift stopped at about 13–10 Ma when it encountered the strong cratonic lithosphere of the Archaean Tanzania craton (Weeraratne et al. 2003; Nyblade, Brazier 2002). Nyblade and Blazier (2002) suggested that some of

the east-west extensional stress was transmitted across the cratonic lithosphere to cause rift faulting in the weaker mobile-belt lithosphere on the west side of the craton. A pronounced splay, the Northern Tanzania Divergence Zone (NTD), structurally and morphologically expresses this termination at the Archaean Tanzania craton. The NTD is ~300–400 km-wide and consists of three separate branches, which are from W to E the Eyasi, the Manyara and the Pangani rifts (Ebinger et al. 1997; Chorowicz 2005). These rift basins are typically some 40–50 km-wide and 60–120 km-long and open at rates of ~3 mm/yr (Ring 2014).

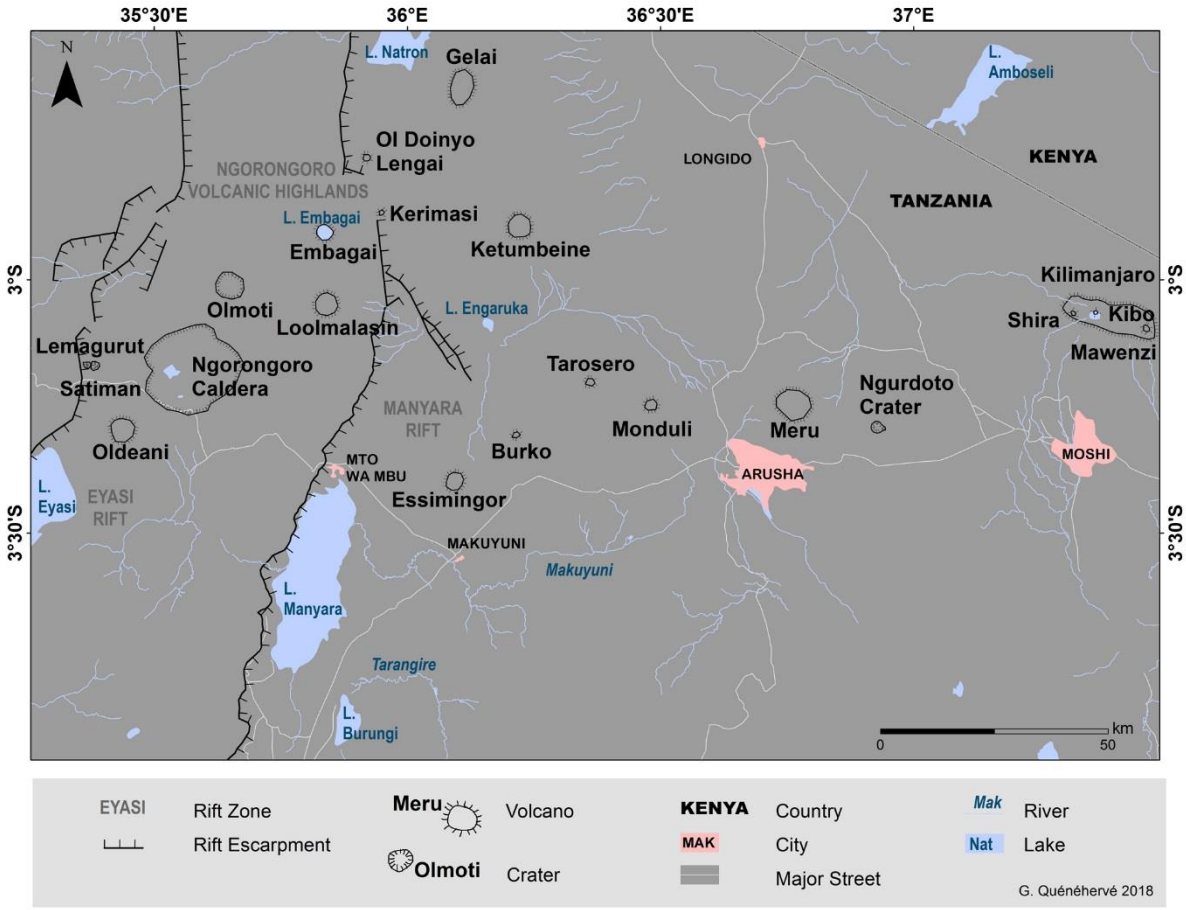

Figure 6. Northern Tanzania volcanic province. Tectonic faults and volcano names: Mollel et al. 2008; Dawson 1992; Mollel et al. 2008. Volcanoes and cities digitized after ESRI Basemap. Lakes, rivers and roads from the 'Digital Chart of the World' product from ESRI.

Volcanic activity began at ~8–4 Ma in the centre of the NTD and continues to the present (Le Gall et al. 2008). Cenozoic volcanism in the eastern branch of the EARS migrates from

north to south and is consistent with the thin lithosphere with a large N–S trending gravimetric negative Bouguer anomaly (Chorowicz 2005). There is a 200 × 50 km transverse volcanic belt (northern Tanzania volcanic province; Figure 6, p.15) from the Ngorongoro crater to the volcano Kilimanjaro.

The Ngorongoro Volcanic Highland (NVH) is part of the volcanic province measuring about 45 × 60 km and is situated on the southern part of the Gregory rift, between the Eyasi and the Manyara rift on the EARS platform (Mollel, Swisher III, Carl C. 2012). The NVH comprises the volcanic uplands adjacent to and east of the Olduvai and Laetoli paleoanthropological sites. The chemistry of the volcanoes is alkaline and silica-undersaturated, the composition of the lavas indicated small volumes of melt beneath a ~140 km-thick lithosphere (Ring 2014).

The earliest volcanic activity in the NTD occurred during the Late Miocene with the eruption of the phonolithic lava at the Essimingor volcano and is associated with the deformation of the mid-Tertiary land surface (Bagdasaryan et al. 1973; Dawson 1992). This first activity produced mainly alkali basalt-trachyte-phonolite lavas, associated with the volcanoes Ol Doinyo Lengai, Olmoti, Loolmalasin, Ngorongoro, Lemagrut, Oldeani, Tarosero, Ketumbeine, Gelai, Kilimanjaro (Shira and Mawenzi centres) (Dawson 1992; Mollel et al. 2008). A second phase of volcanic activity occurred after the 1.2 Ma faulting. This phase was highly explosive with an ultra-basic to ultra-alkaline magma and rocks mainly phonolites and feldspathoidal syenites at the pyroclastic volcanic cones of Meru, Monduli, Ol Doinyo Lengai and Kerimasi. Carbonatite lavas, pyroclasts, nephelinites and phonolites occurred at Ol Doinyo Lengai and Kerimasi (Mollel 2007; Dawson 1992).

Essimingor, which is closest to the study area, is mainly formed of pyroclastic deposits namely nephelinitic and phonolitic tuffs as well as agglomerates (Dawson 1992, 2008). It is the oldest volcano in northern Tanzania with K-Ar ages of 8.1 Ma on a mela-nephelinite and 4.68 and 3.22 Ma on two nephelinites (Dawson 2008). However, Mana et al. (2009) report a maximum age approximately 2 Ma earlier then the previously considered. They present a new 40Ar/39Ar laser-incremental heating and geochemical analyses of twelve lava samples and yielding ages of 5.81±0.01 Ma to 6.20±0.03 Ma. These ages restrict the duration of the volcanism of Essimingor to ~370 ka.

The Manyara rift is underlain by the Archaean Tanzania craton (W) and Precambrian basement rocks of the Mozambique Belt (E). Three major half-graben basins (Natron

basin, Engaruka basin and Manyara basin, from N to S) are bounded by a faulted rift escarpment on one side and a flexural warp on the other (Le Gall et al. 2008). Since its initiation at ~8 Ma the Manyara rift has recorded several episodes of faulting; the earliest evidence of extensional faulting is on the western flank of the Natron basin where 3 Ma-old basalts are located, there is evidence for multi-stage extensional faulting in the Engaruka basin, the Manyara basin has its major activity at 1.2 Ma (Le Gall et al. 2008). A series of small lakes that are presently partly alkaline has developed in the eastern branch since the Pliocene (Trauth et al. 2005). A general overview of the geologic basement is illustrated in Figure 7.

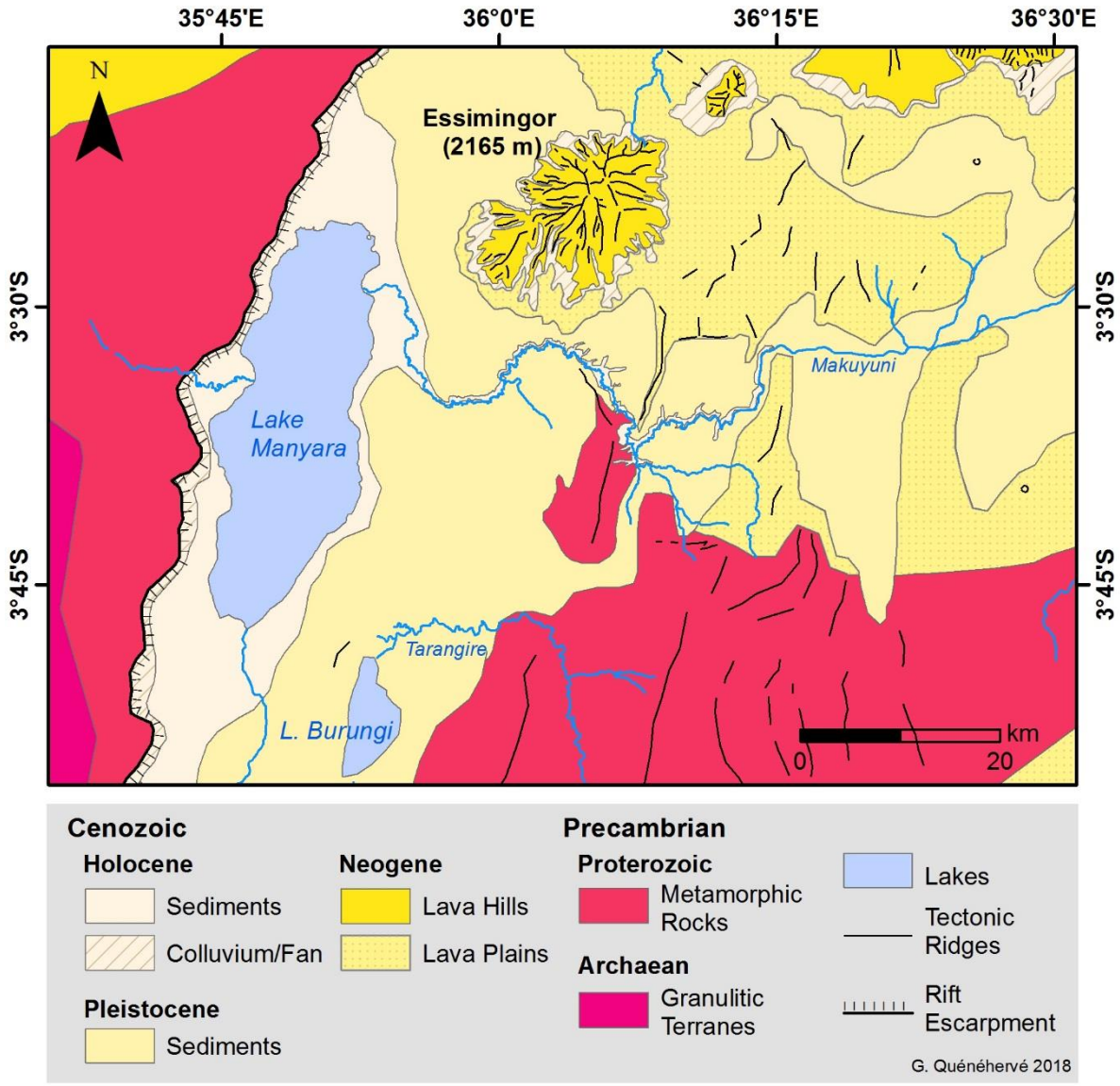

Figure 7. Geological overview of the study area. Interpretation based on field surveys and additional information from Vaidyanadhan et al. 1993 and Schlüter 2008.

The Manyara basin (20 × 50 km half-graben, ~3 km-thick fill material) initiated at ~4.9 Ma in shallow lacustrine environments with little extensional faulting (Foster et al. 1997). The present Lake Manyara is the residual of a larger paleolake that was much deeper (Bachofer et al. 2014). There are two drilling cores from Lake Manyara (Holdship 1976; Barker 1990). The rocks laid down in the lake basin include carbonate rocks, tuffs and reworked volcanic detritus, ashy clays and marls with horizons of chert nodules and calcareous algal concretions known as stromatolites. The ridges on the E of the lake are formed by carbonate rocks and stromatolites (Bachofer et al. 2014). The footwall block of the Manyara basin is primarily composed of Late Proterozoic basement rocks overlain to the N by basaltic lava flows ranging in age from ~4.9 Ma to ~1.3 Ma (Le Gall et al. 2008; Foster et al. 1997). The basement rocks are primarily metasediments (hornblende-garnet gneiss, biotite gneiss, quartzo-feldspathic gneiss, quartzites etc.) along the W margin of Lake Manyara, Neogene volcanic extrusive rocks in the N of the Manyara basin are basaltic (Vaidyanadhan et al. 1993).

2.2 Geomorphology and Soils

The broader area (see Figure 7, p. 17), from west to east, can be divided into the volcanic plateau area on top of the graben with the volcanic hills of the Ngorongoro area and the Archaean craton. The escarpment hills are made of Proterozoic metamorphic rock formations, they are sloping towards NNE (Vaidyanadhan et al. 1993). The Proterozoic gneisses are overlie by Neogene lavas that form high mountains (Ngorongoro Volcanic Highland). Undulating and incised plains form the landscape east of the Makuyuni River.

As the geomorphology is the main topic of this dissertation, the synthesis (Chapter 5) provides a comprehensive interpretation of the geomorphology. Please see additionally the inlay map in the inner back cover for reference as well as Manuscript V.

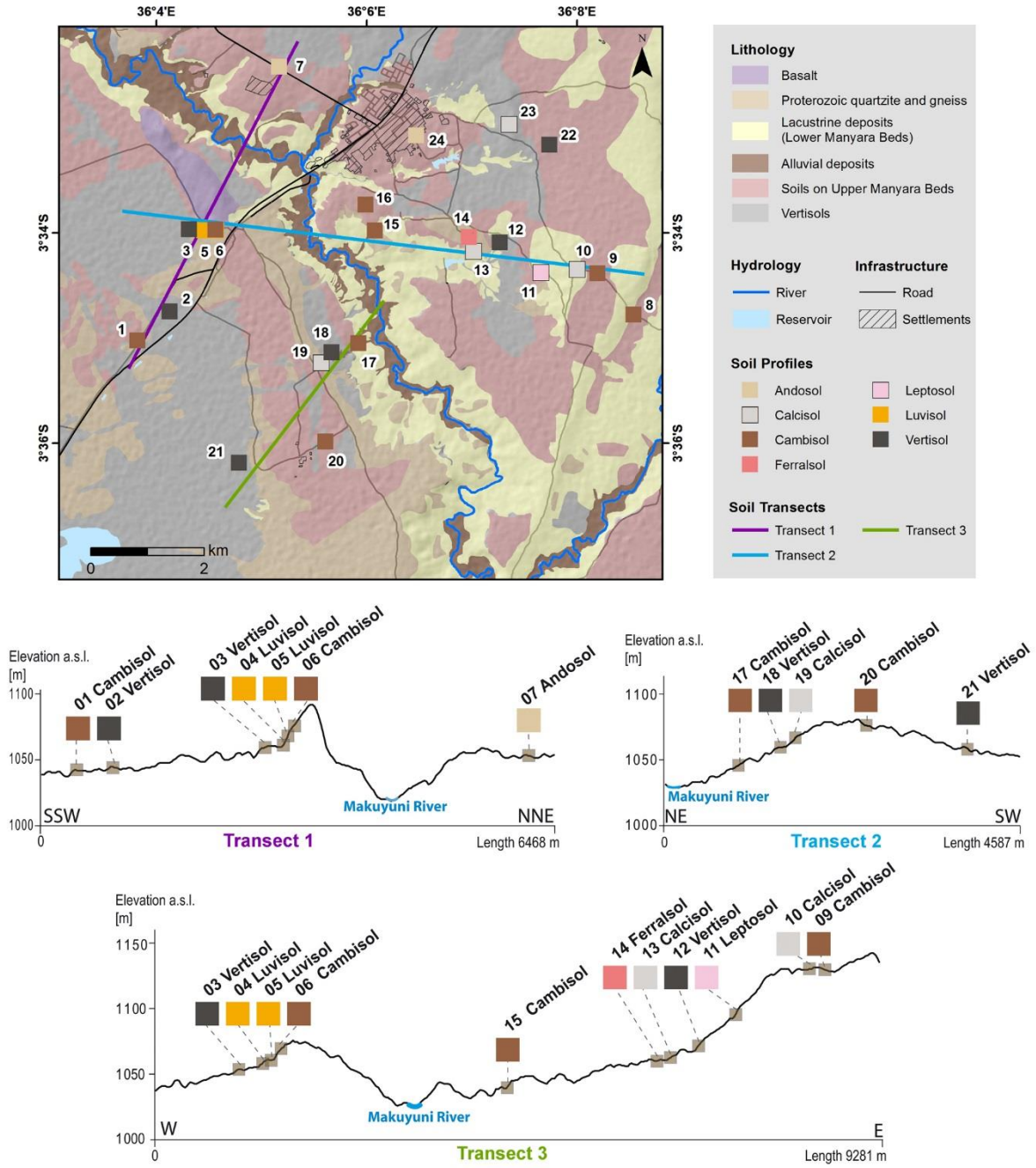

Figure 8. Soil transects and lithologies. Location of the soil profiles and derivated lithologies.

The main stratigraphy is explained in Schwartz et al. (2012), the lacustrine deposits (Figure 8) are the so-called Lower Manyara beds. They are separated by a tuff layer overlaid by soils of the Upper Manyara beds. Soil changes reflect variations in lithology, drainage and erosional history. Figure 8 provide an overview about the soil types along transects; see also Appendix II.

On ridges, most often Haplic or Leptic Calcisols or, more rare, Rendzic Leptosols occur. On the interfluvial crests, on mid-slopes, deep, highly weathered, brown and reddish sandy clay loam or sandy clay soils occur (Andic and Rhodic Cambisols, Rhodic Luvisols). Cambisols (Colluvic) occur close to the Makuyuni River bed and slope toes. On plane areas, least affected by erosion, deep cracked Grumic and Haplic Vertisols, on some parts Andosols, are prevalent. For typical profiles, see Figure 9.

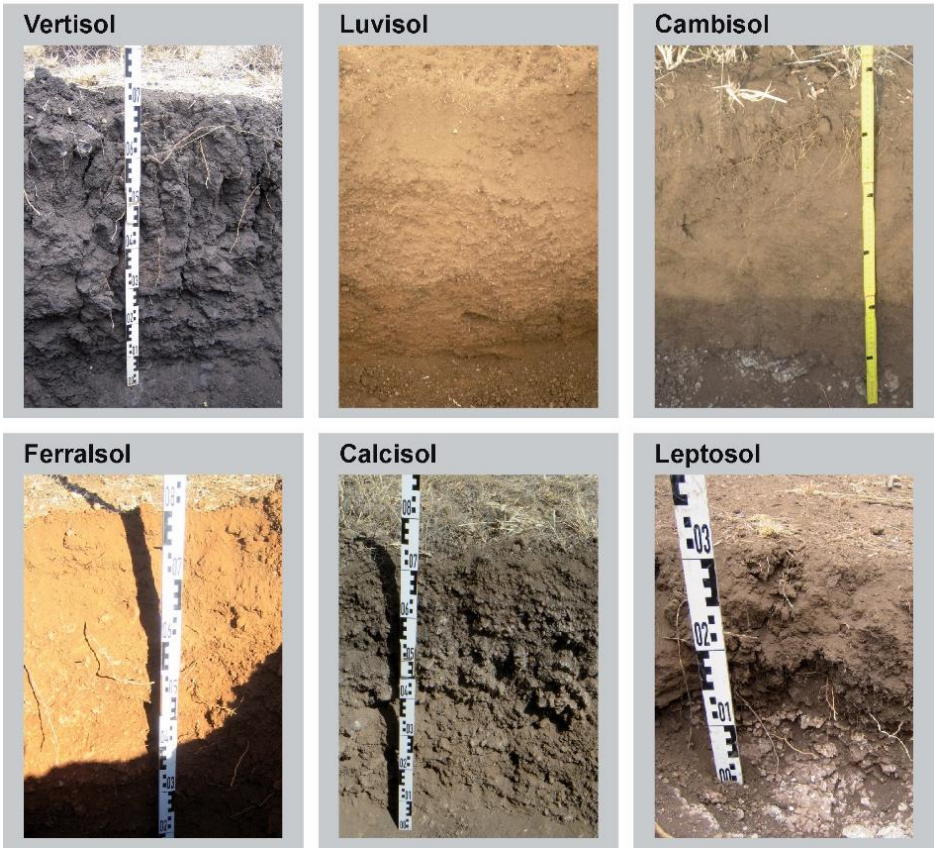

Figure 9. Soil Profiles. Pictures of typical soil profiles in the Makuyuni area. Photos: Quénéhervé 2012, 2013.

2.3 Climate, Hydrology and Vegetation

The East African climate has been and continues to be dynamic. Late Miocene (~8–10 Ma) climate in East Africa was humid and supported a variety of savannah and forest habitats, including rain forests (Trauth et al. 2010). Following this humid period, from ~7–5 Ma, the ice volume of the Antarctic ice sheet expanded and global temperatures fell. This time period is also associated with an aridification across East Africa, as well as the uplift of the Himalayas and the resulting intensification of the Indian Monsoon, which

may also have contributed to increased aridity. The early Pliocene (5–3 Ma) is characterized by warmer and wetter conditions across Africa (deMenocal 1995). The interval beginning at ~2.8 Ma represents the onset of the glacial-interglacial cycles that characterizes the Pleistocene as the Northern Hemisphere Glaciation expanded (deMenocal 2004; Trauth et al. 2005).

Simultaneous with this onset of bipolar glaciation and glacial-interglacial cyclicity, a cyclic trend in aridity across Africa occurs. In particular during the last 500 ka, the climate in East Africa has been extremely variable, transitioning between wet and dry intervals that have caused significant fluctuations in the East African lake levels (Hillaire-Marcel et al. 1986; Gasse 2006; Trauth et al. 2003; Garcin et al. 2009). During the Last Glacial Maximum (LGM, ~20–15 ka), Africa again experienced an increase in aridity (Gasse 2000). The Holocene represents an interval of a moderately fluctuating climate during which there have been modest fluctuations in the lake levels of the African Great Lakes (Cohen et al. 1997; Bergner et al. 2009).

During March 2010 and December 2013, with measurement gaps, meteorological data have been recorded on a climate station close to the town of Makuyuni. The recent prevailing tropical savannah climate (Aw after Köppen-Geiger climate system; Geiger 1961) is characterized by bi-modal rainy seasons (October-December and March-May) with annual rainfall of less than 500 mm. The climate is influenced by the south eastern trade wind in mid-year and the north eastern trade wind during the turn of the year but rainfall pattern is very erratic. Air temperatures vary little; the mean annual temperature is about 22° C.

The broader area is drained by the endorheic basin of the Lake Manyara. The saline lake is located at the NE margin of the Manyara basin and varies from 410 to 480 km^2 in area and has dried up completely at certain times (Yanda, Madulu 2005). Deus *et al.* (2013) reported a maximum water depth of 1.18 m with an average depth of 0.81 m was measured in 2010. The lake is enclosed by the rift escarpment on the west, on the flanks, freshwater runs in cascades and rapids down to the lake. There are few waterfalls along the E margin of the W ranges. Some hot springs (*maji moto*) are located close to the W shores of the lake that are an indication of recent tectonic activity (Vaidyanadhan et al. 1993). Broad lake flats are stretching along its eastern shoreline, on the W of the lake they are narrow and are flanked by the alluvial fans of the escarpment drainages.

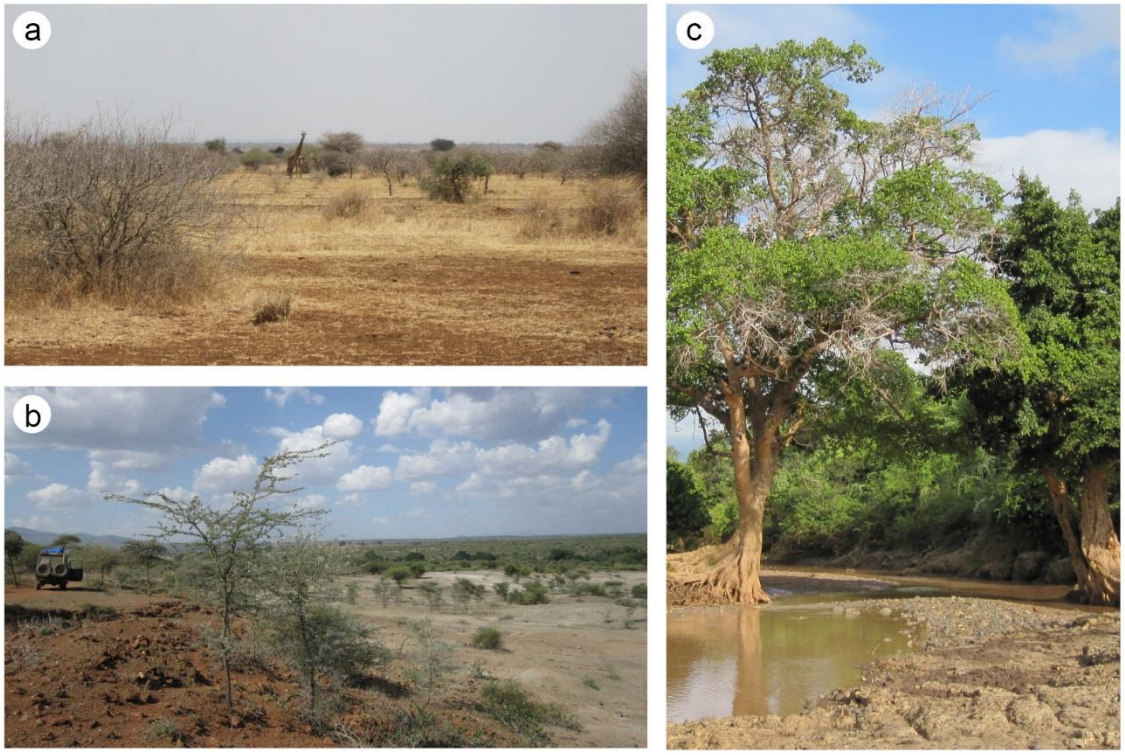

Figure 10. Typical vegetation communities in the Makuyuni area. a) Sparsely vegetated savannah bushland with grasslands and bushes. b) In the foreground on the reddish Upper Manyara beds agricultural fields, on the slopes mostly whistling thorn acacia (*Vachellia drepanolobium),* in the greyish Lower Manyara beds open substrates with few bushes. In the background on Upper Manyara beds and quartzite substrates bushy vegetation with baobabs (*Adansonia digitata*) on hill crests. c) Along the Makuyuni River banks dense, bushy vegetation with trees. Photos: Quénéhervé 2011, 2014.

The lakes largest tributary is the Makuyuni River with a catchment area of ~3080 km^2 that is flowing from the volcanic highlands to the northeast westwards up to its outlet point in the Lake Manyara. East of the lake flats, within the Makuyuni River catchment, the landscape is gently undulating. Some faults in the E trigger the secondary streams of the Makuyuni River to follow their lines. On the southernmost part of the Makuyuni, there is distinct evidence of a former discharge valley running southwards towards the Tarangire River system. Due to uplifting, the river is running now westward up to its outlet point into the Lake Manyara. Along the Makuyuni River, where first and second tributaries cut deep into the sediments, the landscape is dominated by erosion features.

Vegetation cover follows substrates as well as the water regime and is parted into small-scale mosaics with homogeneous grass vegetation, woodlands and bushlands. The following description of relevant communities on typical landscape units follows Loth and Prins (1986) and van Breugel et al. (2015); for typical plant communities see Figure 10.

The riverine vegetation on alluvial terraces along ephemeral streams, the 'African caper (*Capparis tomentosa*) – paperbark thorn (*Acacia sieberiana*)' community occurs. On lacustrine terraces the 'umbrella thorn (*Acacia tortilis*) – feather fingergrass (*Chloris virgata*)' community is found. In moderately steep slopes, the latter is replaced by the Asbos-vernonia shrub (*Vernonia cinerascens*). On plains 'Acacia-Commiphora deciduous wooded grasslands' intermixed with 'Combretum wooded grasslands' and 'Somalia-Masai Acacia-Commiphora deciduous bushland and thicket' are prevailing. The first persists of bushy plants, mainly *Acacia* and *Commiphora,* and by the relative abundance of grasses (especially perennial grass species). The latter is intermediate between bushland and shrubland. On volcanic soils, edaphic grasslands occur; with an estimated tree cover >10%, they are classified as edaphic woody grasslands.

The valley bottom west of Makuyuni town, around Mto wa Mbu is used mainly for irrigated banana and rice plantations. Maize and beans are also important crops; many Croton trees (*Croton macrostachys*) have been cleared to generate those fields (Loth, Prins 1986). Around Makuyuni town, the Cambisols and Vertisols are mainly used for Maize fields. Most of the area is used as feeding grounds for goats, however.

3 Materials and Methods

This study was accompanied by extensive fieldwork; six campaigns have been held from 2010 to 2014. We measured different kind of field parameters that are presented in the following part of this chapter.

A brief look into spatial data analysis as well as geostatistical modelling approaches are shown in the first subchapter. This is followed by the presentation of morphotectonic digital analyses. Soils, gullies and pedo-hydrologic characteristics have been measured in the field as well as analysed – in the laboratory and/or digitally. The present mapping of geomorphic forms and features finalizes this chapter.

3.1 Digital Data Analyses

Geographic Information Systems (GIS) are a necessity working with spatial datasets; to not only synthesize and visualize the data and results, but also to perform quantitative – more precisely geomorphometric – analyses of the landscape. Different kind of terrain indices, based on derivatives of digital elevation models (DEM), have been used throughout the presented publications. Most relevant for this thesis are works of following authors: Beven, Kirkby 1979; Moore et al. 1991; Wilson, Gallant 2000; Jenness 2006; Gruber, Peckham 2009; Olaya, Conrad 2009; Jasiewicz, Stepinski 2013.

For the identification and mapping on aerial and satellite data, a certain familiarity of the environment is a necessity. Reference and ground truth data have been recorded to support satellite classifications (see e.g. Bachofer et al. 2015a and Bachofer et al. 2015b). Especially for mapping approaches, these are useful additional data that support the on-screen interpretation.

Geostatistics and the depending regionalization are an important part working with spatial datasets. In order to generate spatially continuous data sets from single point information, an appropriate method is necessary. Various methods have been explored within the last decades, especially from the 1990s onwards in research publications (Journel 1993) and tool developments (Deutsch, Journel 1998). Relevant for this synopsis is the boosted regression tree approach (BRT), a stochastic gradient boosting model (Elith et al. 2006). BRTs combine classification and regression trees with the gradient

boosting algorithm (Friedman 2002). It identifies the best relationship between a feature set and the target classes (Bachofer et al. 2016).

3.2 Morphotectonic Analyses

Morphotectonic analyses, lineament extraction and base level map production are methods that identify landscape elements of recent tectonic activities associated with drainage networks (Kirby, Whipple 2001).

Morphometric variables in basins can be determined by hypsometric analysis of a DEM. DEMs and remote sensing images are used to analyse regional tectonic features from topography (Wobus et al. 2006). Basin hypsometry identifies the stage of drainage evolution. The hypsometric integral (HI) values provide a simple index of the depth distribution within the area under consideration and represent different evolution stages: HI > 0.6 youthful phase, HI 0.35–0.6 equilibrium phase, HI < 0.35 monadnock phase (Strahler 1952; Shahzad, Gloaguen 2011b). When the basins represent similar HI values but have different shapes, hypsometric curves and their statistical moments (skewness and kurtosis) can be calculated (Pérez-Peña et al. 2009). Skewness represents the amount of headward erosion in the upper reach of the basin; kurtosis represents the erosion on the upper and lower reaches of a basin. The calculation is automated within the TecDEM software (Shahzad, Gloaguen 2011a, 2011b). The TecDEM extracts automatically the drainage network based on Strahler (1957) order.

Lineaments are manually and automatically extracted and compared to the neotectonic map of Dawson (2008). This was done to classify them into four types of linear tectonic structures: faults, inferred faults, escarpments and lithological contacts.

The concept of base level is defined as a level “below which the dry lands cannot be eroded”, the ultimate base level is therefore the local sea level (Grohmann et al. 2011). Base level maps express a relationship between valley order and topography. They are related to similar erosional stages and are a product of erosional tectonic events (Golts, Rosenthal 1993). The method attempts to identify areas with possible tectonic influence within lithological uniform domains (Grohmann et al. 2011). These approaches allow to assess further the influence of tectonics on current gully erosion processes.

3.3 Soil Analyses

The categorization of soils and their mapping is a complex process. During the field campaigns, we digged in total 24 profiles and collected 69 profile samples. In the field, x-y-location coordinates using a handheld GPS and pictures of each profile were taken. For each 10 cm, a profile sample was taken and data recorded in situ (Table 1, p. 33):

(i) Sample depth [cm];
(ii) Landuse around the soil profile;
(iii) Soil skeleton in vol.-% after sieving with a 2 mm sieve;
(iv) Finger testing of the soil matrix, according to USDA Guide to texture by feel (USDA n.y.).
(v) Soil colour in dry and wet conditions following the Munsell Soil Colour Charts (Munsell Color (Firm) 2010),
(vi) CaCO3 with the 10%-conc. HCl soluble, after AG Boden (2005);
(vii) Roots distribution (for thick and thin roots), following AG Boden (2005).

After the samples have been air-dried and sieved in the laboratory (<2 mm), they have been physically and chemically analysed (Table 2, p. 34**Fehler! Textmarke nicht definiert.**):

(viii) Soil texture according to USDA classification (USDA 2014);
(ix) soil pH;
(x) Carbonate content ($CaCO_3$);
(xi) cation exchange capacity (CEC);
(xii) exchangeable bases (Ca^{2+}, Mg^{2+}, Na^{+} and K^{+});
(xiii) Carbon (C) and Nitrogen (N) content to analyse the soil degradation and fertility;
(xiv) Phosphate (P) content which is controlled by soil organic matter levels, soil pH and soil aluminium and iron contents.
(xv) Iron (Fe) and Aluminium (Al) content [mg/kg].

Note that due to the change of laboratories, we have a change of methods and sometimes not available data for some of the characteristics.

3.4 Pedo-hydrological Measurements

In the study area, notable surface runoff is produced when the soil is very dry on the moment precipitations starts, especially in homogeneous soils with low activity clays. When rainfall exceeds the rate at which water can infiltrate the ground, surface runoff will be produced, called Hortonian overland flow (Bracken, Croke 2007). Overland flow in semiarid areas – that are only sparsely and patchy vegetated – occurs on stretched slopes as laminar sheetflow. Lauenroth & Bradford (2006) stated, that the runoff part of the water balance in semiarid regions is close to zero, and hence often ignored.

We measured soil infiltration and texture of the top soils as well as surface runoff for individual rainfall events between October 10, 2010 and December 6, 2010 using a simple experimental setting. With a tension infiltrometer, water infiltrability is determined on the soil surface (Schwärzel, Punzel 2007). In this study, the hood infiltrometer (Umwelt-Geräte-Technik 2005) was used. Rainfall was obtained by a multi-sensor climate station (Meteo, EcoTech Germany) in a 10 min interval. Soil texture was obtained by finger testing (according to USDA Guide to texture by feel, USDA (n.y.).

Overland flow was measured with the innovative, experimental automatic surface runoff detectors (SRD) that measure surface runoff height and duration. The SRD devices are placed on the surface whilst the logger unit is buried in the soil (Figure 11).

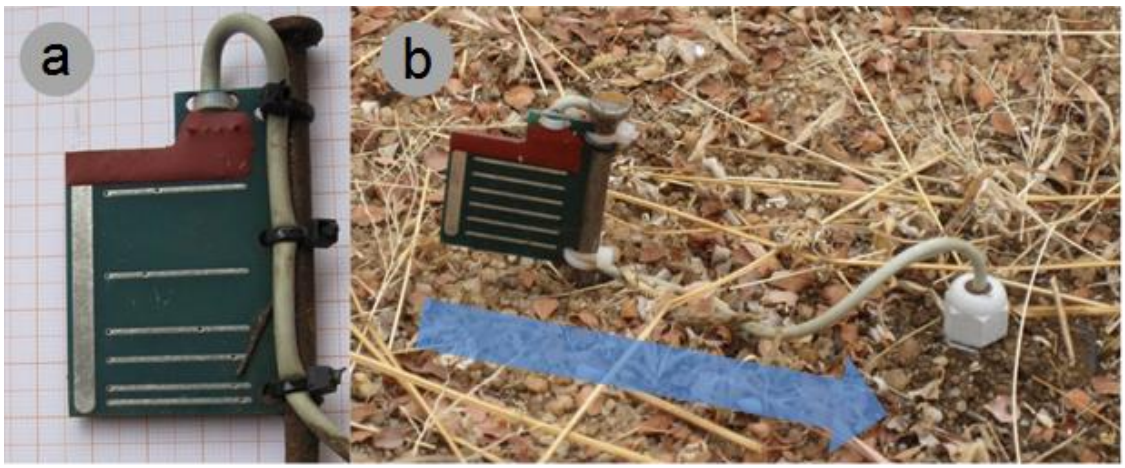

Figure 11. Surface runoff detector. a) Close up of the sensor head. b) Installed device on the test slope; drainage line is shown in blue. Photos: G. Quénéhervé.

When runoff height grows, the electric contacts are closed sequentially transmitting a signal that is then reported to the logger storage unit. In this experimental setup, we placed logger units according to Figure 11b with equal spacing of contacts. The distances

between the electric contacts are 5 mm, reaching up to 3 cm above ground. Hence, the device is able to measure a water column of 3 cm and has a sensitivity of 5 mm.

Terrain indices are based on a very high-resolution DEM. With a ProMark-3 differential GPS, a DEM was obtained, visible drainage lines with a minimum depth of 5 cm were mapped separately with a kinematic survey and function as stream lines for the building of the DEM. The applied interpolation method is based on the ANUDEM algorithm, which allows the consideration of drainage enforcement to create a hydrological correct DEM (Hutchinson 1989). Following indices have been delineated: (i) topographic wetness index (TWI) (after Beven, Kirkby 1979), (ii) vertical distance to channel network, (iii) channel network base level (both after Olaya, Conrad 2009), and (iv) transport capacity (TCI) (Moore et al. 1991).

To get a spatially continuous data set of infiltration values and soil texture, a stochastic gradient boosting model, in this case, a boosted regression tree (BRT) approach was used (Friedman 2002).

3.5 Linear Erosion Feature Analyses

We collected field reference samples and coordinates to be able to distinguish different linear erosion forms and features of remote sensing data. Particular attention was given to the identification and mapping of gully erosion forms and features. Gully erosion is one of the most severe soil erosion processes leading to the loss of fertile topsoil and intensive sediment transport towards the drainage system.

For eight gullies, we conducted a close-up analysis that included detail field measurements. Using handheld GPS devices we measured x- and y-coordinates, moving along the gully thalwegs from upstream (gully head) to downstream (gully mouth, reaching the Makuyuni River channel). For each x-,y-location we also performed a classical cross section measurement, registering the gully depth and width using a measuring tape and stick.

This data, especially the depth values were utilized in the DEM interpolation. We also took geo-tagged photos of gully profiles at the recorded GPS points to document general

features such as soil skeleton, structure and colour of the substrates. Moreover, we performed a finger test to estimate the soil texture. This information is important for the interpretation of gully dynamics after the GIS analyses were conducted.

The formula used for the classification of dynamic and static gully phases is:

$$ratio\ \% = \frac{AH - TCA}{TCA}$$

where AH is the contributing area at gully head [m²], TCA is the total contributing area at the downstream situated gully mouth [m²] (Sidorchuk 1999).

In this study, we utilized the gully area to divide between dynamic and stable gully evolution phases. A ratio greater than 60% indicate static gully systems, ratios below 60% reveal dynamic systems.

3.6 Geomorphic Mapping

Important for the compilation of geomorphic maps is the field mapping as well as the scale issues (Smith, Pain 2011). Doornkamp (1971) suggests to begin the data collection in the field with a reconnaissance survey that includes no actual mapping but only an examination and definition of the features. This was undertaken in the first campaigns 2010 and 2011.

The field mapping has been performed following the guidelines proposed by Knight et al. (2011). The structure of the mapped features, and hence the structure of the database, was established prior to field surveying. We carried out several campaigns of geomorphic field mapping between March 2012 and February 2014 in which we recorded an abundant number of information at x-y-location coordinates using handheld GPS (Geographic Position System). Those include e.g. lithologies, landuse, landforms, erosion features, rock outcrops, water bodies, paths, soil surface types, drainage lines, and landfills.

We followed a multiscale approach with (i) extensive field mapping, (ii) interpretation of multi-spectral and microwave remote sensing images and (iii) the delineation of topographic derivatives (based on DEM). Geomorphic features of the final product were compiled using GIS software. All mapped features are stored as single layers for flexible data management.

4 Results and Discussion

This section summarizes the main goals of the introduced papers according to the research questions stated in this thesis. The questions are addressed by research objectives, in order to perform a scientific analysis and to answer the raised hypotheses.

Tectonic processes in the basin of Lake Manyara have significantly contributed to the formation of the current drainage systems and landforms. Paper I focuses on the morphotectonics of the Makuyuni catchment with an analysis of topography, drainage networks, stream longitudinal profiles and lineaments. Following research question and its deliveries (RD) are stated:

RQ1 How strong is the influence of active tectonics within the Makuyuni River basin and which geomorphic markers are suitable for their delineation?

RD1 Examination of the morphotectonics of the Makuyuni River basin subcatchments:

- Tilting and asymmetric development of the river network.
- Hypsometric curve analyses.
- Stream longitudinal profile delineation and knickpoints analyses.
- Role of tectonics as a triggering mechanism of gully erosion.

This analysis points to a morphostructural control with an N–S trend for the uplifted Masai Block, as well as tectonic deformation in the Makuyuni catchment area (NE of Lake Manyara). The data on the basin tilting, basin hypsometry and the morphology of the stream longitudinal profiles suggests that tectonic activity is an important factor governing Quaternary geomorphic processes, such as river incision and soil erosion, and hence, the landscape evolution of this region.

Hypsometry curves reveal that subcatchments on the right side of the Makuyuni River are in a mature equilibrium phase, whereas those at the left side are in a younger stage of maturity. An investigation of base level and statistical moments of the hypsometric curves provides evidences for the spatial distribution of gully erosion phenomena. Such erosion processes are due to tectonic deformation in the northern parts of the Makuyuni catchment.

Though the soil must be considered as a three dimensional medium, a wide range of remote sensing sensors provide useful information in assessing various details of the mineral composition and other physical and/or chemical properties of the uppermost parts of the soils, as well as for spatially contiguous areas (Anderson, Croft 2009). The topsoils have complex genetic origins related to different substrates, resulting in a high spatial heterogeneity. Paper II pursues the mapping of the distribution of topsoils and surface substrates. Nine soil and lithological target classes were selected through field-work and laboratory analysis of soil samples.

Additionally, 24 soil profiles and collected 69 profile samples have been conducted and analyses in the laboratory. Following work was done, to answer the research question:

RQ2 What soil types are available and how are the soils distributed over the study area?

RD2 Describing soil characteristics and regionalizing them:

- Laboratory analysis of surface samples in order to categorize and characterize the topsoils (Table 1, p. 31; and 2, p.32).
- Compare and discuss the final mapping results with (laboratory-derived) soil catenae covering characteristic transects of the study area.
- Regionalizing the distribution of topsoil and surface substrates using topographic derivatives based on DEMs and additional remote sensing information.

The classification of the nine soil and lithological classes was conducted applying a non-linear support vector machine approach. With the recursive feature elimination approach, the most input-relevant features for separating the target classes were selected. Despite multiple target classes, an overall accuracy of 71.9% was achieved. Inaccuracies occurred between classes with high $CaCO_3$ content and between classes of silica-rich substrates. The incorporation of different input feature datasets improved the classification accuracy. An in-depth interpretation of the classification result was conducted with three soil profile transects introducing 24 soil profiles.

Table 1. Soil properties of the field documentation.

Soil profile number	Soil sample number	Sample depth [cm]	Landuse	Soil skeleton [vol-%]	Soil Matrix by Feel	Munsell Color [dry]	Munsell Color [dry] - Name	Munsell Color [wet]	Munsell Color [wet] - Name	CaCO3 [with 30%-HCl]	Roots [> 2 mm]	Roots [< 2 mm]
3	1	10	grazing	15	scL	7.5YR 4/3	brown	7.5YR 2.5/2	very dark brown	c0	Wg0	Wf6
	2	20	grazing	13	scL	7.5YR 2.5/3	very dark brown	7.5YR 2.5/2	very dark brown	c0	Wg0	Wf6
	3	40	grazing	15	scL	2.5YR 2.5/2	very dusky red	2.5YR 3/2	dusky red	c0	Wg0	Wf4
4	4	10	grazing	25	cL	5YR 3/1	very dark gray	2.5YR 2.5/1	reddish black	c0	Wg0	Wf4
	5	20	grazing	60	CL	5YR 2.5/1	black	7.5YR 2.5/1	black	c0	Wg0	Wf2
	6	30	grazing	50	CL	7.5YR 2.5/1	black	7.5YR 2.5/2	very dark brown	c0	Wg0	Wf2
	7	40	grazing	40	sicL	5YR 2.5/1	black	7.5YR 2.5/1	black	c2	Wg0	Wf2
	8	50	grazing	40	siL	2.5YR 2.5/1	reddish black	7.5YR 2.5/1	black	c2	Wg0	Wf3
	9	60	grazing	40	siL	7.5YR 2.5/1	black	10YR 2/1	black	c2	Wg0	Wf1
5	10	10	n/a	25	SL	10YR 3/4	dark yellowish brown	7.5YR 2.5/3	very dark brown	c0	Wg1	Wf4
	11	20	n/a	45	SL	7.5YR 4/6	strong brown	7.5YR 2.5/3	very dark brown	c0	Wg1	Wf3
	12	30	n/a	55	scL	5YR 4/4	reddish brown	5YR 3/4	dark reddish brown	c0	Wg0	Wf3
	13	40	n/a	60	cL	5YR 4/6	yellowish red	2.5YR 2.5/3	dark reddish brown	c0	Wg1	Wf4
	14	50	n/a	55	sL	5YR 4/6	yellowish red	5YR 3/3	dark reddish brown	c0	Wg0	Wf3
	15	60	n/a	55	scL	7.5YR 4/6	strong brown	5YR 3/3	dark reddish brown	c0	Wg1	Wf3
19	16	10	grazing	80	sicL	5YR .5/2	reddish gray	7.5YR 2.5/2	very dark brown	c5	Wg0	Wf4
	17	20	grazing	75	sicL	7.5YR 4/3	brown	7.5YR 2.5/2	very dark brown	c5	Wg0	Wf3
	18	30	grazing	60	L	7.5YR 5/4	brown	7.5YR 3/4	dark brown	c5	Wg0	Wf3
	19	40	grazing	50	lS	7.5YR 5/4	brown	7.5YR 4/3	brown	c5	Wg0	Wf3
	20	50	grazing	60	siL	7.5YR 5/4	brown	7.5YR 3/3	dark brown	c5	Wg0	Wf0
	21	60	grazing	40	sicL	7.5YR 4/4	brown	7.5YR 3/4	dark brown	c5	Wg0	Wf0
13	22	10	grazing	10	scL	7.5YR 3/3	dark brown	10YR 3/2	very dark grayish brown	c5	Wg0	Wf4
	23	40	grazing	60	cL	5YR 4/4	reddish brown	5YR 3/4	dark reddish brown	c5	Wg0	Wf3
	24	80	grazing	55	cL	7.5YR 4/4	brown	7.5YR 2.5/3	very dark brown	c5	Wg0	Wf1
	25	110	grazing	0	scL	2.5Y 5/2	weak red	2.5Y 3/3	dark reddish brown	c5	Wg0	Wf0
11	26	10	n/a	0	n/a	7.5YR 4/3	brown	n/a	n/a	c0	Wg0	Wf3
	27	15	n/a	5	SL	7.5YR 2.5/2	very dark brown	n/a	n/a	c0	Wg2	Wf3
20	28	15	farming	1	L	5YR 3/4	dark reddish brown	2.5YR 2.5/2	very dusky red	c0	Wg0	Wf4
	29	30	farming	1	siC	2.5YR 3/4	dark reddish brown	2.5YR 3/2	dusky red	c0	Wg0	Wf5
	30	50	farming	2	C	2.5YR 3/6	dark red	2.5YR 2.5/3	dark reddish brown	c0	Wg0	Wf3
21	31	5	grazing	2	sC	5YR 2.5/1	black	7.5YR 2.5/1	black	c0	Wg4	Wf3
	32	30	grazing	0	sC	5YR 2.5/1	black	7.5YR 2.5/1	black	c2	Wg1	Wf4
	33	50	grazing	0	C	5YR 2.5/1	black	7.5YR 2.5/1	black	c2	Wg1	Wf3
18	34	10	grazing	1	sC	7.5YR 2.5/1	black	10YR 2/1	black	c0	Wg1	Wf5
	35	30	grazing	1	sC	10YR 2/1	black	10YR 2/1	black	c0	Wg0	Wf4
	36	60	grazing	1	sC	7.5YR 2.5/1	black	10YR 2/1	black	c1	Wg0	Wf2
14	37	20	grazing	55	SL	7.5YR 4/6	strong brown	7.5YR 2.5/3	very dark brown	c0	Wg1	Wf6
	38	60	grazing	65	SL	5YR 5/8	yellowish red	5YR 3/4	dark reddish brown	c0	Wg1	Wf2
17	39	15	grazing	5	cL	7.5YR 4/3	brown	10Yr 3/3	dark brown	c5	Wg1	Wf5
	40	40	grazing	60	SL	2.5YR 2.5/1	reddish black	5YR 2.5/2	dark reddish brown	c5	Wg0	Wf3
	41	50	grazing	1	scL	7.5YR 3/2	dark brown	7.5 3/2	dark brown	c5	Wg0	Wf0
22	42	15	farming	5	siC	7.5YR 2.5/1	black	7.5YR 2.5/2	very dark brown	c4	Wg1	Wf5
	43	40	farming	1	siC	7.5YR 2.5/1	black	10YR 2/1	black	c4	Wg0	Wf2
	44	75	farming	45	scL	2.5YR 4/1	dark reddish gray	2.5YR 3/2	dusky red	c5	Wg0	Wf0
23	45	5	village	30	scL	7.5YR 3/2	dark brown	7.5YR 2.5/2	very dark brown	c5	Wg0	Wf4
	46	15	village	80	scL	7.5YR 3/2	dark brown	7.5YR 3/3	dark brown	c5	Wg1	Wf3
	47	10	farming	0	SiCL	7.5YR 3/3	dark brown	7.5YR 2.5/2	very dark brown	c0	Wg1	Wf4
	48	40	farming	0	cL	7.5YR 3/3	dark brown	7.5YR 2.5/2	very dark brown	c0	Wg1	Wf0
7	49	10 - 15	bush	0	sicL	7.5 YR 4/4	brown	7.5 YR 2.5/2	very dark brown	c0	Wg1	Wf6
	50	30	bush	0	sicL	7.5 YR 3/4	dark brown	7.5 YR 2.5/3	very dark brown	c0	Wg0	Wf6
	51	50	bush	0	scL	7.5 YR 3/4	dark brown	7.5 YR 2.5/2	very dark brown	c0	Wg0	Wf5
6	52	10	bush	50	n/a	7.5 YR 3/4	dark brown	7.5 YR 2.5/3	very dark brown	c0	Wg2	Wf6
	53	40	bush	60	n/a	7.5 YR 4/6	strong brown	7.5 YR 2.5/3	very dark brown	c0	n/a	n/a
12	54	15	grazing	1	n/a	10 YR 3/1	very dark grey	10 YR 3/1	very dark grey	c2	Wg0	Wf6
	55	50	grazing	< 1	n/a	10 YR 3/1	very dark grey	10 YR 3/1	very dark grey	c2	Wg0	Wf4
9	56	15	bush	60	n/a	10 YR 3/2	very dark greyish brown	10 YR 2/2	very dark brown	c5	Wg2	Wf5
	57	40	bush	60	n/a	10 YR 3/2	very dark greyish brown	10 YR 2/2	very dark brown	c5	Wg2	Wf5
8	58	15	farming	1	n/a	7.5 YR 3/4	dark brown	7.5 YR 2.5/2	very dark brown	c0	Wg0	Wf3
	59	40	farming	0	n/a	7.5 YR 3/3	dark brown	7.5 YR 2.5/2	very dark brown	c0	Wg1	Wf2
16	60	15	bush	0	SC	10 YR 3/2	very dark greyish brown	10 YR 2/1	black	c0	Wg3	Wf5
	61	40	bush	1	SCL	10 YR 3/2	very dark greyish brown	10 YR 2/1	black	c0	Wg0	Wf2
15	62	15	farming	0	SCL	10 YR 4/3	brown	10 YR 2/2	very dark brown	c0	Wg0	Wf5
	63	40	farming	1	SCL	10 YR 3/4	dark yellowish brown	10 YR 2/2	very dark brown	c4	Wg0	Wf5
1	64	15	bush	40	sicL	10 YR 4/3	brown	10 YR 2/2	very dark brown	c3	Wg1	Wf6
	65	30	bush	20	CL	10 YR 4/4	dark yellowish brown	10 YR 3/2	very dark greyish brown	c3	Wg0	Wf5
2	66	15	grazing	0	C	7.5 YR 3/3	dark brown	7.5 YR 2.5/2	very dark brown	c0	Wg1	Wf4
	67	40	grazing	0	C	7.5 YR 3/2	dark brown	10 YR 2/2	very dark brown	c0	Wg1	Wf3
12	68	15	bush	0	sicL	10 YR 3/1	very dark grey	10 YR 2/1	black	c0	Wg0	Wf4
	69	40	bush	0	sicL	10 YR 2/1	black	10 YR 2/1	black	c0	Wg0	Wf0

n/a: not available.

Table 2. Soil properties of laboratory analyses.

Soil profile number	Soil sample number	Soil Texture Analysis									pH		$CaCO_3$		CEC		Exchangeable Cations				C		N				
		C. sand %	M. sand %	F.sand %	Sand %	C. silt %	F. silt %	Silt %	Clay %	Class USDA	pH (H_2O)	pH (KCl)	$CaCO_3$ [%]	$CaCO_3$ [g/kg]	[cmol+/kg]	[meq/100g]	Ca^{2+}	Mg^{2+}	Na^{+}	K^{+}	C [%]	C org. [g/kg]	N tot. [g/kg]	N tot. [%]	P [mg/kg]	Fe [mg/kg]	Al [mg/kg]
3	1	28	7	6	41	19	20	39	20	L	7	6	—	n/a	22	n/a	14	5	0	2	1	n/a	n/a	0	33	1	1
	2	29	6	4	39	18	12	30	31	CL	7	6	—	n/a	23	n/a	15	6	0	2	1	n/a	n/a	0	6	1	1
	3	28	5	4	38	14	12	26	36	CL	6	6	—	n/a	24	n/a	16	6	0	1	1	n/a	n/a	0	7	1	2
4	4	33	5	4	42	15	22	37	21	L	8	7	—	n/a	28	n/a	19	5	3	1	1	n/a	n/a	0	2	1	1
	5	28	4	3	35	12	17	29	36	CL	9	7	—	n/a	35	n/a	25	5	4	1	1	n/a	n/a	0	1	1	2
	6	29	3	3	35	14	12	25	40	CL	9	7	—	n/a	37	n/a	27	5	4	1	1	n/a	n/a	0	2	1	2
	7	29	3	3	35	15	10	24	41	C	9	7	—	n/a	34	n/a	24	4	5	1	1	n/a	n/a	0	2	1	1
	8	25	3	3	31	14	13	27	41	C	9	7	—	n/a	36	n/a	25	4	5	1	1	n/a	n/a	0	2	1	1
	9	25	3	3	31	14	10	24	44	C	9	7	—	n/a	36	n/a	26	4	5	1	1	n/a	n/a	0	4	1	1
5	10	35	10	8	54	16	18	34	12	SL	7	6	—	n/a	16	n/a	12	3	0	1	1	n/a	n/a	0	7	1	1
	11	36	9	8	53	18	18	35	11	SL	7	6	—	n/a	15	n/a	11	3	0	1	1	n/a	n/a	0	<1	1	2
	12	33	9	9	51	21	15	36	12	L	7	6	—	n/a	17	n/a	12	3	0	1	1	n/a	n/a	0	<1	1	3
	13	34	8	9	52	22	15	37	11	L	7	6	—	n/a	16	n/a	12	3	0	1	1	n/a	n/a	0	<1	n/a	n/a
	14	29	9	9	47	19	18	37	16	L	7	6	—	n/a	16	n/a	12	3	0	1	1	n/a	n/a	0	<1	n/a	n/a
	15	30	8	8	46	20	17	37	17	L	7	6	—	n/a	16	n/a	12	3	0	1	1	n/a	n/a	0	<1	n/a	n/a
19	16	37	11	10	58	18	15	33	9	SL	8	8	23	n/a	22	n/a	n/a	2	0	1	3	n/a	n/a	0	2	n/a	n/a
	17	32	11	9	52	18	18	36	12	L	8	8	26	n/a	32	n/a	n/a	1	0	1	2	n/a	n/a	0	1	n/a	n/a
	18	n/a	n/a	n/a	n/a	n/a	n/a	n/a	n/a	n/a	8	8	50	n/a	n/a	n/a	n/a	n/a	n/a	n/a	1	n/a	n/a	0	n/a	n/a	n/a
	19	37	9	7	53	16	19	35	12	SL	8	7	33	n/a	17	n/a	n/a	2	0	0	1	n/a	n/a	0	<1	n/a	n/a
	20	39	8	6	54	17	17	34	12	SL	8	7	27	n/a	19	n/a	n/a	3	0	0	1	n/a	n/a	0	<1	n/a	n/a
	21	40	8	6	54	15	18	33	12	SL	8	7	28	n/a	17	n/a	n/a	3	0	0	1	n/a	n/a	0	<1	n/a	n/a
13	22	31	11	7	48	20	22	42	10	L	8	7	—	n/a	21	n/a	n/a	6	0	2	2	n/a	n/a	0	<1	n/a	n/a
	23	33	10	6	49	15	18	32	19	L	8	7	3	n/a	17	n/a	n/a	5	0	1	1	n/a	n/a	0	<1	n/a	n/a
	24	29	13	7	49	16	15	31	20	L	8	8	9	n/a	19	n/a	n/a	9	0	1	1	n/a	n/a	0	<1	n/a	n/a
	25	29	12	8	49	23	19	43	8	L	9	8	17	n/a	8	n/a	n/a	9	0	0	0	n/a	n/a	0	<1	n/a	n/a
11	26	n/a	n/a	n/a	n/a	n/a	n/a	n/a	n/a	n/a	n/a	n/a	n/a	n/a	n/a	n/a	n/a	n/a	n/a	n/a	n/a	n/a	n/a	n/a	n/a	n/a	n/a
	27	25	12	12	50	24	19	43	7	SL	8	7	2	n/a	22	n/a		3	0	1	2	n/a	n/a	0	<1	n/a	n/a
20	28	20	5	5	30	21	29	49	20	L	7	6	—	n/a	22	n/a	12	6	0	4	2	n/a	n/a	0	4	n/a	n/a
	29	19	4	4	27	21	21	41	32	CL	7	6	—	n/a	18	n/a	11	6	0	2	1	n/a	n/a	0	<1	n/a	n/a
	30	18	4	3	25	17	17	34	42	C	7	6	—	n/a	19	n/a	11	6	0	2	1	n/a	n/a	0	<1	n/a	n/a
21	31	24	2	2	29	15	18	34	38	CL	8	7	—	n/a	44	n/a	35	8	1	1	1	n/a	n/a	0	<1	n/a	n/a
	32	33	2	2	36	10	11	21	43	C	9	7	—	n/a	41	n/a	31	8	1	1	2	n/a	n/a	0	<1	n/a	n/a
	33	23	2	2	27	12	12	24	49	C	9	7	—	n/a	44	n/a	31	9	3	1	1	n/a	n/a	0	<1	n/a	n/a
18	34	25	4	3	31	19	16	35	33	CL	9	7	—	n/a	40	n/a	32	5	1	1	1	n/a	n/a	0	<1	n/a	n/a
	35	30	4	3	36	14	12	27	37	CL	9	7	—	n/a	36	n/a	27	5	3	1	1	n/a	n/a	0	<1	n/a	n/a
	36	23	3	3	29	16	11	27	44	C	9	7	—	n/a	37	n/a	26	5	4	1	1	n/a	n/a	0	<1	n/a	n/a
14	37	43	8	6	58	14	18	32	11	SL	8	6	—	n/a	15	n/a	10	3	0	1	1	n/a	n/a	0	<1	n/a	n/a
	38	51	6	4	61	13	18	31	8	SL	8	7	—	n/a	12	n/a	7	3	0	1	0	n/a	n/a	0	<1	n/a	n/a
17	39	29	19	13	62	19	11	30	9	SL	9	8	11	n/a	12	n/a	n/a	5	2	1	1	n/a	n/a	0	2	n/a	n/a
	40	63	9	3	74	7	8	16	10	SL	9	8	13	n/a	16	n/a	n/a	4	1	0	0	n/a	n/a	0	<1	n/a	n/a
	41	27	8	5	40	14	12	26	33	CL	10	8	12	n/a	21	n/a	n/a	8	8	1	1	n/a	n/a	0	<1	n/a	n/a
22	42	6	7	7	21	28	12	40	39	CL	9	7	3	n/a	42	n/a	n/a	6	1	2	1	n/a	n/a	0	<1	n/a	n/a
	43	3	3	4	10	19	17	35	55	C	9	7	3	n/a	48	n/a	n/a	7	5	2	1	n/a	n/a	0	<1	n/a	n/a
	44	23	3	2	28	14	19	32	39	CL	9	7	25	n/a	31	n/a	n/a	6	4	2	0	n/a	n/a	0	1	n/a	n/a
23	45	24	11	11	46	21	23	44	9	L	8	8	32	n/a	23	n/a	n/a	4	0	2	2	n/a	n/a	0	5	n/a	n/a
	46	n/a	n/a	n/a	n/a	n/a	n/a	n/a	n/a	n/a	n/a	n/a	41	n/a	n/a	n/a	n/a	n/a	n/a	n/a	3	n/a	n/a	0	n/a	n/a	n/a
	47	3	5	7	16	23	33	56	28	SiCL	8	6	—	n/a	36	n/a	20	12	0	4	2	n/a	n/a	0	2	n/a	n/a
	48	3	4	5	12	21	31	52	36	SiCL	8	7	—	n/a	38	n/a	21	12	0	4	1	n/a	n/a	0	<1	n/a	n/a
7	49	1	2	28	31	n/a	n/a	48	21	L	n/a	7	n/a	20	n/a	35	n/a	n/a	n/a	n/a	n/a	14	1	n/a	n/a	6	0
	50	1	2	22	24	n/a	n/a	42	34	CL	n/a	6	n/a	32	n/a	33	n/a	n/a	n/a	n/a	n/a	13	1	n/a	n/a	8	1
	51	1	1	12	15	n/a	n/a	32	53	C	n/a	6	n/a	22	n/a	34	n/a	n/a	n/a	n/a	n/a	12	1	n/a	n/a	9	0
6	52	25	13	30	68	n/a	n/a	21	12	SL	n/a	6	n/a	14	n/a	18	n/a	n/a	n/a	n/a	n/a	21	2	n/a	n/a	9	0
	53	27	8	23	58	n/a	n/a	24	18	SL	n/a	6	n/a	11	n/a	19	n/a	n/a	n/a	n/a	n/a	12	1	n/a	n/a	4	1
12	54	12	7	24	43	n/a	n/a	38	19	L	n/a	7	n/a	141	n/a	33	n/a	n/a	n/a	n/a	n/a	36	4	n/a	n/a	6	1
	55	10	8	22	40	n/a	n/a	37	24	L	n/a	7	n/a	241	n/a	29	n/a	n/a	n/a	n/a	n/a	28	2	n/a	n/a	6	1
9	56	2	2	16	20	n/a	n/a	45	35	CL	n/a	6	n/a	19	n/a	34	n/a	n/a	n/a	n/a	n/a	17	1	n/a	n/a	8	0
	57	3	2	14	18	n/a	n/a	32	50	C	n/a	6	n/a	19	n/a	35	n/a	n/a	n/a	n/a	n/a	15	1	n/a	n/a	7	0
8	58	11	10	34	56	n/a	n/a	31	12	SL	n/a	7	n/a	22	n/a	24	n/a	n/a	n/a	n/a	n/a	18	2	n/a	n/a	4	1
	59	9	10	35	54	n/a	n/a	26	20	SCL	n/a	6	n/a	22	n/a	27	n/a	n/a	n/a	n/a	n/a	14	1	n/a	n/a	14	0
16	60	9	8	19	35	n/a	n/a	27	38	CL	n/a	7	n/a	18	n/a	32	n/a	n/a	n/a	n/a	n/a	13	1	n/a	n/a	5	1
	61	6	7	20	34	n/a	n/a	30	37	CL	n/a	7	n/a	60	n/a	31	n/a	n/a	n/a	n/a	n/a	15	1	n/a	n/a	5	1
15	62	11	17	27	55	n/a	n/a	23	22	SCL	n/a	8	n/a	94	n/a	20	n/a	n/a	n/a	n/a	n/a	13	1	n/a	n/a	4	1
	63	16	15	20	51	n/a	n/a	24	26	SCL	n/a	8	n/a	166	n/a	18	n/a	n/a	n/a	n/a	n/a	10	1	n/a	n/a	4	1
1	64	2	1	13	16	n/a	n/a	24	60	C	n/a	6	n/a	30	n/a	40	n/a	n/a	n/a	n/a	n/a	17	1	n/a	n/a	14	0
	65	1	1	10	12	n/a	n/a	22	65	C	n/a	6	n/a	18	n/a	40	n/a	n/a	n/a	n/a	n/a	14	1	n/a	n/a	11	0
2	66	5	2	7	14	n/a	n/a	23	63	C	n/a	7	n/a	60	n/a	17	n/a	n/a	n/a	n/a	n/a	14	1	n/a	n/a	10	1
	67	5	2	12	18	n/a	n/a	18	64	C	n/a	7	n/a	65	n/a	18	n/a	n/a	n/a	n/a	n/a	13	1	n/a	n/a	12	0
12	68	7	3	13	23	n/a	n/a	36	41	C	n/a	7	n/a	33	n/a	39	n/a	n/a	n/a	n/a	n/a	12	1	n/a	n/a	4	0
	69	5	2	12	19	n/a	n/a	38	43	C	n/a	7	n/a	57	n/a	39	n/a	n/a	n/a	n/a	n/a	11	1	n/a	n/a	4	0

n/a: not available; —: not detectable.

The applied methodological approach seems suitable for multiscale and multisensoral datasets of large areas. The study showed that the topsoil classification can be associated with soil profiles obtained by fieldwork and certain terrain positions derived from DEM, thus allowing a distinct spatial attribution of soil types.

The main objective of Paper III is to propose a simple approach to assess surface infiltration and runoff generation processes under semiarid climate conditions on hillslope scale. The infiltration rates and potential surface runoff at the end of the dry seasons are interesting, as these are the periods of potentially high soil loss. The hypothesis is that soils – especially after the dry seasons – have high water tensions and hence, the isolated rainfall events produce high amounts of surface runoff especially on fine-grained soils. Thus, water conduction is lower than in saturated conditions and consequently the overall infiltration rates are quite low.

RQ3 How can surface runoff be quantified in semiarid savannah type environments?

RD3 Modelling of soil hydrological characteristics using following setup:

- Testing an experimental setup of several SRDs within a slope system
- Using a stochastic gradient boosting modelling approach with soil texture and infiltrabilities as response variables and terrain indices as environmental variables.

The author observed that in the study area, notable surface runoff is produced when the soil is very dry on the moment precipitations starts, especially in homogeneous soils with low activity clays. Infiltration characteristics in particular are highly variable, both spatially and temporally. Here, the Horton overland flow is strongly related to soil properties. The automatic SRDs proved to be a helpful instrument in quantification of overland flow dynamics over time. The example demonstrates the importance of integrated fieldwork measurements and computer-based simulation in pedo-hydrological research.

During fieldwork, eight gully systems close to Makuyuni town were thoroughly measured. The focus of Paper IV is to assess gully erosion dynamics using improved DEMs with resolutions of 30 m and 20 m, respectively. To improve the DEMs, we integrated information deduced from satellite images as well as from acquired GPS field data. We assessed terrain characteristics to extract information on environmental drivers. To evaluate gully evolution we assessed also the measured longitudinal slope profiles. Finally, the gully evolution phases of each gully were classified according to the concept proposed by Kosov et al. (1978).

RQ4 Are the local gullies in stable or in dynamic conditions? How can these analyses contribute to a better understanding of landscape developments?

RD4 Modelling gully erosion and evolution:

- Field measurements and GPS tracking of the gully drainage networks and profiles.
- Pre-processing and interpolation of different DEM sources.
- Analysis of linear erosion processes.
- Analysis of gully morphometric characteristics.
- Classifying of dynamic and static gullies.
- Assessment of gully development phases and their implications for the landscape development.

Best results for the interpolation of the DEMs were obtained by applying the hydrological forcing option of the ANUDEM algorithm 'Topo to Raster'. This algorithm guarantees a hydrological correct DEM without sinks. The derived DEMs show a good performance in terms of the hydrological and geomorphic process dynamics, which were assessed by terrain analysis.The calculation of topographic indices showed that specific gully features such as head cuts, catchment areas and erosion/deposition zones can be assessed.

The investigated gully systems seem to be very old and belonging to the static gully phase (according to Kosov et al. 1978). Additionally, areas identified as having a greater risk of gully erosion have been confirmed by observations and survey carried out in the field.

The aim of Manuscript V is to understand the morphology and morphogenesis of the landforms in the proximity of Makuyuni town in Northern Tanzania. Particular attention was given to the identification and mapping of gully erosion forms and features. For the geomorphic assessment, we combine information on morphology and morphogenesis with secondary information on sampling and laboratory data. We use GIS for the mapping procedure. The data are stored in a geomorphic database.

The main objective and its result as the thesis' synthesis (see below):

MO Understanding geomorphic processes, their spatial extent and location.

Syn Geomorphic data collection and interpretation:

- Extensive field mapping of landforms and related processes, genesis and ages
- Spatial extent and location of geomorphic forms and features.
- A synthesis of landscape processes, forms and features is provided below.

The geomorphic map product, due to its detail, provides a reliable base document, which yield valuable information on features of interests for geomorphologists and related disciplines, e.g. soil scientists, geologists. In particular, the map supports the planning of detailed fieldwork. In semiarid regions, where irrigation farming is necessary, a knowledge of land and drainage conditions contributes to water conservation and land use planning processes, especially in agricultural areas. Field mapping and ground truthing must remain an important part to calibrate and validate remote sensing and GIS techniques.

5 Synthesis

The highly complex landscapes and its processes, forms and features of the undulating plains of the half graben in the East African Rift valley in Northern Tanzania are explained here; according to the geomorphic map compiled for Manuscript V.

On the very southern part of the Makuyuni River, one can detect the (proposed) former flow of the river in a southern direction (entering the Tarangire River). Nowadays, there is a major bend (close to 160°) and the river follows the tectonic fault in a northwestern direction. The river flows in a rather narrow bed in the southern part of the mapping extent, then while eroding a broader riverbed, there are broad alluvial deposits and the river is actively meandering within the alluvial material. The tectonic fault lines, forming a "V" within the mapping extent, and according lithologies dominate the landscape. Following Schwartz et al. (2012), surface materials are distinguished in

- Lithologies: volcanic deposits (nephelinite, volcanic agglomerate/conglomerate; basalt dyke) and basement (Proterozoic quartzite and gneiss).
- Consolidated surface formations: terrestrial deposits (Upper Manyara beds) and lacustrine deposits (Lower Manyara Beds).
- Unconsolidated surface formations : recent alluvial/colluvial deposits.

On Makuyuni Rivers' western banks, the ridge formed by quartzite and basalt material has only allowed some erosion and is separating the erosional front line with a distinct scarp edge of often more than 5 m in height. The following fluvial and slope landforms formed due to surface runoff:

- Gully thalwegs,
- Gully head cut areas,
- Areas affected by rill erosion,
- Scarp edges.

On its eastern banks, there are major gully formation up to ephemeral stream confluences. A dominant gully was eroding a rather big area and exposing lacustrine deposits and quartzic materials. On the southeastern part of Makuyuni town, another major gully

is still cutting deep into Holocene soil formations, but was clearing and exposing lacustrine material only in the confluencing part. Within those major gully systems, archaeological and palaeontological artefacts and fossils are outcropping. This is also the area, where the hominin-bearing site MK4 is located.

The Makuyuni River shows three different kind of channel types (compare Figure 12, p.41):

- Type A can be identified as a relatively new channel incision into the well-developed floodplain. The river bed is characterized by pools and point bars, sorted sands and cobbles that are deposited especially after intense rainfalls in the upper catchment.
- Type B developed its bed running through sedimentary rocks of the Lower Manyara Bed section. The steeper gradient is expressed by step/pool formation along its course and a narrow river channel.
- Type C is dominant where the Manyara River is running over cemented tephra outcrops. This rather horizontal layer is relatively strong compared to the surrounding lithology and therefore its incision is very slow. The channel is showing an anastomosing stream system bedded into the lower substrates within former alluvial river terraces. On the sidewalls of the terraces, recent material is accumulated on the toes of the terrace.

Actively, erosion processes dominate the areas left and right of the Makuyuni River. Here, gullies are cutting through alluvial deposits of the Makuyuni River terraces and, more upslope, event through the soft tuff layers of the Upper Manyara beds. In between Upper and Lower Manyara beds – in stable positions –fossils and artefacts are outcropping.

One flat parts within the mapping extent, there are mostly lacustrine members of the Lower Manyara Beds where erosion features have cleared the top material. Vertisols are in the northern and eastern part of the mapping extent flat areas prevalent. On top of the Upper Manyara beds, especially on sloping areas, Cambisols as well as Andosols and Leptosols have been formed. On the volcanic tuff deposits in plain areas, reddish soils (mainly Cambisols) have been developed.

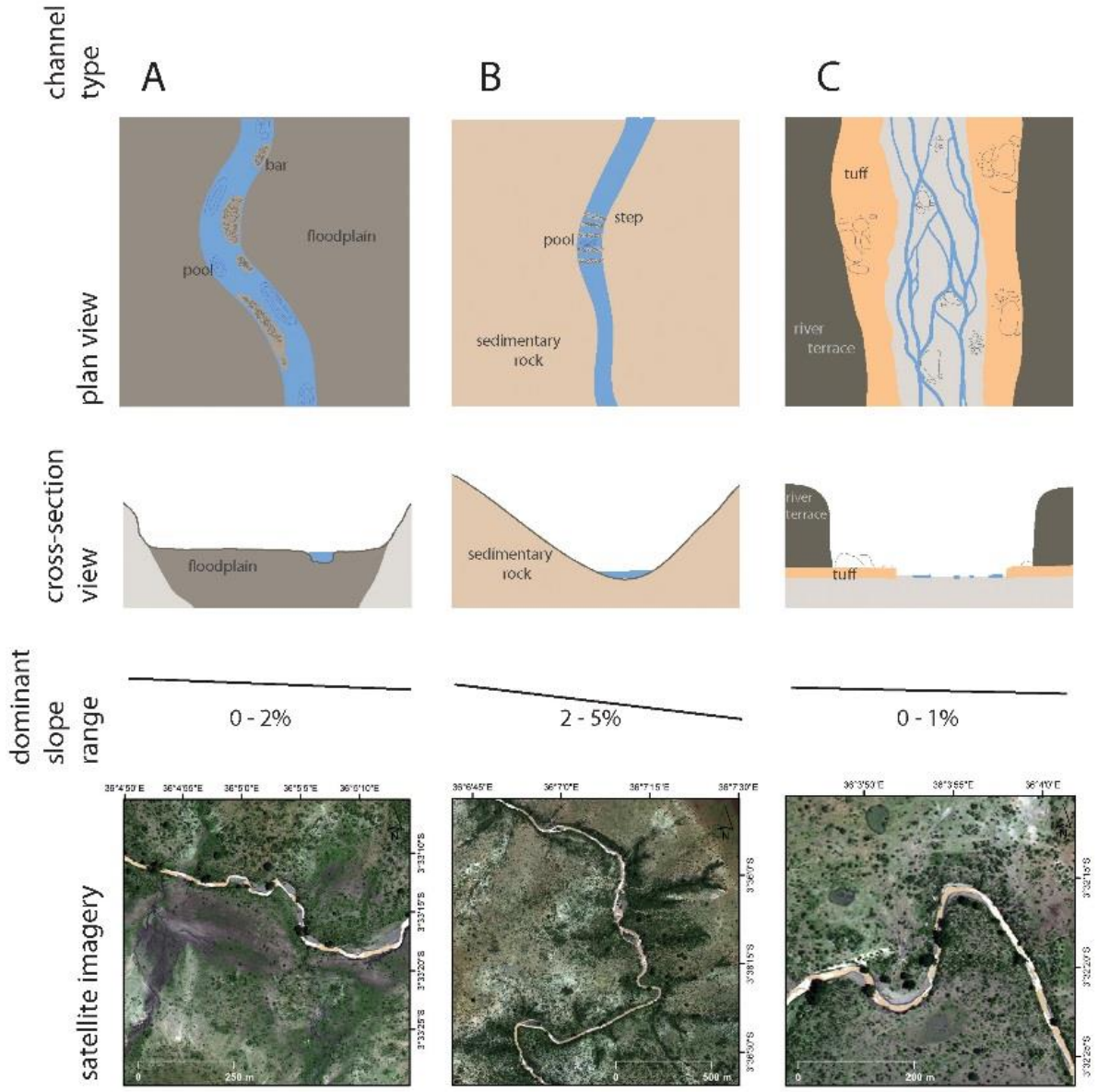

Figure 12. Makuyuni River channel types. **Type A** is a relatively new channel incision into the well-developed floodplain. **Type B** developed its bed running through sedimentary rocks and follows a narrow river channel of the Lower Manyara Bed section. **Type C** is running over tephra outcrops as anastomosing stream. Satellite imagery: WorldView-2 scene from 2011-02-21.

The geomorphological synthesis yield valuable information to identify areas that are recently exposed for archaeologists and palaeontologists and for the recognition of features of interests for physical geographers and related disciplines, e.g. soil scientists, geologists.

6 Conclusion

This dissertation work shows an integrated approach of scale, methods, devices, models and input/measured data, and therefore, an in-depth analysis of geomorphological research. The author was able to tackle specific questions with the proposed methods and input information (weather measured in the field, in the laboratory or obtained digitally from various sources). This contributes to the knowledge of present geomorphic processes and features and the landscape evolution around Makuyuni town in Northern Tanzania.

In summary, drainage network, stream longitudinal profiles, basin analysis and lineament extraction can be used as tools for identifying tectonic activity and related features in rift areas. This morphotectonic interpretations may be applicable to similar areas in the African rift, where landscapes are governed by extensional, tectonic, volcanic and erosional processes.

Combining surface characteristics and terrain features, a spatial distribution of topsoils and related soil types was achieved. Topsoils have a complex genetic origin related to different substrates, resulting in a high spatial heterogeneity. The applied methodological approach seems suitable for multiscale and multisensoral datasets of larger areas. The topsoil classification is associated with soil profiles obtained by fieldwork and certain terrain positions derived from DEM, thus allowing a distinct spatial attribution of soil types.

The example from a hillslope scale water balance model demonstrates the importance of integrated fieldwork measurements (especially the incorporation of surface runoff detectors) and computer-based simulations in hydrological research. The automatic surface runoff detectors offer a helpful insight into actual overland flow dynamics and, especially, for the quantification of those. This approach is providing useful additional information on water balance modelling and are recommended for usage especially in semiarid conditions.

Gully assessment can be derived with a certain combination of terrain indices from digital elevation models. To a certain degree, even specific gully features such as head cuts, catchment areas and erosion/deposition zones can be assessed. Additional topographic

information to improve the DEMs are collected by fieldwork (GPS points and gully cross sections) and the mapping of thalwegs on optical imagery.

The results of the geomorphological surveys carried out in the Lake Manyara basin from 2012 to 2014 led to a composed geomorphological map. Underlying data layers from various satellite data sources proved to be very helpful and should be considered to be included in any mapping work.

The above mentioned methods and analyses may be applicable to similar areas in the African rift, where landscapes are governed by extensional, tectonic, volcanic and erosional processes. At the same time, new questions have emerged, which shall be solved in future research. E.g. the quantification of soil erosion is of importance, regarding future soil loss and badland development in this water-scare area.

In general, the understanding of highly complex landscapes – such as in Northern Tanzania – their relevant forms and features as well as the related processes is sophisticated and time-consuming work. Field mapping and ground truthing must remain an important part to calibrate and validate remote sensing and GIS techniques. The geomorphic interpretation, especially the map product, provides, due to its detail, a reliable base document, which yield valuable information to e.g. identify areas that are recently exposed for archaeologists and palaeontologists or for the recognition of features of interests for physical geographers and related disciplines, e.g. soil scientists, geologists.

References

AG Boden (2005): Bodenkundliche Kartieranleitung. 5th. Hannover. [in German]

Anderson, K. & Croft, H. (2009): Remote sensing of soil surface properties. *Progress in Physical Geography* 33(4), 457–473.

Bachofer, F. (2015): Assessment of Paleo-Landscape Features using Advanced Remote Sensing Techniques, Modelling and GIS Methods in the Lake Manyara Basin, Northern Tanzania. Dissertation, Universität Tübingen.

Bachofer, F.; Quénéhervé, G.; Hochschild, V.; Maerker, M. (2015a): Multisensoral Topsoil Mapping in the Semiarid Lake Manyara Region, Northern Tanzania. *Remote Sensing* 7(8), 9563–9586.

Bachofer, F.; Quénéhervé, G.; Märker, M. (2014): The Delineation of Paleo-Shorelines in the Lake Manyara Basin Using TerraSAR-X Data. *Remote Sensing* 6(3), 2195–2212.

Bachofer, F.; Quénéhervé, G.; Märker, M.; Hochschild, V. (2015b): Comparison of SVM and Boosted Regression Trees for the Delineation of Lacustrine Sediments using Multispectral ASTER Data and Topographic Indices in the Lake Manyara Basin. *Photogrammetrie, Fernerkundung, Geoinformation* 1, 81–94.

Bachofer, F.; Quénéhervé, G.; Zwiener, T.; Maerker, M.; Hochschild, V. (2016): Comparative analysis of Edge Detection techniques for SAR images. *European Journal of Remote Sensing* 49(1), 205–224.

Bagdasaryan, G. P.; Gerasimovski, V. I.; Palyakov, A. I.; Gukasyan, R. K. (1973): Age of volcanic rocks in the rift zones of East Africa. *Geochemistry International* 10, 66–71.

Bailey, G. N.; Reynolds, S. C.; King, G. C. P. (2011): Landscapes of human evolution: models and methods of tectonic geomorphology and the reconstruction of hominin landscapes. *Journal of Human Evolution* 60(3), 257–280.

Baker, B. H.; Mohr, P. A.; Williams, L. A. J. (1972): Geology of the eastern rift system of Africa. Geological Society of America, Special paper 136.

Barker, P. A. (1990): Diatoms as paleolimnological indicators: a reconstruction of Late Quaternary environments in two East African salt lakes. Doctoral thesis. Loughborough University of Technology.

Baumann, O. (1894): Durch Massailand zur Nilquelle. Reisen und Forschungen der Massai-Expedition des deutschen Antisklaverei-Komitee in den Jahren 1891 - 1893. Berlin: Reimer. [in German]

Bergner, A. G. N.; Strecker, M. R.; Trauth, M. H.; Deino, A. L.; Gasse, F.; Blisniuk, P.; Dühnforth, M. (2009): Tectonic and climatic control on evolution of rift lakes in the Central Kenya Rift, East Africa. *Quaternary Science Reviews* 28(25-26), 2804–2816.

Berking, J.; Meister, J.; Burkart, U.; Schott, M.; Kaufmann, G.; Schütt, B. (2011): Geoarchaeological Methods for Landscape Reconstruction at the Excavation Site of Naga, Central Sudan. *Die Erde* 142(3), 289–313.

Beven, K. J. & Kirkby, M. J. (1979): A physically based, variable contributing area model of basin hydrology. *Bulletin of the International Association of Scientific Hydrology* 24(1), 43–69.

Bird, P. (2003): An updated digital model of plate boundaries. *Geochemistry, Geophysics, Geosystems* 4(3), 1027.

Bishop, M. P.; Shroder, J. F. (Eds.) (2004): Geographic Information Science and Mountain Geomorphology. Berlin: Springer.

Bishop, P. (2007): Long-term landscape evolution. Linking tectonics and surface processes. *Earth Surf. Proc. Landforms* 32(3), 329–365.

Blaszczynski, J. S. (1997): Landform Characterization with Geographic Information Systems. *Photogramm. Eng. Remote Sens* 63(2), 183–191.

Bracken, L. J. & Croke, J. (2007): The concept of hydrological connectivity and its contribution to understanding runoff-dominated geomorphic systems. *Hydrol. Process.* 21(13), 1749–1763.

Broll, G.; Brauckmann, H.-J.; Overesch, M.; Junge, B.; Erber, C.; Milbert, G. et al. (2006): Topsoil characterization—recommendations for revision and expansion of the FAO-Draft (1998) with emphasis on humus forms and biological features. *Z. Pflanzenernähr. Bodenk.* 169(3), 453–461.

Bull, L. J. & Kirkby, M. J. (1997): Gully processes and modelling. *Progress in Physical Geography* 21(3), 354–374.

Burbank, D. W. & Anderson, R. S. (2001): Tectonic geomorphology. Malden, Mass.: Blackwell Science.

Chang, S.-J. & Van der Lee, S. (2011): Mantle plumes and associated flow beneath Arabia and East Africa. *Earth and Planetary Science Letters* 302(3–4), 448–454.

Chesley, J. T.; Rudnick, R. L.; Lee, C.-T. (1999): Re-Os systematics of mantle xenoliths from the East African Rift: age, structure, and history of the Tanzanian craton. *Geochimica et Cosmochimica Acta* 63(7–8), 1203–1217.

Chorowicz, J. (2005): The East African rift system. Phanerozoic Evolution of Africa. *Journal of African Earth Sciences* 43(1-3), 379–410.

Cohen, A. S.; Talbot, M. R.; Awramik, S. M.; Dettman, D. L.; Abell, P. (1997): Lake level and paleoenvironmental history of Lake Tanganyika, Africa, as inferred from late Holocene and modern stromatolites. *Geological Society of America Bulletin* 109(4), 444–460.

Conacher, A. J. & Dalrymple, J. B. (1977): The nine-unit landsurface model: an approach to pedogeomorphic research. *Geoderma* 18(1-2), 1–154.

Conoscenti, C.; Agnesi, V.; Angileri, S.; Cappadonia, C.; Rotigliano, E.; Märker, M. (2013): A GIS-based approach for gully erosion susceptibility modelling: a test in Sicily, Italy. *Environ Earth Sci* 70(3), 1–17.

Costanzo, D.; Cappadonia, C.; Conoscenti, C.; Rotigliano, E. (2012): Exporting a Google Earth™ aided earth-flow susceptibility model: a test in central Sicily. *Nat Hazards* 61(1), 103–114.

Dawson, J. B. (1992): Neogene tectonics and volcanicity in the North Tanzania sector of the Gregory Rift Valley: contrasts with the Kenya sector. *Tectonophysics* 204(1–2), 81–92.

Dawson, J. B. (2008): The Gregory Rift Valley and neogene-recent-volcanoes of Northern Tanzania. London: Geological Society Memoir, 33.

Demek, J.; Kirchner, K.; Mackovčin, P.; Slavík, P. (2011): Geomorphodiversity derived by a GIS-based geomorphological map: case study the Czech Republic. *Z. Geomorph.* 55(4), 415–435.

deMenocal, P. B. (1995): Plio-Pleistocene African Climate. *Science* 270(5233), 53–59.

deMenocal, P. B. (2004): African climate change and faunal evolution during the Pliocene-Pleistocene. *Earth Planet. Sci. Lett.* 220(1-2), 3–24.

Deus, D.; Gloaguen, R.; Krause, P. (2013): Water Balance Modeling in a Semi-Arid Environment with Limited in situ Data Using Remote Sensing in Lake Manyara, East African Rift, Tanzania. *Remote Sensing* 5(4), 1651–1680.

Deutsch, C. V. & Journel, A. G. (1998): Geostatistical Software Library and user's guide. Applied geostatics series. Oxford University Press.

Doornkamp, J. C. (1971): Geomorphological Mapping. In Ominde, S. H. (Ed.): Studies in East African Geography and Development. Berkeley: Heinemann, 9–28.

Ebinger, C. J.; Djomani, Y. P.; Mbede, E.; Foster, A.; Dawson, J. B. (1997): Rifting Archaean lithosphere: the Eyasi-Manyara-Natron rifts, East Africa. *Journal of the Geological Society* 154(6), 947–960.

Ebinger, C. J.; Yemane, T.; Harding, D. J.; Tesfaye, S.; Kelley, S.; Rex, D. C. (2000): Rift deflection, migration, and propagation: Linkage of the Ethiopian and Eastern rifts, Africa. *Geological Society of America Bulletin* 112(2), 163–176.

Elith, J.; Graham, C. H.; Anderson, R. P.; Dudík, M.; Ferrier, S.; Guisan, A. et al. (2006): Novel methods improve prediction of species' distributions from occurrence data. *Ecography* 29(2), 129–151.

FAO (1998): Topsoil Characterization for Sustainable Land Management. Land and Water Development Division, Soil Resoures, Management and Conservation Service.

FAO (2014): World reference base for soil resources. International soil classification system for naming soils and creating legends for soil maps. World Soil Resources Report, 106.

Finkl, C. W.; Becerra, J. E.; Achatz, V.; Andrews, J. L. (2008): Geomorphological Mapping along the Upper Southeast Florida Atlantic Continental Platform; I: Mapping Units, Symbolization and Geographic Information System Presentation of Interpreted Seafloor Topography. *Journal of Coastal Research* 246, 1388–1417.

Foster, A.; Ebinger, C. J.; Mbede, E.; Rex, D. C. (1997): Tectonic development of the northern Tanzanian sector of the East African Rift System. *Journal of the Geological Society* 154(4), 689–700.

Frankl, A.; Zwertvaegher, A.; Poesen, J.; Nyssen, J. (2013): Transferring Google Earth observations to GIS-software: example from gully erosion study. *International Journal of Digital Earth* 6(2), 196–201.

Friedman, J. H. (2002): Stochastic gradient boosting. Nonlinear Methods and Data Mining. *Computational Statistics & Data Analysis* 38(4), 367–378.

Frost, S. R.; Harvati, K.; Saanane, C.; Giemsch, L.; Schrenk, F.; Morgan, L. E. et al. (2010): Preliminary report of new research in the Lake Manyara Beds, Arusha Region, Tanzania. *Journal of Physical Anthropology* S50, 108.

Frost, S. R.; Schwartz, H. L.; Giemsch, L.; Morgan, L. E.; Renne, P. R.; Wildgoose, M. M. et al. (2012): Refined age estimates and Paleoanthropological investigations of the Manyara Beds, Tanzania. *JASs* 90, 151–169.

García-Ruiz, J. M. (2015): Why geomorphology is a global science. *Cuadernos de Investigación Geográfica* 41(1), p. 87.

García-Ruiz, J. M.; Beguería, S.; Nadal-Romero, E.; González-Hidalgo, J. C.; Lana-Renault, N.; Sanjuán, Y. (2015): A meta-analysis of soil erosion rates across the world. *Geomorphology* 239, 160–173.

Garcin, Y.; Junginger, A.; Melnick, D.; Olago, D. O.; Strecker, M. R.; Trauth, M. H. (2009): Late Pleistocene-Holocene rise and collapse of Lake Suguta, northern Kenya Rift. *Quaternary Science Reviews* 28(9-10), 911–925.

Gasse, F. (2000): Hydrological changes in the African tropics since the Last Glacial Maximum. *Quaternary Science Reviews* 19(1-5), 189–211.

Gasse, F. (2006): Climate and hydrological changes in tropical Africa during the past million years. *Comptes Rendus Palevol* 5(1-2), 35–43.

Geiger, R. (1961): Überarbeitete Neuausgabe von Geiger, R.: Köppen-Geiger / Klima der Erde. (Wandkarte 1:16 Mill.). Klett-Perthes, Gotha. [in German]

Giemsch, L. (2015): Makuyuni. Fundstellen des Acheuléen am Lake Manyara, Tansania. Ein Beitrag zur Erforschung der mittelpleistozänen Kultur in Ostafrika. Tübinger Arbeiten zur Urgeschichte, 7. [in German]

Giemsch, L.; Hertler, C.; Märker, M.; Quénéhervé, G.; Saanane, C.; Schrenk, F. (2018): Acheulean Chronology and Technology at Makuyuni (Lake Manyara, Tanzania). Results of archaeological fieldwork and classification of the lithic assemblages. *African Archaeological Review* 2(3), 12–15.

Golts, S. & Rosenthal, E. (1993): A morphotectonic map of the northern Arava in Israel, derived from isobase lines. *Geomorphology* 7(4), 305–315.

Grohmann, C. H.; Riccomini, C.; Chamani, M. A. C. (2011): Regional scale analysis of landform configuration with base-level (isobase) maps. *Hydrol. Earth Syst. Sci.* 15(5), 1493–1504.

Grove, A. T. (1986): Geomorphology of the African Rift System. In Frostick, L. E.; Renaut, R. W.; Reid, I.; Tiercelin, J.-J. (Eds.): Sedimentation in the African Rifts. Geological Society Special Publications 25. Blackwell Scientific Publications, 9–16.

Gruber, S. & Peckham, S. D. (2009): Land-surface Parameters and Objects in Hydrology. In Hengl, T. & Reuter, H. I. (Eds.): Geomorphometry. Concepts, Software, Applications. Developments in Soil Science, 33, 171–194.

Gustavsson, M.; Kolstrup, E.; Seijmonsbergen, A. C. (2006): A new symbol-and-GIS based detailed geomorphological mapping system. *Geomorphology* 77 (1–2), 90–111.

Haidle, M. N.; Bolus, M.; Bruch, A. A.; Hertler, C.; Kandel, A. W.; Märker, M. et al. (2010): The role of culture in early expansions of humans - A new research center. *Quaternary International* 223-224, 429–430.

Hancock, G. R. & Evans, K. G. (2010): Gully, channel and hillslope erosion - An assessment for a traditionally managed catchment. *Earth Surf. Proc. Landforms* 35(12), 1468–1479.

Hillaire-Marcel, C.; Carro, O.; Casanova, J. (1986): 14C and Th/U dating of Pleistocene and Holocene stromatolites from East African paleolakes. *Quaternary Research* 25(3), 312–329.

Holdship, S. A. (1976): The palaeolimnology of Lake Manyara, Tanzania. A diatom analysis of a 56 meter sediment core. Dissertation. Duke University North Carolina, Duluth, USA.

Howard, A. D. (1994): A detachment-limited model of drainage basin evolution. *Water Resour. Res.* 30(7), 2261–2285.

Hutchinson, M. F. (1989): A new procedure for gridding elevation and stream line data with automatic removal of spurious pits. *J. Hydrol.* 106(3–4), 211–232.

Jäger, F. (1911): Das Hochland der Riesenkrater und die umliegenden Hochländer Deutsch-Ostafrikas. Ergebnisse einer amtlichen Forschungsreise ins abflußlose Gebiet des nördlichen Deutsch-Ostafrika 1906/1907. Teil I. Ergänzungshefte der Mitteilungen aus den deutschen Schutzgebieten, 4. [in German]

Jasiewicz, J. & Stepinski, T. F. (2013): Geomorphons — a pattern recognition approach to classification and mapping of landforms. *Geomorphology* 182, 147–156.

Jenness, J. (2006): Topographic Position Index (tpi jen.avx) extension for ArcView 3.x, v. 1.3a. Jenness Enterprises, Technical Report.

Jensen, M. E.; Burman, R. D.; Allen, R. G. (1990): Evapotranspiration and irrigation water requirements. A manual. ASCE manuals and reports on engineering practice, No. 70.

Journel, A. G. (1993): Geostatistics. Roadblocks and Challenges. In Soares, A. (Ed.): Geostatistics Tróia '92. Quantitative Geology and Geostatistics 5, 213–224.

Kaiser, T. M. (1997): Die Taphonomie plio-pleistozäner Hominidenfundstellen Ostafrikas mit besonderer Berücksichtigung der Säugetierfaunen des Laetoli- und Lake-Manyara-Gebietes in Nordtansania. Dissertation. Hochschule Darmstadt. [in German]

Kaiser, T. M.; Bromage, T. G.; Schrenk, F. (1995): Hominid Corridor Research Project update: New Pliocene fossil localities at Lake Manyara and putative oldest Early Stone Age occurrences at Laetoli (Upper Ndolanya Beds), northern Tanzania. *Journal of Human Evolution* 28(1), 117–120.

Kaiser, T. M.; Fiedler, L.; Schrenk, F.; Schwartz, H. L.; Bromage, T. G.; Seiffert, C. et al. (2005): Makuyuni, eine neue altpaläolithische Hominidenfundstelle in Tansania. *Jahrb. RGZM* 52, 1–41. [in German]

Kaiser, T. M.; Seiffert, C.; Hertler, C.; Fiedler, L.; Schwartz, H. L.; Frost, S. R. et al. (2010): Makuyuni, a new Lower Palaeolithic Hominid Site in Tanzania. *Mitt. hamb. zool. Mus. Inst.* 106, 69–110.

Keller, C. M.; Hansen, C.; Alexander, C. S. (1975): Archaeology and Paleoenvironments in the Manyara and Engaruka Basins, Northern Tanzania. *Geographical Review* 65(3), 364–376.

Kent, P. E. (1942): A Note on Pleistocene Deposits near Lake Manyara, Tanganyika. *Geological Magazine* 79, 72–77.

Kirby, E. & Whipple, K. (2001): Quantifying differential rock-uplift rates via stream profile analysis. *Geology* 29(5), 415–418.

Klimaszeski, M. (1990): Thirty years of detailed geomorphological mapping. *Geographia Polonica* 58, 11–18.

Knight, J.; Mitchell, W. A.; Rose, J. (2011): Geomorphological Field Mapping. In Smith, M. J.; Paron, P.; Griffiths, J. S. (Eds.): Geomorphological mapping. Methods and applications, 151–188.

Knighton, D. (1998): Fluvial Forms and Processes: a New Perspective. London, New York: Routledge.

Kohl-Larsen, L. (1943): Auf den Spuren des Vormenschen. Stuttgart: Strecker und Schröder. [in German]

Kosov, B. F.; Nikol'skaya, I. I.; Zorina, Y. F. (1978): Eksperimental'nyye issledovaniya ovragoobrazovaniya. In Makkaveev, N. I. (Ed.**)**: Eksperimental'naya Geomorfologiya 3, 113–140. [in Russian]

Langlands, B. W. (1964): East African Landscapes and the study of Physical Geograpy. *E. Afr. Geogr. Rev.* 2, 1–16.

Lauenroth, W. K. & Bradford, J. B. (2006): Ecohydrology and the Partitioning AET Between Transpiration and Evaporation in a Semiarid Steppe. *Ecosystems* 9(5), 756–767.

Le Gall, B.; Nonnotte, P.; Rolet, J.; Benoit, M.; Guillou, H.; Mousseau-Nonnotte, M. et al. (2008): Rift propagation at craton margin: Distribution of faulting and volcanism in the North Tanzanian Divergence (East Africa) during Neogene times. *Tectonophysics* 448(1–4), 1–19.

Leakey, L. S. B. & Reck, H. (1951): Olduvai Gorge: a report in the evolution of the hand-axe culture in beds I-IV. Cambridge University Press.

Leakey, M. D. (1979): Olduvai Gorge: my search for early man. London: Collins.

Leakey, M. D. (Ed.) (1987): Laetoli: a pliocene site in Northern Tanzania. Oxford: Clarendon Press.

Leakey, R. E. F. (1973): Evidence for an Advanced Plio-Pleistocene Hominid from East Rudolf, Kenya. *Nature* 242(5398), 447–450.

Loth, P. E. & Prins, H. H. T. (1986): Spatial patterns of the landscape and vegetation of Lake Manyara National Park. *ITC Journal* 2, 115–130.

Mana, S.; Mollel, G. F.; Feigenson, M.; Carr, M. J.; Turrin, B. D.; Furman, T.; Swisher, C. C. (2009): Geochemistry and age of the Essimingor volcano, northern Tanzania (East Africa). *AGU Fall Meeting Abstracts*, p. 2075.

Manya, S.; Kobayashi, K.; Maboko, M. A. H.; Nakamura, E. (2006): Ion microprobe zircon U–Pb dating of the late Archaean metavolcanics and associated granites of the Musoma-Mara Greenstone Belt, Northeast Tanzania: Implications for the geological evolution of the Tanzania Craton. *Journal of African Earth Sciences* 45(3), 355–366.

Märker, M.; Bachofer, F.; Quénéhervé, G.; Hertler, C.; Sanaane, C.; Giemsch, L.; Thiemeyer, H. (2013): Modelling the spatial distribution of Paleontological sites in the Makuyuni region, Tanzania. In Contreras, F.; Farjas, M.; Melero, F. J. (Eds.): Proceedings of the 38th Annual Conference on Computer Applications and Quantitative Methods in Archaeology, Granada, Spain, April 2010. 2494 volumes. Oxford: BAR International Series, 147–150.

McBratney, A. B.; Mendonça-Santos, M. L. de; **Minasny, B. (2003)**: On digital soil mapping. *Geoderma* 117(1–2), 3–52.

Meyer, H. (Ed.) (1909): Das deutsche Kolonialreich. Band 1. Ostafrika und Kamerun. Leipzig, Wien: Verl. d. Bibliogr. Inst. [in German]

Minasny, B.; McBratney, A. B.; Salvador-Blanes, S. (2008): Quantitative models for pedogenesis — A review. *Geoderma* 144(1-2), 140–157.

Minasny, B. & McBratney, A.B. (1999): A rudimentary mechanistic model for soil production and landscape development. *Geoderma* 90(1-2), 3–21.

Mollel, G. F. (2007): Petrochemistry and Geochronology of Ngorongoro Volcanic Highland Complex (NVHC) and its Relationship to Laetoli and Olduvai Gorge, Tanzania. Rutgers University, New Brunswick, New Jersey.

Mollel, G. F. & Swisher III, Carl C. (2012): The Ngorongoro Volcanic Highland and its relationships to volcanic deposits at Olduvai Gorge and East African Rift volcanism. *Five Decades after Zinjanthropus and Homo habilis: Landscape Paleoanthropology of Plio-Pleistocene Olduvai Gorge, Tanzania* 63(2), 274–283.

Mollel, G. F.; Swisher III, Carl C.; Feigenson, M. D.; Carr, M. J. (2008): Geochemical evolution of Ngorongoro Caldera, Northern Tanzania: Implications for crust–magma interaction. *Earth and Planetary Science Letters* 271(1–4), 337–347.

Moore, I. D.; Grayson, R. B.; Ladson, A. R. (1991): Digital terrain modelling. A review of hydrological, geomorphological, and biological applications. *Hydrol. Process.* 5(1), 3–30.

Morgan, W. T. W. (1972): East Africa. Its peoples and resources. 2d ed. Nairobi, New York: Oxford University Press.

Mulder, V. L.; Bruin, S. de; **Schaepman, M. E.; Mayr, T. R. (2011)**: The use of remote sensing in soil and terrain mapping — A review. *Geoderma* 162(1–2), 1–19.

Munsell Color (2010): Munsell soil color charts with genuine Munsell color chips. Grand Rapids, MI.

Nyblade, A. A. & Brazier, R. A. (2002): Precambrian lithospheric controls on the development of the East African rift system. *Geology* 30(8), 755–758.

Olaya, V. & Conrad, C. (2009): Geomorphometry in SAGA. In Hengl, T. & Reuter, H. I. (Eds.): Geomorphometry. Concepts, Software, Applications. Developments in Soil Science, 33, 293–308.

Pérez-Peña, J. V.; Azañón, J. M.; Azor, A.; Tuccimei, P.; Della Seta, M.; Soligo, M. (2009): Quaternary landscape evolution and erosion rates for an intramontane Neogene basin (Guadix-Baza basin, SE Spain). *Geomorphology* 106(3-4), 206–218.

Poesen, J.; Vandekerckhove, L.; Nachtergaele, J.; Oostwoud Wijdenes, D.; Verstraeten, G.; van Wesemael, B. (2002): Gully erosion in dryland environments. In Bull, L. J. (Ed.): Dryland rivers. Hydrology and geomorphology of Semi-arid channels. Chichester: Wiley, 229–262.

Rădoane, M.; Cristea, I.; Rădoane, N. (2011): Geomorphological Mapping. Evolution and Trends. *Revista de geomorfologie* 13, 19–39.

Rahnama, M. & Gloaguen, R. (2014): TecLines: A MATLAB-Based Toolbox for Tectonic Lineament Analysis from Satellite Images and DEMs, Part 2: Line Segments Linking and Merging. *Remote Sensing* 6(11), 11468–11493.

Reck, H. (1933): Oldoway, die Schlucht des Urmenschen: die Entdeckung des altsteinzeitlichen Menschen in Deutsch-Ostafrika. Leipzig: Brockhaus. [in German]

Ring, U. (2014): The East African Rift System. *Austrian Journal of Earth Sciences* 107(1), 132–146.

Ring, U.; Schwartz, H. L.; Bromage, T. G.; Sanaane, C. (2005): Kinematic and sedimentological evolution of the Manyara Rift in northern Tanzania, East Africa. *Geological Magazine* 142(4), 355–368.

Sanchez, P. A.; Ahamed, S.; Carré, F.; Hartemink, A. E.; Hempel, J.; Huising, J. et al. (2009): Digital Soil Map of the World. *Science* 325(5941), 680–681.

Scheidegger, A. E. (2004): Morphotectonics. Berlin, Heidelberg: Springer.

Schlüter, T. (2008): Geological Atlas of Africa. With Notes on Stratigraphy, Tectonics, Economic Geology, Geohazards, Geosites and Geoscientific Education of Each Country. Berlin, Heidelberg: Springer.

Schoorl, J. M.; Sonneveld, M. P. W.; Veldkamp, A. (2000): Three-dimensional landscape process modelling: the effect of DEM resolution. *Earth Surf. Proc. Landforms* 25(9), 1025–1034.

Schwartz, H. L.; Renne, P. R.; Morgan, L. E.; Wildgoose, M. M.; Lippert, P. C.; Frost, S. R. et al. (2012): Geochronology of the Manyara Beds, northern Tanzania: New tephrostratigraphy, magnetostratigraphy and 40Ar/39Ar ages. *Quaternary Geochronology* 7, 48–66.

Schwärzel, K. & Punzel, J. (2007): Hood Infiltrometer A New Type of Tension Infiltrometer. *Soil Sci. Soc. Am. J.* 71(5), 1438–1447.

Shahzad, F. & Gloaguen, R. (2011a): TecDEM: A MATLAB based toolbox for tectonic geomorphology, Part 1: Drainage network preprocessing and stream profile analysis. *Computers & Geosciences* 37(2), 250–260.

Shahzad, F. & Gloaguen, R. (2011b): TecDEM: A MATLAB based toolbox for tectonic geomorphology, Part 2: Surface dynamics and basin analysis. *Computers & Geosciences* 37(2), 261–271.

Sidorchuk, A. (1999): Dynamic and static models of gully erosion. *CATENA* 37(3–4), 401–414.

Sidorchuk, A.; Märker, M.; Moretti, S.; Rodolfi, G. (2003): Gully erosion modelling and landscape response in the Mbuluzi River catchment of Swaziland. *CATENA* 50(2-4), 507–525.

Smith, M. J. & Pain, C. F. (2011): Geomorphological Mapping. In Gregory, K. J. & Goudie, A. S. (Eds.): The SAGE handbook of geomorphology, 142–153.

Soil Survey Staff (1999): Soil taxonomy: A basic system of soil classification for making and interpreting soil surveys. U.S. Department of Agriculture Handbook, 436.

Strahler, A. N. (1952): Hypsometric (Area-Altitude) Analysis of Erosional Topography. *Geological Society of America Bulletin* 63(11), 1117–1142.

Strahler, A. N. (1957): Quantitative analysis of watershed geomorphology. *Trans. AGU* 38(6), p. 913.

Summerfield, M. A. (1991): Global geomorphology. An introduction to the study of landforms. Harlow: Pearson.

Toya, H.; kadomura, H.; Tamura, T.; Hori, N. (1973): Geomorphological Studies in Southeastern Kenya. Geographical reports of Tokyo Metropolitan University 8, 51–137.

Trauth, M. H.; Deino, A. L.; Bergner, A. G. N.; Strecker, M. R. (2003): East African climate change and orbital forcing during the last 175 kyr BP. *Earth Planet. Sci. Lett.* 206 (3-4), 297–313.

Trauth, M. H.; Maslin, M. A.; Deino, A. L.; Junginger, A.; Lesoloyia, M.; Odada, E. O. et al. (2010): Human evolution in a variable environment: the amplifier lakes of Eastern Africa. *Quaternary Science Reviews* 29(23–24), 2981–2988.

Trauth, M. H.; Maslin, M. A.; Deino, A. L.; Strecker, M. R. (2005): Late Cenozoic Moisture History of East Africa. *Science* 309 (5743), 2051–2053.

Tricart, J. (1972): Landforms of the humid tropics, forests and savannas. Geographies for advanced study, USA: St. Martin's Press

Umwelt-Geräte-Technik (2005): Operating instructions for Hood Infiltrometer. Available online at www.ugt-online.de/fileadmin/Public/downloads/Produkte/Bodenkunde/Leitfaehigkeit/Hood-Infiltrometer_-_IL_2700.pdf, checked on 20/9/2018.

USDA: Guide to Texture by Feel. Modified from S.J. Thien. 1979. A flow diagram for teaching texture by feel analysis. *Journal of Agronomic Education* 8, 54-55.

USDA (2014): Soil Survey Field and Laboratory Methods Manual. 2nd ed. Soil Survey Investigations Report, 51.

Vaidyanadhan, R.; Dixit, P. C.; Schlüter, T. (1993): Geomorphology and Sedimentology of Lake Manyara Environs, Tanzania, East Africa. *Documenta naturae* 77, 41–62.

van Breugel, P.; Kindt, R.; Barnekow Lillesø, J.-P.; van Breugel, M. (2015): Environmental gap analysis to prioritize conservation efforts in eastern Africa. *PloS one* 10 (4), e0121444.

Venzke, E. (2013): Global Volcanism Program, Volcanoes of the World, v4.7.3. Available online at https://doi.org/10.5479/si.GVP.VOTW4-2013, checked on 20/09/2018.

Viscarra Rossel, R. A. & Chen, C. (2011): Digitally mapping the information content of visible–near infrared spectra of surficial Australian soils. *Remote Sensing of Environment* 115(6), 1443–1455.

Viscarra Rossel, R. A.; McBratney, A. B.; Minasny, B. (Eds.) (2010): Proximal Soil Sensing. Progress in soil science. Springer Netherlands.

Weeraratne, D. S.; Forsyth, D. W.; Fischer, K. M.; Nyblade, A. A. (2003): Evidence for an upper mantle plume beneath the Tanzanian craton from Rayleigh wave tomography. *J. Geophys. Res.* 108(B9), p. 2427.

Wilson, J. P. & Gallant, J. C. (2000): Digital Terrain Analysis. In Wilson, J. P. & Gallant, J. C. (Eds.): Terrain analysis. Principles and applications. New York: Wiley, 1–27.

Wobus, C.; Whipple, K. X.; Kirby, E.; Snyder, N.; Johnson, J.; Spyropolou, K. et al. (2006): Tectonics from topography: Procedures, promise, and pitfalls. *Geological Society of America Special Papers* 398, 55–74.

Yanda, P. Z. & Madulu, N. F. (2005): Water resource management and biodiversity conservation in the Eastern Rift Valley Lakes, Northern Tanzania. *Integrated Water Resources Management (IWRM) and the Millennium Development Goals: Managing Water for Peace and Prosperity* 30(11–16), 717–725.

Zema, A. D.; Bombino, G.; Denisi, P.; Licciardello, F.; Zimbone, S. M. (2012): Prediction of Surface Runoff and Soil Erosion at Watershed Scale: Analysis of the AnnAGNPS Model in Different Environmental Conditions. In Godone, D. (Ed.): Research on Soil Erosion: InTech, 3–31.

I Morphotectonic Interpretation of the Makuyuni Catchment in Northern Tanzania using DEM and SAR Data

Authors

Elio Flores-Prieto, **Geraldine Quénéhervé**, Felix Bachofer, Faisal Shahzad and Michael Maerker

Paper History

The study design was constructed by Michael Maerker and Geraldine Quénéhervé. It was adapted by the Master of Science Thesis of Elio Flores-Prieto "Morphotectonic interpretation of the quaternary evolution of the Lake Manyara Basin using DEM and radar data analyses: a case study in the East African rift system, Tanzania" at the University of Tübingen in 2014. This thesis was closely supervised by Michael Maerker with data preparation and structure assistance by Geraldine Quénéhervé.

Own Contribution

study design, structure of the paper, contribution to data preparation, completion to figures and substantial writing.

Published in

Geomorphology **248**, 427–439, (2015).

doi:10.1016/j.geomorph.2015.07.049

ISSN: 0169-555X
Impact Factor (2015): 2.813

License

Geomorphology 248 (2015) 427–439

Contents lists available at ScienceDirect

Geomorphology

journal homepage: www.elsevier.com/locate/geomorph

Morphotectonic interpretation of the Makuyuni catchment in Northern Tanzania using DEM and SAR data

Elio Flores-Prieto [a], Geraldine Quénéhervé [a], Felix Bachofer [a], Faisal Shahzad [b], Michael Maerker [c,d,*]

[a] Department of Geosciences, Institute of Geography, University of Tübingen, Rümelinstraße 19-23, 72070 Tübingen, Germany
[b] LiDAR Research and Development, Zoller and Froehlich GmbH, Simoniousstraße 22, 88299 Wangen im Allgaeu, Germany
[c] Heidelberg Academy of Sciences and Humanities, c/o Institute of Geography, University of Tübingen, Rümelinstraße 19-23, 72070 Tübingen, Germany
[d] Department of Earth Sciences, University of Florence, Italy

ARTICLE INFO

Article history:
Received 23 October 2014
Received in revised form 30 July 2015
Accepted 31 July 2015
Available online 4 August 2015

Keywords:
Morphotectonics
SAR data
TecDEM
Lineament extraction

ABSTRACT

Landscapes in the East African Rift System are formed by complex effects of the active continental extension zone. These effects are caused by the Somalian micro-plate's eastward drift away from the Nubian plate, as well as by volcanic, erosional and depositional processes. Tectonic processes in this region have significantly contributed to the formation of the current drainage systems and landforms. This study focuses on the morphotectonics of the Makuyuni catchment with an analysis of topography, drainage networks, stream longitudinal profiles and lineaments. This analysis reveals a morphostructural control with an N–S trend for the uplifted Masai Block, as well as tectonic deformation in the Makuyuni catchment area (NE of Lake Manyara). Whereas basin asymmetry analysis shows basin tilting associated with active faulting and uplifting near the Essimingor volcanic cone, in this catchment the steepness and concavity indices, coupled with lineaments obtained from interpretations of Synthetic Aperture Radar satellite scenes, show an uplifting along micro-faults. Hypsometry curves reveal that subcatchments on the right side of the Makuyuni River are in a mature equilibrium phase, whereas those at the left side are in a younger stage of maturity. An investigation of base level and statistical moments of the hypsometric curves provides evidences for the spatial distribution of gully erosion phenomena. Such erosion processes are due to tectonic deformation in the northern parts of the Makuyuni catchment. These results of regional tectonic instability suggest that tectonic processes are a significant factor for the current landscape evolution in the Lake Manyara basin.

1. Introduction

Quaternary evolution of landscapes in active rift areas is primarily formed by the effects of tectonic, volcanic and climatic factors. Tectonic factors are controlled by extensional processes of accommodating zones on major bounding faults (Ebinger and Scholz, 2011). Volcanic activity results from structural weaknesses in the crust and the high heat flow associated directly with rifting (Nichols, 2013). Climatic factors influence the weathering and water availability for transport, which determine the morphology and lithology of sedimentary bodies in rift regions (Tiercelin, 1990). Tectonic landscapes in rift areas are highly dynamic and are liable to undergo relatively rapid re-molding of its physical surface (Bailey et al., 2000). Traces of these dynamics are in part preserved in high escarpments, discontinuities in relief patterns, inland lake formation, and drainage network control, which are actively manifested by faulting and seismicity.

The study of relief structure and its morphology in tectonically active regions using geospatial data is usually called morphotectonics (Goudie, 2013). Morphotectonics is considered synonymous with tectonic geomorphology and defines the study of the interaction of tectonics and geomorphology (Scheidegger, 2004; Goudie, 2013). Morphotectonic studies are particularly addressed to locate anomalies in landform distribution, river courses, channel forms, terrace profiles, local relief or specific landforms such as slope breaks (Burbank and Anderson, 2011; Goudie, 2013). Digital Elevation Models (DEMs) and remote sensing data in general, are especially useful to analyze regional tectonic features from topography (Codilean et al., 2006; Wobus et al., 2006). The spatial data used as input in these analyses are commonly geomorphological and drainage pattern maps, DEMs and their various derivatives e.g., slope, aspect, and curvature (Burbank and Anderson, 2011). Morphotectonic analyses have been recently applied using global DEMs for active tectonic regions in the Himalayas, Andes, Alps and other mountain ranges showing their possibilities for applying geologic mapping and tectonic interpretations (Leverington et al., 2002; Jordan et al., 2005; Wulf et al., 2006; Gloaguen et al., 2007; Grohmann et al., 2007; Ramli et al., 2010; Shahzad and Gloaguen, 2011a, b; Anoop et al., 2012;

* Corresponding author at: Heidelberg Academy of Sciences and Humanities, c/o Institute of Geography, University of Tübingen, Rümelinstraße 19-23, 72070 Tübingen, Germany.
E-mail addresses: elio.flores_prieto@yahoo.de (E. Flores-Prieto), geraldine.queneherve@uni-tuebingen.de (G. Quénéhervé), felix.bachofer@uni-tuebingen.de (F. Bachofer), geoquaidian@gmail.com (F. Shahzad), michael.maerker@ggi.uni-tuebingen.de (M. Maerker).

http://dx.doi.org/10.1016/j.geomorph.2015.07.049
0169-555X/

Ferraris et al., 2012; Fisher et al., 2013; Gao et al., 2013; Soto-Pinto et al., 2013; Rahnama and Gloaguen, 2014; Scherler et al., 2014).

To investigate earth surface deformation due to tectonic processes, it is necessary to identify geomorphic markers that were displaced. The best markers are readily recognizable landforms, surfaces or linear trends (Burbank and Anderson, 2011). Linear trends can be identified in spatial data sets as lineaments. A lineament is a traceable, simple or composite linear feature shown on the surface whose parts are aligned in a rectilinear or slightly curvilinear relationship and which differs distinctly from the patterns of adjacent features, presumably reflects a subsurface phenomenon (O'Leary et al., 1976). Consequently, lineaments can be valley systems as well as rectilinear convex landforms. However, the automatic detection of valley features in the study area is difficult due to the ground resolution of the data in relation to the target structures as well as vegetation and shadowing effects. Therefore, we consider only convex rectilinear landforms as lineaments. Recent studies have demonstrated that remote sensing data are valuable sources for evaluating lineaments (Marghany and Hashim, 2010a; Soto-Pinto et al., 2013; Rahnama and Gloaguen, 2014). The appearance of lineaments is related to the occurrence of faults in the earth's crust and the depth of these faults. A fault which is close to the surface appears as a clear high-contrast lineament, and is better detectable in high resolution images. A deeper located fault is reflected in more subtle and often smeared lineaments, detectable in the lower-resolution and larger area images where the "noise", caused by fine details, is reduced (Arlegui and Soriano, 1998).

The aim of this study is to examine the morphotectonics of the Lake Manyara area focusing on the Makuyuni River basin, located in the East African Rift System (EARS). The tectonics of this region were previously studied in terms of i) kinematic and structural geology (Ring et al., 2005), ii) faulting, iii) Neogene tectonics and volcanism (Dawson, 1992, 2008; Le Gall et al., 2008; Albaric et al., 2009), iv) and structural geology (Albaric et al., 2010). Nevertheless, the link between landscape morphology and tectonics still has not been directly addressed.

This study identifies tectonic processes through a detailed analysis of topography, drainage networks, basins and river longitudinal profiles using DEMs derived from the Shuttle Radar Topography Mission (SRTM). This analysis is complemented by a lineament analysis performed using Synthetic Aperture Radar (SAR) data with different imaging geometry, wavelength and polarization. Different studies have proven the suitability of microwave remote sensing images for lineament detection and extraction (Tzong-Dar and Lee, 2007; Marghany and Hashim, 2010b). A specific focus of the study consists of assessing the suitability of different sensors for the detection of lineaments. The applied sensors are: ALOS Phased Array type L-band Synthetic Aperture Radar (PALSAR), Envisat Advanced Synthetic Aperture Radar (ASAR) and TerraSAR-X. We also investigate the role of tectonics as a triggering mechanism of gully erosion.

2. Regional setting

The EARS is one of the most remarkable geomorphic features in the African continent that results from the combination of the effects of the active continental extension zone caused by the eastward drift of the Somalia microplate away from the Nubian plate (Dawson, 2008) (Fig. 1). The EARS encompasses several Precambrian terrains that have experienced Cenozoic extension related to uplift and rifting. These terrains include the Archean Tanzanian craton, located in the center of the EARS that is mechanically strong and is surrounded by less resistant Proterozoic mobile belts, demonstrating strong control of lithospheric heterogeneities in strain localization during rift initiation (Ebinger et al., 1997; Ebinger and Scholz, 2011). The EARS splits into a western and an eastern branch around the Tanzania craton. The eastern branch runs over a distance of 2200 km through Ethiopia and Kenya up to northern Tanzania, largely following an N–S trend, composed of the Afar, Ethiopian, Kenya and Gregory rifts and the North Tanzania Divergence zone (NTD) from north to south (Tiercelin, 1990; Chorowicz, 2005; Dawson, 2008). As the EARS enters northern Tanzania, it splays into a 300 km wide zone of block faulting, in contrast to the well-defined, 80 km wide graben formed to the north of Kenya (Le Gall et al., 2008). The NTD is an elongated N–S depression flanked on its western side by a high, east-facing escarpment. The rift structures within the NTD are marked by a change in the rift morphology. Both sides of the depression are extensive areas of Neogene volcanic rocks (Dawson, 1992).

According to Dawson (1992) two intensive faulting processes took place in the NTD. The earlier was associated with the deformation of the mid Tertiary land surface and the uplifting of the Victoria and Masai Blocks causing a tectonic depression bounded by faults and warps. The second major phase of faulting took place at about 1.2 Ma during the Pleistocene phase of lower intensities, explosive nephelinite–phonolite–carbonatite volcanism (Dawson, 2012). Both episodes of faulting have created the present-day rift valley depression at the NTD.

The main manifestation of this faulting is seen in the major rift escarpment that runs from Lake Natron in the North to the South of Lake Manyara. This Eastern branch of the EARS has a relative elevation of ~500 m above the basin floor and is the surface expression of the major Manyara–Natron Fault (Macintyre et al., 1974).

The Lake Manyara basin is geographically located in the north-central part of Tanzania (3°00′–5°12′ S, 35°24′–36°48′ E), covers about 18,400 km^2 and lies between 954 and 3611 m a.s.l. It is an endorheic basin that straddles a complex occurrence of geological and geomorphological processes associated with volcanism, faulting, erosion and denudation (Dawson, 2008). The basin corresponds largely to the Manyara rift and has an asymmetrical geometry typical of a half-graben located in continental rift zones. In the west it is bordered by the Manyara escarpment, whose base is formed by several poorly sorted alluvial fan deposits. In the central part the shallow and saline Lake Manyara is located. The half-graben structure of the Lake Manyara basin is filled with continental sediments (Mutakyahwa, 2002). Today the seismic activity concentrates in the southern part of the basin (Macheyeki et al., 2008). East of Lake Manyara, paleolake terraces indicate former lake levels (Bachofer et al., 2014). A W-dipping warp in basement rocks is located in the east of the basin and minor *en echelon* step faults that dip to the NNE and to the E. (Macintyre et al., 1974; Ring et al., 2005).

The Makuyuni River catchment (3084 km^2) drains into Lake Manyara. The prevailing savannah climate is characterized by bi-modal rainy seasons with an annual rainfall of ca. 700 mm. The mean annual temperature is about 26 °C. In the north the border of the catchment is defined by steep valleys and volcanic sediments from the volcano Essimingor and the Monduli volcanoes and in general undulated structures (Fig. 2). The southern part is dominated by lowland areas followed by the undulating Masai plain stretching to the southeast. The Proterozoic metamorphic rocks are nearly completely covered by Holocene soils and lacustrine sediments adjacent to the lake. Close to the village of Makuyuni the so-called Manyara Beds are well exposed due to the incision of the Makuyuni River and gully erosion (Bachofer et al., 2015). They are divided in two sections: the Lower Members which are formed of lacustrine facies from the former paleolake Manyara (>0.633 Ma) and the Upper Members formed by floodplain, channel and debris flow facies (Ring et al., 2005; Frost et al., 2012).

3. Materials and methods

In this study we used multisensoral remote sensing data at various spatial scales. The data include: i) SRTM X-band data (SRTM-X) with 30 m ground resolution and those from three medium–high spatial resolution Synthetic Aperture Radar (SAR) sensors with different wavelengths and polarizations: ii) ALOS PALSAR (HH/HV polarization, L-band), iii) Envisat ASAR (HH/VV polarization, C-band) and iv) TerraSAR-X (HH polarization, X-band).

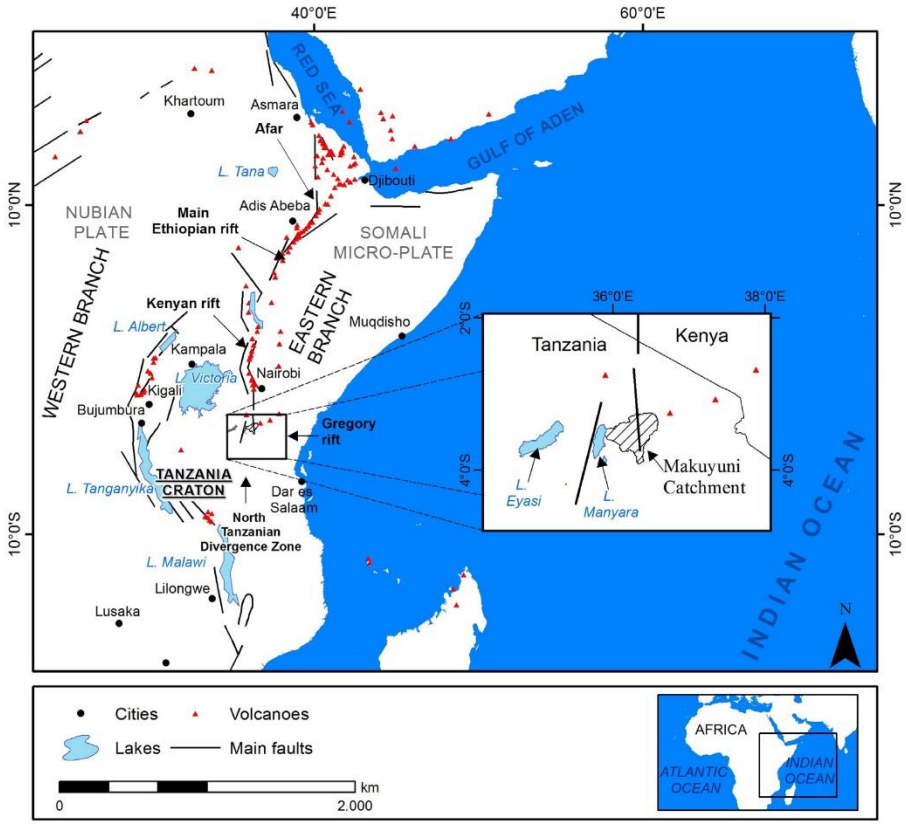

Fig. 1. Map of East Africa showing the EARS, its main structural units and associated volcanism, the location of the Lake Manyara and the Makuyuni River catchment in northern Tanzania. Source: Geology from the U.S. Geological Service (http://www.usgs.gov/), and Toponyms from Dawson (2008).

These data sets were examined to identify landscape elements reflecting recent tectonic activity such as drainage networks and lineaments. We combined morphotectonic parameters derived by terrain analysis to synthesize and visualize the results in a GIS (Geographic Information Systems) environment. This approach allows us to assess the influence of tectonics on current gully erosion processes.

3.1. Morphotectonic analyses

3.1.1. Stream profile analysis

For this analysis an SRTM-X DEM with a ground resolution of 30 m was used. Stream longitudinal profiles were extracted using TecDEM (http://www.tecdem.org). This toolbox is implemented into the MATLAB environment for understanding tectonics from DEMs and is able to generate stream profiles, determine flow directions, delineate watersheds, select knickpoints and generate morphometric maps for surface dynamics and basin analyses (Shahzad and Gloaguen, 2011a, b).

The first step is the extraction of the drainage network. This is based on the calculation of flow directions using the deterministic flow direction algorithm (D8) and contributing area. During the next step, on the basis of the extracted drainage system, longitudinal profiles of 22 channels were generated.

The stream profile analysis involved the calculation of the concavity (θ) and the steepness (k_s) indices.

θ and k_s values depend on basin morphology, underlying rock strengths and hydraulic geometry (Snyder et al., 2000; Shahzad and Gloaguen, 2011a; Anoop et al., 2012). They allow us to describe the stream longitudinal profiles through a relation between the channel gradient and the contributing drainage area (Schoenbohm et al., 2004). They are especially used for evaluating river system response to different landscape forming and modifying processes, including patterns of tectonic uplift and deformation (Wobus et al., 2006). This relation is expressed by the following predictable power law equation:

$$S = k_s A^{-\theta} \quad (1)$$

where S represents channel slope and A is the upstream drainage area. Because k_s is highly correlated to θ, we calculated a normalized steepness k_n using as reference $\theta = 0.45$ as suggested by Schoenbohm et al. (2004). θ and k_n values for concave segments along the longitudinal profiles were automatically calculated using a logarithmic regression analysis of area and slope values of selected trends. This calculation yields steepness distribution for the area with steady state landscape, as calculated by Shahzad and Gloaguen (2011a).

In the last step, knickpoints along the longitudinal profiles of the 22 tributaries were identified using a semi-automatic approach in TecDEM. This approach consists of the manual identification of the knickpoints in terms of slope breaks along the longitudinal profiles. The identification is based on expert knowledge and field work experience.

3.1.2. Drainage basin tilting

Drainage basin tilting was evaluated to examine the presence of tectonic tilting at the scale of the subcatchments. Therefore, we chose

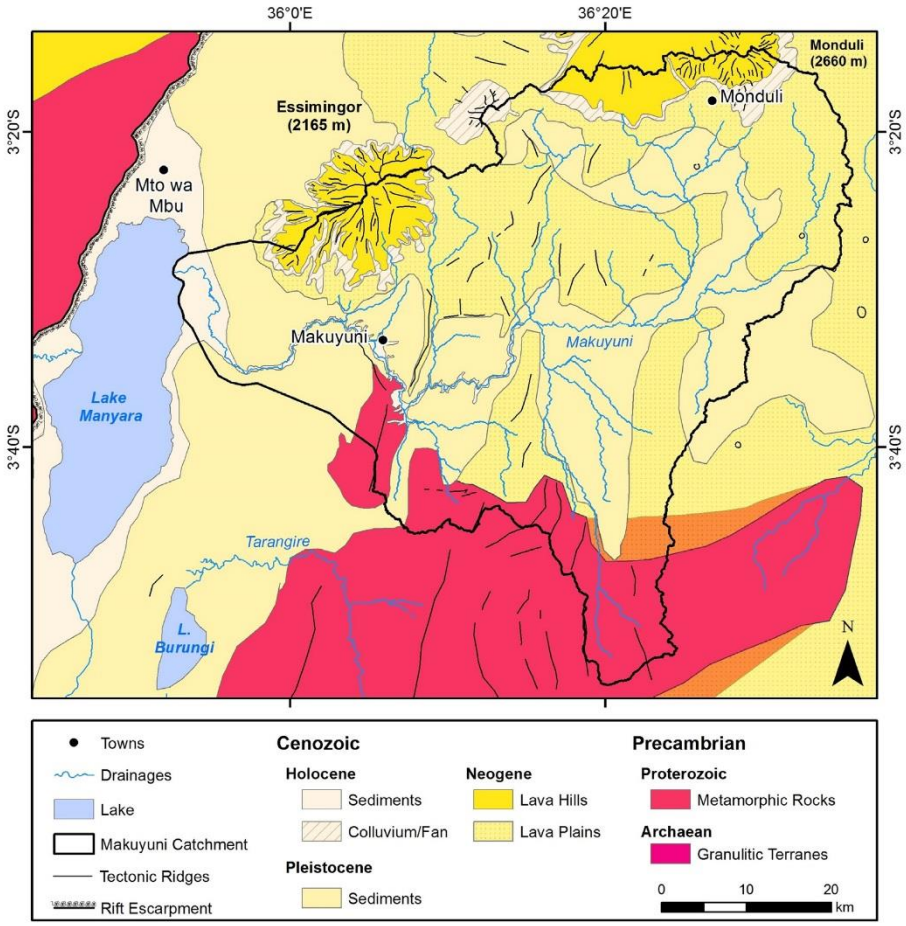

Fig. 2. Geological main units of the area. Based on field surveys and additional information from Vaidyanadhan et al. (1993) and Schlüter (2008).

Strahler order 4 which represents the mayor tributaries. Drainage basin tilting was estimated by means of the asymmetry factor *AF*, which is sensitive to tilting perpendicular to the direction of the stream (Hare and Gardner, 1985). *AF* values close to 50 show little or no tilting perpendicular to the direction of the trunk channel. *AF* values significantly above or below 50 results from drainage basin tilting, either due to tectonic activity or to lithological control. In order to determine the tilting direction of the subcatchments, following equation was used:

$$AF = 100 \cdot \frac{A_r}{A_t} \quad (2)$$

where A_r represents the basin area to the right side of the trunk stream, and A_t represents the total area of the drainage basin.

3.1.3. Basin hypsometry

Basin hypsometry is an appropriate parameter for identifying the stage of drainage evolution (Pérez-Peña et al., 2009). It represents the relative extent of the watershed area below or above a given height. The hypsometry integral (*HI*) and hypsometric curves can be used in classical conceptual geomorphic models of landscape and drainage evolution as follows: for *HI* values above 0.6, the area is at a youthful stage; for *HI* values in the range of 0.35–0.6 the area is in equilibrium (mature) phase; and *HI* values below 0.35 characterizes a monadnock phase in landscape evolution, a stage even more mature than the equilibrium stage (Strahler, 1957; Shahzad and Gloaguen, 2011b). Convex curves are typical for youthful stages of maturity whereas S-shaped curves and concave curves are typical for mature and old stages (Ohmori, 1993). Hypsometric curves and their statistical moments (skewness and kurtosis) were calculated using TecDEM software (see Shahzad and Gloaguen, 2011b). Skewness represents the asymmetry of the normal distribution in respect to the mean. Skewness is 0 when the variable distribution is symmetrical. Kurtosis is used to measure the "peakness" (>3) or "flatness" (<3) of the distribution in respect to the normal distribution (Pérez-Peña et al., 2009). These statistics can be interpreted in terms of erosion; skewness represents the amount of headward erosion in the upper reach of the basin, and kurtosis represents the erosion on both upper and lower reaches of a basin (Luo, 2000). Usually, these statistics are useful for hypsometric analysis when the basins present a similar hypsometry integral but different shapes (Pérez-Peña et al., 2009).

3.2. Lineament extraction

There are several algorithms that are available for automated lineament extraction, e.g. Hough Transform, Haar Transform and Segment Tracing (Jinfei and Howarth, 1990). In this study the automated lineament extraction was carried out by the LINE module of PCI

Geomatica software. This module is similar to the Segment Tracing algorithm and automatically detects a line of pixels as a vector element by evaluating local variance of the gray level in a digital image (Koike et al., 1998). All SAR scenes were radiometrically calibrated and topographically corrected. The automated lineament extraction method was performed for all available SAR scenes, and a complementary visual interpretation and manual extraction were conducted for the data of the Envisat ASAR (VH polarization) sensor. Complementary visual interpretation was performed only for this SAR sensor because its spatial scale resolution of 15 m provided the best basis for generalizing and identifying continuous linear features. The interpretation takes tonal and textural changes in the image as well as abrupt changes within the drainage network pattern into consideration — an example is shown in Fig. 3.

Manually and automatically extracted lineaments were compared using an overlay technique with a map of neotectonics created by

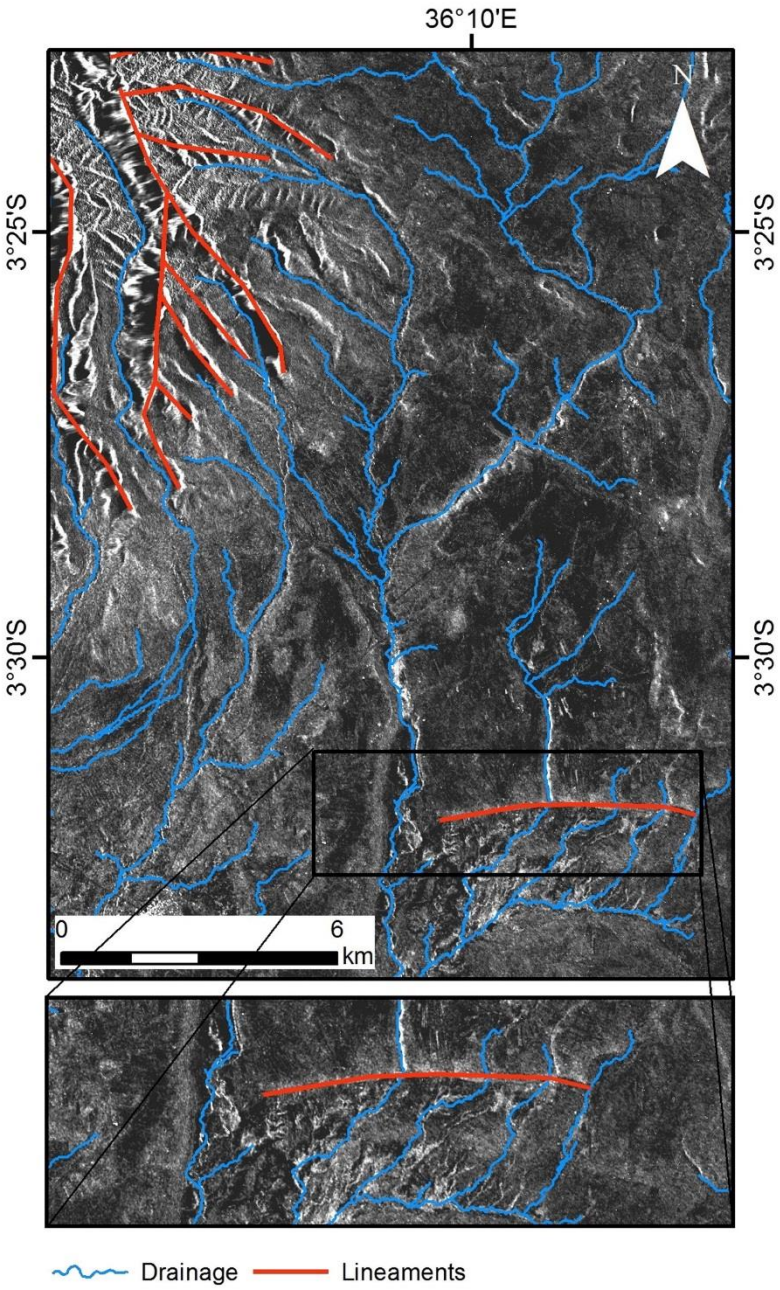

Fig. 3. Section of an Envisat ASAR scene (VH) of an area in the north of the Makuyuni catchment. Lineaments are indicated with segmented lines in white. The lineament in the enlarged section represents a local fault that deflects the four stream lines to the SW.

Dawson (2008). This allowed the classification of the lineaments into four types of linear tectonic structures: faults, inferred faults, escarpments and lithological contacts.

3.3. Base level maps and erosion areas

In a GIS environment we combined georeferenced tectonic structures (lineaments), morphotectonic data and a shapefile showing the current distribution of gully erosion phenomena digitalized from Google Earth™ images. We assessed the tectonic influence on the spatial distribution of gully erosion comparing the base level map with the current topography of the Makuyuni catchment shown by interpolated contours. The base level map was prepared in TecDEM by interpolating the elevation at the location of 2nd and 3rd Strahler order streams. Base levels can be used to study the dynamics of streams with different Strahler orders and topographic variations. Each base level surface is related to similar erosional stages, and can be considered a product of tectonic events (Golts and Rosenthal, 1993; Grohmann, 2004; Grohmann et al., 2007). To interpret the development and migration of knickpoints due to changes in the base level, they can be related to any geomorphological feature, e.g. the geomorphological evolution of a normal fault scarp. A response to the sudden base-level fall is knickpoint migration or propagation, which is an important aspect of channel incision and evolution in a wide range of geologic, tectonic, and climatic settings (Whipple and Tucker, 1999). Here we compared the knickpoint location with the location of gully systems in order to reveal a specific spatial correlation.

4. Results

All data and calculated results were validated during several field campaigns between 2010 and 2014. A total of 22 streams of the Makuyuni River were selected for a detailed analysis (Fig. 4). These streams correspond to the Strahler orders 3 and 4. Streams numbers 1 to 13 have their headwaters in the northern volcanic region, flowing southward to reach the Makuyuni River. The stream number 14 is part of the highest section of the Makuyuni River and follows an N–S trend for the first 10 km before undergoing a 45° deflection to an NE–SW direction. The streams numbers 15 to 22 flow northwards until they reach the Makuyuni main channel.

4.1. Stream longitudinal profiles

Longitudinal profiles of the 22 tributaries of the Makuyuni River consist of one to several channel segments. We identified these channel segments according to morphologic categories of the stream longitudinal profiles. These segments are frequently separated by knickpoints. The

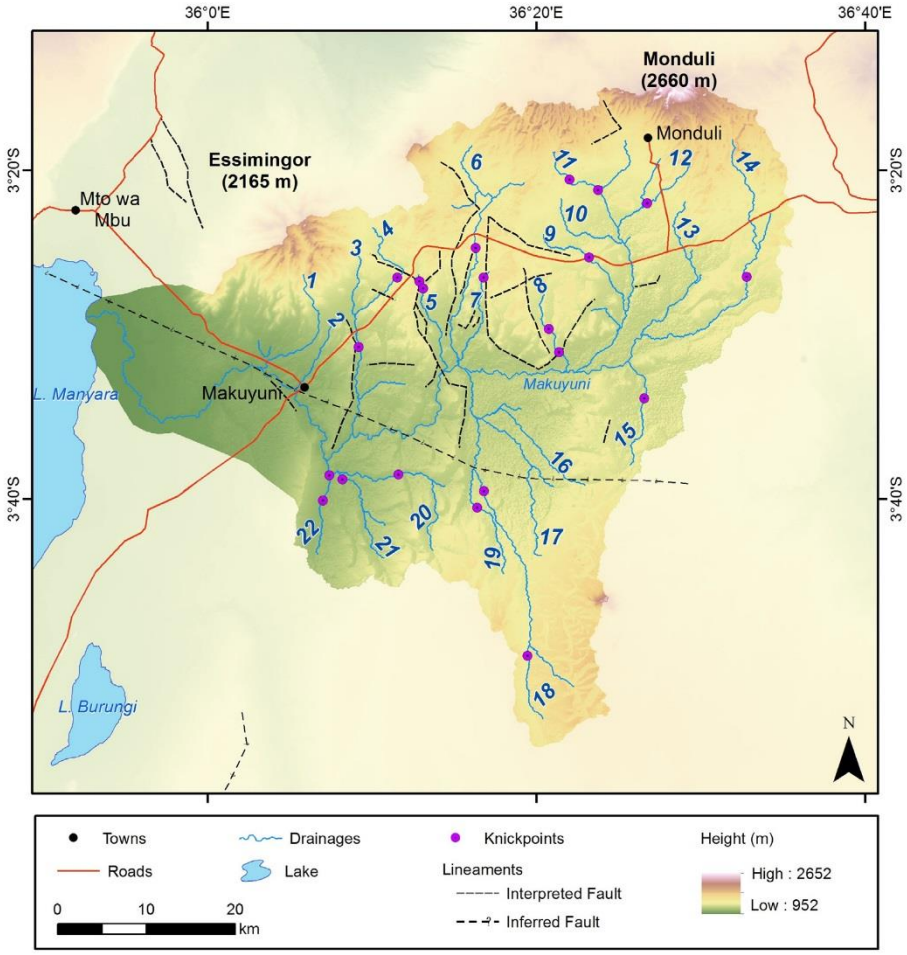

Fig. 4. Topographic map of the Makuyuni catchment showing the 22 selected tributaries, knickpoints and lineaments.

position of the channel segments allows the classification of the longitudinal profiles into four categories, corresponding to Fig. 5: A) fully equilibrated profiles without knickpoints (eight profiles), B) equilibrated profiles with knickpoints on their sections (nine profiles), C) profiles with two well-defined channel segments (two profiles), and D) profiles with three well-defined channel segments (three profiles).

θ and k_n values of the selected profiles are shown in the log area–log slope plots of Fig. 5. Values of θ and k_n of the 22 analyzed tributaries are grouped into three major segments that are defined by the morphology of the longitudinal profiles (Table 1), an upper segment that travels over the relict landscape, an intermediate segment corresponding to the middle section of the tributaries, and a lower segment dominated by fluvial incision. Table 1 shows increasing θ and k_n from the upper, middle to lower segments, as well as high variabilities of θ and k_n in the lower segments.

The distribution of knickpoints is related to the occurrence of faults (Fig. 4). The knickpoints located on the streams on the right side of the Makuyuni River (Nos. 3 to 8), coincide with minor lineaments detected through radar analysis, which were also classified by Dawson (2008) as micro or minor faults. Stream No. 14, situated in the eastern part of the catchment (Fig. 4), reveals one knickpoint located at the contact between Neogene rocks and recent alluvial deposits. No. 15, on the left side of the Makuyuni River, also shows a knickpoint located at this geological contact zone. The other knickpoints on the left side of the Makuyuni River are correspondingly related to a distinct lithological contact. There, the geological structure built by the Precambrian basement of the Masai Plateau is superimposed by the Quaternary alluvial and lacustrine deposits of the Manyara beds. Fig. 4 shows that the knickpoints of streams Nos. 20 to 22 are clearly alienated over this geological contact zone.

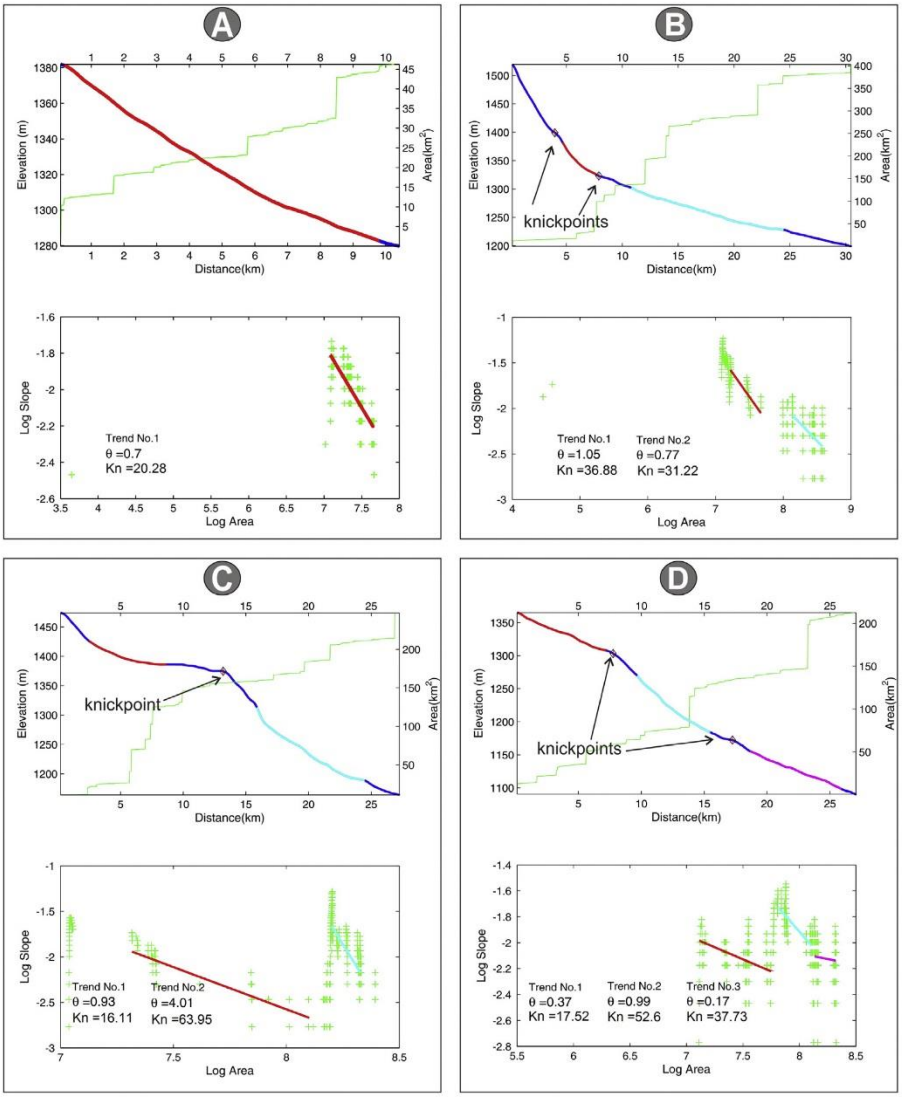

Fig. 5. Stream profile analysis (top of each set: longitudinal profile and cumulative catchment area, bottom: log area–log slope data) and knickpoints representing four categories of longitudinal profiles of the tributaries. (A) Fully equilibrated profile without knickpoints: stream No. 10. (B) Equilibrated profile with knickpoints on its section: No. 11. (C) Profile with two well-defined channel segments: No. 9. (D) Profile with three well-defined channel segments: No. 8.

Table 1
θ and k_n values.

Segment	Total segments	θ	k_n
Upper	22	1.394 ± 1.029	24.390 ± 11.890
Middle	9	3.731 ± 3.793	31.941 ± 16.835
Lower	2	9.070 ± 8.900	33.345 ± 43.850

4.2. Basin indices of tectonic activity

The calculated asymmetry index (*AF*) shows a strong asymmetry of the 12 subcatchments (Fig. 6A). The values of *AF* vary from 3.50 (almost symmetric; subcatchment 7) to 27.58 (highly asymmetric; subcatchment 8). The black arrows in Fig. 6A indicate the direction of tilt. All the subcatchments, with the exception of the Nos. 1 and 12, show an E–W direction of tilt.

Fig. 6B shows higher steepness values in the northern part of the Makuyuni catchment. This demonstrates higher tectonic deformation in this region of the catchment.

The hypsometric curves of the 12 subcatchments show two landscape maturity stages. A combined illustration of these subcatchments is shown in Fig. 7. Blue colored curves represent the subcatchments located on the right side of the Makuyuni River (northern subcatchments) and reveal a concave shape that suggests maturity, while the hypsometric curves of the subcatchments situated on the left side of the river (red curves) exhibit a more convex behavior (southern part). This shape type is attributed to more youthful drainage systems.

Statistical moments were used to quantify these hypsometric curves (Fig. 8A). In the case of the northern subcatchments, the values of hypsometric kurtosis are very irregular. They have a strong eastward increase up to subcatchment 3 and then a sudden decrease. Hypsometric skewness also increases slightly eastwards. In the southern subcatchments, there is an irregular behavior in hypsometric kurtosis and hypsometric skewness, with a general westward decrease (Fig. 8B). The hypsometric integral values are very similar for both northern and southern subcatchments.

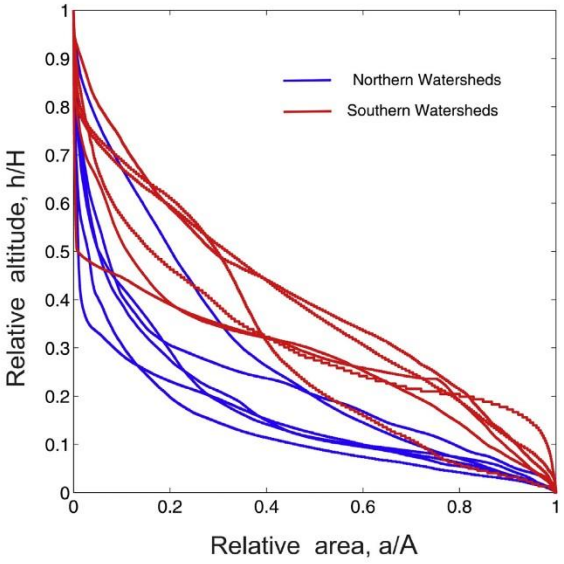

Fig. 7. Hypsometric curves for the northern and southern subcatchments of the Makuyuni River catchment. (H = maximum elevation difference of the basin; h = height of a given point in the basin; A = total area of the basin; a = surface area within basin above h).

4.3. Lineaments

The lineaments were automatically and manually extracted from the SAR images. The results of the automatic lineament extraction for each

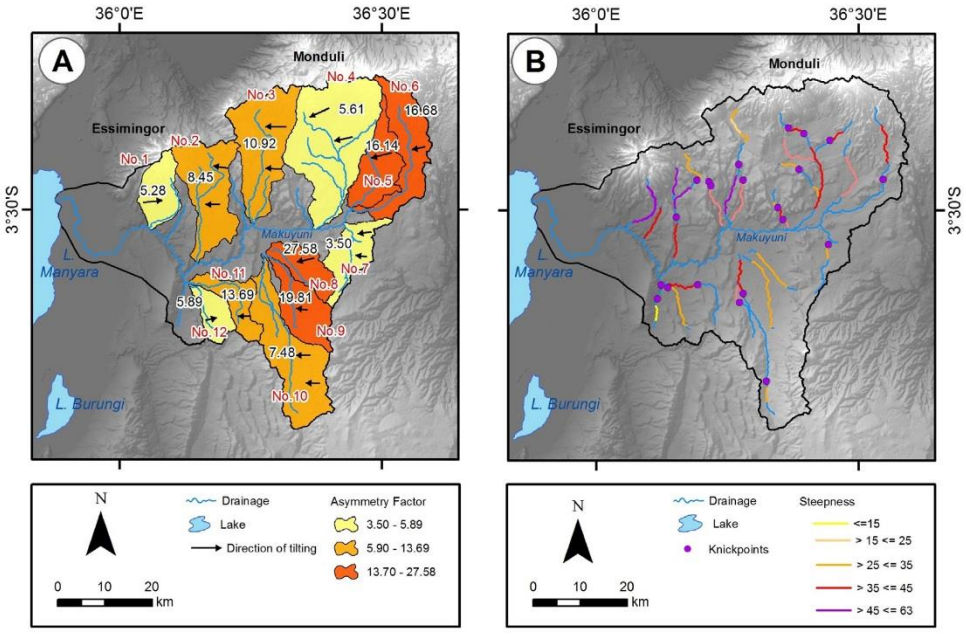

Fig. 6. Basin indices of tectonic activity. (A) Map showing subcatchments order 4 used to prepare hypsometric curves and their tilt directions according to the basin asymmetry. (B) Steepness and knickpoints of the Makuyuni River tributaries.

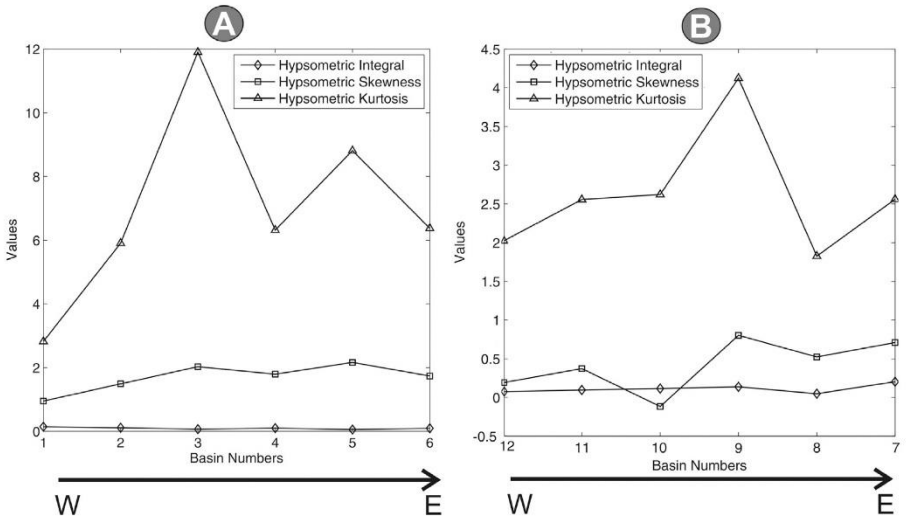

Fig. 8. Statistical moments of the hypsometric curves for the northern (A) and southern (B) subcatchments.

available SAR scene and all polarizations are summarized in Table 2 and Fig. 9. The length and number of detected lineaments were similar to the results computed with the ALOS PALSAR and Envisat ASAR data whereas the TerraSAR-X scenes provide a considerably higher number of lineaments. These differences are explained by the spatial resolution. Rose diagrams show a predominant N–S orientation of the extracted lineaments (Fig. 9A–C). Nonetheless, the Envisat ASAR Stripmap (VV; Fig. 9D) and the mosaicked TerraSAR-X Stripmap (HH; Fig. 9E) scenes indicate that a significant number of lineaments also have an NNE–SSW and an NNW–SSE orientation.

The visual interpretation was conducted for the Envisat scene, because the scene specific image acquisition geometry provided the best basis for the manual extraction of the lineaments. The automatically and the manually extracted lineaments are shown in Fig. 10. The number of automatically detected lineaments (503, Fig. 10A) is more than 24 times higher than the manually extracted ones (21, Fig. 10B). The most important reason for this is, that lineaments in automated analysis are shorter in length so that few of them could be combined to form one line as in the manually extracted map. The majority of the other detected lineaments are classified as artifacts, resulting from changes in vegetation cover, topography or geomorphologic structures and also roads and paths. The TerraSAR-X scenes in particular are highly affected by these artifacts, due to their high spatial resolution and a higher sensitivity to vegetation. Instead, the longer wavelengths of C- and L-band sensors show less sensitivity. The LINE algorithm cannot combine segmented lines. The total length of all the lineaments is higher in automated lineaments than the total length of the lineaments identified by manual extraction (342.3 vs 195.8 m). Nevertheless, the mean length of the lineaments from the manual interpretation is considerably higher than the automated ones.

Despite these differences, the spatial distribution of the lineaments in both maps is similar in that most of the lineaments are located in the north of the central Makuyuni catchment (Fig. 10).

4.4. Morphotectonics and current erosion processes

A base-level map of the 2nd and 3rd Strahler order streams and a colored shaded relief of the Makuyuni catchment are illustrated in Fig. 11. The base-level map gives a clear delimitation of the Makuyuni basin and the contour lines demarcate theoretical lines of equal uplift and hence, erosional surfaces (Fig. 11A). These lines show an E–W striking in the northern part of the Makuyuni catchment with a dip towards SSE, while the southern part is striking NE–SW and dipping towards NE. The proximity between these lines in the northern part suggests that this area is subject to tectonic activities. This might be in part correlated to uplift produced by the formation of the Monduli and Essimingor volcanoes. The major occurrence of knickpoints at considerably similar altitudes in this northern part indicates that they might have formed at similar stages of uplifting. In the northeastern and northern parts of the catchment, a high concentration of gully systems close to, or above the knickpoints can be observed. The knickpoints act as local erosion base level, and any changes in the knickpoint location leads to a response of erosional processes in the watershed above the knickpoints. Hence gully systems might indicate neotectonic activities as one of the triggering factors in gully formation.

Table 2
Automatically extracted lineaments from SAR data.

SAR sensor, mode & polarization	Acquisition date	Pass & incident angle (deg.)	Number of lineaments	Average length of lineaments (m)
ALOS PALSAR Fine Beam (HH)	2010-07-15	Ascending 38.78°	382	847
ALOS PALSAR Fine Beam (HV)	2010-07-15	Ascending 38.78°	310	824
Envisat ASAR Stripmap (VH)	2011-08-02	Descending 33.82°	503	680
Envisat ASAR Stripmap (VV)	2011-08-02	Descending 33.82°	391	633
TerraSAR-X Stripmap Mosaic (HH)	2013-01-25 & 2013-01-26	Ascending 24.49° & 28.11°	50,169	97

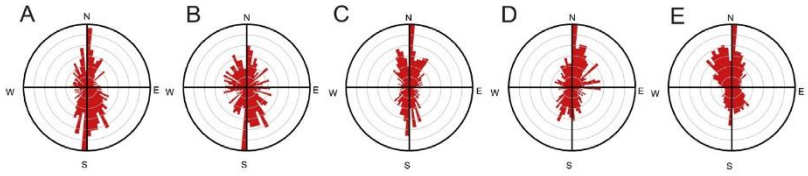

Fig. 9. Rose diagrams of the automatically delineated lineaments: (A) ALOS PALSAR Fine Beam (HH), (B) ALOS PALSAR Fine Beam (HV), (C) Envisat ASAR Stripmap (VH), (D) Envisat ASAR Stripmap (VV) and (E) Mosaicked TerraSAR-X Stripmap (HH).

5. Discussion

The assessment of morphotectonics based on DEM and SAR data analyses have yielded evidences of recent tectonics in the Makuyuni catchment.

5.1. Tilting of the subcatchments

Three categories of tectonic tilting for subcatchments of Strahler order 4 inferred from the *AF* value suggest that the drainage evolution in the Makuyuni catchment is sensitive to recent tectonics (Fig. 6A). These categories also reveal a non-uniform intensity of tilting. Highest values (>16) are located in the south-central and western parts of the Makuyuni catchment. There are several explanations for this result. Structural control caused by the boundary of the Pangani Rift at the western part of the Makuyuni catchment may have resulted in a strong shift of the basin midline of the subcatchments. Recent faulting and the contact of the tectonic depression of the Makuyuni River with the Masai Block (south) in the south-center of the Makuyuni River may also have affected the asymmetry of the subcatchments.

The *AF* factor also reveals a predominant E–W trend of tilting orientation for 10 out of 12 subcatchments. This trend can be explained by extensional E–W processes of the Manyara Rift and by the effects of local *en echelon* micro-faults. The other two subcatchments in the western part of the Makuyuni have a W–E tilt orientation. A possible explanation for this might be the local pushing forces of the ground movements (orogeny forces), associated with volcanism (Essimingor volcano).

5.2. Geomorphic stages of the subcatchments

The convexity of the hypsometric curves indicates erosional stages of the subcatchments. Older, more eroded drainage systems, show concave shapes. The difference in the curves of the northern and southern sides of the Makuyuni River reveals two stages of maturity (Fig. 7). Since the climatic conditions are similar for both sides of the river, these differences can be attributed to tectonic and lithological factors.

The northern part of the Makuyuni River catchment is affected by several *en echelon* micro-faults, while the southern part has no relevant fault lines (Fig. 4). The faults to the north of the Makuyuni River have been active during the late Pleistocene (Dawson, 2008) and were affected by uplifting. This uplifting is responsible for changes in the base level of the tributaries, which can also be interpreted as high incision rates. Thus, the subcatchments of the northern part of the Makuyuni River might have developed more concave hypsometric curves.

Lithological factors might also explain these differences in hypsometric curves. In the south of the catchment, where the Precambrian basement crops out, the relief is more resistant to the river incision, preserving convex stream profiles over time. In the north, the longitudinal profiles are more concave, revealing not only older states of maturity, but also major susceptibilities for the outcropping Quaternary deposits and Neogene rocks to river incision.

The statistical moments of the hypsometric curves provide additional information about the morphodynamics in the Makuyuni catchment. Since hypsometric integral values are very low and similar for both northern and southern curves (see Fig. 8), we had to use hypsometric skewness and kurtosis to interpret the spatial distribution and intensities of erosion processes.

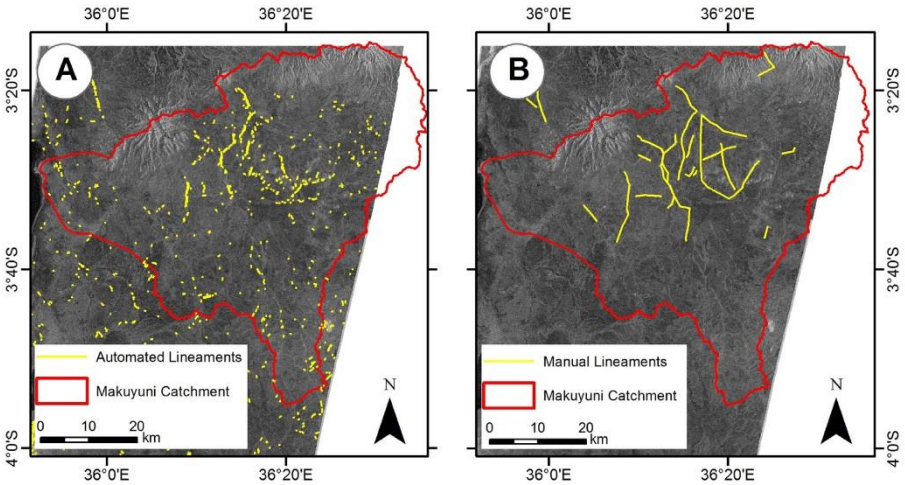

Fig. 10. Lineaments extracted (A) automatically and (B) manually.

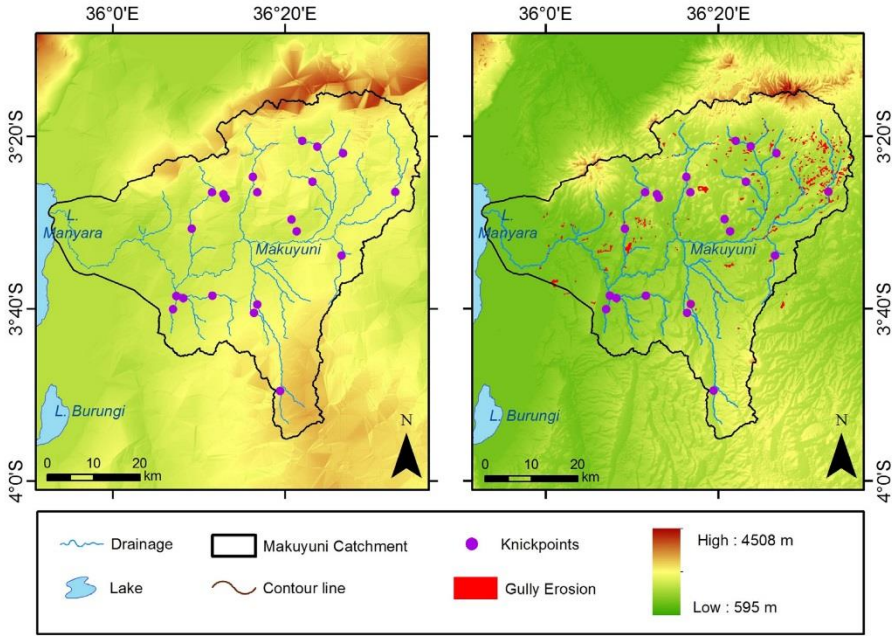

Fig. 11. Landforms reflecting: active tectonics and gully erosion. (A) Base-level map constructed for the 2nd and 3rd Strahler order streams and knickpoints. (B) Colored shaded relief, knickpoints of the Makuyuni catchment and gully erosion distribution. (For interpretation of the references to color in this figure legend, the reader is referred to the web version of this article.) Digitalized from Google Earth™ images and validated in the field.

Hypsometric skewness and kurtosis values increase eastwards in both the northern and southern hypsometric curves, revealing an increase in erosion in the upper and lower reaches of the subcatchments. These values also show a higher magnitude of incision on the northern side of the Makuyuni River around the Essimingor volcano, thus confirming the effect of the tectonic and lithological control on the erosion processes.

5.3. Evidence of tectonic activity in stream longitudinal profiles

Despite some irregularities that produced "noise" during the processing of some stream longitudinal profiles, the profile analysis seems to have yielded reliable results. Stream longitudinal profiles with different shapes suggest complex morphologies and morphodynamics that is primarily explained by changes in the lithology and tectonic activity.

A strong relationship between faults and the location of knickpoints was observed in the northern part of the Makuyuni catchment. The sequence of knickpoints on the tributaries Nos. 3 to 8 is directly related to tectonic control (micro-faults). The location of these knickpoints "over" the fault lines means that tectonic processes have taken place recently, and the location of knickpoints upstream of the fault lines is related to knickpoint migration (stream No. 8). Knickpoints on the streams Nos. 20, 21 and 22 (in the southern part) are spatially located over the lithological contact between Precambrian rocks and Quaternary deposits. One interpretation of the existence of these knickpoints might be that they are related to the low resistance of the Quaternary deposits. Once the streams reach the Quaternary deposits, the river incision increases, producing a distinct inflection in the river bed. Thus, these knickpoints are directly related to the predominant lithology. The latter was also confirmed by field observations in 2014. Stream longitudinal profiles classified as equilibrated profiles with knickpoints on their sections, and profiles with two and three well-defined channel segments are considered as a clear sign of tectonic activity and erosion.

The highest concavity index values were found in the lower channel segments. An explanation may be that the alluvial sediments which crop out close to the main channel of the Makuyuni River are less resistant to river incision. In the same way, the highest normalized steepness values in the lower channel segments are explained by the relative base level fall. The highest variability of these values in the middle segment is a consequence of the major uplift rates in the middle sections of the tributaries of the Makuyuni River.

Some authors (Whipple and Tucker, 1999; Snyder et al., 2000) argue that θ is relatively insensitive to tectonics (or climate), and that k_n is correlated with the rate of rock uplift. Streams that have different k_n values for different segments may be responding to tectonic perturbations to the fluvial system (e.g. tributaries Nos. 8 and 9 in Fig. 5), since uplift along a fault will send a wave of incision through the fluvial network which is directly reflected in steepened profiles and in knickpoint generation and migration (Wobus et al., 2006). Although tectonic forces are often responsible for these variations in the channel slopes and/or concavity, there are other factors such as lithological differences or variations in rock strength and debris flow or landslide frequency which can influence stream longitudinal profiles, including changes in incision rates, channel morphology, and bed condition (Whipple and Tucker, 1999). The estimation of steepness distribution from the concavity and steepness values was conducted by assuming steady state incision processes. The steepness map (Fig. 6B) confirms that in the northern side of the Makuyuni River, a more intense uplift has taken place in comparison to the southern side.

5.4. Landscape dynamics: active tectonics and gully erosion

Base-levels of the 2nd and 3rd Strahler order streams reveal that the northern part of the Makuyuni catchment was intensively affected by tectonic activity (Fig. 11A). This might have caused important differences in the effects of the geomorphic processes within the Makuyuni catchment. For example, the statistical moments of the hypsometric curves (Fig. 8) showed that the erosion in this northern part of the catchment is considerably higher. These findings are consistent with field validation

identifying a higher spatial occurrence of gully systems in the northern part, especially in the north-eastern part of the basin (Fig. 11B). This suggests that gully erosion processes in this area might be triggered by local active tectonics.

Similarly, stream longitudinal profiles with knickpoints and with two or three segments reveal changes at the base level of the tributaries of the Makuyuni River. Changes at the base level may lead to a subsequent incision of the streams, which result in a direct or indirect propagation of this incision in the upstream catchments (Harvey, 2002). This incision causes frequently a higher complexity of the drainage net, such as the development of tributaries of first order and gully formation. The distribution of gully erosion in Fig. 11B shows that several gully erosion systems are located upstream of the knickpoints in the northeastern part of the Makuyuni catchment. This points to a direct relation between the upstream migration of knickpoints and gully formation. Quantifying this relation is an important issue for future research for understanding the landscape dynamics in this part of the EARS.

6. Conclusions

The morphotectonics and the drainage evolution of the Lake Manyara area, with a focus on the Makuyuni River basin in the south of the EARS, were studied based on DEM analysis and lineament interpretations of SAR images. These analyses were performed using morphotectonic methods based on automated tools and software. Through these analyses the influence of tectonic activity on landscape evolution was investigated. The effect of the tectonics had already previously been consistently documented but without specific or local evidences. This study contributes to understanding the dynamics of Quaternary landscape evolution in this region as follows:

i. Relief and landscape patterns of the Lake Manyara basin reflect the evolution of a complex part of the rift systems that underwent the combined effects of tectonic factors inherent to its geological settings and Quaternary geomorphological processes. Generally, the morphostructures related to the EARS show a dominant N–S orientation. In the Makuyuni catchment, these structures reveal tectonic activity characterized by deviations and knickpoints of stream beds and the occurrence of erosion processes.
ii. The general increase of concavity and steepness values in the longitudinal profiles from the headwaters to lower sections indicate uplift associated with tectonic activity in the Makuyuni catchment.
iii. The spatial location of the knickpoints and its correlation with the lineament structures allowed the differentiation of the Makuyuni catchment into two distinctive areas: a) the hydrological controlled northern part of the catchment which is greatly influenced by tectonic activity, and b) a more stable southern part of the catchment, where the Precambrian lithology and less intense tectonics dominate.
iv. The data on the basin tilting, basin hypsometry and the morphology of the stream longitudinal profiles suggest that tectonic activity is an important factor governing Quaternary geomorphological processes, such as river incision and soil erosion, and hence, the landscape evolution of this region.

In summary, drainage network, stream longitudinal profiles, basin analysis and lineament extraction can be used as tools for identifying tectonic activity and related features in rift areas. The use of DEMs and SAR data in this kind of study permits the characterization and comparison of rift landscapes. Although there were initial limitations imposed by the low spatial resolution of the SRTM-X DEMs (30 m), their combination with high resolution radar data produced a better understanding of the superficial morphostructures. Moreover, in our case lineament interpretations for the regional analyses of morphotectonics, based on the use of C-band Envisat SAR images, yielded the best results with a medium spatial resolution. The above mentioned morphotectonic interpretations may be applicable to similar areas in the African rift, where landscapes are governed by extensional, tectonic, volcanic and erosional processes.

Acknowledgments

We are grateful for the support of the ROCEEH project: The Role of the Culture in Early Expansions of Humans, funded by the Heidelberg Academy of Sciences and Humanities. We would like to thank the DLR and the German Remote Sensing Data Center (DFS) for providing the TerraSAR-X and the SRTM/X-SAR data. Envisat ASAR and ALOS PALSAR data were provided by the European Space Agency. Furthermore, we would like to thank Jan Kalvoda and two more anonymous reviewers for their valuable comments.

References

Albaric, J., Déverchère, J., Petit, C., Perrot, J., Le Gall, B., 2009. Crustal rheology and depth distribution of earthquakes: insights from the central and southern East African Rift System. Tectonophysics 468 (1–4), 28–41.
Albaric, J., Perrot, J., Déverchère, J., Deschamps, A., Le Gall, B., Ferdinand, R.W., Petit, C., Tiberi, C., Sue, C., Songo, M., 2010. Contrasted seismogenic and rheological behaviours from shallow and deep earthquake sequences in the North Tanzanian Divergence, East Africa. J. Afr. Earth Sci. 58 (5), 799–811.
Anoop, A., Prasad, S., Basavaiah, N., Brauer, A., Shahzad, F., Deenadayalan, K., 2012. Tectonic versus climate influence on landscape evolution: a case study from the upper Spiti valley, NW Himalaya. Geomorphology 145–146, 32–44.
Arlegui, L.E., Soriano, M.A., 1998. Characterizing lineaments from satellite images and field studies in the central Ebro basin (NE Spain). Int. J. Remote Sens. 19 (16), 3169–3185.
Bachofer, F., Quénéhervé, G., Märker, M., 2014. The delineation of Paleo-Shorelines in the Lake Manyara Basin using TerraSAR-X data. Remote Sens. 6 (3), 2195–2212.
Bachofer, F., Quénéhervé, G., Märker, M., Hochschild, V., 2015. Comparison of SVM and Boosted regression trees for the delineation of lacustrine sediments using multispectral ASTER data and topographic indices in the Lake Manyara Basin. Photogrammetrie - Fernerkundung - Geoinformation (PFG) 1, 81–94.
Bailey, G., Manighetti, I., King, G., Bailey, G., Manighetti, I., King, G., 2000. Tectonics, volcanism, landscape structure and human evolution in the African Rift. In: Bailey, G., Charles, R., Winder, N., Bailey, G., Charles, R., Winder, N. (Eds.), Human Ecodynamics. Symposia of the Association for Environmental Archaeology en_GB. Oxbow Books, pp. 31–46.
Burbank, D., Anderson, R., 2011. Tectonic geomorphology. John Wiley & Sons 480 pp.
Chorowicz, J., 2005. The East African rift system. J. Afr. Earth Sci. 43 (1–3), 379–410.
Codilean, A.T., Bishop, P., Hoey, T.B., 2006. Surface process models and the links between tectonics and topography. Prog. Phys. Geogr. 30 (3), 307–333.
Dawson, J.B., 1992. Neogene tectonics and volcanicity in the North Tanzania sector of the Gregory Rift Valley: contrasts with the Kenya sector. Tectonophysics 204 (1–2), 81–92.
Dawson, J., 2008. The Gregory Rift Valley and Neogene-recent Volcanoes of Northern Tanzania. Geological Society (102 pp.).
Dawson, J.B., 2012. Nephelinite–melilitite–carbonatite relationships: evidence from Pleistocene–recent volcanism in northern Tanzania. Lithos 152, 3–10.
Ebinger, C., Scholz, C.A., 2011. Continental rift basins: the East African perspective, tectonics of sedimentary basins. John Wiley & Sons, Ltd, pp. 183–208.
Ebinger, C., Djomani, Y.P., Mbede, E., Foster, A., Dawson, J.B., 1997. Rifting Archaean lithosphere: the Eyasi–Manyara–Natron rifts, East Africa. J. Geol. Soc. 154 (6), 947–960.
Ferraris, F., Firpo, M., Pazzaglia, F.J., 2012. DEM analyses and morphotectonic interpretation: the Plio-Quaternary evolution of the eastern Ligurian Alps, Italy. Geomorphology 149–150, 27–40.
Fisher, G.B., Bookhagen, B., Amos, C.B., 2013. Channel planform geometry and slopes from freely available high-spatial resolution imagery and DEM fusion: Implications for channel width scalings, erosion proxies, and fluvial signatures in tectonically active landscapes. Geomorphology 194, 46–56.
Frost, S., Schwartz, H., Giemsch, L., Morgan, L., Renne, P., Wildgoose, M., Saanane, C., Schrenk, F., Harvati, K., 2012. Refined age estimates and Paleoanthropological investigation of the Manyara Beds, Tanzania. J. Anthropol. Sci. 90, 151–161.
Gao, M., Zeilinger, G., Xu, X., Wang, Q., Hao, M., 2013. DEM and GIS analysis of geomorphic indices for evaluating recent uplift of the northeastern margin of the Tibetan Plateau, China. Geomorphology 190, 61–72.
Gloaguen, R., Marpu, P.R., Niemeyer, I., 2007. Automatic extraction of faults and fractal analysis from remote sensing data. Nonlinear Process. Geophys. 14 (2), 131–138.
Golts, S., Rosenthal, E., 1993. A morphotectonic map of the northern Arava in Israel, derived from isobase lines. Geomorphology 7 (4), 305–315.
Goudie, A., 2013. Encyclopedia of geomorphology. Taylor & Francis (1200 pp.).
Grohmann, C.H., 2004. Morphometric analysis in geographic information systems: applications of free software GRASS and R. Comput. Geosci. 30 (9–10), 1055–1067.
Grohmann, C.H., Riccomini, C., Alves, F.M., 2007. SRTM-based morphotectonic analysis of the Poços de Caldas Alkaline Massif, southeastern Brazil. Comput. Geosci. 33 (1), 10–19.
Hare, P.W., Gardner, T., 1985. Geomorphic indicators of vertical neotectonism along converging plate margins, Nicoya Peninsula, Costa Rica. In: Morisawa, M., Hack, J. (Eds.), Tectonic Geomorphology. Allen and Unwin, pp. 75–104.
Harvey, A.M., 2002. Effective timescales of coupling within fluvial systems. Geomorphology 44 (3–4), 175–201.

Jinfei, W., Howarth, P.J., 1990. Use of the Hough transform in automated lineament. IEEE Trans. Geosci. Remote Sens. 28 (4), 561–567.
Jordan, G., Meijninger, B.M.L., Hinsbergen, D.J.J.v., Meulenkamp, J.E., Dijk, P.M.v., 2005. Extraction of morphotectonic features from DEMs: development and applications for study areas in Hungary and NW Greece. Int. J. Appl. Earth Obs. Geoinf. 7 (3), 163–182.
Koike, K., Nagano, S., Kawaba, K., 1998. Construction and analysis of interpreted fracture planes through combination of satellite-image derived lineaments and digital elevation model data. Comput. Geosci. 24 (6), 573–583.
Le Gall, B., Nonnotte, P., Rolet, J., Benoit, M., Guillou, H., Mousseau-Nonnotte, M., Albaric, J., Deverchère, J., 2008. Rift propagation at craton margin. Tectonophysics 448 (1–4), 1–19.
Leverington, D.W., Teller, J.T., Mann, J.D., 2002. A GIS method for reconstruction of late Quaternary landscapes from isobase data and modern topography. Comput. Geosci. 28 (5), 631–639.
Luo, W., 2000. Quantifying groundwater-sapping landforms with a hypsometric technique. J. Geophys. Res. 105 (E1), 1685–1694.
Macheyeki, A.S., Delvaux, D., Batist, M.D., Mruma, A., 2008. Fault kinematics and tectonic stress in the seismically active Manyara–Dodoma Rift segment in Central Tanzania — implications for the East African Rift. J. Afr. Earth Sci. 51 (4), 163–188.
Macintyre, R.M., Mitchell, J.G., Dawson, J.B., 1974. Age of fault movements in Tanzanian Sector of East African rift system. Nature 247 (5440), 354–356.
Marghany, M., Hashim, M., 2010a. Lineament mapping using multispectral remote sensing satellite data. Res. J. Appl.Sci. 5 (2), 126–130.
Marghany, M., Hashim, M., 2010b. Developing adaptive algorithm for automatic detection of geological linear features using RADARSAT-1 SAR data. Int. J. Phys. Sci 5, 2223–2229.
Mutakyahwa, M.K.D., 2002. Mineralogy and chemistry of bentonite (?) deposits at Minjingu, Lake Manyara, North Tanzania. J. Afr. Earth Sci. 34 (3–4), 213–221.
Nichols, G., 2013. Sedimentology and stratigraphy. Wiley (423 pp.).
Ohmori, H., 1993. Changes in the hypsometric curve through mountain building resulting from concurrent tectonics and denudation. Geomorphology 8 (4), 263–277.
O'Leary, D.W., Friedman, J.D., Pohn, H.A., 1976. Lineament, linear, lineation: some proposed new standards for old terms. Geol. Soc. Am. Bull. 87 (10), 1463.
Pérez-Peña, J.V., Azañón, J.M., Azor, A., 2009. CalHypso: an ArcGIS extension to calculate hypsometric curves and their statistical moments. Applications to drainage basin analysis in SE Spain. Comput. Geosci. 35 (6), 1214–1223.
Rahnama, M., Gloaguen, R., 2014. TecLines: a MATLAB-based toolbox for tectonic lineament analysis from satellite images and DEMs, part 1: line segment detection and extraction. Remote Sens. 6 (7), 5938–5958.
Ramli, M.F., Yusof, N., Yusoff, M.K., Juahir, H., Shafri, H.Z.M., 2010. Lineament mapping and its application in landslide hazard assessment: a review. Bull. Eng. Geol. Environ. 69 (2), 215–233.
Ring, U.W.E., Schwartz, H.L., Bromage, T.G., Sanaane, C., 2005. Kinematic and sedimentological evolution of the Manyara Rift in northern Tanzania, East Africa. Geol. Mag. 142 (04), 355.
Scheidegger, A.E., 2004. Morphotectonics. Springer (197 pp.).
Scherler, D., Bookhagen, B., Strecker, M.R., 2014. Tectonic control on ^{10}Be-derived erosion rates in the Garhwal Himalaya, India. J. Geophys. Res. Earth Surf. 119 (2), 83–105.
Schlüter, T., 2008. Geological Atlas of Africa. With notes on stratigraphy, tectonics, economic geology, geohazards, geosites and geoscientific education of each country. Springer (307 pp.).
Schoenbohm, L.M., Whipple, K.X., Burchfiel, B.C., Chen, L., 2004. Geomorphic constraints on surface uplift, exhumation, and plateau growth in the Red River region, Yunnan Province, China. Geol. Soc. Am. Bull. 116 (7), 895.
Shahzad, F., Gloaguen, R., 2011a. TecDEM: a MATLAB based toolbox for tectonic geomorphology, Part 1: drainage network preprocessing and stream profile analysis. Comput. Geosci. 37 (2), 250–260.
Shahzad, F., Gloaguen, R., 2011b. TecDEM: a MATLAB based toolbox for tectonic geomorphology, part 2: surface dynamics and basin analysis. Comput. Geosci. 37 (2), 261–271.
Snyder, N.P., Whipple, K.X., Tucker, G.E., Merritts, D.J., 2000. Landscape response to tectonic forcing: digital elevation model analysis of stream profiles in the Mendocino triple junction region, northern California. Geol. Soc. Am. Bull. 112 (8), 1250–1263.
Soto-Pinto, C., Arellano-Baeza, A., Sánchez, G., 2013. A new code for automatic detection and analysis of the lineament patterns for geophysical and geological purposes (ADALGEO). Comput. Geosci. 57, 93–103.
Strahler, A., 1957. Quantitative analysis of watershed geomorphology. Defense Technical Information Center, pp. 913–920.
Tiercelin, J.J., 1990. Rift-basin sedimentation: responses to climate, tectonism and volcanism. Examples of the East African Rift. J. Afr. Earth Sci. 10 (1–2), 283–305.
Tzong-Dar, W., Lee, M.T., 2007. Geological lineament and shoreline detection in SAR images, Geoscience and Remote Sensing Symposium, 2007. IGARSS 2007. IEEE International, pp. 520–523.
Vaidyanadhan, R., Dixit, P.C., Schlüter, T., 1993. Geomorphology and sedimentology of Lake Manyara Environs, Tanzania, East Africa. Doc. Naturae 77, 41–62.
Whipple, K.X., Tucker, G.E., 1999. Dynamics of the stream-power river incision model: implications for height limits of mountain ranges, landscape response timescales, and research needs. J. Geophys. Res. 104 (B8), 17661–17674.
Wobus, C., Whipple, K.X., Kirby, E., Snyder, N., Johnson, J., Spyropolou, K., Crosby, B., Sheehan, D., 2006. Tectonics from topography: procedures, promise, and pitfalls. Geol. Soc. Am. Spec. Pap. 398, 55–74.
Wulf, H., Schoenbohm, L., Strecker, M., 2006. Analysis of large-scale Quaternary landslide deposits: El Cajon basin, south-eastern Puna margin, NW Argentina, geophysical research abstracts. European Geosciences Union General Assembly.

II Multisensoral Topsoil Mapping in the Semiarid Lake Manyara Region, Northern Tanzania

Authors

Felix Bachofer, **Geraldine Quénéhervé**, Volker Hochschild and Michael Maerker

Own Contribution

Contribution to study design, field work, contribution to structure of the paper, soil profile analysis, contribution to figures, interpretation and writing.

Published in

Remote Sensing **7**(8), 9563–9586, (2015).

doi: 10.3390/rs70809563

ISSN: 2072-4292

Impact Factor (2015): 3.036

License

Remote Sens. **2015**, *7*, 9563-9586; doi:10.3390/rs70809563

OPEN ACCESS

remote sensing

ISSN 2072-4292

www.mdpi.com/journal/remotesensing

Article

Multisensoral Topsoil Mapping in the Semiarid Lake Manyara Region, Northern Tanzania

Felix Bachofer [1,*], Geraldine Quénéhervé [1], Volker Hochschild [1] and Michael Maerker [2,3]

[1] Institute of Geography, University of Tuebingen, Ruemelinstr. 19-23, 72070 Tuebingen, Germany; E-Mails: geraldine.queneherve@uni-tuebingen.de (G.Q.); volker.hochschild@uni-tuebingen.de (V.H.)

[2] Heidelberg Academy of Sciences and Humanities, Ruemelinstr. 19-23, 72070 Tuebingen, Germany; E-Mail: michael.maerker@geographie.uni-tuebingen.de

[3] Earth Science Department, University of Florence, Via G. La Pira, 50121 Florence, Italy

* Author to whom correspondence should be addressed; E-Mail: felix.bachofer@uni-tuebingen.de; Tel.: +49-7071-29-77528; Fax: +49-7071-29-5378.

Academic Editors: Nicolas Baghdadi and Prasad S. Thenkabail

Received: 21 May 2015 / Accepted: 20 July 2015 / Published: 28 July 2015

Abstract: This study pursues the mapping of the distribution of topsoils and surface substrates of the Lake Manyara area of northern Tanzania. The nine soil and lithological target classes were selected through fieldwork and laboratory analysis of soil samples. High-resolution WorldView-2 data, TerraSAR-X intensity data, medium-resolution ASTER spectral bands and indices, as well as ENVISAT ASAR intensity and SRTM-X-derived topographic parameters served as input features. Objects were derived from image segmentation. The classification of the image objects was conducted applying a nonlinear support vector machine approach. With the recursive feature elimination approach, the most input-relevant features for separating the target classes were selected. Despite multiple target classes, an overall accuracy of 71.9% was achieved. Inaccuracies occurred between classes with high $CaCO_3$ content and between classes of silica-rich substrates. The incorporation of different input feature datasets improved the classification accuracy. An in-depth interpretation of the classification result was conducted with three soil profile transects.

Keywords: topsoil mapping; ASTER; SAR; WorldView-2; topographical indices; multisensoral; SVM; multiscale

1. Introduction

The spatial distribution of soils and lithology provides essential input information for different scientific and economic applications, including landscape reconstruction [1], digital soil mapping (DSM) and mineral exploration for agricultural [2] or mining applications [3]. Though the soil must be considered as a three dimensional medium, a wide range of remote sensing sensors provide useful information in assessing various details of the mineral composition and other physical and/or chemical properties of the uppermost parts of the soils, as well as for spatially contiguous areas [4–6]. The topsoil is generally the most relevant part of the soil, considering food production, degradation and soil management [7]. Although the definition of topsoil varies in different soil taxonomies [7–10], the uppermost part of the soil belongs to the topsoil. The topsoil thickness is related to local conditions of pedogenesis, erosion and deposition processes. Normally, topsoil is characterized by a thickness of 10–30 cm [7,8]. In this study, we regard the soil surface properties as topsoil/lithology proxy. We hypothesize that the analysis of physical-chemical properties, the collection of field reference data and the remote sensing analysis of the upper surface strata yield valuable information about the topsoil and/or lithologic characteristics. Moreover, the topographic position and geomorphological processes also influence the topsoil characteristics and, hence, should be included in a comprehensive analysis of the spatial distribution of topsoils.

The surface reflectance of the mineral composition of a surface, which is received by a multi- or hyper-spectral sensor, is influenced by soil organic matter, moisture content, as well as texture and surface roughness [11]. Backscatter signals from Synthetic Aperture Radar (SAR) sensors of different wavelengths are dependent on the surface roughness and are sensitive to the dielectric properties of soils [12–14]. Soil mapping using remote sensing data show limitations due to the complex physical and chemical nature of soils. Remotely derived datasets can characterize the surface (optical remote sensing systems) or the uppermost part of soils (SAR systems) [5,15]. Since soils are complex three-dimensional structures, the surface characteristics may not represent the underlying layers of soil. The remote sensing signal may also be a product of different soil surface properties. This effect will increase with a lower spatial resolution of the datasets. Very high-resolution sensors, like WorldView-2 and GeoEye-1, provide a high spatial differentiation. On the other hand, lower spatial resolution sensors, like the Landsat series or ASTER, provide a better spectral coverage, especially in the mid-infrared region, which is important for mineral mapping purposes [5,16]. Vegetation cover is another important factor to consider. Already sparse vegetation cover may influence the identification of soil attributes using remote sensing methods [17,18]. Spectral indices from multi- or hyper-spectral remote sensing images are effective tools for the classification and evaluation of photosynthetic vegetation activity. Vegetation indices (VI), like the Normalized Difference Vegetation Index (NDVI), utilize the difference of absorption and reflection in the spectral wavelengths of the red (0.625–0.74 μm) and near-infrared (IR; 0.74–1 μm) [19]. Dead materials in grasslands blur VI, making it hard to distinguish between dead materials and some other land cover [20]. This is especially a problem in arid and semiarid regions, due to relatively long dry periods. A strategy to resolve these problems consists of long-term monitoring via remote sensing and collection of ground information [21,22].

A wide range of studies proved the applicability of techniques using remote sensing data for topsoil mapping. In the following, some of them are described. Landsat 5 TM imagery was used to detect basalt

outcrops for supporting soil mapping, applying reflectance values, band ratios and indices [23]. Landsat 7 ETM+ data were used to determine surface soil properties with the help of laboratory-analyzed surface soil samples [24]. The ASTER multispectral bands and derived indices and ratios were often utilized for lithological mapping [25–28]. ASTER data were also used to identify mineral components in tropical soils using reflectance spectroscopy signatures from soil samples [29].

Various studies include additional variables, especially in geostatistical approaches of the spatial soil distribution [5]. Topographical features, in particular, provide information on the terrain and, hence, on soil formation processes [30]. Mulder *et al.* [31] used ASTER data and derivatives, as well as elevation as topographical proxy for DSM. Hahn and Gloaguen [32] compared different input variable combinations of ASTER-derived land use, geology, topographical parameters and others to estimate soil distribution by support vector machines (SVM). Rossel and Chen [33] used Landsat data and derivatives, topographical derivatives, climate parameters, as well as soil, geological and radiometric maps and spectrometry results from soil samples to determine the surface soil properties for Australia. Selige *et al.* [34] found out that soil organic matter and soil texture of topsoil correlate with the spectral properties of a hyperspectral sensor. They were also able to model the distribution of sand, clay, organic carbon (C_{org}) and nitrogen. SAR backscatter intensity information from X-, C- and L-band sensors proved to be sensitive for soil moisture differences, surface roughness and, to some extent, also to soil texture [13,14,35–41]. Hengl *et al*. [42] applied an automated random forest approach to map soil properties of Africa with DEM-based landforms parameters and MODIS data at a spatial resolution of 250 m for the Africa Soil Information Service (AfSIS) project. A comprehensive overview about remote sensing in soil mapping is provided by Mulder *et al.* [5] and with a special focus on Africa by Dewitte *et al*. [6].

The lithologies and the soils of the Lake Manyara basin have complex genetic origins. The Proterozoic gneissic basement, tectonic and volcanic processes, as well as the (paleo-)hydrological processes and the sedimentation of the paleolake Manyara influence soil formation. This results in a small-scale distribution and fuzzy transitions of today's soils, topsoils and outcropping lithology, which cannot be depicted by the available soil map for the region with a scale of 1:2,000,000 [43]. Consequently, the categorization of soils is a complex process due to their three-dimensional nature. Hence, remotely-sensed surface features yield auxiliary information of topsoil characteristics and their distribution. Combined with topographic information, the analysis results in valuable information that allows also a rough identification of soil types.

The aim of this study is to map the distribution of the topsoil and surface substrate characteristics using multispectral, topographical and SAR input data. The laboratory analysis of surface samples provides soil properties used to categorize and characterize the topsoils and surface substrates. In order to improve the topsoil classification, we followed a multiscale approach using: (i) image object segments from a high-resolution WorldView-2 scene; (ii) low-resolution ASTER multispectral data and indices; (iii) X- and C-band SAR backscatter; as well as (iv) topographical derivatives. We compare and discuss the final mapping results with soil catenae covering characteristic transects of the study area.

2. Study Area

The study area is located within the East African Rift System of northern Tanzania; in the surroundings of the Makuyuni village. The area is drained towards the west by the Makuyuni River

disemboguing into the endorheic Lake Manyara Basin (Figure 1). The precipitation calculations from the daily Rainfall Estimate Product 3B42 (V7) of the Tropical Rainfall Measurement Mission (TRMM) show a bimodal rainfall pattern for the years 2000–2013 [44]. For this period, the average annual precipitation of 651 mm is mainly caused by two wet seasons. One occurs between November and January and a second between March and May [45]. This results in a sparsely-vegetated semiarid environment dominated by bushy grassland. The study area is also characterized by a variety of degradation processes due to long dry periods and short, but intensive rainfall events, as well as contributing anthropological factors, like overgrazing [46].

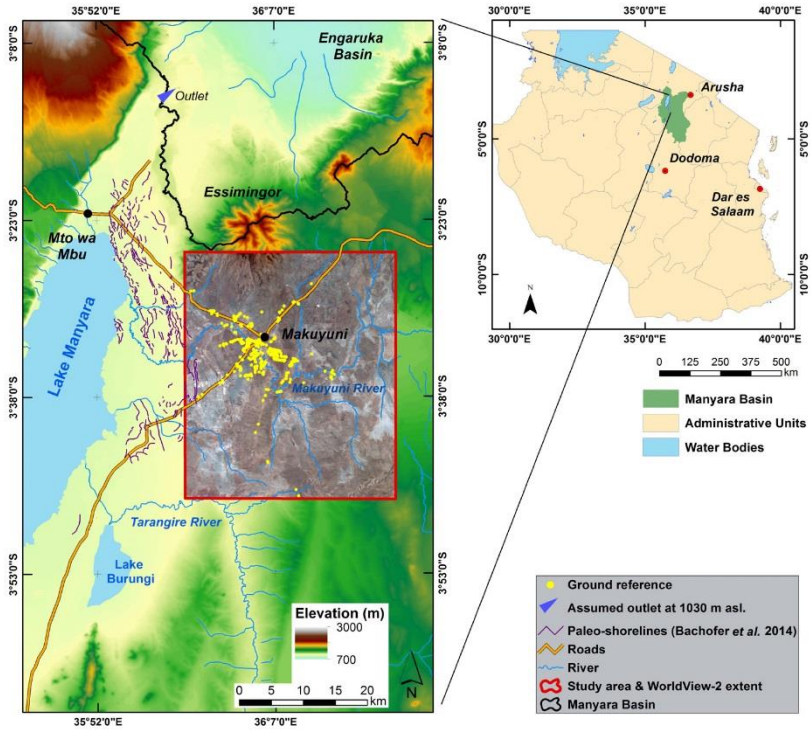

Figure 1. Study area.

The lithology of the study area is very complex, because different lithological units interleave here. The underlying basement of the Masai Plateau is formed of Proterozoic intermediate quartzite and gneisses and is exposed by tectonic faults [47]. Explosive volcanism, especially from the volcano Essimingor, and faulting associated with the rifting of the basin produced alkaline lavas, like alkali basalt, phonolite, nephelinite and tuffs. The volcano Ol Doinyo Lengai (90 km north of the study area) has a carbonate volcanism, and its carbonate tephra deposits are widespread [47–49]. Lacustrine and fluvially deposited sediments can be found 140 m above today's level of Lake Manyara. The so-called Manyara Beds crop out where the Makuyuni River and gully system incise into the lacustrine and terrestrial deposits. The lower member of the Manyara Beds is of lacustrine origin and is composed mainly of mudstones, siltstones, diatomites, marls and tuff that have been deposited in a reducing

environment. These sediments have an age of approximately 1.03–0.633 Ma. A tephra layer, which was dated to 0.633 Ma, marks the transition of the younger upper member of the Manyara Beds [50–52].

3. Input Data and Pre-Processing

Multiscale remote sensing data and their derivatives, as well as topographic indices delineated from a Shuttle Radar Topography Mission (SRTM) DEM served as input information for the analysis. All image datasets were co-registered to ensure complementary datasets.

3.1. WorldView-2

WorldView-2 is a commercial multispectral sensor, which was launched in October 2009. It has a very high geometrical resolution for its' eight multispectral bands (MS) at 1.85 m ground resolution and for the panchromatic band of 0.46 m at nadir [53]. The scene was acquired on 21 February 2011 (Table 1); following the winter wet season and a strong precipitation event mid-February (Figure 2).

Table 1. Optical remote sensing sensors. MS: multispectral.

Sensor	Date	Time (UTC)	No. of Bands	Wavelength	Spatial Resolution
WorldView-2	21 February 2011	08:22	8	0.40–1.04 µm	1.85 m (MS)
ASTER-VNIR	23 August 2006	08:07	3	0.52–0.86 µm	15 m
ASTER-SWIR	23 August 2006	08:07	6	1.60–2.43 µm	30 m

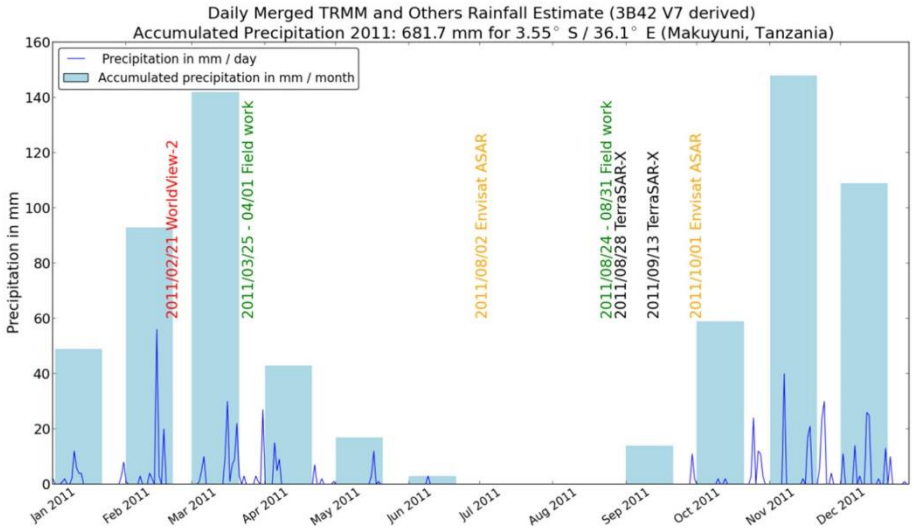

Figure 2. Precipitation, fieldwork and remote sensing data of the year 2011.

3.2. ASTER Bands and Indices

The Advanced Spaceborne Thermal Emission and Reflection Radiometer (ASTER) consists of three subsystems with a spectral coverage in the visible-near infrared (VNIR), the shortwave infrared (SWIR) and the thermal infrared (TIR) wavelength regions (Table 1). ASTER was launched onboard NASA's

TERRA spacecraft in December 1999. The spectral resolution was mainly designed for vegetation, soil and mineral mapping [54]. An ASTER L1B scene was obtained on 23 August 2006 after a long dry season. Because of the cross-detector leakage between the SWIR bands, crosstalk correction was applied using a correction tool from the Earth Remote Sensing Data Applications Centre (ERSDAC) [55].

The six spectral bands of the SWIR system were selected as input features for the analysis. Spectral indices derived from the ASTER VNIR and SWIR bands were also included as input parameters (Table 2). The purpose of these indices is a relative amplification of selective absorption and reflection features, which are caused by different surface materials at distinct wavelengths. They help to detect different mineral compositions, but also to emphasize the spectral differences of target objects. The indices listed in Table 2 are based on a comprehensive literature review.

Table 2. Spectral indices of ASTER VNIR and SWIR bands.

Index with Literature Reference	Formula	Index with Literature Reference	Formula
Alunite/Kaolinite/Pyrophyllite Index [25]	(4 + 6)/5	AlOH Group Index [56]	(5/7)
Alteration/Laterite Index [57]	(4/5)	Alunite Index [28]	(7/5) × (7/8)
Calcite Index [28]	(6/8) × (9/8)	Carbonate/Chlorite/Epidot Index [25]	(7 + 9)/8
Clay—1 Index [25]	(5 + 7)/6	Clay—2 Index [57]	(5 × 7)/(6 × 6)
Dolomite Index [25]	(6 + 8)/7	Ferric Iron (Fe^{3+}) Index [25]	(2/1)
Ferric Oxide Index [56]	(4/3)	Ferrous Iron (Fe^{2+})—1 Index [26]	(1/2)
Ferrous Iron (Fe^{2+})—2 Index [26]	(5/3) + (1/2)	Ferrous Iron/Silicates Index [56]	(5/4)
Kaolinite Index [28]	(4/5) × (8/6)	Kaolin Group Index [56]	(6/5)
Kaolinitic Index [58]	(7/5)	MgOH—1 Index [58]	(6 + 9)/8
MgOH—2 Index [56]	(7/8)	Muscovite Index [58]	(7/6)
OH Bearing Altered Minerals—1 Index [28]	(7/6) × (4/6)	OH Bearing Altered Minerals—2 Index [59]	(4 × 7/6/6)
OH Bearing Altered Minerals—3 Index [59]	(4 × 7/5/5)	Opaque Index [56]	(1/4)
Phengitic Index [58]	(5/6)	Relative Band Depth 6 (RBD6) [26]	(4 + 7)/(6 ×2)
Relative Band Depth 8 (RBD8) [26]	(7 + 9)/(8 × 2)		

3.3. Topographic Indices

During the Shuttle Radar Topography Mission (SRTM) in the year 2000, X-band data were acquired, which provided a DEM with 25 m ground resolution. The SRTM-X dataset has no full coverage worldwide; however, one track covers the study area. The DEM was projected to the Earth Gravitational Model (EGM96) vertical datum. The short wave X-band-derived DEM resulted in good elevation accuracy [60], but also yielded small-scale noise at the surface. To reduce this effect while preserving the topography, we applied a multidirectional Lee filter [61]. The DEM was used to calculate different topographic indices, which characterize the topographic position of the topsoils in the study area (Table 3).

Table 3. Topographic indices.

Index with Literature Reference	Index with Literature Reference
Elevation (height above sea level; a.s.l) [62]	Geomorphons [63]
Slope Length Factor [64]	Morphometric Protection Index [51]
Multiresolution Index of Ridge Top Flatness (MRRTF) [65]	Multiresolution Index of Valley Bottom Flatness [65]
Negative Openness [66]	Positive Openness [51]
Plan Curvature [67,68]	Slope [69]
Stream Power Index [64]	Terrain Classification Index for Lowlands [70]
Terrain Ruggedness Index [71]	Topographic Position Index [72]
Topographic Wetness Index [73]	Vertical Distance to Channel Network [74]

3.4. SAR Data

We acquired two TerraSAR-X (TSX1) (~9.65 GHz; X-band) StripMap and two Envisat ASAR (~5.331 GHz; C-band) scenes for different dates (Table 4). Precise orbits were applied to the ASAR scenes. All SAR scenes were calibrated and radiometrically corrected for topographic effects to gamma naught (γ) using the local incident angle derived from the SRTM-X DEM. The scenes were terrain corrected, and speckle effects were reduced by applying a Lee filter [61]. The two TSX1 scenes were mosaicked to a single dataset in order to cover the whole study area. The images were acquired in the dry season (Table 4; Figure 2), to minimize the influence of soil moisture on the backscatter intensity signal [36–38,75].

Table 4. SAR images. TSX1, TerraSAR-X.

Sensor	Mode	Date	Time (UTC)	Orbit	Incident Angle Range (Degrees)	Polarization	Spatial Resolution
Envisat ASAR	AP	2 August 2011	07:22	Descending	31.0–36.3°	VV/VH	30 m
Envisat ASAR	AP	1 October 2011	07:22	Descending	31.0–36.3°	VV/VH	30 m
TSX1	StripMap	28 August 2011	15:46	Ascending	26.3° (scene center)	HH	3 m
TSX1	StripMap	13 September 2011	15:54	Ascending	44.4° (scene center)	HH	3 m

3.5. Field Reference Data, Laboratory Analysis and Target Classes

During six field campaigns from 2010 to 2014, 602 reference sites were visited within the study area, including fieldwork conducted one month after the acquisition of the WV-2 scene. Because the southern and eastern parts of the study area are remote and partly inaccessible, we decided on a random clustered sampling strategy (Figure 1). The landscape is considered as stable and the mineral components as conservative in relation to the resolution of the input data. The collected parameters consist of: texture, calcium carbonate ($CaCO_3$) content (with hydrochloride acid), soil color, visible mineral components of surface substrates, vegetation cover, topographic position, GPS and photo references. The reference points serve as training and test data for the SVM analysis.

The categorization of soils and topsoils is a complex process. In addition to the description of field reference points, we also conducted laboratory analyses for a better understanding and for the target class selection. From 27 reference locations, surface substrate samples (0–2 cm) were collected and physical and chemical analyses conducted (Table 5). Soil samples were air-dried and sieved (<2 mm).

Texture was analyzed with the Bouyoucos hydrometer method after dispersing the samples with 1N sodium hexametaphosphate and represented according to the United States Department of Agriculture (USDA) classification [8]. $CaCO_3$ was measured using the methods proposed in Buurman *et al.* [76]. C_{org} was determined using the Springer and Klee method [77]. Available fractions of heavy metals (Fe and Mn) were extracted according to the Lindsay–Norwell procedure [78]. Exchangeable bases (K, Ca, Mg and Na) are analyzed based on the Mehlich 3 method [79]. The field reference collection and the laboratory samples resulted in seven topsoil classes (Table 5), two additional lithological classes (Figure 3) and a class for surface water (Class 1), which includes the Makuyuni River and water reservoirs for cattle farming and irrigation.

Table 5. Laboratory analysis of topsoil samples (meq = milliequivalents; mmol = millimoles).

		Laboratory Analysis														
Class	**Number of topsoil Samples**	**Coarse Sand (0.5–2 mm) in g/kg**	**Fine/Medium Sand (0.05–0.5 mm) in g/kg**	**Silt (0.002– 0.05 mm) in g/kg**	**Clay (<0.002 mm) in g/kg**	**Calcium Carbonate $CaCO_3$ in g/kg**	**Organic Carbon (C_{org}) in g/kg**	**Iron (Fe) in mg/kg**	**Manganese (Mn) in mg/kg**	**Aluminium (Al) in mg/kg**	**Calcium Cation (Ca^{2+}) in meq/100 g**	**Magnesium Cation (Mg^{2+}) in meq/100 g**	**Sodium Cation (Na^{+}) in meq/100 g**	**Potassium Cation (K^{+}) in meq/100 g**	**Chlorides (Cl) in mg/kg**	**Water soluble Sulfate (SO_4) in mmol/kg**
2	4	117.25	503.75	166.00	279.50	128.00	2.75	4.01	7.60	0.28	7.53	4.40	4.87	0.97	91.37	8.87
3	5	74.80	344.80	143.80	367.60	115.60	20.62	6.54	20.72	0.17	18.88	5.09	6.77	1.80	59.90	45.78
4	4	92.60	216.00	416.60	274.80	26.79	14.61	9.64	36.80	0.21	24.13	6.07	6.31	1.88	13.86	8.54
5	1	83.00	280.00	134.00	475.00	2.00	9.80	9.17	20.14	0.22	22.46	3.70	6.10	1.08	7.20	7.80
6	7	134.86	327.57	317.14	220.43	12.29	15.47	9.09	49.80	0.25	14.98	4.66	5.81	2.24	10.01	6.94
7	4	384.00	374.50	156.75	120.75	0.75	10.05	5.70	40.48	0.25	4.79	1.54	0.26	1.46	18.68	10.20
8	2	41.00	235.50	101.00	278.50	25.00	15.85	26.40	76.04	0.47	18.25	7.77	0.21	2.44	14.25	8.90

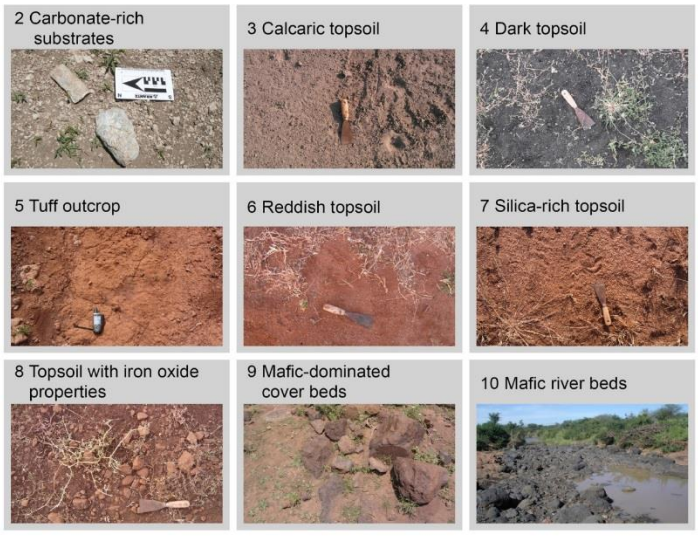

Figure 3. Target classes identified by field surveys and laboratory analysis (Class 1 = water).

"Carbonate-rich substrate" (Class 2) mostly consists of erosive areas with lacustrine sediments and more than 20% carbonate gravel or concretions. Class 2 appears with the Lower Manyara Beds, associated calcaric Regosols and secondary hardened carbonates. The $CaCO_3$ content is rather high (128 g/kg) and the C_{org} content relatively low (2.75 g/kg). "Calcaric topsoil" (Class 3) features a high $CaCO_3$ content and a comparatively high clay content. "Dark topsoil" (Class 4) shows the highest silt content, is dark in color (Munsell® color: hue of 7.5 or 10 YR (yellow red); values of ≤3 or lower; chroma of ≤2), has a low $CaCO_3$ content compared to "Class 3" and a low Fe content compared to "Class 8". It is associated with colluvial and fluvial deposits. "Tuff outcrop" (Class 5) defines distinct outcropping layers of hardened tuff. "Reddish topsoil" (Class 6) has a distinct hue of 5 YR or redder (Munsell® color) and can be distinguished from "Class 3" by a low $CaCO_3$ content, from "Class 4" by color and texture, from "Class 7" by texture, cations and Fe content and from "Class 8" by Fe and Mn content. "Silica-rich topsoil" (Class 7) is associated with the felsic basement and the high quartz sand and grit content, which is a surface residual due to selective erosion. The hue of the soil is 5–7.5 YR; the color value is 4; and the chroma 6–4 (Munsell® color). The "Topsoil with iron oxides properties" (Class 8) class describes a soil associated with mafic lithology (Class 9) and with a high Fe and Mn content, which makes it clearly distinguishable from "Class 3" and "Class 4". "Mafic-dominated cover beds" (Class 9) describe outcroppings and weathered mafic (nephelinite, phonolite, basalt) ridges and the Essimingor volcano. "Mafic river beds" (Class 10) are the same material as "Class 9", but the boulders are hardly weathered, which results in different spectral properties and concentrates within the river beds.

In order to validate and interpret the results of the topsoil and surface substrates' classification procedure, we conducted three soil catenae consisting of 24 soil profiles with detailed profile descriptions according to the World Reference Base for Soil Resources (WRB) 2014 [80].

4. Methods

The workflow consists of several steps (Figure 4): (I) image segmentation based on the high-resolution WorldView-2 images; (II) vegetation and areas affected by clouds and shadowing effects were excluded from further processing; (III) for each remaining segment, mean values of the input feature sets listed in the previous section (Tables 3 and 4) were extracted; (IV) an SVM model was built; (V) SVM-recursive feature elimination (RFE) reduced the number of variables before classifying the segments with the SVM approach; (VI) we compared the results of various input feature set combinations; (VII) accuracy assessment; and (VIII) external validation using soil catenae.

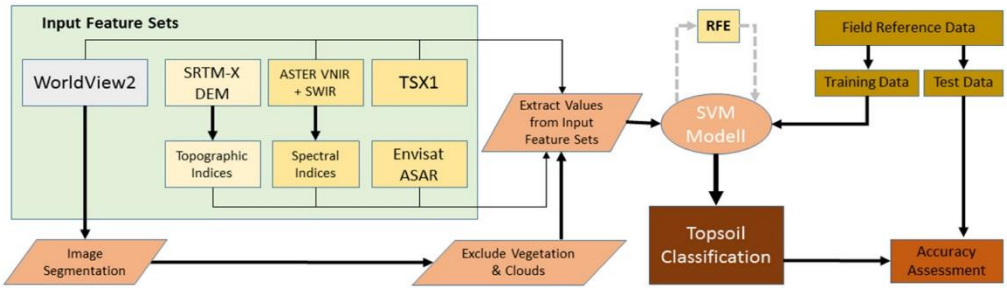

Figure 4. Proposed workflow. RFE, recursive feature elimination.

4.1. Image Object Segmentation

Image objects, which represent contiguous areas in the image, were delineated by multi-resolution segmentation [81]. The segmentation is purely based on the WorldView-2 bands. The reasons for applying an object-oriented approach are reduced processing costs, the possibility to extract values from multiple scales and the option to generate additional object-based input features. The multi-resolution segmentation is a bottom-up approach, which applies region merging beginning with the pixel level [82]. The heterogeneity measurement f (Equation 1), which defines if objects are merged, is controlled by a threshold. If the heterogeneity measure exceeds the threshold, which is determined by the scale parameter, the merging of image objects is terminated. Δh_{color} defines the difference in spectral heterogeneity and Δh_{shape} the consideration of the smoothness and compactness of the image objects. w_{color} and w_{shape} are the according weight measures [82].

$$f = w_{\text{color}} \times \Delta h_{\text{color}} + w_{\text{shape}} \times \Delta h_{\text{shape}}, w_{\text{color}} \in [0, 1,], w_{\text{shape}} \in [0, 1,] \, w_{\text{color}} + w_{\text{shape}} = 1 \quad (1)$$

Roads and buildings were easily identified from the resulting segments by spectral values, shape and spatial relations. Since the image acquisition took place shortly after the winter rainy season, we could verify in the field that, with the exception of some rare occasions, all vegetation cover was photosynthetic active. Therefore, vegetation cover was determined by NDVI thresholding, utilizing a histogram. These three land cover types were excluded from further processing, since they are not the focus of the research objective. This is especially important for the vegetation, because the influence on the spectral response (dead organic materials, as well as photosynthetic vegetation) is considered high [20].

After this pre-selection, 47% of the study area of 1200 km^2 was considered as open soil or vegetation-free lithology. Some of the reference points had to be excluded from further analysis, leading to 432 vegetation-free reference points. The 1,005,058 image segments result in an average mapping unit of 550 km^2. For these image objects, mean values from the SAR images, ASTER bands and indices, as well as from topographic parameters were extracted. The following additional input features were computed from WV2: (i) standard deviation for all spectral bands; (ii) NDVI [19]; (iii) spectral brightness; and (iv) texture homogeneity measure following Haralick *et al.* [83].

4.2. Support Vector Machines

The machine learning concept of SVM was developed to solve binary problems in pattern recognition applications. The development and theoretical background is published by Vapnik [84,85], Hearst [86], Burges [87] and Schölkopf and Smola [88]. Remote sensing studies make use of SVM properties, like high computation performance and high classification accuracies with small numbers of training samples [89]. Recent studies used SVM approaches to identify lithological units with remote sensing data [90,91].

The fundamental principle of SVM is the maximization of margins between training samples of two target classes. Not all features of the training dataset are used for this approach; only those samples that are close to the margin. They serve as support vectors, which are used to define the boundaries of the margin. A maximized margin is referred to as the optimal separating hyperplane [87]. To prevent an over-fitting of the hyperplane caused by outliers in the training dataset, a “soft margin” approach was introduced [92]. This approach uses a cost parameter (C), which determines a penalty for the support

vectors. Low *C* values indicate a stronger generalization of the model; high values provide more influence for single input features [93].

For this study, we utilized a support vector classifier (C-SVC) provided by the Library for Support Vector Machines (LIBSVM) [94]. C-SVC works as a "one-against-one" classifier that discriminates between two target classes. A multi-class approach is solved by constructing multiple target value pairs. In some cases, including soil-related issues, it is hardly possible to separate the target classes in a single input space with a linear function [32]. SVMs therefore project the input features in an n-dimensional feature space. To avoid the computational effort of projecting all input features into a multi-dimensional feature space, kernels can be used to calculate their dot product in the feature space. Various kernels can be applied with SVMs. In this study, a radial basis kernel function (RBF) was utilized, which is widely used when a nonlinear distribution of feature values is expected [32,95]. A linear kernel serving as reference was also applied. The width of the RBF, and hence, the influence of a training sample on the adjacent feature space, is controlled by the constant γ. High values indicate a strong influence, whereas low values indicate a weak influence. Thirty percent of the reference samples (130) were randomly selected to serve exclusively as test datasets, and the remaining 70% was used for the training of the SVM model. All input feature sets were scaled to a range of $[-1, +1]$. For the derivation of the constants *C* and γ, a grid search was conducted by an iterative cross-validation of the performance of fitting the model to the training data [94].

4.3. Recursive Feature Selection

In order to identify a minimum subset of features that contribute to the discrimination of the target classes, a RFE technique was applied [96]. Many of the spectral and topographical input features carry redundant information. A subset of features provides, in addition to a higher computation performance, the possibility for a better interpretation of the interrelation between the topsoil reference and the spectral and topographic parameters of the datasets explaining the topsoil distribution. RFE is a backward elimination method, which starts with a full set of features and iteratively reduces their number according to their contribution to the classification accuracy [97]. For this, the SVM classifier is trained at each iteration, and a ranking criterion is computed for all features. The feature with the smallest criterion is then removed before the next iteration [98]. SVM-RFE was performed with the e1071 package [99].

5. Results and Discussion

The comparison of different input feature groups shows that all additional input features increase the overall accuracy of the classification (Table 6). The classification of only the spectral bands of WorldView-2 with an RBF-kernel reaches an accuracy of 62.9%. By incorporating more features from the ASTER data, SAR scenes and topographic indices, an overall accuracy of 70.4% was achieved. By conducting the classification with the parameters selected by RFE (Table 7), the highest accuracy of 71.9% was reached. The application of a linear kernel instead of an RBF-kernel led to lower accuracies.

Table 6. Overall accuracies for different input feature groups. RBF, radial basis function.

Input Feature Groups	No. of Input Features	*C*	g	Overall Accuracy
WorldView-2	8	1896.0	0.0625	62.9%
WorldView-2 + WV2 derivatives	8 + 11	185,363	0.00006	63.7%
WorldView-2 and SAR scenes	8 + 5	16	0.0625	65.2%
WorldView-2 and ASTER bands / indices	8 + 33	181.02	0.0055	64.4%
WorldView-2 and topographic parameters	8 + 16	65,536.0	0.00005	67.4%
All available parameters	73	2.82	0.0883	70.4%
Selection from RFE (linear kernel)	24	1.41	-	66.6%
Selection from RFE (RBF-kernel)	38	4.00	0.1250	71.9%

Table 7. Relevance ranking of RFE selected input features. SD, standard deviation.

RFE Rank	Input Feature	RFE Rank	Input Feature	RFE Rank	Input Feature
1	Geomorphons	2	MRRTF	3	WV2—Band 3
4	Ferric Iron (Fe^{3+}) Index	5	WV2—Band 1	6	Calcite Index
7	AlOH Group Index	8	WV2—SD Band 3	9	Ferrous Iron 1 Index
10	Ferric Oxide Index	11	RBD8	12	WV2—Band 8
13	WV2—Band 4	14	WV2—SD Band 1	15	Alteration/ Laterite Index
16	ASTER SWIR Band 6	17	Opaque Index	18	Clay 2 Index
19	MgOH 2 Index	20	WV2—SD Band 4	21	WV2—Band 2
22	Kaolinite Index	23	Terrain Ruggedness Index	24	TSX1 HH intensity
25	Envisat ASAR (1 October 2011 VV)	26	WV2 NDVI	27	ASTER SWIR Band 4
28	Morphometric Protection Index	29	WV2—Band 7	30	ASTER SWIR Band 3
31	WV2—SD Band 8	32	WV2—Brightness	33	Envisat ASAR (2 August 2011 VV)
34	Elevation (height a.s.l.)	35	Topographic Wetness Index	36	Texture (homogeneity)

An RFE was performed for the dataset with all 73 input features. The RFE shows that with seven input features, an accuracy exceeding 60% can be attained (Figure 5). The classification accuracy for the SVM, with an RBF-kernel, peaks with a selection of 36 input features, then performs relatively stable until the maximum number of input features is reached. The so-called Hughes phenomenon, which describes the decrease in classification accuracy when additional input features are added to an already large dataset, cannot be observed with the RBF-kernel [100]. Yet, a small decrease can be noted for the linear kernel (Figure 5). The 36 input features from the RFE selection represent all input feature groups (Table 7). Out of the first seven input features, two are topographic indices. The MRRTF results in high values for flat elevated areas [65], and the geomorphons (geomorphologic phonotypes) classify the topography into landscape elements [63]. Both features describe the position of the target classes in the study area. WV2 contributes, along with the spectral Bands 3 and 1, two further

input datasets. The ASTER Calcite Index and the Ferric Iron (Fe^{3+}) Index may explain the distribution of the two target classes with high $CaCO_3$ content (Classes 2 and 3) and the topsoil class with iron oxide properties (Class 8). The AlOH Group Index may support the discrimination of clay minerals [56].

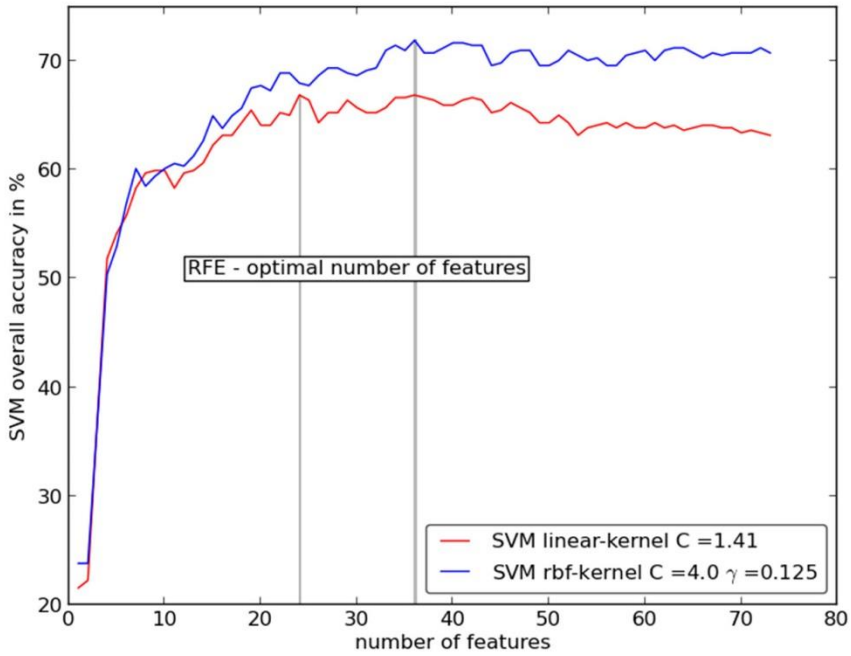

Figure 5. Accuracy curves from RFE for a linear and an RBF-kernel.

The confusion matrix of the RFE-selected input feature dataset reveals that the most competitive classes, concerning the user's and the producer's accuracy, are Class 2 "carbonate-rich substrates" and Class 3 "calcaric topsoil" (Table 8). Both classes have high carbonate content, and the topographic position is overlapping. The difference between both classes is related to the amount of $CaCO_3$ concretions, which are much higher in the lacustrine deposits. If we were to merge both classes, the overall accuracy would reach 79%. However, the visual validation shows a reasonable distribution for both classes. Class 3 also overlaps with Class 4 "dark topsoil". Class 4 is associated mainly with colluvial and fluvial deposits and shows low $CaCO_3$ content. The transition to Class 3 is gradual. The low producer's accuracy of Class 5 "tuff outcrop" can be explained by the relatively small area of these outcrops. The producer's accuracy of this particular class is higher (75%) when only applying the WV2-related input parameters, but the medium-resolution information of the ASTER- and DEM-derived features seems to corrupt the correct identification.

Table 8. Confusion matrix for RFE classification with RBF-kernel ($C = 4$, $g = 0.125$).

		Classified Data										Producers Accuracy
		1	**2**	**3**	**4**	**5**	**6**	**7**	**8**	**9**	**10**	
Reference Class	**1**	6	0	0	0	0	0	0	0	0	0	100%
	2	0	8	5	0	0	0	0	0	0	0	62%
	3	0	5	12	3	0	0	0	0	0	0	60%
	4	0	0	2	19	0	0	0	0	0	1	86%
	5	0	1	0	0	5	1	2	1	0	0	50%
	6	0	0	0	0	0	9	3	0	0	0	75%
	7	0	1	1	0	0	0	12	0	0	0	86%
	8	0	0	1	2	0	0	1	10	2	0	63%
	9	0	0	2	2	0	0	0	0	6	0	60%
	10	0	0	2	0	0	0	0	0	0	10	83%
Users Accuracy		100%	53%	48%	73%	100%	90%	67%	91%	75%	91%	Overall Accuracy 97/135 = 71.9%

"Carbonate-rich substrates" mainly represent the lacustrine lower member of the Manyara Beds, which are exposed prevalently at the foot of slope and mid-slope positions of the Makuyuni River system, as well as in associated gully systems (Figure 6). The class "calcaric topsoil" indicates soils that show an enrichment of $CaCO_3$ due to inputs from carbonatic volcanic ash deposits or development processes upon the "carbonate-rich substrates". In some cases, $CaCO_3$-rich soils developed on secondary translocated carbonates or consist of eroded soils exposing $CaCO_3$ concretions. The latter ones were identified during fieldwork in areas with higher slope degrees or large specific catchment areas. "Tuff outcrops" (Class 5) were recognized at a stratigraphic position above the lower member of the Manyara Beds, which coincides with the results of fieldwork and reviewed scientific literature [47]. The outcrops are too minuscule to be displayed in the map (Figure 6). The class "reddish topsoil" is identified with satisfying accuracy. This class is located mainly on stable flat ridge tops and is used agriculturally. Consequently, topsoils are disturbed and reworked by ploughing activity, bringing leached $CaCO_3$ back to the surface (Table 5). This makes the difference in Class 7 "silica-rich topsoil". These soils are not disturbed, and consequently, silica enriches at the surface due to selective erosion processes. "Silica-rich topsoils" and "reddish topsoils" developed on the Proterozoic intermediate quartzite and gneisses of the Masai Plateau, occur especially in the south of the study area. However, also, these areas were subject to carbonatic volcanic ash deposits. The topsoils with iron oxide properties (Class 8) occur in association with mafic ridges (phonolite, nephelinite) or along the slopes of the Essimingor volcano (Figure 6). Class 9 "Mafic-dominated cover beds" was identified well. Like Class 8, Class 9 can be found at the volcano slopes and on the mafic ridges. Since the cover beds are densely vegetated by shrubs, only small, vegetation-sparse areas were used for the classification. The "mafic river beds" are often covered by vegetation and water. Nevertheless, the mafic material at point bars in the Makuyuni River was traced with high accuracies.

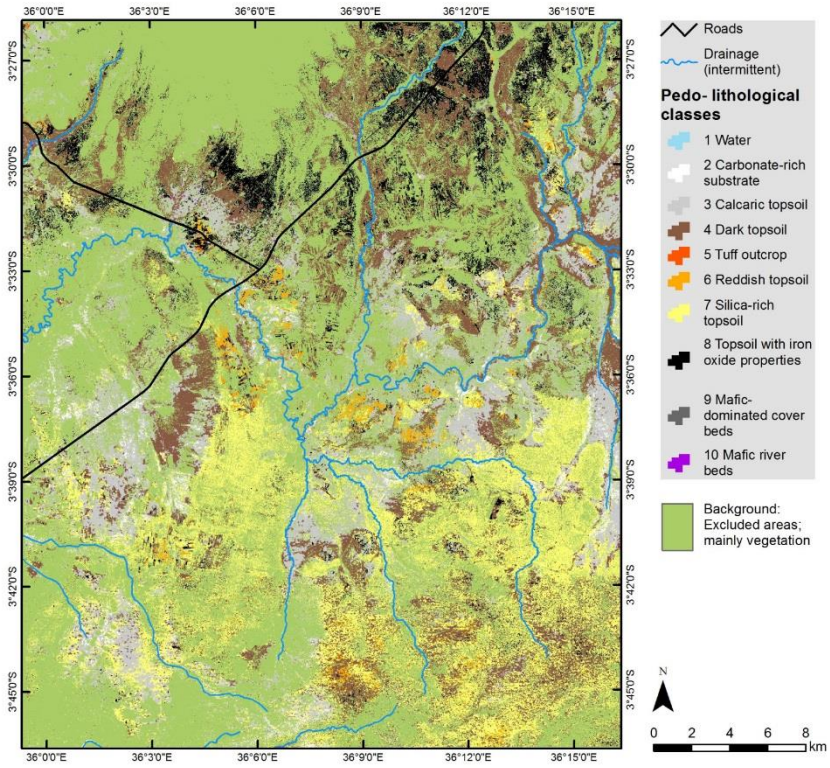

Figure 6. Final classification of topsoil distribution in the study area.

Out of 24 soil profile analyses conducted in the study area, we identified seven main soil types (see Figure 7). In the following, we show that these topsoils can be related to or associated with specific WRB soil types according to the applied catena approach. Vertisols are found in flat areas and in depressions characterized by high clay contents and representing formerly wet positions, related to a high biomass production. They are associated with "dark topsoil" (Class 4). Vertisols occur in association with Vertic Cambisols (Clayic) (Soil Profile 1; Figure 7b) that also relates to the pedo-lithological Class 4 "dark topsoil". In the study area, Calcisols occur with lacustrine "carbonate-rich substrates" (Class 2) and "calcaric topsoils" (Class 3), which are characterized by eroded Luvisols exposing $CaCO_3$ concretions.

Andosols are located on flat and stable ridge positions with low erosion potential. These soils developed from parent material of volcanic origin, such as volcanic ash, tuff and pumice. They show high mineral proportions indicating fertile soils suitable for crop production. In our analysis, Andosols co-exist with "reddish topsoils" (Class 6). Cambisols are widely distributed in the study area and occur mainly on relatively flat mid-slope positions. Along the Makuyuni River terraces, they are distinguished as Cambisols (Colluvic) (Soil Profiles 15–17; Figure 7). On flat ridge positions, they develop as Andic Cambisol (Soil Profiles 6, 8 and 9, Figure 7). Rhodic Cambisols (Soil Profile 20; Figure 7c) are particularly located on intensively-used agricultural fields and correlate with "reddish topsoils" (Class 6), showing a dark reddish brown 5 YR 3/4 Munsell® color for the first 15 cm of soil depth. Cambisols and Luvisols are associated with each other and correlate with "silica-rich topsoils" (Class 7) and

"reddish topsoils" (Class 6). The Haplic Ferralsol (Soil Profile 14; Figure 7d) correlates with "silica-rich topsoil" (Class 7). These soils developed on a weathered felsic basement.

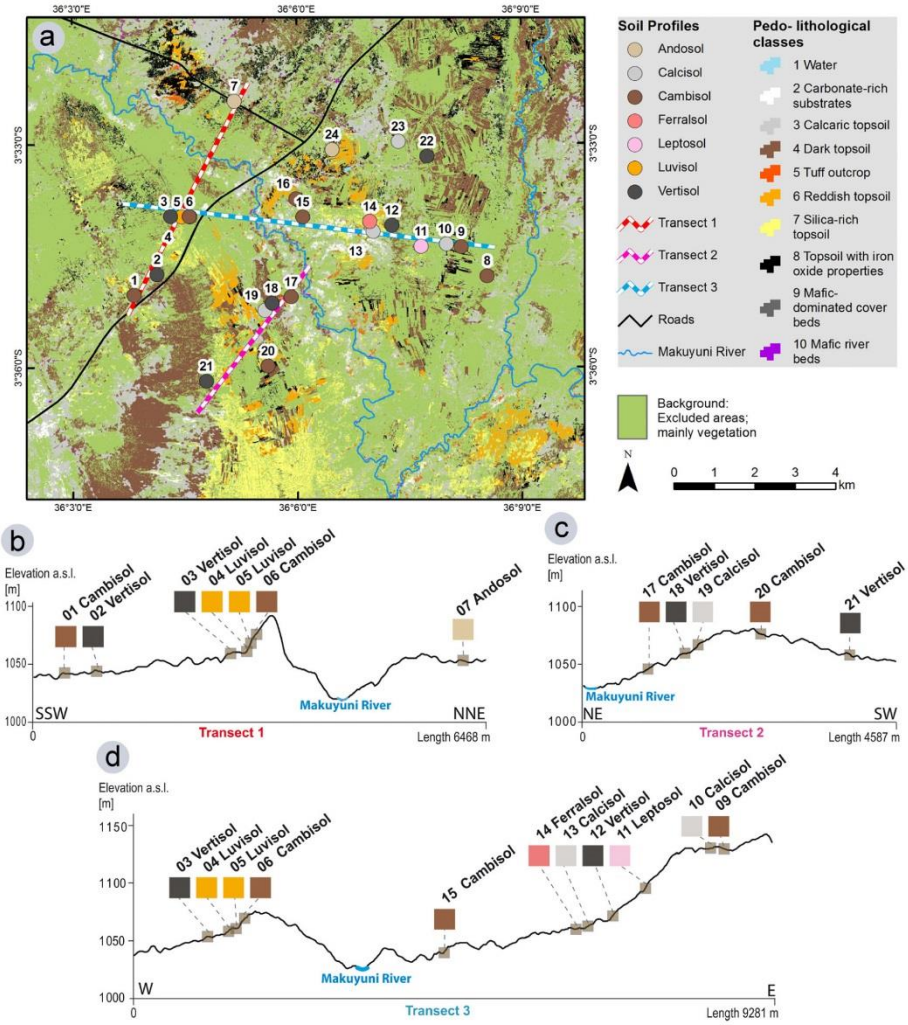

Figure 7. Section of the classification with soil profile transects. (**a**) Map with soil profile transects; (**b**) Soil profile transect 1 (SSW – NNE orientation); (**c**) Soil profile transect 2 (NE–SW orientation); (**d**) Soil profile transect 3 (W–E orientation).

The resulting map provides a very detailed distribution of topsoils and surface substrates for the study area, which outcompetes other spatial soil information available for this region, like the official soil map by De Pauw [43], the 250 m Africa Soil Information Service (AfSIS) product [42] or the products from the Soil and Terrain Database (SOTER) program [101]. Furthermore, the comparison with the soil profile catenae shows that the detailed topsoil information can be related to specific WRB-based soil types with little additional fieldwork and/or expert knowledge. Nevertheless, providing detailed

information on topsoils and surface substrates in comparison to other DSM studies [31,32,42] remains the main intention of the paper.

6. Conclusions

The introduced study has mapped the distribution of topsoils and lithology in a study area in the semiarid Lake Manyara Basin. Applying an integrated approach, combining surface characteristics and terrain features, the spatial distribution of topsoils and related soil types was derived. The topsoils have complex genetic origins related to different substrates, resulting in a high spatial heterogeneity. The non-vegetated areas were classified with a multisensoral approach, which included WV2 and ASTER multispectral data, the TSX1 and Envisat ASAR SAR scenes, and topographical indices were derived from SRTM-X data. With a C-SVC and an RBF-kernel, an overall accuracy of 71.9% was achieved for a challenging classification depth of 10 target classes. The final map is coherent with field observations and laboratory analysis of 27 soil samples. The applied methodological approach seems suitable for multiscale and multisensoral datasets of large areas. We show that the topsoil classification can be associated with soil profiles obtained by fieldwork and certain terrain positions derived from DEM, thus allowing a distinct spatial attribution of soil types.

The results of the topsoil classification and the related soil type association give valuable information, which can help to find locations for agricultural projects in the region and may thereby support the transition to the sustainable self-subsistence of the local population. This may contribute to a reduction of cattle-induced overgrazing and subsequent land degradation. For many applications, like archaeological field studies and paleontological surveys, high-resolution topsoil and surface substrate information yields greater insight than low-resolution soil type maps. The results of this work also help to explain the geological situation of the study area and the landscape evolution. Despite the potential influence of different fluvial and mass movement processes on the topsoil distribution, this study draws a valuable picture of the general situation.

Acknowledgments

This study was financed by the Heidelberg Academy of Sciences and Humanities research center: “The Role of Culture in Early Expansions of Humans” (ROCEEH). The WorldView-2 scene is courtesy of the DigitalGlobe Foundation. We would like to thank the DLR and the German Remote Sensing Data Center (DFD) for providing the TerraSAR-X and the SRTM/X-SAR data. The European Space Agency (ESA) provided the Envisat ASAR data. We acknowledge the support of Deutsche Forschungsgemeinschaft and Open Access Publishing Fund of Tuebingen University. We also want to acknowledge the EU International Research Staff Exchange Scheme (IRSES) Fluvial processes and sediment dynamics of slope channel systems (FLUMEN) (PIRSES-GA-2012-318969) project financing the exchange of researchers.

Author Contributions

Felix Bachofer designed and implemented the research of this study. He processed the remote sensing data, conducted the analysis and drafted the manuscript. Geraldine Quénéhervé analyzed the soil profiles. Felix Bachofer, Geraldine Quénéhervé and Michael Maerker contributed to the collection of

ground reference data during three field campaigns from 2010–2014. Furthermore, Felix Bachofer, Geraldine Quénéhervé, Volker Hochschild and Michael Maerker contributed to the data interpretation and supervised the manuscript construction.

Conflicts of Interest

The authors declare no conflict of interest.

References

1. Solomon, A.M.; Webb, T., III. Computer-aided reconstruction of late-quaternary landscape dynamics. *Annu. Rev. Ecol. Syst.* **1985**, *16*, 63–84.
2. Moore, I.D.; Gessler, P.E.; Nielsen, G.A.; Peterson, G.A. Soil attribute prediction using terrain analysis. *Soil Sci. Soc. Am. J.* **1993**, *57*, 443–452.
3. Sabins, F.F. Remote sensing for mineral exploration. *Ore Geol. Rev.* **1999**, *14*, 157–183.
4. Anderson, K.; Croft, H. Remote sensing of soil surface properties. *Prog. Phys. Geogr.* **2009**, *33*, 457–473.
5. Mulder, V.L.; de Bruin, S.; Schaepman, M.E.; Mayr, T.R. The use of remote sensing in soil and terrain mapping—A review. *Geoderma* **2011**, *162*, 1–19.
6. Dewitte, O.; Jones, A.; Elbelrhiti, H.; Horion, S.; Montanarella, L. Satellite remote sensing for soil mapping in Africa: An overview. *Prog. Phys. Geogr.* **2012**, *36*, 514–538.
7. FAO. *Topsoil Characterization for Sustainable Land Management, Draft*; Food and Agriculture Organization of the United Nations, Land and Water Development Division, Soil Resources, Management and Conservation Service: Rome, Italy, 1998; p. 74. Available online: ftp://ftp.fao.org/agl/agll/docs/topsoil.pdf (accessed on 23 July 2015).
8. USDA (United States Department of Agriculture). *Soil Survey Manual*; Soil Survey Division: Washington, DC, USA, 1993; p. 437.
9. Broll, G.; Brauckmann, H.J.; Overesch, M.; Junge, B.; Erber, C.; Milbert, G.; Baize, D.; Nachtergaele, F. Topsoil characterization-recommendations for revision and expansion of the FAO-Draft (1998) with emphasis on humus forms and biological features. *J. Plant Nutr. Soil Sci.* **2006**, *169*, 453–461.
10. Graefe, U.; Baritz, R.; Broll, G.; Kolb, E.; Milbert, G.; Wachendorf, C. Adapting humus form classification to WRB principles. In Proceedings of the 4th International Congress of the European Soil Science Societies—Eurosoil, At Bari, Italy, 2–6 July 2012; p. 954.
11. Ben-Dor, E.; Goldlshleger, N.; Benyamini, Y.; Agassi, M.; Blumberg, D.G. The spectral reflectance properties of soil structural crusts in the 1.2- to 2.5-μm spectral region. *Soil Sci. Soc. Am. J.* **2003**, *67*, 289–299.
12. Baghdadi, N.; Cerdan, O.; Zribi, M.; Auzet, V.; Darboux, F.; El Hajj, M.; Kheir, R.B. Operational performance of current synthetic aperture radar sensors in mapping soil surface characteristics in agricultural environments: Application to hydrological and erosion modelling. *Hydrol. Process.* **2008**, *22*, 9–20.

13. Aubert, M.; Baghdadi, N.; Zribi, M.; Douaoui, A.; Loumagne, C.; Baup, F.; El Hajj, M.; Garrigues, S. Analysis of TerraSAR-X data sensitivity to bare soil moisture, roughness, composition and soil crust. *Remote Sens. Environ.* **2011**, *115*, 1801–1810.
14. Aubert, M.; Baghdadi, N.N.; Zribi, M.; Ose, K.; El Hajj, M.; Vaudour, E.; Gonzalez-Sosa, E. Toward an operational bare soil moisture mapping using TerraSAR-X data acquired over agricultural areas. *IEEE J. Sel. Top. Appl. Earth Obs. Remote Sens.* **2013**, *6*, 900–916.
15. Schmugge, T.J.; Kustas, W.P.; Ritchie, J.C.; Jackson, T.J.; Rango, A. Remote sensing in hydrology. *Adv. Water Resour.* **2002**, *25*, 1367–1385.
16. Ben-Dor, E.; Chabrillat, S.; Demattê, J.A.M.; Taylor, G.R.; Hill, J.; Whiting, M.L.; Sommer, S. Using imaging spectroscopy to study soil properties. *Remote Sens. Environ.* **2009**, *113* (Suppl. 1), S38–S55.
17. Bartholomeus, H.; Epema, G.; Schaepman, M. Determining iron content in Mediterranean soils in partly vegetated areas, using spectral reflectance and imaging spectroscopy. *Int. J. Appl. Earth Obs. Geoinf.* **2007**, *9*, 194–203.
18. Grebby, S.; Cunningham, D.; Tansey, K.; Naden, J. The impact of vegetation on lithological mapping using airborne multispectral data: A case study for the north Troodos region, Cyprus. *Remote Sens.* **2014**, *6*, 10860–10887.
19. Rouse, J.W.; Haas, R.H.; Shell, J.A.; Deering, D.W.; Harlan, J.C. *Monitoring the Vernal Advancement of Retrogradation of Natural Vegetation*; NASA/GSFC: Greenbelt, MD, USA, 1974; p. 371.
20. Yang, X.; Guo, X. Quantifying responses of spectral vegetation indices to dead materials in mixed grasslands. *Remote Sens.* **2014**, *6*, 4289–4304.
21. Pickup, G.; Chewings, V.H.; Nelson, D.J. Estimating changes in vegetation cover over time in arid rangelands using landsat MSS data. *Remote Sens. Environ.* **1993**, *43*, 243–263.
22. Trodd, N.M.; Dougill, A.J. Monitoring vegetation dynamics in semi-arid African rangelands: Use and limitations of earth observation data to characterize vegetation structure. *Appl. Geogr.* **1998**, *18*, 315–330.
23. Mitchell, J.; Shrestha, R.; Moore-Ellison, C.; Glenn, N. Single and multi-date Landsat classifications of basalt to support soil survey efforts. *Remote Sens.* **2013**, *5*, 4857–4876.
24. Dogan, H.M.; Kılıç, O.M. Modelling and mapping some soil surface properties of Central Kelkit Basin in Turkey by using Landsat-7 ETM+ images. *Int. J. Remote Sens.* **2013**, *34*, 5623–5640.
25. Rowan, L.C.; Mars, J.C. Lithologic mapping in the Mountain Pass, California area using Advanced Spaceborne Thermal Emission and Reflection Radiometer (ASTER) data. *Remote Sens. Environ.* **2003**, *84*, 350–366.
26. Rowan, L.C.; Mars, J.C.; Simpson, C.J. Lithologic mapping of the Mordor, NT, Australia ultramafic complex by using the Advanced Spaceborne Thermal Emission and Reflection Radiometer (ASTER). *Remote Sens. Environ.* **2005**, *99*, 105–126.
27. Mars, J.C.; Rowan, L.C. Spectral assessment of new ASTER SWIR surface reflectance data products for spectroscopic mapping of rocks and minerals. *Remote Sens. Environ.* **2010**, *114*, 2011–2025.
28. Pour, A.B.; Hashim, M. Application of advanced spaceborne thermal emission and reflection radiometer (ASTER) data in geological mapping. *Int. J. Phys. Sci.* **2011**, *6*, 7657–7668.

29. Vicente, L.E.; de Souza Filho, C.R. Identification of mineral components in tropical soils using reflectance spectroscopy and advanced spaceborne thermal emission and reflection radiometer (ASTER) data. *Remote Sens. Environ.* **2011**, *115*, 1824–1836.
30. Conacher, A.J.; Dalrymple, J.B. The nine unit land surface model and pedogeomorphic research. *Geoderma* **1977**, *18*, 127–144.
31. Mulder, V.L.; de Bruin, S.; Weyermann, J.; Kokaly, R.F.; Schaepman, M.E. Characterizing regional soil mineral composition using spectroscopy and geostatistics. *Remote Sens. Environ.* **2013**, *139*, 415–429.
32. Hahn, C.; Gloaguen, R. Estimation of soil types by non linear analysis of remote sensing data. *Nonlinear Process. Geophys.***2008**, *15*, 115–126.
33. Rossel, R.A.V.; Chen, C. Digitally mapping the information content of visible–near infrared spectra of surficial Australian soils. *Remote Sens. Environ.* **2011**, *115*, 1443–1455.
34. Selige, T.; Böhner, J.; Schmidhalter, U. High resolution topsoil mapping using hyperspectral image and field data in multivariate regression modeling procedures. *Geoderma* **2006**, *136*, 235–244.
35. Gaber, A.; Koch, M.; El-Baz, F. Textural and compositional characterization of Wadi Feiran deposits, Sinai Peninsula, Egypt, using Radarsat-1, PALSAR, SRTM and ETM+ Data. *Remote Sens.* **2010**, *2*, 52–75.
36. Zribi, M.; Chahbi, A.; Shabou, M.; Lili-Chabaane, Z.; Duchemin, B.; Baghdadi, N.; Amri, R.; Chehbouni, A. Soil surface moisture estimation over a semi-arid region using ENVISAT ASAR radar data for soil evaporation evaluation. *Hydrol. Earth Syst.Sci.* **2011**, *15*, 345–358.
37. Zribi, M.; Kotti, F.; Lili-Chabaane, Z.; Baghdadi, N.; Ben Issa, N.; Amri, R.; Duchemin, B.; Chehbouni, A. Soil texture estimation over a semiarid area using TerraSAR-X radar data. *IEEE Geosci. Remote Sens. Lett.* **2012**, *9*, 353–357.
38. Baghdadi, N.; Aubert, M.; Zribi, M. Use of TerraSAR-X data to retrieve soil moisture over bare soil agricultural fields. *IEEE Geosci. Remote Sens. Lett.* **2012**, *9*, 512–516.
39. Vaudour, E.; Baghdadi, N.; Gilliot, J.M. Mapping tillage operations over a peri-urban region using combined SPOT4 and ASAR/ENVISAT images. *Int. J. Appl. Earth Obs. Geoinf.* **2014**, *28*, 43–59.
40. Gorrab, A.; Zribi, M.; Baghdadi, N.; Mougenot, B.; Chabaane, Z. Potential of X-band TerraSAR-X and COSMO-SkyMed SAR data for the assessment of physical soil parameters. *Remote Sens.* **2015**, *7*, 747–766.
41. Baghdadi, N.; Cresson, R.; El Hajj, M.; Ludwig, R.; la Jeunesse, I. Estimation of soil parameters over bare agriculture areas from C-band polarimetric SAR data using neural networks. *Hydrol. Earth Syst. Sci.* **2012**, *16*, 1607–1621.
42. Hengl, T.; Heuvelink, G.B.M.; Kempen, B.; Leenaars, J.G.B.; Walsh, M.G.; Shepherd, K.D.; Sila, A.; MacMillan, R.A.; Mendes de Jesus, J.; Tamene, L.; *et al*. Mapping soil properties of Africa at 250 m resolution: Random forests significantly improve current predictions. *PLoS One* **2015**, *10*, e0125814.
43. De Pauw, E. Soils, physiography and agro-ecological zones of tanzania. In *Crop Monitoring and Early Warning Systems Project, Food and Agriculture Organization of the United Nations. GCPS/URT/047/NET*; Ministry of Agriculture: Dar es Salaam, Tanzania, 1983.

44. Huffman, G.J.; Adler, R.F.; Bolvin, D.T.; Gu, G.J.; Nelkin, E.J.; Bowman, K.P.; Hong, Y.; Stocker, E.F.; Wolff, D.B. The TRMM multisatellite precipitation analysis (TMPA): Quasi-global, multiyear, combined-sensor precipitation estimates at fine scales. *J. Hydrometeorol.* **2007**, *8*, 38–55.
45. Bachofer, F.; Quénéhervé, G.; Märker, M. The delineation of paleo-shorelines in the Lake Manyara basin using TerraSAR-X data. *Remote Sens.* **2014**, *6*, 2195–2212.
46. Kiunsi, R.B.; Meadows, M.E. Assessing land degradation in the Monduli District, northern Tanzania. *Land Degrad. Dev.* **2006**, *17*, 509–525.
47. Schwartz, H.; Renne, P.R.; Morgan, L.E.; Wildgoose, M.M.; Lippert, P.C.; Frost, S.R.; Harvati, K.; Schrenk, F.; Saanane, C. Geochronology of the Manyara Beds, northern Tanzania: New tephrostratigraphy, magnetostratigraphy and 40Ar/39Ar ages. *Quat. Geochronol.* **2012**, *7*, 48–66.
48. Dawson, J.B. *The Gregory Rift Valley and Neogene-Recent Volcanoes of Northern Tanzania*; Geological Society: London, UK, 2008; p. 102.
49. Dawson, J.B. Neogene tectonics and volcanicity in the North Tanzania sector of the Gregory Rift Valley: Contrasts with the Kenya sector. *Tectonophysics* **1992**, *204*, 81–92.
50. Ring, U.; Schwartz, H.L.; Bromage, T.G.; Sanaane, C. Kinematic and sedimentological evolution of the Manyara Rift in northern Tanzania, East Africa. *Geol. Mag.* **2005**, *142*, 355–368.
51. Frost, S.R.; Schwartz, H.L.; Giemsch, L.; Morgan, L.E.; Renne, P.R.; Wildgoose, M.; Saanane, C.; Schrenk, F.; Harvati, K. Refined age estimates and Paleoanthropological investigation of the Manyara Beds, Tanzania. *J. Anthropol. Sci.* **2012**, *90*, 151–161.
52. Bachofer, F.; Quénéhervé, G.; Märker, M.; Hochschild, V. Comparison of SVM and boosted regression trees for the delineation of lacustrine sediments using multispectral ASTER data and topographic indices in the Lake Manyara basin. *Photogramm. Fernerkund. Geoinf.* **2015**, *1*, 81–94.
53. DigitalGlobe WorldView-2. Available online: https://www.digitalglobe.com/sites/default/files/DG_WorldView2_DS_PROD.pdf (accessed on 20 January 2015).
54. Yamaguchi, Y.; Kahle, A.B.; Tsu, H.; Kawakami, T.; Pniel, M. Overview of advanced spaceborne thermal emission and reflection radiometer (ASTER). *IEEE Trans. Geosci. Remote Sens.* **1998**, *36*, 1062–1071.
55. Iwasaki, A.; Fujisada, H.; Akao, H.; Shindou, O.; Akagi, S. Enhancement of spectral separation performance for ASTER/SWIR. *Proc. SPIE* **2002**, *4486*, 42–50.
56. Cudahy, T. *Satellite ASTER Geoscience Product—Notes for Australia*; Commonwealth Scientific and Industrial Research Organisation (CSIRO): Dickson, Australia, 2012; p. 26.
57. Bierwirth, P. *Evaluation of ASTER Satellite Data for Geological Applications*; Consultancy Report to Geoscience Australia: Canberra, Australia, 2002; p. 50.
58. Hewson, R.D.; Cudahy, T.J.; Mizuhiko, S.; Ueda, K.; Mauger, A.J. Seamless geological map generation using ASTER in the Broken Hill-Curnamona province of Australia. *Remote Sens. Environ.* **2005**, *99*, 159–172.
59. Ninomiya, Y.; Fu, B.; Cudahy, T.J. Detecting lithology with Advanced Spaceborne Thermal Emission and Reflection Radiometer (ASTER) multispectral thermal infrared "radiance-at-sensor" data. *Remote Sens. Environ.* **2005**, *99*, 127–139.
60. Hoffmann, J.; Walter, D. How complementary are SRTM-X and -C band digital elevation models? *Photogramm. Eng. Remote Sens.* **2006**, *72/3*, 261–268.

61. Lee, J.S. Digital image enhancement and noise filtering by use of local statistics. *IEEE Trans. Pattern Anal. Mach. Intell.* **1980**, *2*, 165–168.
62. DLR SRTM Digital Elevation Models/SRTM-X Specifications. Available online: https://centaurus.caf.dlr.de:8443/eoweb-ng/licenseAgreements/DLR_SRTM_Readme.pdf (accessed on 3 April 2015).
63. Jasiewicz, J.; Stepinski, T.F. Geomorphons—A pattern recognition approach to classification and mapping of landforms. *Geomorphology* **2013**, *182*, 147–156.
64. Moore, I.D.; Grayson, R.B.; Ladson, A.R. Digital terrain modelling: A review of hydrological, geomorphological, and biological applications. *Hydrol. Process.* **1991**, *5*, 3–30.
65. Gallant, J.C.; Dowling, T.I. A multiresolution index of valley bottom flatness for mapping depositional areas. *Water Resour. Res.* **2003**, *39*, 1347.
66. Yokoyama, R.; Shirasawa, M.; Pike, R.J. Visualizing topography by openness: A new application of image processing to digital elevation models. *Photogramm. Eng. Remote Sens.* **2002**, *68*, 257–266.
67. Zevenbergen, L.W.; Thorne, C.R. Quantitative analysis of land surface topography. *Earth Surf. Proc. Landf.* **1987**, *12*, 47–56.
68. Dikau, R. *Entwurf Einer Geomorphographisch-Analytischen Systematik von Reliefeinheiten*; Heidelberger Geographische Bausteine: Heidelberg, Germany, 1988.
69. Travis, M.R.; Elsner, G.H.; Iverson, W.D.; Johnson, C.G. *VIEWIT: Computation of Seen Areas, Slope, and Aspect for Land-Use Planning*; Pacific Southwest Research Station, Forest Service, U.S. Department of Agriculture: Berkeley, CA, USA, 1975.
70. Bock, M.; Böhner, J.; Conrad, O.; Köthe, R.; Ringeler, A. Methods for Creating Functional Soil Databases and Applying Digital Soil Mapping with SAGA GIS. In *Status and Prospect of Soil Information in South-Eastern Europe*; Office for Official Publications of the European Communities: Luxembourg, 2007; pp. 149–162.
71. Riley, S.J.; DeGloria, S.D.; Elliot, R. A terrain ruggedness index that Quantifies topographic heterogeneity. *Intermt. J. Sci.* **1999**, *5*, 23–27.
72. Guisan, A.; Weiss, S.; Weiss, A. GLM *versus* CCA spatial modeling of plant species distribution. *Plant Ecol.* **1999**, *143*, 107–122.
73. Beven, K.; Kirkby, M.J. A physically based, variable contributing area model of basin hydrology. *Hydrol. Sci. J.* **1979**, *24*, 43–69.
74. Conrad, O. Terrain Parameters described in the SAGA-GIS Software v.2.1.0. Available online: http://sourceforge.net/projects/saga-gis/files/latest/download?source=files (accessed on 10 February 2015).
75. Baghdadi, N.; Camus, P.; Beaugendre, N.; Issa, O.M.; Zribi, M.; Desprats, J.F.; Rajot, J.L.; Abdallah, C.; Sannier, C. Estimating surface soil moisture from TerraSAR-X data over two small catchments in the Sahelian part of western Niger. *Remote Sens.* **2011**, *3*, 1266–1283.
76. Buurman, P.; Lagen, B.V.; Velthorst, E.J.; Lagen, B.; Velthorst, E. *Manual for Soil and Water Analysis*; Backhuys: Leiden, The Netherlands, 1996.
77. Springer, U.; Klee, J. Prüfung der Leistungsfähigkeit von einigen wichtigeren Verfahren zur Bestimmung des Kohlenstoffs mittels Chromschwefelsäure sowie Vorschlag einer neuen Schnellmethode. *J. Soil Sci. Plant Nutr.* **1954**, *64*, 1–26.

78. Lindsay, W.L.; Norvell, W.A. Development of a dtpa soil test for zinc, iron, manganese, and copper. *Soil Sci. Soc. Am. J.* **1978**, *42*, 421–428.
79. Mehlich, A. Mehlich-3 soil test extractant—A modification of mehlich-2 extractant. *Commun. Soil Sci. Plant Anal.* **1984**, *15*, 1409–1416.
80. FAO. *World Reference Base for Soil Resources 2014—International Soil Classification System for Naming Soils and Creating Legends for Soil Maps*; Food and Agriculture Organization of the United Nations: Rome, Italy, 2014.
81. Baatz, M.; Schäpe, A. Multiresolution Segmentation: An optimization approach for high quality multi-scale image segmentation. In *Angewandte Geographische Informationsverarbeitung XII. Beiträge zum AGIT-Symposium Salzburg*; Strobl, J., Blaschke, T., Griesebner, G., Eds.; Wichmann: Heidelberg, Germany, 2000; Volume 12, pp. 12–23.
82. Benz, U.C.; Hofmann, P.; Willhauck, G.; Lingenfelder, I.; Heynen, M. Multi-resolution, object-oriented fuzzy analysis of remote sensing data for GIS-ready information. *ISPRS J. Photogramm. Remote Sens.* **2004**, *58*, 239–258.
83. Haralick, R.M.; Shanmugam, K.; Dinstein, I.H. Textural features for image classification. *IEEE Trans. Syst. Man Cybern.* **1973**, *SMC-3*, 610–621.
84. Vapnik, V.N. *The Nature of Statistical Learning Theory*; Springer: New York, NY, USA, 1995; p. 188.
85. Vapnik, V.N. An overview of statistical learning theory. *IEEE Trans. Neural Netw.* **1999**, *10*, 988–999.
86. Hearst, M.A. Support vector machines. *IEEE Intell. Syst.* **1998**, *13*, 18–28.
87. Burges, C. A tutorial on support vector machines for pattern recognition. *Data Min. Knowl. Discov.* **1998**, *2*, 121–167.
88. Schölkopf, B.; Smola, A.J. A short introduction to learning with kernels. In *Advanced Lectures on Machine Learning*; Mendelson, S., Smola, A.J., Eds.; Springer-Verlag: Berlin/Heidelberg, Germany, 2003; pp. 41–64.
89. Mountrakis, G.; Im, J.; Ogole, C. Support vector machines in remote sensing: A review. *ISPRS J. Photogramm. Remote Sens.* **2011**, *66*, 247–259.
90. Wang, X.; Niu, R.; Wu, K. Lithology intelligent identification using support vector machine and adaptive cellular automata in multispectral remote sensing image. *Opt. Eng.* **2011**, *50*, 076201.
91. Othman, A.; Gloaguen, R. Improving lithological mapping by SVM classification of spectral and morphological features: The discovery of a new chromite body in the Mawat ophiolite complex (Kurdistan, NE Iraq). *Remote Sens.* **2014**, *6*, 6867–6896.
92. Cortes, C.; Vapnik, V. Support-vector networks. *Mach. Learn.* **1995**, *20*, 273–297.
93. Schölkopf, B.; Smola, A.J. *Learning with Kernels: Support Vector Machines, Regularization, Optimization, and Beyond*; MIT Press: Cambridge, MA, USA, 2002; p. 626.
94. Chang, C.C.; Lin, C.J. LIBSVM: A library for support vector machines. *ACM Trans. Intell. Syst. Technol.* **2011**, *2*, 1–27.
95. Foody, G.M.; Mathur, A. Toward intelligent training of supervised image classifications: Directing training data acquisition for SVM classification. *Remote Sens. Environ.* **2004**, *93*, 107–117.
96. Guyon, I.; Elisseeff, A. An introduction to variable and feature selection. *J. Mach. Learn. Res.* **2003**, *3*, 1157–1182.

97. Kohavi, R.; John, G.H. Wrappers for feature subset selection. *Artif. Intell.***1997**, *97*, 273–324.
98. Guyon, I.; Weston, J.; Barnhill, S.; Vapnik, V. Gene selection for cancer classification using support vector machines. *Mach. Learn.* **2002**, *46*, 389–422.
99. Karatzoglou, A.; Meyer, D.; Hornik, K. Support vector machines in R. *J. Stat. Softw.* **2006**, *15*, 1–28.
100. Pal, M.; Foody, G.M. Feature selection for classification of hyperspectral data by SVM. *IEEE Trans. Geosci. Remote Sens.* **2010**, *48*, 2297–2307.
101. ISRIC; Global and National Soils and Terrain Databases (SOTER). *Procedures Manual, Version 2.0*; ISRIC—World Soil Information: Wageningen, The Netherlands, 2013; p. 198.

III Experimental Assessment of Runoff Generation Processes on Hillslope Scale in a Semiarid Region in Northern Tanzania

Authors

Geraldine Quénéhervé, Felix Bachofer and Michael Maerker

Author contribution:

Study design, structure of the paper, data preparation, data analyses, figures, interpretation and writing.

Current status

Published 2015 in *Geografia Fisica e Dinamica Quaternaria* **38**(1), 55–66.

doi:10.4461/GFDQ.2015.38.06

ISSN: 0391-9838

Impact Factor (2015): 0.641

Geogr. Fis. Dinam. Quat.
38 (2015), 55-66, 8 figg., 6 tab.

DOI 10.4461/GFDQ.2015.38.06

GERALDINE QUÉNÉHERVÉ (*), FELIX BACHOFER (**) & MICHAEL MAERKER (*,**)

EXPERIMENTAL ASSESSMENT OF RUNOFF GENERATION PROCESSES ON HILLSLOPE SCALE IN A SEMIARID REGION IN NORTHERN TANZANIA

ABSTRACT - QUÉNÉHERVÉ G., BACHOFER F., & MAERKER M., *Experimental Assessment of Runoff Generation Processes on Hillslope Scale in a Semiarid Region in Northern Tanzania.* (IT ISSN 0391-9838, 2015).

In runoff modelling often saturated conductivities or infiltration rates for saturated surfaces are used to calculate the soil water balance and subsequently surface runoff. These infiltration rates are often too high and thus no or very little runoff is generated. However, after long dry periods even with small precipitation events surface runoff is observed. In this study we focus on the infiltration rates at different tensions to study their effect on surface runoff generation on a typical soil catena of northern Tanzania. The area is characterized by very little information on surface runoff and soil characteristics. Therefore, we measured soil infiltration and texture at the surface as well as overland flow volumes for individual rainfall events between October 10, 2010 and December 6, 2010 using a simple experimental setting. We examined rough water balance quantities for single rainfall events. A simplistic hydrological modelling of the surface runoff and accumulation was performed and compared to measured surface runoff. The study shows that infiltration at 0 water tension clearly overestimates infiltration quantities. However, even when soil characteristics like crusting of sealing are not considered, our simple approach yield much better surface runoff volumes using infiltration rates at higher soil water tensions instead of saturated infiltration conditions. The interaction between rainfall and soil surface conditions is relevant for understanding the hydrology of semiarid savannas with gentle slopes. However, we show that our approach integrating simple field measurements and basic hydrological budget models yield much better results than conventional approaches.

KEY WORDS: Surface Runoff; Hydrological Modelling; Rainfall-Runoff; Hillslope Scale; Tanzania; Surface Runoff Detectors.

INTRODUCTION

Runoff generation in direct response to a precipitation event triggers soil particle detachment and accordingly soil erosion phenomena which are a major threat in sparsely vegetated regions. The factors affecting runoff for event-based analyses are i) rainfall characteristics and climatic conditions (rainfall intensity, duration and distribution), ii) the soil type (soil evaporation, infiltrability, hydraulic conductivity, antecedent condition of the soil moisture, water repellent characteristics, bulk density, surface crusting and surface roughness), iii) vegetation (vegetation cover, organic matter, macropores and root systems), and iv) the catchment area (slope steepness, slope length, landscape position) (after Critchley & Siegert, 1991; Borselli & *alii*, 2001; Bracken & Croke, 2007; Ritter & *alii*, 2011).

However, for a detailed surface runoff assessment especially the soil parameters are often not available or only hardly obtainable requiring sophisticated instruments, trained personnel and the economic resources to measure them. Particularly, semiarid areas around the globe are often characterized by scarce infrastructure and rural environments with no or sparse information on the spatial distribution of soils or related parameters on institutional levels. Moreover, semiarid regions generally show low precipitation that is highly variable (Sala & Lauenroth, 1982; Mualem & Assouline, 1996). Hence, simple low budget approaches are needed to overcome these problems.

In order to assess surface runoff processes in semiarid areas, precipitation events have to be addressed as pulses,

(*) *Institute of Geography, University of Tübingen, Ruemelinstr. 19-23, 72070 Tuebingen, Germany.*

(**) *Heidelberg Academy of Sciences and Humanities, c/o University of Tübingen, Ruemelinstr. 23, 72070 Tübingen, Germany.*

(***) *Dipartimento di Scienze della Terra, Università di Firenze, Italia.*

Corresponding author: Geraldine Quénéhervé, Tel.: +49 7071 2972131. E-Mail address: geraldine.queneherve@uni-tuebingen.de

This work was funded by the Heidelberg Academy of Sciences and Humanities' research centre: 'The Role of Culture in Early Expansions of Humans'. We thank the Tanzania Commission for Science and Technology (COSTECH) for their support and the Manyara Ranch Conservancy, held in trust by the African Wildlife Foundation (AWF) up to 2013, for their access permit. Furthermore, we would like to thank Hauke Sattler for the assemblage of the surface runoff detectors. Finally we would like to thank the EU IRSRS project FLUMEN for support and assistance.

FIG. 1 - Surface runoff shortly after a precipitation event of 15 mm (in 40 min) in the Lake Manyara region (2013-03-16; photo G. Quénéhervé).

isolated in time (Huxman & *alii*, 2004). Small rainfall pulses falling on dry soil surfaces wet only the uppermost part of the soil and a great amount of the soil moisture is accordingly lost by direct evaporation of the bare soil (Sala & Lauenroth, 1982). The soil evaporation front, deepening over time into the soil profile following the topsoil drying, is based on the solar energy reaching the soil surface as well as soil hydraulic properties and root densities (Wallace & *alii*, 1999; Schwinning & Sala, 2004). Rainfall on bare soils change the properties at the vicinity of the soil surface due to physical and chemical processes (Mualem & Assouline, 1996).

When overland flow in sparsely vegetated semiarid regions is generated, it occurs on stretched slopes as prevalent laminar sheetflow. When runoff concentrates further down the slope it becomes turbulent and promotes sediment detachment that leads to linear depressions called rills that are consequently deepened into gullies (Ritter & *alii*, 2011; Wainwright & Bracken, 2011). The runoff on dryland slopes may be highly discontinuous because of spatial and temporal variability in precipitation and in surface properties. The surface roughness significantly affects the pathways and rates of flow transfer. In general, runoff after small precipitation events can only be short distance runoff (Lauenroth & Bradford, 2006). The authors also stated that the common assumption for semiarid regions is that the runoff part of the water balance is close to zero, and hence it is often ignored. Jensen et al. (1990) reported that runoff depends on the characteristics of precipitation and can only be neglected for a particular type of soil, i.e. coarse textured (sand and loamy sand) and moderately coarse textured soils (sandy loams). However, at the event scale there can occur remarkable amounts of surface runoff on top of all kinds of soil texture types (Zema & *alii*, 2012) especially after dry periods, as also experienced by the authors. Figure 1 shows a surface runoff immediately after a 15 mm (in 40 min) event close to the Makuyuni village.

The rate at which water enters the soil is called infiltration rate or infiltration capacity, typically measured in mm/h. Most dryland soils are rarely saturated (Wainwright & Bracken, 2011), therefore the infiltration rate has normally a high initial value that decreases with time until it becomes fairly steady, called final infiltration rate. When rainfall exceeds the rate at which water can infiltrate the ground, surface runoff will be produced, accordingly called Hortonian overland flow (Bracken & Croke, 2007). Generally, as shown by various authors (Mualem, 1976; van Genuchten, 1980; Kutílek & Nielsen, 1994), infiltration rate (Q) is a function of soil water content (Θ) and soil water tension (Ψ). When water is applied into a dry soil, initially, most of the water is absorbed by the capillary potential of the soil matrix. The capillary force triggers the initial water infiltration process. Subsequently, as infiltration proceeds, the gravitational force becomes dominant (Philip, 1957). The critical matrix potential at which air enters the largest pores of a saturated soil is expressed as air entry value. As shown by Regner & *alii* (1999) infiltration processes consist of a soil matrix triggered micropore flow and a soil structure dependent macropore flow. In soils with dominant matrix driven processes, such as coherent soils, the infiltration from 0 tension up to the air entry value normally decreases. When macropores are present, water penetrates the soil mainly by these. The soils dominated by macropores show an immediate increase in infiltration when water tension is rising (Renger & *alii*, 1999; Schwärzel & Punzel, 2007). Apart of other factors like slacking, clogging, drop impact and air entrapment

that we do not consider in this study, infiltration and thus, surface runoff processes are strongly related to the soil's micro- and macropore distribution. Infiltration equation as stated of Philip (1975):

$$I = S \cdot t^{-\frac{1}{2}} \pm A \cdot t \qquad (1)$$

where I is infiltration rate; S is sorptivity; t is infiltration interval; and A is a constant, depending on water content (Θ) and soil water tension (Ψ).

The main objective of this study is to propose a simple approach to assess surface infiltration and runoff generation processes under semiarid climate conditions on hillslope scale. Especially we are interested in the infiltration rates and potential surface runoff at the end of the dry season. This goal is achieved using basic low budget, non-invasive methods that are easily applicable. We focus on the runoff generation mechanisms at hillslope scale with a characteristic soil catena for specific rainfall events. We do not tackle effects such as surface sealing, clogging or crusting since in the described conditions of semiarid environments a sophisticated measurement of these parameters is often not feasible. Instead, we concentrate on infiltration rates triggered by water content and water tension. The hypothesis is that, especially after the dry seasons soils have high water tensions and hence, the isolated rainfall events produce high amounts of surface runoff especially on fine-grained soils. Thus, water conduction is lower than in saturated conditions and consequently the overall infiltration rates quite low. Therefore, we performed detailed surface infiltration measurements using a tension infiltrometer and gained information about surface soil texture distribution. We monitored rainfall events over a three years period and estimated the evapotranspiration dynamics and land cover patterns and validated overland flow volumes with automatic surface runoff detectors.

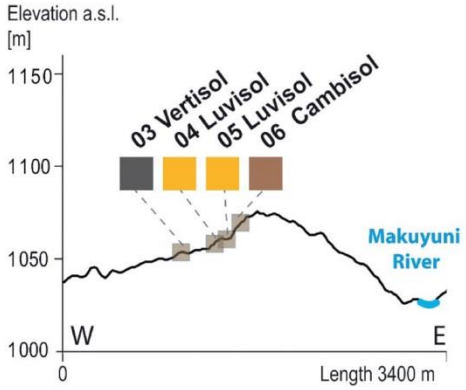

FIG. 2 - Soil transect with three different soil types according to World reference base for soil resources (FAO, 2014).

MATERIALS AND METHODS

STUDY AREA

The study area is located in Northern Tanzania in the eastern branch of the East African Rift System. It is drained by the Makuyuni River (catchment area ~3080 km²) which is flowing into the endorheic Lake Manyara. The prevailing savannah climate is characterized by bi-modal rainy seasons (Sep – Dec and Mar – May) with mean annual rainfall of ca. 500 mm and a strong inter-annual variability. The mean annual temperature is about 27°C, during short dry season (Jan – Feb) 30°C, during long rain season (Mar – May) 26°C, during long dry season (Jun – Sep) 22°C, and during short rain season (Oct – Dec) 27°C.

The study area has an extent of ca. 50 hectares and is located at the Manyara Ranch Conservancy. The morphology is characterized by a low angle stretched slope between 0 – 2.7° dipping towards north west (fig. 2). On the upper slopes Cambisols occur that are developed on tephra deposits and have therefore remaining andic properties (FAO, 2014). They also show leaching of carbonates towards the subsoil where $CaCO_3$ concretions are forming. On the midslope Rhodic Luvisols are located with loamy testure. The soil types in these localities are characterized by a high silica skeleton content with an average quartz mineral diameter of 1 cm. The Luvisol grade laterally into vertic horizons in lower landscape positions, the clay content is increasing and more active layer clays are accumulated. Thus, in the lower slope positions normally Vertisols are found.

FIELD DATA AND REMOTE SENSING ANALYSIS

To test the hypotheses, we conducted detailed surface infiltration measurements and gained information about surface soil texture distribution. Moreover, we monitored rainfall events over a three years period and estimated the evapotranspiration dynamics and landuse patterns. Overland flow volumes were assessed with automatic surface runoff detectors. The calculation of the runoff volumes were performed for single precipitation events. Moreover, we measured the relevant parameters (described below) in the field and in the laboratory or estimated these using remote sensing techniques as outlined below.

DGPS survey

We used a ProMark-3 differential GPS (DGPS) system in order to get very high-resolution digital topographic information. About 36,400 kinematic point measurements were measured and then post processed to orthometric heights (EGM96). The kinematic survey performance of the equipment is 0.012 m + 2.50 ppm (horizontal) and 0.015 m + 2.50 ppm (vertical) (ashtech, 2010). As the rover device was installed on a pole and variations occurred while it was carried over different landforms, we expect a vertical accuracy < 0.1 m + 2.50 ppm. Data acquisition took place in early March 2012, at the end of a short dry period. Thus vegetation and especially leaf cover was sparse and the sky

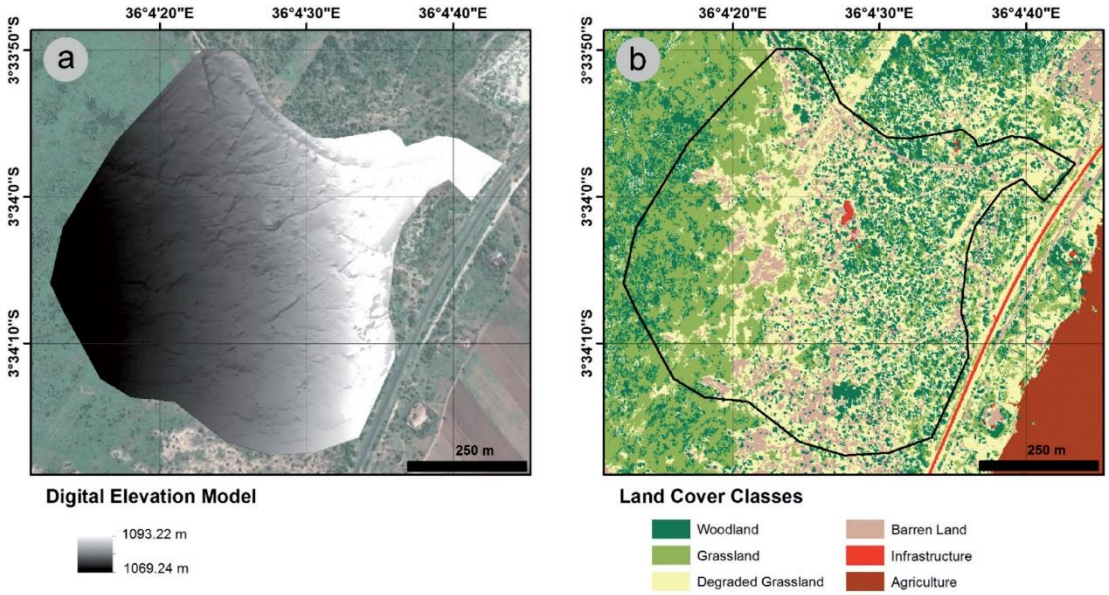

FIG. 3 - Surface runoff shortly after a precipitation event of 15 mm (in 40 min) in the Lake Manyara region (2013-03-16; photo G. Quénéhervé).

visibility of the GPS antenna and the resulting GPS signal lock was excellent. The sampling strategy was adapted to the constrained accessibility by bush vegetation.

The accuracy of the resulting digital elevation model (DEM) depends on the operational GPS precision, as well as the distribution and density of the GPS samples (Nico & *alii*, 2005). Visible drainage lines with a minimum depth of 5 cm were mapped separately with a kinematic survey and function as stream lines for the DEM building. The applied interpolation method is based on the ANUDEM algorithm, which allows the consideration of drainage enforcement to create a hydrological correct DEM (Hutchinson, 1989); Figure 3.

Land cover classification

For the derivation of land cover classes within the study area a multispectral WorldView-2 scene (acquired 2011-02-21; pan-sharpened to 0.5 m ground sampling distance) was utilized. For the analysis the three visible bands (RGB) as well as one near infrared band were available. Following an object based image analysis approach (Blaschke, 2010) five different land cover classes were distinguished (tab. 1) and validated in the field.

Soil characteristics

The calculation of the runoff volumes for single precipitation events is based on relevant parameters measured in the field and in the laboratory or estimated using remote sensing techniques. We measured soil texture for topsoil at 61 locations with a simple finger test method, according to USDA (1993). Additionally, we conducted laboratory analyses from four soil profile locations along a transect (fig. 1). Soil samples were air-dried and sieved (<2 mm). Texture was measured with the Bouyoucos Hydrometer Method after dispersing the samples with 1N Sodium hexametaphosphate and represented according to the United States Department of Agriculture classification (USDA, 1993). Organic Carbon was analysed using the Springer and Klee method (Springer & Klee, 1954). The field reference collection and the laboratory samples resulted into three soil classes, namely Cambisol, Luvisol, and Vertisol (tab. 2).

Meteorological parameters

Our study area is equipped with a multi-sensor climate station (Meteo combined with EnviLog MAXI data logger

TABLE 1 - Land cover classes

Class Number	Class Name	Description
1	Woodland	Trees and shrubs (> 1m)
2	Grassland	Grass, small bushes and sedges (permanent)
3	Degraded Grassland	Dry and sparse grassland (> 33% bare soil)
4	Barren Land	> 66% bare soil
5	Infrastructure	Buildings and paved roads

by EcoTech, Germany) that measures 6 parameters: wind speed and direction, precipitation, air temperature, relative humidity as well as air pressure. Data are measured with high temporal resolution of 10 min intervals and have been collected from March 2010 up to present.

Soil infiltration

With the hood infiltrometer (Umwelt-Geräte-Technik GmbH, Germany), which is a type of tension infiltrometer (Schwärzel & Punzel, 2007), water infiltrability is determined for the soil surface. The unsaturated conductivity was calculated following Wooding (1968) (Equation 2) and (Umwelt-Geräte-Technik, 2005) (Equation 3):

$$Q = \pi a^2 k_u \left(1 + \frac{4}{\pi \alpha a}\right) \quad (2)$$

$$\alpha = \frac{\ln\left(\frac{Q_1}{Q_2}\right)}{h1 - h2} \quad (3)$$

where Q is steady-state flow; a is radius of the infiltration area; k_u is hydraulic conductivity as a function of water tension; and h is water tension.

Accordingly, hydraulic conductivities for different tensions can be calculated using Equations 4 and 5, after Umwelt-Geräte-Technik (2005):

$$k(h_1) = \frac{\frac{Q_1}{\pi a^2}}{\left(1 + \frac{4}{\pi \alpha a}\right)} \quad (4)$$

$$k(h_2) = \frac{\frac{Q_2}{\pi a^2}}{\left(1 + \frac{4}{\pi \alpha a}\right)} \quad (5)$$

The capillary theory can be used to estimate the size of pores excluded from the transmission of infiltration at different pressure heads. Pore diameters can be predicted from Equation 6 (Sauer & Logsdon, 2002):

TABLE 2 - Soil Properties of the Soil Profiles[a].

Soil Depth	Particle size composition %			Class USDA	Corg (%)	Munsell soil colour
	Sand	Silt	Clay			
				03 Haplic Vertisol		
10 cm	42·3	36·8	20·9	L	0·77	5 YR 3/1
20 cm	35·0	28·7	36·3	CL	0·94	5 YR 2.5/1
30 cm	34·7	25·3	40·0	CL	1·23	7.5 YR 2.5/1
40 cm	35·1	24·2	40·7	C	1·03	5 YR 2.5/1
50 cm	31·2	27·3	41·5	C	0·93	7.5 YR 2.5/1
60 cm	31·1	24·5	44·4	C	1·05	7.5 YR 2.5/1
				04 Rhodic Luvisol		
10 cm	41·2	39·1	19·7	L	1·41	7.5 YR 4/3
20 cm	39·5	30·0	30·5	CL	1·27	7.5 YR 2.5/3
40 cm	37·7	26·0	36·3	CL	0·81	2.5 YR 2.5/2
				05 Rhodic Luvisol		
10 cm	54·3	34·1	11·6	SL	1·32	10 YR 3/4
20 cm	53·1	35·5	11·4	SL	0·95	7.5 YR 4/6
30 cm	51·4	36·4	12·2	L	0·90	5 YR 4/4
40 cm	51·5	37·3	11·2	L	0·65	5 YR 4/6
50 cm	47·3	37·0	15·8	L	0·72	5 YR 4/6
60 cm	46·0	37·2	16·8	L	0·64	7.5 YR 4/6
				06 Andic Cambisol		
10 cm	67·6	20·9	11·5	SL	20·5	7.5 YR 3/4
40 cm	57·7	24·2	18·1	SL	11·8	7.5 YR 4/6

[a]Soil classes after USDA (1993): L loam, CL clay loam, C clay, SL sandy loam; Soil colour under dry conditions after Munsell Soil Color Charts.

$$d = -\frac{4\,\sigma\,cos\alpha}{\rho\,g\,h} \quad (6)$$

where σ is the surface tension of water, N/m, assumed to be 0.072 at 25°C; α is the contact angle between water and pore wall, assumed = 0°, cos(0) = 1; ϱ is the density of water, kg/m³; and g is the gravitational acceleration, 9.8 m/s². Therefore, a higher suction or tension corresponds to an infiltration where the bigger pore sizes in the soil matrix are successively excluded from water transmission. The water tensions of -2 cm and -4 cm equal to pore sizes of 1.47 mm and 0.73 mm, respectively. In general, we assumed that soil pores are represented to be cylindrical, vertical tubes. Generally, the pressure 0 cm water column and two suctions have been measured at 40 locations.

Spatial modelling of soil hydrological characteristics

To get a spatially continuous data set of infiltration values and soil texture we utilized a stochastic modelling approach. In this study, a boosted regression tree approach (BRT) (Friedman, 2002) is applied using dependent and independent variables. BRTs employ a learning algorithm to identify a model that best fits the relationship between the predictor variables (an attribute set of, in this case, environmental variables) and the response variables, here the soil texture and infiltrability. The dependent variable is the soil texture measured for 61 locations within the study area, analysed with finger test (according to USDA (1993)). As independent variables the delineated landcover from multispectral WorldView-2 data as well as four terrain indices have been selected: (i) land cover classes, (ii) topographic wetness index (TWI) (after Beven & Kirkby, 1979), (iii) vertical distance to channel network, (iv) channel network base level (both after Olaya & Conrad, 2009), and (v) transport capacity (TCI) (Moore & *alii*, 1991). The indices ii to v are based on the derived hydrological correct DEM (see Moore & *alii*, 1993).

We utilized the TreeNet model (Salford Systems) also known as stochastic gradient boosting (Elith & Leathwick, 2009). The models' predictive performance is assessed by constructing the receiver operating characteristics (ROC) curves for each response variable, both for training and test data (Fielding & Bell, 1997). In a ROC curve the sensitivity is plotted over the false positive rate (1-Specificity) for all possible cut-off points (Swets, 1988). The quality of a ROC curve is quantified by the measurement of the parameter area under the ROC curve (AUC; Hanley & McNeil, 1982). The AUC is shown to be independent of prevalence (Manel & *alii*, 2001) and is considered a highly effective measure for the performance of ordinal score models. A perfect discrimination between positives and negatives has a ROC plot that passes through the upper left corner (100% sensitivity, 100% specificity), so that the AUC is equal to 1 (Reineking & Schröder, 2006). According to (Hosmer & *alii*, 2013) AUC values exceeding 0.7/0.8/0.9 indicate acceptable/excellent/outstanding predictions.

Automatic surface runoff detectors

Surface runoff was measured with automatic surface runoff detectors (SRD) that measure surface runoff height and duration. SRDs were distributed along the slope system to account for the runoff generation dynamics on different slope segments and thus, topographic positions. The SRD devices are placed on the surface whilst the logger unit is buried in the soil (fig. 4). When runoff height grows the electric contacts are closed sequentially transmitting a signal that is then reported to the logger storage unit. In this experimental setup, we placed logger units according to Figure 4b right side with equal spacing of contacts. The distances between the electric contacts are 5 mm, reaching up to 3 cm above ground. Hence, the device is able to measure a water column of 3cm and has a sensitivity of 5mm. The advantage of our study area and of semiarid environments in general is the sparse vegetation cover during dry periods, and hence the disturbance of runoff due to plants is minimized. Moreover, in most of the cases precipitation is moderate to low, so runoff is normally not accumulating deeper than the contact zone of the SRDs.

Runoff calculation

To calculate a simple water balance model, the relevant input parameters such as i) the precipitation input, ii) the evapotranspiration, iii) the infiltration rate, and iv) the resulting runoff hast to be measured (tab. 3).

The measured infiltration values are further attached to the regionalized model of the surface texture. This cre-

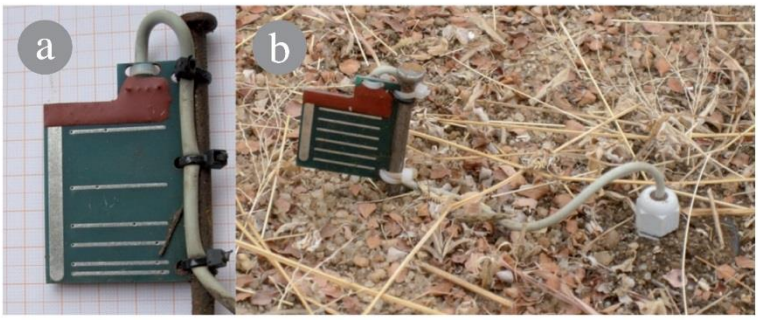

Fig. 4 - a) Close up of the sensor head of the Surface Runoff Detector. b) Installed device on the Manyara Ranch Conservancy test slope with the drainage coming from the right, shown with the blue arrow. (Photos: G. Quénéhervé).

TABLE 3 - Rainfall events, potential evapotranspiration, and calculated runoff characteristics.

Event number	Day of year	Rainfall duration [min]	Rainfall depth [mm]	Average rainfall intensity [mm/h]	PET_{Turc} [mm/ event][a]	Rainfall depth (P) - PET [mm]	Infiltration, tension $h0_2$ [mm]	Q_{h0} = P - PET - I [mm][b]	Infiltration, tension h2 [mm]	Qh_2 = P - PET - I [mm]	Infiltration, tension h2max [mm]	Q_{h2max} = P - PET - I [mm]
1	283	80	54.61	40.96	4.89	49.72	26.85	22.87	20.59	2.28	14.19	35.53
2	296	260	21.46	4.95	7.16	14.30		~		~		0.11
3	232 + 233	310	10.38	2.01	-	10.38		~		~		~
4	335	150	27.99	11.20	8.10	19.89		~		~		5.70
5	340	280	16.49	3.53	-	16.49		~		~		2.30

[a]PET: - indicates a night event, evapotranspiration is set to 0; bQ: ~ no runoff, all P is infiltrated into the soil column

ates a raster model with infiltration values as attributes. A single-cell raster based water balances model (Equation 7) was then utilized for a weighted flow algorithm based on a deterministic infinity flow approach following (Tarboton, 1997), the GIS modelling was done with SAGA GIS (Conrad, 2006). For the sake of simplicity the runoff calculation do not take into account surface roughness parameters.

$$R = P - I \quad (7)$$

where R is water balance and P is precipitation.

RESULTS

PRECIPITATION ANALYSIS

For this study we focus on the period October to December 2010, where 5 rainfall events occurred, which produced substantial runoff that was captured by the surface runoff detectors. Table 4 shows the mean daily meteorological data for each day of the recorded events and Table 5 the soil hydraulic conditions.

DGPS AND REMOTE SENSING DATA PROCESSING

For the evaluation of DGPS measurements, a regular 1 m point grid was computed for the study area (ca. 440,000 points). For each point of the produced digital elevation model (the centroid of the 1 x 1 m grid) the distance to the closest DGPS measurement was calculated. The average distance to a reference point is 5.43 m with a standard deviation of 4.7 m and a maximum distance of 32.65 m. 48.8% of all interpolated points are within a maximum distance of 4 m to a DGPS measurement point, whereas only 1.2 % within a distance greater than 20 m.

Including spectral and textural attributes, we discriminated five land cover classes with an overall accuracy of 88.98% (Kappa 0.86), validated with ground reference information. In contrast to the land use class "Grassland" the

TABLE 4 - Mean daily climatic dataa for the recorded events in 2010.

Day of year	Tmax [°C]	Tmin [°C]	mean T [°C]	mean RH [%]	meanhPa	PETTurc [mm/d]
283	34.0	17.6	24.8	37.65	893.01	219.89
296	29.6	18.6	23.2	38.74	892.39	198.35
232	31.2	18.6	23.4	43.99	892.73	187.64
233	32.6	18.7	24.7	44.64	891.90	199.9
335	32.1	18.1	23.4	41.23	890.98	194.47
340	31.9	19.6	23.1	42.87	889.74	186.72

[a]T temperature; RH relative humidity; hPa hectopascal; PET potential evapotranspiration

TABLE 5 - Measured tensions and according infiltration rates with hood infiltrometer.

Mess_ID	Tension h0	Infiltration h0 [mm/h]	Tension h1	Infiltration h1 [mm/h]	Tension h2	Infiltration h2 [mm/h]	Air entrytension
1	0	20.52	-2.0	13.99	none	none	-5.8
2	0	29.23	-3.4	21.14	-5.5	16.79	-9.5
4	0	14.93	-2.5	11.82	none	none	-7.1
5	0	34.83	-3.0	33.58	none	none	-5.2
8	0	31.00	-1.2	30.87	-3.1	29.63	-15.1
10	0	19.28	-4.0	13.68	-8.0	9.33	-15.1
11	0	15.55	-4.0	9.33	-9.0	7.46	-22.0
13	0	32.34	-1.5	26.12	-2.4	19.90	-7.8
14	0	21.77	-3.4	18.66	none	none	-7.1
15	0	84.58	-4.0	31.72	none	none	-6.9
16	0	32.96	-4.0	25.50	-8.0	19.90	-10.7
17	0	24.25	-3.5	20.52	-6.0	15.55	-12.4
19	0	38.56	-2.7	29.85	-2.8	29.02	-7.5
20	0	43.53	-4.0	18.35	-6.0	13.68	-9.3
22	0	13.33	-2.5	8.71	-4.8	6.66	-8.5
23	0	26.65	none	none	none	none	-11.0
23	0	36.07	none	none	none	none	-11.0
24	0	14.66	-6.3	9.95	-9.2	2.69	-13.0
25	0	14.61	-4.0	7.00	-7.5	4.35	-8.8
26	0	114.01	-4.0	62.19	-7.2	38.35	-8.6
27	0	74.63	-3.0	43.53	-5.1	33.17	-18.0
28	0	202.11	-3.9	128.26	-7.0	90.17	-9.5
29	0	15.55	-4.4	9.33	-9.5	7.46	-13.1
30	0	18.66	-4.4	11.19	-7.0	5.60	-7.6
31	0	32.34	-6.0	34.83	-12.0	23.01	-17.4
32	0	33.58	-3.0	22.39	-5.4	18.66	-9.6
33	0	97.95	-4.0	60.63	-5.5	23.63	-7.6
34	0	69.44	-2.2	49.13	-4.6	42.91	-9.7
35	0	98.46	-4.0	66.85	-6.0	65.30	-9.0
36	0	31.09	-4.4	18.66	none	none	-7.5
37	0	71.52	-1.4	59.08	-2.2	49.13	-3.0
38	0	39.18	-3.5	32.34	-7.0	26.85	-13.3
39	0	18.66	-4.4	15.55	-6.7	12.83	-8.7
40	0	11.11	-4.6	7.15	none	none	-14.1
41	0	37.31	-2.0	41.04	-5.0	31.72	-10.3
42	0	55.19	-3.0	23.32	-6.1	13.33	-9.1
43	0	15.55	-4.4	9.33	-8.8	6.53	-13.8
44	0	37.31	-2.7	20.52	-5.3	13.60	-8.6
45	0	29.85	-3.2	24.88	-7.1	16.17	-7.7

62

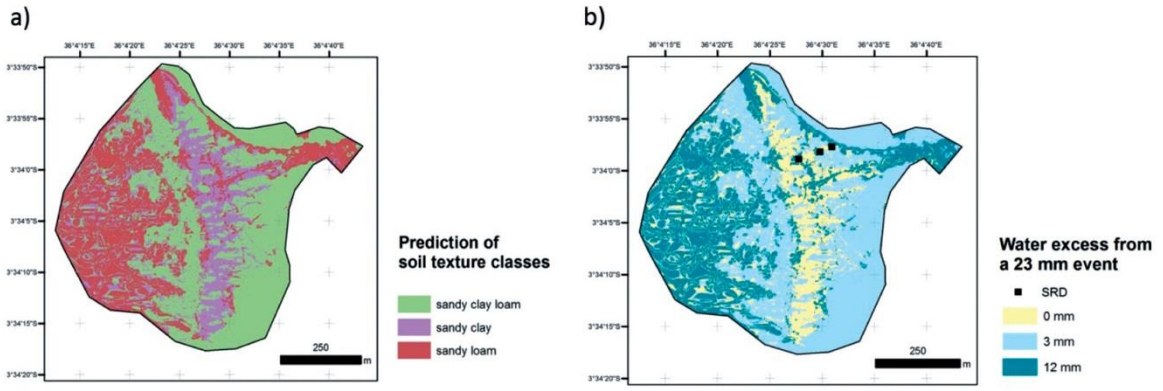

FIG. 5 - a) Prediction of soil texture classes (USDA taxonomy) according to the boosted regression tree based classification model. b) Spatial distribution of water excess calculated for a precipitation event of 23 mm (~event number 1), based on the predicted soil texture class.

classes "Degraded Grassland" and "Barren Land" show a high percentage of bare soil. The later ones are highly affected by dry and wet seasons concerning their vegetation share and are in result highly affected by overgrazing and erosional processes. The highest confusion between the classes turned out to occur between "Grassland" and "Degraded Grassland" (fig. 3b).

REGIONALIZATION OF SOIL SURFACE TEXTURE

All DEM-based independent variables show a high contribution to the best fitted classification tree model. Only the land cover classification is found to be of no significance to soil texture distribution. The modelling based on the remaining four terrain indices shows a very good model performance. The modelled classes 'sandy loam' and 'sandy clay loam' with an AUC value of more than 0.8 show an excellent prediction output. The class 'sandy clay' with an AUC value of 0.93 indicates to have an outstanding prediction performance.

The according regionalization based on the TreeNet model is shown in Figure 5a. The results show a sequence of textures from sandy clay loam on the eroded cambisols in the upper slope positions to sandy clay textures at mid slope positions. Toe slopes are characterized by sandy loam textures and vertic features. In Figure 6 the relation of texture and infiltration is shown for the 0 tension measurements in boxplots a) to d). As expected there is a close relation between texture and infiltration rates at 0 tension. The higher tensions h_2 are measured in relation to the specific air entry value of the soil's matric potential see boxplots e) to h). Figure 7 shows the relation between texture and reached tensions. As expected the highest tensions are measured in the soils with highest clay content and they are lowest in the soils with dominant sand fractions. The median tension infiltration value of the respective textures classes were then attributed to the soil texture map for the runoff modelling.

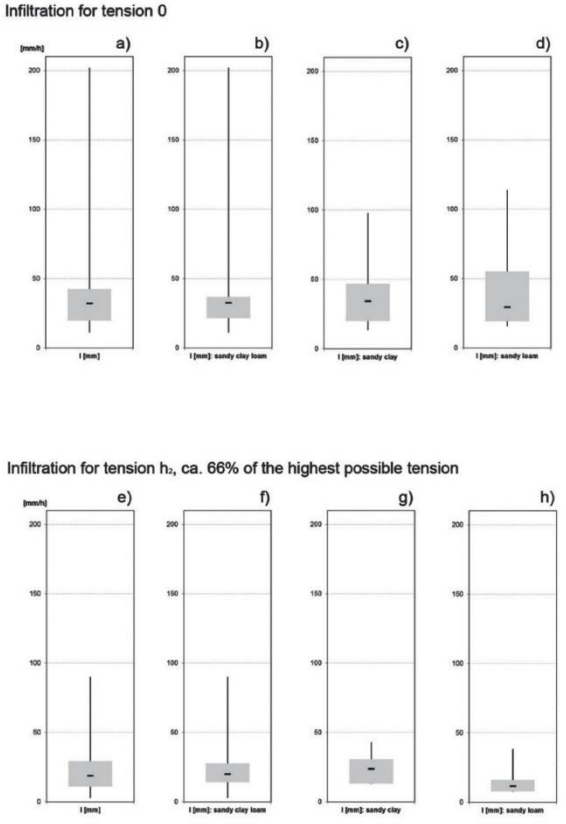

FIG. 6 - Infiltration rate (I) of 0 tension, in mm/h, for all locations a), and for the different soil texture classes b) – d). Accordingly infiltration rate of tension h2 for all locations e), and for the different soil texture classes f) – h).

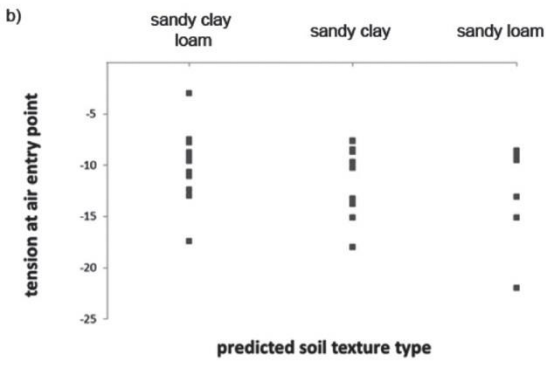

FIG. 7 - The relation between predicted soil texture class and reached tensions, in a) the tensions measured at h2, and in b) tensions at air entry value.

WATER BALANCE MODELLING

The water balance was calculated after Equation 7 for the test area on a 1m x 1m pixel basis. The calculation was performed for the surface infiltration at 0 tension and highest measured tensions (h_2). Figure 5b shows the spatial distribution of the infiltration excess for the highest measured tension. Sandy loam soils (in dark blue) show a fast response to surface sealing due to their texture partitioning. They are therefore prone to a fast surface runoff development. The Luvisols (sandy loam and loam fraction) show a high water flux and only small runoff is calculated (in light blue) or even none (yellow). Within the soil column, the picture will be the other way round, with a high micropore flux (Luvisols) lower infiltration values at higher tension values are expected, whereas soils with macropores (Vertisols) show a higher infiltration. The water balances were subsequently utilized as weighting surface in a weighted flow accumulation algorithm. This model is based on the Multiple Flow Direction algorithm (after Seibert & McGlynn, 2007) and counts the number of cells draining into a given cell. Figure 8 shows the produced runoff volumes for the infiltration scenario shown in Figure 5b.

SURFACE RUNOFF MEASUREMENT VIA SRD

For each of the 5 rainfall events (>5 mm rainfall within 1 hour) occurring from October to December 2010, we compared the data to the recorded discharge height in the SRDs. All 5 events have been recorded in each of the available SRDs. Generally, the SRDs characterize the actual surface-runoff amounts on hillslope scale in a very high temporal resolution (5 min intervals). Consequently, SRDs can be used to roughly validate water balance calculations and related runoff processes. For the single SRD locations we estimated the upslope contributing area with SAGA-GIS software using a deterministic infinity flow direction algorithm following Tarboton (1997). Measured values of surface runoff are shown in Table 6.

DISCUSSION

In this study we focus on the spatial distribution of infiltration rates. As shown, infiltration in semiarid savannah dry lands of northern Tanzania is mainly depending on spe-

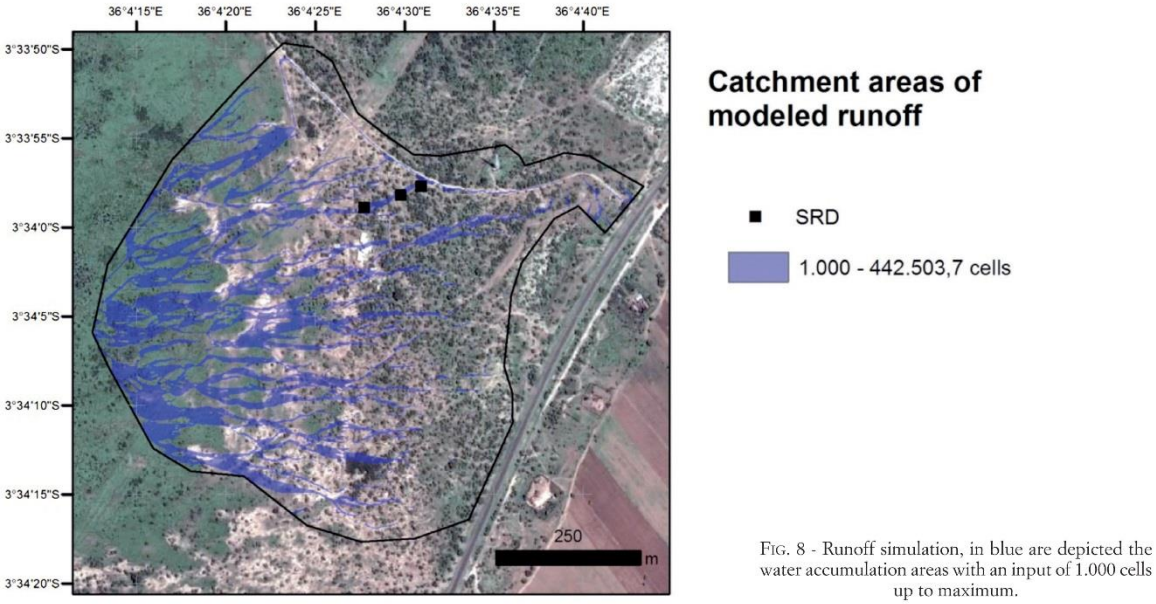

FIG. 8 - Runoff simulation, in blue are depicted the water accumulation areas with an input of 1.000 cells up to maximum.

TABLE 6 - Measured discharge from surface runoff detectors..

ID	Catchment area [m²]	Rainfall event	runoff [mm]	RI [mm/h]	Rainfall event	runoff [mm]	RI [mm/h]	Rainfall event	runoff [mm]	RI [mm/h]	Rainfall event	runoff [mm]	RI [mm/h]	Rainfall event	runoff [mm]	RI [mm/h]
A	278.62	1	107.5	1.34	2	117.5	1.47	3	25	0.31	4	203	2.54	5	108.5	1.36
B	608.08		22	0.28		240	3.00		85	1.06		321.5	4.02		171	2.14
C	569.68		202.5	2.53		300	3.75		95	1.19		298.5	3.73		162	2.03

[a]RI: average runoff intensity

cific soil physical characteristics and climatic conditions. The carbonatic volcanic ash and tuff/tephra deposits of the Makuyuni area are characterized by Andic Cambisols and Rhodic Luvisols with low activity clays developed on the upper slopes and flat summit areas. These soils show an intensive carbonate leaching (decalcification) and accumulation of carbonates (concretions) in the deeper subsoil or further downslope. On the slope ridges the soils are often eroded. The material is washed along the surface and deposition dominates in the toe slope situations. The structure of the soils is changing from matrix dominated soils on the slope ridges and mid-slope positions, towards vertic soils showing a distinct secondary macropore structures due to active layer clays (typically consisting of smectite and illite clays). The soil catena itself documents the intense sediment transport with surface runoff. Infiltration at different textures vary significantly. Especially in micropore dominated soils the infiltration is mainly triggered by the tension values or in other words is triggered by different humidity conditions of the uppermost soil horizon before rainfall starts. Generally, infiltration is decreasing for highest measured tensions by 18.74 %. For the sake of simplicity, we kept the evapotranspiration constant and do not consider soil water storage to calculate the water balance and hence, overland flow generation.

The GIS-based simulation of runoff depending on pixel water balances shows that for a detailed hillslope scale analysis a high-resolution digital elevation model is crucial. This is because all further analyses such as topographic indices, e.g. runoff direction and accumulation, are based on the accuracy of the height estimations. Particularly, the creation of a hydrological correct DEM is essential for further hydrological modeling. Therefore, sophisticated statistical methods provide accurate spatial pattern of soil surface texture. Finally, we calculated the different runoff volumes in mm/h and, make them comparable, converting also the rainfall events to average rainfall intensity in mm/h. We show that for 0 tension only the highest event of 40.6 mm/h (rainfall intensity) produced runoff whereas all other events do not show surface runoff. If tension increase the runoff is getting higher for the highest rainfall event (event 1) but still no runoff is produced for the other events (events 2-5). Only when the highest measured tension is utilized the runoff even for the other events can be modelled as shown in Table 3.

For all events runoff is produced and detected in the distributed SRDs. This means that the infiltration values for 0 and h_2 tension used in the modelling are too high for the events 2-5. Only if we use the highest tension (h_{2max}) realistic surface runoff values are simulated. This means that the contributing area for the three SRDs is mainly characterized by homogeneous soils dominated by matrix pore triggered infiltration with small pore sized at sandy loam textures. Tension for this texture (sandy loam) can reach very high suctions characterized by a high air entry value. Hence, the measured highest tensions may be even higher if the measurement is performed close to the air entry point. Consequently, the infiltration becomes even lower.

CONCLUSIONS

The study presents a simple low budget approach to assess soil infiltration and surface runoff values. We show that infiltration processes in semiarid dryland conditions are mainly depending on the soil physical characteristics such as soil water tension and the moisture conditions of the topsoil before the precipitation event starts. Saturated conductivities often used to calculate the surface runoff yield too high infiltration values to explain observed surface runoff. In this study we measured the shallow laminar runoff at the surface using SRDs. Moreover, infiltrations were measured at different tensions simulating various soil humidity conditions. We illustrated with a simple water balance approach, that infiltrations measured at 0 tension produce too high infiltration values in order to generate surface runoff. Especially in micropore dominated homogeneous soils water tension triggered infiltration rates play a crucial role. Thus, on the slope system studied in this investigation surface runoff was only produced if the highest tension infiltration rates were used corresponding to "drier" soil conditions. Consequently, it is very important what kind of soil types are present in a catchment and to what kind of infiltration scheme they are belonging to. Especially in homogeneous soils with low activity clays notable surface runoff can be produced if the soil is very dry when precipitation starts. This example from a hillslope scale water balance model demonstrates the importance of integrated field work measurements (especially the incorporation of surface runoff detectors) and computer-based simulations in hydrological research.

The automatic surface runoff detectors offer a helpful insights into actual overland flow dynamics and, especially, for the quantification of those. This approach can provide useful additional information on water balance modelling. Primarily the verification of single parameters of the water balance equation can further be validated and evaluated.

References

ASHTECH (2010) - *ProMark 3 RTK.* http://www.spectraprecision.com/products/gnss-surveying/promark3-rtk-2655.kjsp, Nov 4, 2014.

Beven K.J. & Kirkby M.J. (1979) - *A physically based, variable contributing area model of basin hydrology.* Bulletin of the International Association of Scientific Hydrology, 24, 43-69.

Blaschke T. (2010) - *Object based image analysis for remote sensing.* ISPRS Journal of Photogrammetry and Remote Sensing, 65, 2-16.

Borselli L., Torri D., Poesen J. & Sanchis P.S. (2001) - *Effects of water quality on infiltration, runoff and interrill erosion processes during simulated rainfall.* Earth Surface Processes and Landforms, 26, 329-342.

Bracken L.J. & Croke J. (2007) - *The concept of hydrological connectivity and its contribution to understanding runoff-dominated geomorphic systems.* Hydrological Processes, 21, 1749–1763.

Conrad O. (2006) - *SAGA - Program structure and current state of implementation.* In: Böhner, J. & MacCloy, K.R. (Eds.) SAGA-analysis and modelling applications. Goltze, Göttingen, 39-52.

Critchley W. & Siegert K. (1991) - *Water Harvesting. A Manual for the Design and Construction of Water Harvesting Schemes for Plant Production,* Rome, Italy, 157 pp.

Elith J. & Leathwick J.R. (2009) - *Species Distribution Models: Ecological Explanation and Prediction Across Space and Time.* Annual Review of Ecology, Evolution, and Systematics, 40, 677-697.

FAO (2014) - *World reference base for soil resources. International soil classification system for naming soils and creating legends for soil maps.* FAO, Natural Resources Management and Environment Department.

Fielding A.H. & Bell J.F. (1997) - *A review of methods for the assessment of prediction errors in conservation presence/absence models.* Environmental Conservation, 24, 38-49.

Friedman J.H. (2002) - *Stochastic gradient boosting. Nonlinear Methods and Data Mining.* Computational Statistics & Data Analysis, 38, 367-378.

Hanley J.A. & McNeil B.J. (1982) - *The meaning and use of the area under a receiver operating characteristic (ROC) curve.* Radiology, 143, 29-36.

Hosmer D.W., Lemeshow S. & Sturdivant R.X. (2013) - *Applied logistic regression,* 3rd ed. Wiley, Hoboken N.J., 1 online resource (xvi, 500 pp.)

Hutchinson M.F. (1989) - *A new procedure for gridding elevation and stream line data with automatic removal of spurious pits.* Journal of Hydrology, 106, 211-232.

Huxman T.E., Snyder K.A., Tissue D., Leffler A.J., Ogle K., Pockman W.T., Sandquist D.R., Potts D.L. & Schwinning S. (2004) – *Precipitation pulses and carbon fluxes in semiarid and arid ecosystems.* Oecologia, 141, 254-268.

Jensen M.E. & Burman R.D. & Allen R.G. (1990) - *Evapotranspiration and irrigation water requirements. A manual.* American Society of Civil Engineers, New York, N.Y., xxviii, 332 pp.

Kutílek M. & Nielsen D.R. (1994) - *Soil hydrology.* Catena Verlag, Cremlingen-Destedt, 370 S. pp.

Lauenroth W.K. & Bradford J.B. (2006) - *Ecohydrology and the Partitioning AET Between Transpiration and Evaporation in a Semiarid Steppe.* Ecosystems, 9, 756-767.

Manel S., Williams H.C. & Ormerod S.J. (2001) - *Evaluating presence–absence models in ecology: the need to account for prevalence.* Journal of Applied Ecology, 38, 921-931.

Moore I.D., Gessler P.E., Nielsen G.A. & Peterson G.A. (1993) - *Soil Attribute Prediction using Terrain Analysis.* Transactions of the American Society of Agricultural Engineers, 57, 443-452.

Moore I.D., Grayson R.B. & Ladson A.R. (1991) - *Digital terrain modelling. A review of hydrological, geomorphological, and biological applications.* Hydrological Processes, 5, 3-30.

Mualem Y. (1976) - *A new model for predicting the hydraulic conductivity of unsaturated porous media.* Water Resources Research, 12, 513-522.

Mualem Y. & Assouline, S. (1996) - *Soil Sealing, Infiltration and Runoff.* In: Issar A. & Resnick S. (Eds.) Runoff, Infiltration and Subsurface Flow of Water in Arid and Semi-Arid Regions. Springer Netherlands, 131-181.

Nico G., Rutigliano P., Benedetto C. & Vespe F. (2005) - *Terrain modelling by kinematical GPS survey.* Natural Hazards and Earth System Science, 5, 293-299.

Olaya V. & Conrad C. (2009) - *Geomorphometry in SAGA.* In: Hengl, T. & Reuter HI (Eds.) Geomorphometry. Concepts, Software, Applications. Elsevier, Amsterdam, 293-308.

Philip J.R. (1957) - *The Theory of Infiltration: 1. The Infiltration Equation and its solution.* Soil Science, 83, 345-358.

Philip J.R. (1975) - *Stability Analysis of Infiltration.* Soil Science Society of America Journal, 39, 1042-1049.

Reineking B. & Schröder B. (2006) - *Constrain to perform: Regularization of habitat models.* Ecological Modelling, 193, 675-690.

Renger M., Stoffregen H., Klocke J., Facklam M., Wessolek G., Roth C.H. & Plagge, R. (1999) - *Ein autoregressives Verfahren zur Bestimmung der gesättigten und ungesättigten hydraulischen Leitfähigkeit.* Journal of Plant Nutrition and Soil Science, 162, 123-130.

Ritter D.F., Kochel R.C. & Miller J.R. (2011) - *Process Geomorphology,* 5. Ed. Waveland Press, Long Grove, Ill., 652 pp.

Sala O.E. & Lauenroth W.K. (1982) - *Small rainfall events: An ecological role in semiarid regions.* Oecologia, 53, 301-304.

Sauer T.J. & Logsdon S.D. (2002) - *Hydraulic and Physical Properties of Stony Soils in a Small Watershed. Soil Science Society of America Journal,* 66, 1947–1956.

Schwärzel K. & Punzel J. (2007) - *Hood Infiltrometer A New Type of Tension Infiltrometer.* Soil Science Society of America Journal, 71, 1438-1447.

Schwinning S. & Sala O. (2004) - *Hierarchy of responses to resource pulses in arid and semi-arid ecosystems.* Oecologia, 141, 211-220.

Seibert J. & McGlynn B.L. (2007) - *A new triangular multiple flow direction algorithm for computing upslope areas from gridded digital elevation models.* Water Resources Research, 43, W04501.

Springer U. & Klee J. (1954) - *Prüfung der Leistungsfähigkeit von einigen wichtigeren Verfahren zur Bestimmung des Kohlenstoffs mittels Chromschwefelsäure sowie Vorschlag einer neuen Schnellmethode.* Zeitschrift für Pflanzenernährung, Düngung, Bodenkunde, 64, 1-26.

Swets J.A. (1988) - *Measuring the accuracy of diagnostic systems.* Science, 240, 1285-1293.

Tarboton D.G. (1997) - *A new method for the determination of flow directions and upslope areas in grid digital elevation models.* Water Resources Research, 33, 309-319.

Umwelt-Geräte-Technik, 2005 - *Operating instructions for Hood Infiltrometer.* http://www.ictinternational.com.au/ugt/brochures/hood-infiltrometer.pdf, Nov 4, 2014.

USDA (1993) - *Soil survey manual. United States Department of Agriculture (USDA). Soil Survey Division, Washington, D.C.,* 437 pp.

van Genuchten, M.T. (1980) - *A Closed-form Equation for Predicting the Hydraulic Conductivity of Unsaturated Soils1.* Soil Sci. Soc. Am. J., 44, 892-898.

Wainwright J. & Bracken L.J. (2011) - *Runoff generation, overland flow and erosion on hillslopes.* In: Thomas, D. (Ed.) Arid Zone Geomorphology. Process, Form and Change in Drylands. Wiley-Blackwell, Oxford, 237-267.

Wallace J.S., Jackson N.A. & Ong C.K. (1999) - *Modelling soil evaporation in an agroforestry system in Kenya.* Agricultural and Forest Meteorology, 94, 189-202.

Wooding R.A. (1968) - *Steady Infiltration from a Shallow Circular Pond.* Water Resources Research, 4, 1259-1273.

Zema A.D., Bombino G., Denisi P., Licciardello F. & Zimbone S.M. (2012) - *Prediction of Surface Runoff and Soil Erosion at Watershed Scale: Analysis of the AnnAGNPS Model in Different Environmental Conditions.* In: Godone D. (Ed.), Research on Soil Erosion. InTech, 3-31.

(ms received 15 December 2014; accepted 15 May 2015)

IV A Simple DEM Assessment Procedure for Gully System Analysis in the Lake Manyara Area, Northern Tanzania

Authors

Michael Maerker, **Geraldine Quénéhervé**, Felix Bachofer and Simone Mori

Paper History

MM and GQ constructed the study design. GQ designed and conducted the field work with assistance by SM. The study was adapted by the Bachelor of Science Thesis of SM "Valutazione di Modelli digitali per l'analisi di sistemi gully nella zona del lago Manyara, nord Tanzania" (in Italian) at the University of Florence, Italy in 2011. This thesis was closely supervised by MM.

Own Contribution

GQ supported study design and the structure of the paper. GQ did data preparation and analyses and provided figures. GQ did substantial manuscript writing as well as proof-reading.

Published in

Natural Hazards **12**(1), 239–279, (2015).

doi: 10.1007/s11069-015-1855-y

ISSN: 0921-030X (Print)
ISSN: 1573-0840 (Online)
Impact Factor (2015): 1.746

Nat Hazards (2015) 79:S235–S253
DOI 10.1007/s11069-015-1855-y

ORIGINAL PAPER

A simple DEM assessment procedure for gully system analysis in the Lake Manyara area, northern Tanzania

Michael Maerker[1,2] · Geraldine Quénéhervé[3] · Felix Bachofer[3] · Simone Mori[4]

Received: 30 August 2014 / Accepted: 30 May 2015 / Published online: 13 June 2015

Abstract Gully erosion is a major threat concerning landscape degradation in large areas along the northern Tanzanian Rift valley. It is the dominant erosion process producing large parts of the sediments that are effectively conducted into the river network. The study area is located in the Lake Manyara—Makuyuni River catchment, Arusha, northern Tanzania. During fieldwork, we measured topographic data of eight gully systems close to Makuyuni Town. The main focus of this study is to assess gully erosion dynamics using improved DEMs with original resolutions of 30 and 20 m, respectively. We assessed terrain characteristics to extract information on environmental drivers. To improve the DEM, we integrated information deduced from satellite images as well as from acquired GPS field data. Topographic indices such as Stream Power Index or Transport Capacity Index were derived from the re-interpolated DEM. To evaluate gully evolution, we assessed also the longitudinal slope profiles. Finally, the gully evolution phases of each gully were classified according to the concept proposed by Kosov et al. (Eksperimental'naya geomorfologiya, vol 3. Moscow University, Moskva, pp 113–140, 1978). The re-interpolated DEMs revealed a positive response especially for the more developed gullies. We show that the extraction of information on this spatial process scale based on "low-resolution" data is feasible with little additional fieldwork and image interpretation. In fact, areas identified as having a greater risk of gully erosion have been confirmed by observations and surveys carried out in the field.

Keywords Soil erosion · Gully erosion · GIS · DEM interpolation · Terrain analysis · Tanzania

✉ Michael Maerker
mmaerker@unifi.it; michael.maerker@ggi.uni-tuebingen.de

[1] Heidelberg Academy of Sciences and Humanities, Rümelinstr. 19-23, 72070 Tübingen, Germany

[2] Department of Earth Sciences, University of Florence, Via La Pira 4, 50121 Florence, Italy

[3] Institute of Geography, Tübingen University, Rümelinstr. 19-23, 72070 Tübingen, Germany

[4] Laboratory of Geo-Information Science and Remote Sensing, Wageningen University, Droevendaalsesteeg 3, 6708 Wageningen, The Netherlands

1 Introduction

The semiarid landscape of the northern Tanzanian Rift is highly sensitive to climate and socio-economic changes. Particularly, along the eastern flanks of the East African Rift half-graben system within the Lake Manyara basin, fertile soils are potentially threatened by soil erosion processes. Particularly gully erosion processes are very effectively destroying entire areas where a suitable and sustainable land management is not implemented (Vrieling et al. 2006; Mwanukuzi 2011). Furthermore, the rift valley is still a very active tectonic area influencing and triggering hydrological and geomorphological processes (Dawson 1997). The study area is also subject to a specific precipitation pattern with long dry periods and intensive rains during the wet seasons. Climatic conditions varied a lot over the last thousands of years, documented by intense fluctuating levels of the Gregory rift lakes and different levels of corresponding fluvial terraces (Trauth et al. 2003; Bergner et al. 2009; Trauth et al. 2009). Generally, gully erosion processes indicate active geomorphic areas where hydraulic settings and sediment dynamics of the terrain are strongly modified. Gullies efficiently concentrate surface runoff, and they transport huge amounts of sediments rapidly down to the river networks (Capra 2013; Shellberg et al. 2013; Rengers and Tucker 2014). Gullies in this area expose archaeological and paleontological finds dated to 78–630 ka BP (Ring et al. 2005; Schwartz et al. 2012). The "off-site damages" of gully erosion processes are related to the transported sediments that are mainly affecting water quality and are causing reservoir sedimentation (Flügel et al. 2003; Sidorchuk et al. 2003). Consequently, a detailed assessment of gullying processes yields valuable information on the landscape and landscape functions such as sediment load, water quality, landscape stability, soil- and groundwater storage as well as soil fertility and soil depth (Sidorchuk 2006; Hancock and Evans 2010).

However, for areas affected by gully erosion processes in Africa and elsewhere, a proper assessment of process dynamics is related to the availability of suitable data and spatial information derived by remote sensing. This is mainly due to the fact that most of those areas are not accessible for comprehensive fieldwork (missing permits; dangerous areas because of conflicts, diseases, etc.). Additionally, analyses are mostly conducted with low financial budgets, even though some remotely sensed data are freely available and can be purchased by the research community; high-resolution data is still cost intensive. Therefore, it is often necessary to find a compromise between the cost and the quality of the data. Consequently, in some studies freely available data such as Shuttle Radar Topographic Mission (SRTM) digital elevation models (DEM) derived from X- or C-band or the Advanced Spaceborne Thermal Emission and Reflection Radiometer (ASTER) GDEM are used in the assessment of erosion processes and feature detection because of their almost global coverage (Brooks et al. 2009; El Haj Tahir et al. 2010). Often these DEMs are the only valuable elevation information in remote areas where no high-quality topographic maps are available. The medium resolution of these DEMs with 30 m is in most of the cases not adequate for assessing erosion processes that have a spatial resolution of less than 10 m like rill or gully features. Consequently, the question remains, whether and how the quality of these models can be enhanced to be able to evaluate gully erosion processes?

The aim of this study is to investigate the potential improvement of freely available data and to develop a simple methodology allowing a proper assessment of soil erosion, especially gully erosion processes, for data-scarce areas. We will explore additional data sources providing topographic information like GoogleEarth™ images in order to enhance

the spatial accuracy and resolution of the datasets. We will test the approach in the Lake Manyara area in northern Tanzania to decipher landscape characteristics and evolutionary phases. Since we are mainly interested in revealing the landscape potential for erosion processes, we primarily concentrate on the triggering topography. Therefore, we consider for this screening approach soils, substrates, vegetation and climate as homogeneous.

2 Materials and methods

2.1 Study area

The Lake Manyara basin is located in an asymmetrically shaped half-graben situated in the eastern branch of the East African Rift System with a 200–600 m high escarpment along the western shoulder and with the Ngorongoro crater as highest elevation (2960 m). The eastern shoulder of the rift is lower in elevation and consists of tectonic blocks that are dipping toward the west. The northeastern part of the catchment area is dominated by the Essimingor volcano (2154 m). Tectonic settings and climatological conditions formed the Lake Manyara catchment in northern Tanzania as an endorheic basin. The Lake Manyara

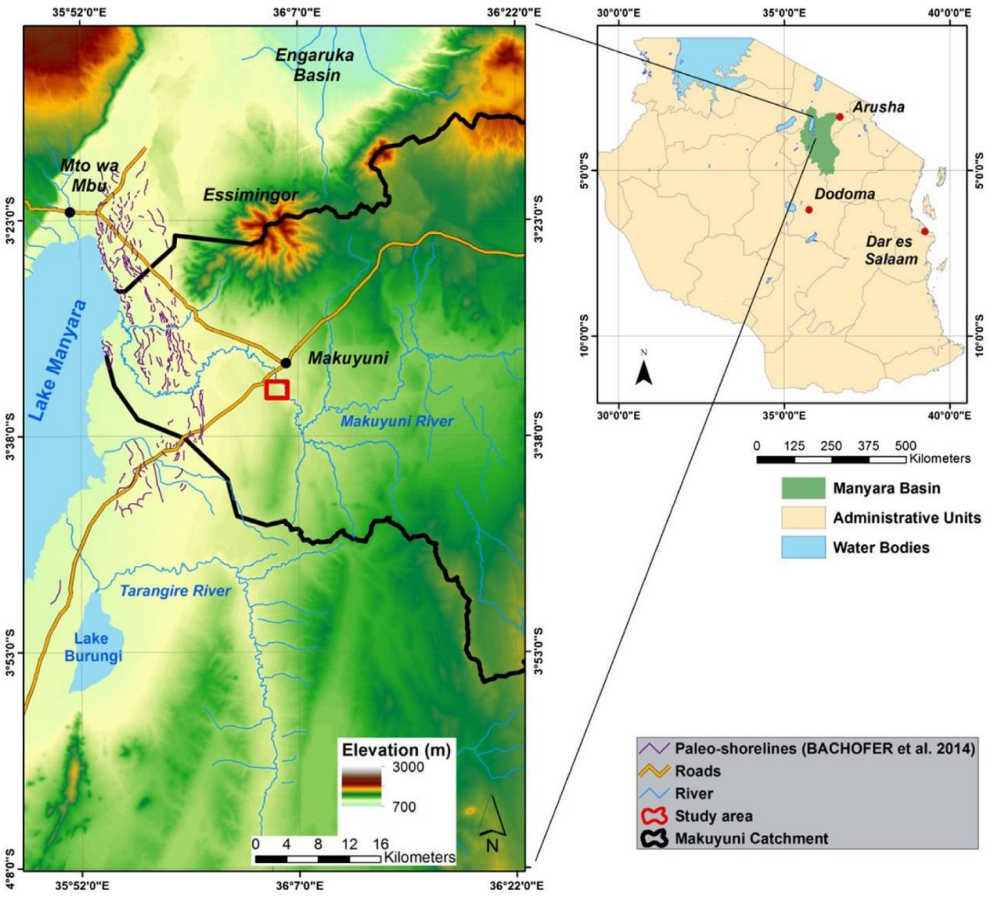

Fig. 1 The regional setting of the Lake Manyara and the study area

(954 m a.s.l.) is a shallow soda lake with a maximum depth of 1.18 m (Deus et al. 2013). Remains of a paleolake Manyara can be found, especially in the eastern part of the basin. Paleoshorelines indicate paleolake levels up to 80 m above today's lake level, which is also the lowest possible outlet point into the northern Engaruka and Lake Natron basins (Keller et al. 1975; Bachofer et al. 2014). Radiocarbon-dated stromatolites (Th/U series) indicate a maximum age of about 140 ka BP (Casanova and Hillaire-Marcel 1992). Today's Lake Manyara is mainly fed with seasonal drainages of the Tarangire and Makuyuni rivers from the east and by some springs at the base of the escarpment in the west. The Makuyuni River catchment east of Lake Manyara is characterized by a bimodal precipitation pattern with an average annual rainfall of about 700 mm that results in a sparse semiarid vegetation cover, dominated by bushed grasslands (Bachofer et al. 2014). The land use consists mainly in pastures and rain-fed agriculture. The study area, located south of the Makuyuni River and east of the road Arusha–Dodoma, is characterized by different fluvial terrace systems related to the lake-level fluctuations in the past (Fig. 1). Fine fluvial deposits formed the substrates and the soils developed on top of them. A paleolake margin is also identified in the study area consisting of tephra deposits with a radiocarbon date of 630 ka BP (Schwartz et al. 2012). These tephra deposits form a distinct escarpment in turn representing harder substrates than the surrounding weathered soil material or outcropping pedogen carbonatic concretions. The underlying geology is characterized by crystalline rocks and basaltic dyke systems (Frost et al. 2012).

2.2 Assessment procedure

The objective of this study is to enhance existing global elevation data with additional topographic information that is available, e.g., via GoogleEarth. Many studies already used this information directly or indirectly to assess soil erosion processes (Costanzo et al. 2012; Conoscenti et al. 2013; Frankl et al. 2013; Zakerinejad and Maerker 2014). However, the data can also be utilized to improve DEM quality and thus may allow a proper erosion process assessment based on these DEMs. The general approach we follow in this study consists in the succeeding steps:

1. GPS tracking of the gully drainage networks and gully profile recording in the study area.
2. Identification and digitalization of gully features and drainage networks from high resolution, freely accessible GoogleEarth images, Google (2012).
3. Preprocessing of available ASTER GDEM, SPOT DEM and SRTM-X DEM (noise and artifact filtering and fill sink procedures).
4. Re-interpolation of ASTER GDEM, SPOT and SRTM-X DEMs at higher resolution taking into account digitized streamlines and GPS-measured ground control points within the gully networks.
5. Assessment of gully erosion processes by detailed Geographic Information System-based (GIS) terrain analysis.
6. Determination of gully development phases according to a gully evolution model.

In the following chapters, we describe in detail the procedure to enhance DEM resolution and quality and the data utilized in the approach. The data sources used in this research can be divided in two categories: remotely sensed and other digital information as well as field acquired data.

2.3 Digital data sources

The remote sensing data consist of DEMs and high-resolution satellite images (Table 1). For gully and drainage network detection, we utilized GoogleEarth, which provides free access to satellite images with high resolution. Regarding the study area, GoogleEarth made two images available: Ikonos-2 (2005) with a resolution of 1 m and GeoEye-1 (2010) with 0.5 m resolution. As a reference, we used a commercial WorldView-2 scene acquired 2010-10-15.

We compared three available DEMs in order to find the most suitable one for our methodological approach:

1. The NASA Shuttle Radar Topography Mission (SRTM) DEM (DLR 2012). In February 2000, a series of synthetic aperture radar (SAR) images was taken by a space shuttle with the aim to build a high-resolution topographic database of the entire world. The result is a DEM with 90 m resolution (3 arcsec, acquired in C-band) and one with 30 m resolution (1 arcsec, acquired in X-band). The major advantage of radar techniques and in particular of the resulting SRTM-X DEM is that microwaves are capable to penetrate clouds and to some degree also the vegetation cover. Even though the SRTM-X DEM offers no global coverage, it covers the study area completely.
2. The Advanced Spaceborne Thermal Emission and Reflection Radiometer (ASTER) Global DEM (GDEM, version 2) is generated using nadir-viewing and backward-viewing bands of the medium resolute ASTER sensor (ASTER GDEM Validation Team 2011). The resulting DEM has a resolution of 30 m at the Equator. The vertical and horizontal accuracy is about 30 m (Nelson et al. 2009).
3. Satellite Pour l'observation De La Terre (SPOT) DEM. The abbreviation SPOT refers to a series of French optical earth observation satellites. The DEM is derived from stereo-pair images of forward- and backward-facing sensors of the SPOT-5 satellite and has a spatial resolution of 20 m. The SPOT DEM is not freely available and does not have a global coverage so far. The DEMs have a vertical accuracy of at least 10 m and a horizontal accuracy of at least 15 m at a confidence level of 90 % (Nelson et al. 2009).

2.4 Fieldwork

Field data were achieved during September/October 2011 southwest of Makuyuni village (Fig. 2). Within the study area, we selected eight gullies (A–H) that are representative for

Table 1 List of DEMs and satellite images used

Dataset name	Resolution	Information
DEM SRTM-X	30 m	NASA SRTM-X DEM 1 arcsec
ASTER GDEM	30 m	ASTER GDEM
DEM SPOT	20 m	Compiled with 4 pairs of satellite images (01/01/2006; 30/07/2004; 23/01/2005; and 27/06/2006)
Ikonos-2	1 m (0.82 m nadir)	Image from Ikonos-2 satellite, available through GoogleEarth™, date 12/09/2005
GeoEye-1	0.5 m (nadir)	Image from GeoEye-1, satellite available through GoogleEarth™, date 25/01/2010
WorldView-2	0.5 m (0.46 m nadir)	15/10/2010

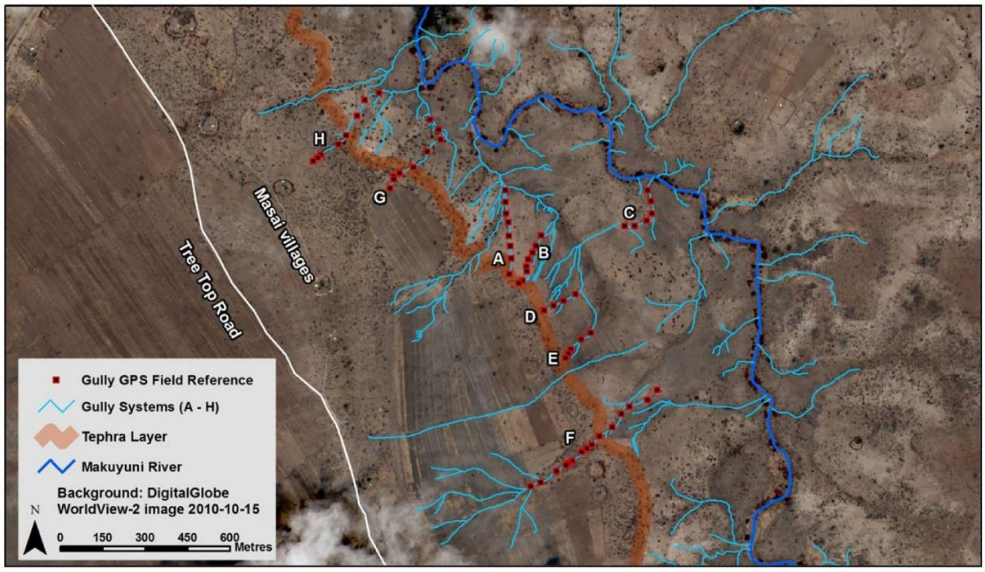

Fig. 2 Digitized gully drainage lines and recorded GPS thalweg points for gully systems *A–H*

this part of the basin and that are used as reference for the terrain analysis. Using Garmin handheld GPS devices, we measured *x*- and *y*-coordinates, moving along the gully from upstream (gully head) to downstream (gully mouth) along the thalwegs, reaching the Makuyuni river channel (Fig. 2). The accuracy of the GPS measurements for *x*- and *y*-coordinates is less than 1 m. For each GPS *x*-, *y*-point, we also performed a classical cross-sectional measurement, registering the exact gully depth and width using a measuring tape and stick (Table 2). These data, especially the depth values, were utilized in the DEM interpolation (see Sect. 3.1). We also took geo-tagged photographs of gully profiles at the recorded GPS points to document general features such as soil skeleton, structure and color of the substrates. Moreover, we performed a finger test to estimate the soil texture. This information is important for the interpretation of gully dynamics after the GIS analyses were conducted.

2.5 Gully drainage detection

Digitizing streamlines by manual photograph-interpretation techniques allows the operator to remove obstructions of vegetation cover and/or delineate flow paths of small-to-medium

Table 2 Figures and averaged values of the sampled gullies A to H

Gully	A	B	C	D	E	F	G	H
Length (m)	298.4	199.3	200.3	128.7	132.5	589.1	364.9	355.1
Average depth (cm)	183.3	96.9	165.8	72	53	174.6	116.4	109.6
Max depth (cm)	270	200	350	102.5	71	373	195	200
Min depth (cm)	50	30	10	33	30	13	28	35
Average width (m)	6.1	2.6	13.6	9.8	11.2	8.8	6.2	7.3
Max width (m)	11.02	5	25.2	14.5	22.5	17.3	15	23.6
Min width (m)	2.5	1.1	0.8	7.1	5.7	2.7	2.4	2.1

scale erosion processes such as gullies. Combined vector elevation information like elevation points, contour lines and streamlines often outperform raster approaches, especially in low-relief areas where moderate elevation errors in remotely sensed data can effectively preclude an accurate determination of the surface shape and drainage lines (Garbrecht and Starks 1995; Wilson and Gallant 2000). Not many interpolation techniques utilize drainage networks or thalwegs without elevation values, but particularly the algorithm developed by Hutchinson (1989) uses drainage lines to improve DEM interpolation.

The GeoEye-1 and the Ikonos-2 satellite images were acquired during the dry season, minimizing the vegetation cover and showing very clear paths of gullies and the river network of the Makuyuni River (Fig. 2). The high resolution of 0.5 m of the GeoEye-1 image allows for an accurate and detailed identification of drainage lines. On the other hand, due to its coarser resolution, the Ikonos-2 image permits only to digitize the more developed gullies that were mainly corresponding to the ones sampled in the field. This drainage lines are an integral part in our study for the DEM improvement and interpolation described in the following chapter.

3 GIS analyses

3.1 DEM interpolation

The ASTER GDEM, SRTM-X and SPOT DEMs were filtered using a simple 3×3 average filter in order to remove noise and to loose as less topographic information as possible. Subsequently, the raster data were transformed in point-type vector data attributing the elevation information to each centroid of the raster cells. We calculated the gully depths from the cross-sectional information at the x- and y-GPS points. The depth was then subtracted from the surrounding raster grid cells in order to estimate the absolute elevation of the gully bottom at the GPS points. We added these points to the raster centroid dataset to generate the point elevation dataset. We digitized the Makuyuni river fluvial network and the visible gullies based on the satellite images (Fig. 2) to provide a linear vector-type thalweg shapefile.

To create an improved DEM for a proper terrain analysis, the different datasets containing absolute (elevation point dataset) or relative elevation information (thalwegs or drainage networks dataset) were again interpolated. This interpolation was conducted using the ANUDEM algorithm developed by Hutchinson (Hutchinson 1986, 1989). This algorithm is an interpolation method specifically designed for the creation of hydrological correct DEMs (Reuter et al. 2009; Arun 2013). The interpolation algorithm is based on thin-plate splines and produces a surface that incorporates ridgelines and stream networks in order to represent as much as possible a natural drainage surface (Reuter et al. 2009). The drainage enforcement option, part of the ANUDEM method, attempts to remove all sink points in the fitted grid (Hutchinson 1989). Removing erroneous (spurious) sinks guarantee a hydrological correct network where water flows from the watershed divides to the respective catchment outlet (Tarboton et al. 1991). A spurious sink is often an erratic feature that does not correspond with actual features of the terrain. These sinks have to be removed to allow accurate hydrologic modeling (Nelson et al. 2009). Hence, the drainage enforcement algorithm significantly increase the accuracy of DEMs interpolated from sparse, but well chosen, surface-specific elevation data (Hutchinson 1989). To interpolate the SPOT DEM, we used the drainage lines digitized on the GeoEye-1 image (0.5 m

Table 3 DEM interpolation scheme

SPOT	SRTM-X	GPS data	Drainage lines	Drainage enforce (on/off)	10 m interpolated DEM
×		×	×	On	SPOT ENF10
×		×	×	Off	SPOT B10
	×	×	×	On	SRTM ENF10
	×	×	×	Off	SRTM B10

ground resolution), and to interpolate the SRTM-X DEM, we utilized the ones digitized on the Ikonos-2 image (1 m ground resolution). The difference between both derived drainage lines is small even though there is a difference in resolution. The main drainage pattern is reproduced well with both datasets, which subsequently are validated by field reference and the WorldView-2 image (0.5 m ground resolution). With the ANUDEM-based method, we interpolated four new elevation models with 10 m resolution based on SRTM-X with 30 m resolution and SPOT with 10 m resolution (Table 3). The ASTER GDEM was not taken into consideration after a first validation because of its low spatial resolution and obvious artifacts resulting from shadowing effects and savanna vegetation. A qualitative assessment was done with a hillshade DEM, checking minimum and maximum values. Moreover, we evaluated visually the differences between the original DEMs and hydrological correct DEMs.

3.2 Terrain analysis

3.2.1 Flow direction

The physics of a purely gravity-driven flow dictates that water always takes the steepest downhill path, such that flow lines cross contour lines at a right angle (Gruber and Peckham 2009). Due to the nature of this study, we took into account two flow direction algorithms: D8 and D∞. The D8 method is the simplest flow direction algorithm: from each cell, all flow is passed to the neighbor with the steepest downslope gradient resulting in 8 possible drainage directions. It can model convergence (several cells draining into one), but not divergence (one cell draining into several cells) (Gruber and Peckham 2009). In the case of ambiguous flow directions, for example if two cells have the same minimum downslope, an arbitrary decision is made. This simple method is often used to extract river networks and is integrated in many GIS packages. D∞ is based on representing flow direction as a single angle taken as the steepest downward slope on the eight triangular facets centered at each grid point. The upslope area is then calculated by proportioning the flow between two downslope pixels according to how close the flow direction is to the direct angle to the downslope pixel (Tarboton 1997). This procedure offers improvements over prior procedures that have restricted a flow to only eight possible directions.

3.2.2 Flow accumulation

The contributing area, also known as basin area, upslope area or flow accumulation, is a planar area and describes the spatial extent of a collecting area over which water from rainfall, snowfall, etc. can be aggregated (Gruber and Peckham 2009). The total contributing area (TCA) is a definite area where values of every raster cell represent the total

number of cells that flows into it, while the specific contributing area (SCA) refers to an area per unit of contour length (SCA = TCA/w).

3.2.3 Potential linear erosion processes

The Stream Power Index (SPI) (Moore et al. 1988) was used to identify and describe potential linear erosion processes such as rills and gullies along slopes based on slope and contributing area (D'Agostino and Vianello 2005). The SPI measures erosive power of flowing water based on the assumption that discharge is proportional to the specific contributing area A_s and flow velocity proportional to the slope gradient (tan β) (Wilson and Gallant 2000). As specific contributing area and slope steepness increase, the amount of water contributed by upslope areas and the velocity of water flow increase, hence stream power and potential erosion increase (Gruber and Peckham 2009). The stream power index SPI is defined as (Wilson and Gallant 2000):

$$\mathrm{SPI} = A_s \cdot \tan\beta \tag{1}$$

3.2.4 Sediment transport

To describe areal or sheet erosion processes, the sediment transport capacity parameter was developed to describe how and where sediments are transported and deposited by the flow. We used the Transport Capacity Index (TCI) (also called LS factor or RUSLE 3D index) (Wischmeier and Smith 1978; Renard et al. 1997). TCI is the 3D equivalent to the Universal Soil Loss Equation (USLE) slope length and steepness factor (LS Factor). TCI substitutes the slope length as proxy for water volume with the contributing area (Desmet and Govers 1996). The modified equation to compute the TCI is (Wilson and Gallant 2000):

$$LS_{(r)} = (m+1) \cdot \left[\frac{A_{(r)}}{22.13}\right]^m \cdot \left[\frac{\sin\beta_{(r)}}{0.09}\right]^n \tag{2}$$

where $A_{(r)}$ is the upslope contributing area (in m^2); $\beta_{(r)}$ is the maximum slope angle (in degrees); and n and m are parameters dependent on the flow. The number values 22.13 m (length) and 0.09 (9 % slope) representing the standard USLE plots.

3.2.5 Flow path profile

Longitudinal profiles are very useful to trace flow path profiles along gully systems and drainage lines. These profiles can be correlated with field measurements and study area morphologies in order to identify and validate fluvial terraces, areas with higher slopes and the spatial distribution of soil characteristics like soil texture. They can furthermore help to explain erosion processes.

3.3 Gully development and evolution

According to gully morphometric characteristics such as gully length, gully depth, gully catchment area and gully volume, we are able to attribute specific gully evolution phases according to Kosov et al. (1978). The authors divided the gully lifetime in a dynamic phase covering just the first 5 % of the gully's lifetime and a static phase covering the remaining

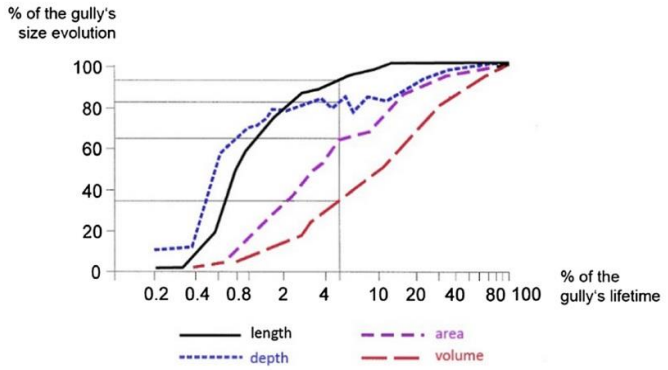

Fig. 3 Gully evolution phases according to gully morphometric characteristics (from Sidorchuk 1999, after Kosov et al. 1978)

95 % of the gully's lifetime. As illustrated in Fig. 3, the dynamic phase is characterized by (1) a gully length up to 90 % of the entire length development, (2) a gully depth that reaches up to 80 % of its final depth, (3) a gully catchment or contributing area of less than 60 % of the entire contributing area and (4) less than 45 % of the final gully volume. The formula used for the classification of dynamic and static gully phases is:

$$\text{ratio}\,\% = \frac{\text{AH} - \text{TCA}}{\text{TCA}}$$

where AH is the contributing area at gully head (m^2), and TCA is the total contributing area at the downstream situated gully mouth (m^2). In this study, we utilized the gully area to divide between dynamic and stable gully evolution phases. A ratio greater then 60 % indicate static gully systems, and ratios below 60 % reveal dynamic systems.

4 Results and discussion

4.1 DEM comparison

Comparing the original DEMs with the interpolated DEMs, we observed a much higher detail and precision for the study of gully erosion for the interpolated DEMs. The enhanced resolution in the interpolated DEMs is the effect of adding crucial information into the interpolation process. Particularly, small-scale erosion processes cannot be derived from the original DEMs because their resolution is too coarse and they do not allow extrapolating information that has a process scale of about 5–10 m. As illustrated in Fig. 4, the interpolated DEMs show more detail and hence allow an assessment of higher spatial erosion process details.

The incorporation of thalwegs and drainage lines as local relative elevation minima provides more realistic and hydrological correct elevation models. We used field measured *x*-/*y*-GPS points and depth information we derived from the cross sections as input in the ANUDEM procedure to increase the elevation accuracy particularly along the gully drainage lines. The models with an enforced drainage system generally show better results than the ones without the enforced drainage option set during the interpolation procedure.

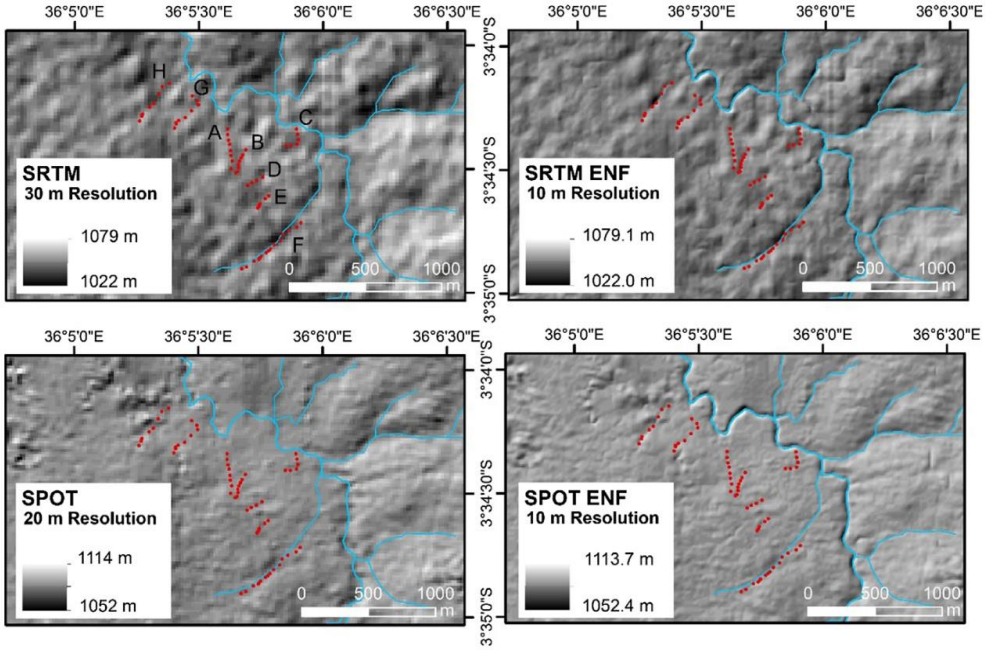

Fig. 4 Comparison between original SRTM-X and SPOT data and their accordingly interpolated DEMs, all shown with underlying hillshade. *Blue lines* are river channels and *red points* the gully thalweg ground truth locations

Hence, in the following we concentrate on the enforced drainage DEMs. Generally, adding digitized drainage lines into raster datasets results in a correction of the drainage networks, especially in areas with very smooth or flat terrain and unclear drainage pattern. The drainage lines were identified and digitized on dry-season high-resolution satellite images GeoEye-1 (0.5 m resolution) and Ikonos-2 (1 m resolution). Due to the low vegetation cover and the high resolution of the satellite images, the delineated drainage network used in the interpolation is very reliable and reflects the real-world situation. The satellite images used to process the SPOT DEM were taken during the long dry season and the short dry season, when the vegetation cover is at its minimum. Therefore, the elevation values of these DEMs are only marginally influenced by the vegetation. To remove the noise generated by big trees like baobab (*Adansonia digitata*), the SPOT DEM has been filtered to smooth these spatial discontinuities. Finally, the use of an interpolation algorithm to generate hydrological correct models like ANUDEM, allowed creating DEMs that are suitable to make terrain analysis for the interpretation of erosion processes such as gullies. The use of different interpolation methods (Kriging, IDW, natural neighbor) results in DEMs that are particularly less suitable for the erosion process assessments (Reuter et al. 2007; Hu et al. 2014).

The main problem with ASTER GDEM data is that the vegetation cover is included in the height information of the cells, due to the stereoscopic methodology of optical image pairs. The surface elevation including vegetation might be useful in some kind of studies, but not for hydro-erosive terrain analyses where the actual ground surface topography is needed. The ASTER GDEM scene for the study area shows a lot of noise and artifacts due to vegetation cover and shadowing effects, especially along the Makuyuni River main

channel and for baobabs located in the study area. The dataset also has a lower resolution compared to the SPOT DEM. Consequently, it was excluded from the analysis because its resolution is not suitable to detect gully processes.

The new interpolation of the original SPOT DEM with 20 m pixel size, to a resolution of 10 m pixel size, means that we divide the original cell into four cells, each with 100 m^2. Theoretically, the information obtained seem to be more accurate. However, we can observe directly from Fig. 5a, b that the surface of the SRTM ENF10 is less homogenous and coarser than the SPOT ENF10, even if the SAR sensor can pass through vegetation. Consequently, we yield a better performance, especially for the terrain analysis, with the SPOT ENF10 DEM because the surface is more regular, reflecting better the real terrain surface.

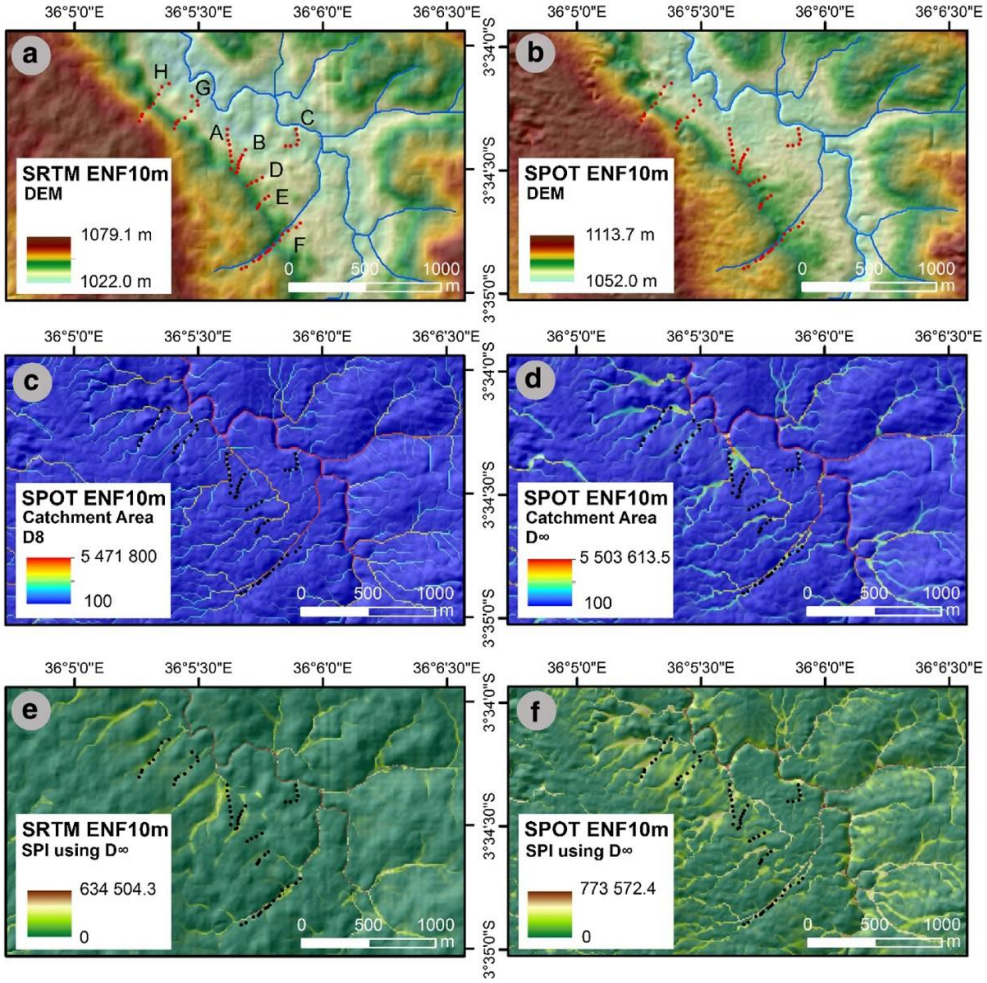

Fig. 5 GIS-based analyses of the different DEMs with underlying hillshade. **a** SRTM-X ENF10, **b** SPOT ENF10, **c** catchment area calculated with D8 from SPOT ENF10, **d** catchment area calculated with D∞ from SPOT ENF10, **e** SPI calculated with D∞ from SRTM-X ENF10, **f** SPI calculated with D∞ from SPOT ENF10

4.2 Terrain analysis

The Stream Power Index (SPI) as a tool to identify linear erosion processes like gullies, is very powerful even when using DEMs with a resolution that is actually lower than the scale of the erosion processes. Moreover, we derive also the Transport Capacity Index (TCI) to understand and identify the more areal erosion like sheet erosion processes.

The flow accumulation generated with D∞ flow accumulation algorithm from the DEM SPOT ENF10 can identify basically all the reference gullies even though there are some uncertainties in the drainage pattern of gully A, especially in the upper part (Fig. 5d). The same conclusions can be drawn for the flow accumulation generated with the D8 algorithm. Nonetheless, D8 is less conform with a real situation because all the water contained in a cell is moved to another cell; consequently water flows are always converging although in reality water can flow in different directions such as in flat or convex areas (Fig. 5c).

The SPI calculated on the DEM SRTM ENF10 identifies successfully the gullies B, C, F, G and H, with some uncertainty in the area around the gully head and the mouth of gully A (see Fig. 5e, f). The gullies E and D can be identified with the SPI values. However, they are not represented by very high SPI values such as the other gullies due to the smaller catchment area and divergent drainage pattern. This is probably caused by a very low depth of the gully systems; hence, it is difficult to interpolate these areas accurately. According to the field measurement, gully D has an average depth of 72 cm and a maximum of 102.5 cm, which is lower than all the other gullies. Gully C on the lower Makuyuni River terrace was also identified by both SRTM ENF10 and SPOT ENF10. The model SPOT ENF10 generally shows a higher accuracy in identifying the gully systems. Where SPI values are medium or high (red to gray color), the energy available for erosion processes is high. Hence, where the index is low (bright green color), the energy is lower. The SPI values of the SPOT ENF10 (Fig. 5f) are high for gullies B, F and H and for lower parts of gully A; are medium for gullies C and G; and are low for gullies D, E and the upstream half of gully A. The same values can be generally observed in the SRTM ENF10 DEM, but with a greater uncertainty (Fig. 5e).

The SPI values show that sites of more intensive gully incision are located in zones with high slope gradient, thus higher surface runoff velocities and/or larger contributing areas and hence larger flow volumes. This correlation of SPI and slope is confirmed also by the longitudinal profiles. Moreover, three zones with high SPI values can be identified: a first one is localized on the banks or lower terraces of the Makuyuni River related to retrogressive erosion and easily erodible fluvial materials, a second one on the escarpment of the second river terrace where all gullies pass through, and a third one on the escarpment next to the Tree Tops road plateau. These three zones have been also identified in the field by a visual evaluation (Figs. 2, 6).

The central zone of the study area, characterized by high SPI and slope values (see Fig. 6 for slope degree values), is dominated by a tephra layer that was dated to 633 ka BP (Schwartz et al. 2012). In this area, most of the gully head cuts are located. The high slope angles of this escarpment increase surface runoff speed. During the rainy season, the surface runoff gets concentrated and hence rills and gullies develop and sediments are eroded and transported downstream to the river. The Transport Capacity Index (TCI) or LS Factor takes into account the specific catchment area and slope degree highlighting the spatial distribution of material transport and deposition. The areas with higher slope gradient identified by the SPI are also the ones where there is more material transport by surface runoff (Fig. 5e, f; yellow to brown colors). The greater the erosional energy,

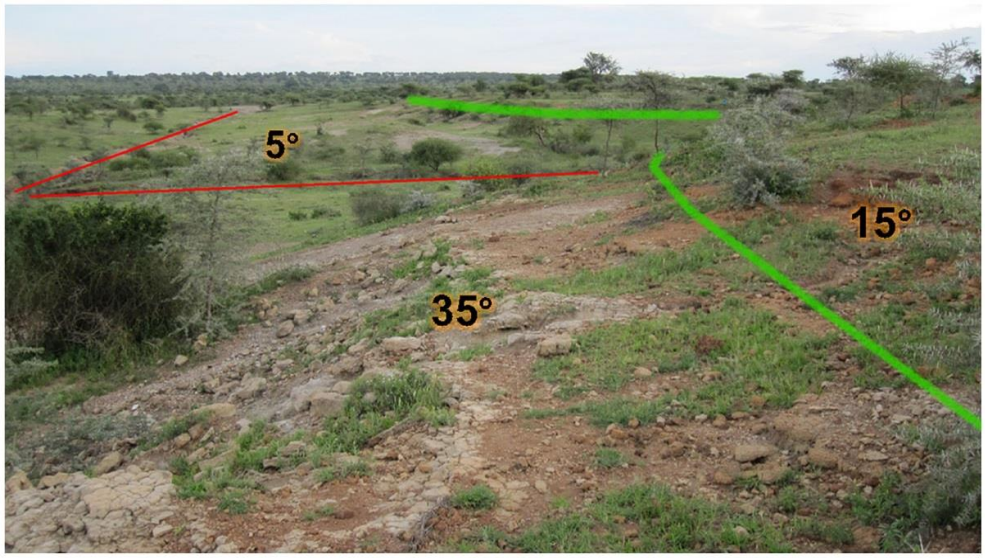

Fig. 6 Second escarpment close to Tree Top road. In *red* are gullies *A* and *B*, and in *green* the tephra outcrops. The fluvial terrace above has a slope of 15° whereas the Tephra escarpment 35° and the lower fluvial terrace a slope of 5°

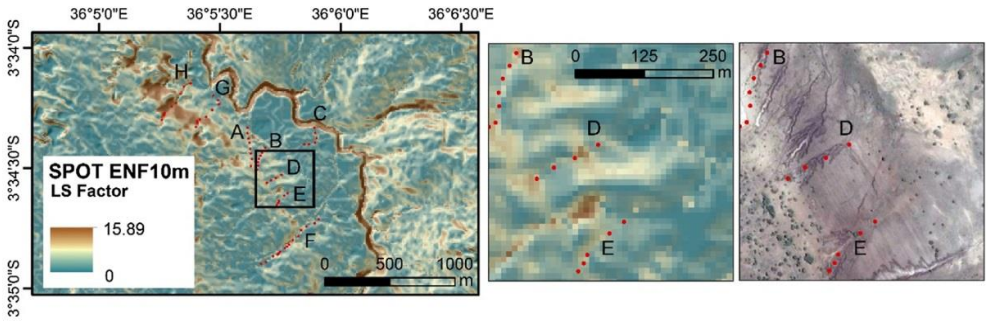

Fig. 7 TCI or LS Factor calculated with D∞ on SPOT ENF10 (*left*); close up of the LS factor for gullies *B*, *D* and *E* (*middle*) as well as a close up underlied by GeoEye-1 data (*right*)

coupled with an increasing soil particle detachment, the more material has to be transported in the water flow. TCI zones showing no transport and thus material deposition and accumulation occur where the transport capacities diminish (shown in blue green colors, Fig. 7 left and middle). For example we identified depositional areas at the downstream parts of gullies B, D and E (zoomed area in Fig. 7 middle and right).

4.3 Gully development and evolution

In order to validate the SPI values in the field, we plotted the SPI values of gully H against the distance from the gully head downstream to the Makuyuni River, shown in Fig. 8. In this figure, a few SPI peaks were identified. The first increase is marked as T and corresponds to the head of the gully where the outcropping tephra layer is located. The peak T_2 is further downstream, where the water starts to concentrate flowing inside the gully itself.

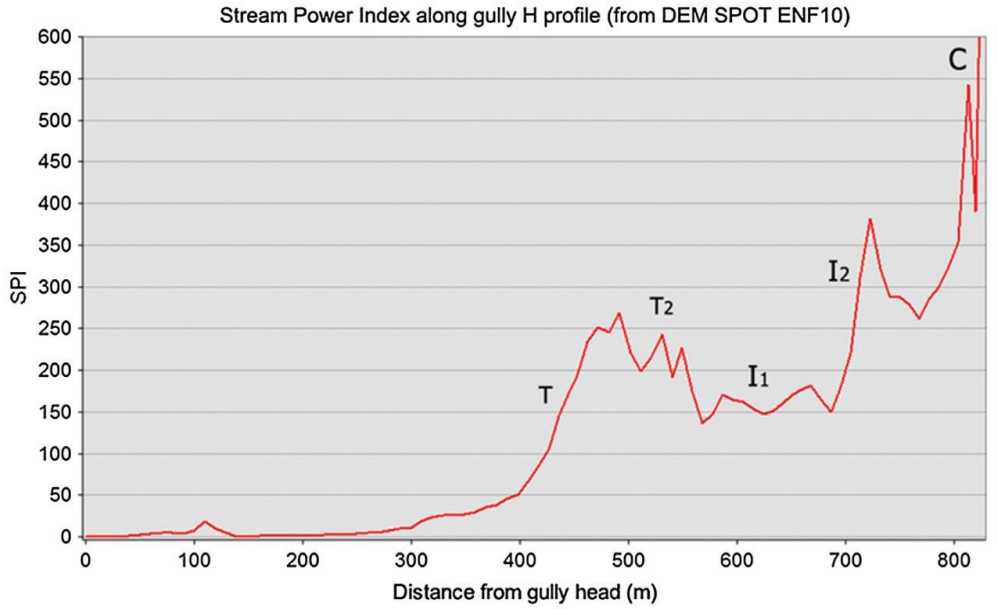

Fig. 8 SPI along the gully H longitudinal profile, from DEM SPOT ENF10

Table 4 Gully phase classification according to the Sidorchuk model

Gully	AH (m^2)	TCA (m^2)	AH – TCA (m^2)	(AH − TCA)/TCA	%	Phase
A	1408	592,435	591,027	0.99762	99.76	Static
B	1196	592,435	591,239	0.99798	99.80	Static
C	153,086	173,053	19,967	0.11538	11.54	Dynamic
D	1161	172,760	171,599	0.99328	99.33	Static
E	1061	172,760	171,699	0.99386	99.39	Static
F	266,877	555,278	288,401	0.51938	51.94	Dynamic
G	1497	382,423	380,926	0.99609	99.61	Static
H	19,196	382,422	363,226	0.94980	94.98	Static

In this area during dry season, there is almost no vegetation, indicating intensive erosion dynamics. Moreover, the SPI values decrease in the area of I_1 (Fig. 5e, f), where the gully depth decreases and gullies almost disappear (lower river terrace). Subsequently, at peak I_2 the gully area increases abruptly due to another tributary gully system that flows into gully H (Fig. 5e, f). The zone C is located close to the Makuyuni River where the material is transported to and deposited.

To asses the evolution stage of the gullies, we applied a methodology based on Kosov et al. (1978). We identified two phases: (1) a static phase that corresponds to 95 % of gully's lifespan and (2) the dynamic developing phase covering the first 5 % of gully lifetime. The model was successfully applied in various studies to classify gully dynamics (e.g., Sidorchuk et al. 2003). We calculated the contributing area at the head cut (AH) and the total contributing area downstream (TCA) for all eight gullies, using the D∞-based catchment area derived from the SPOT ENF10, and the results are shown in Table 4.

The classification shows that most of the gullies are in the static phase. Only gullies C and F show a dynamic pattern. The stable gullies do not significantly grow anymore in their area, and therefore, they are supposed to be quite old systems. The contributing area at the upstream of gully C shows very high values due to many gullies flowing into gully C at this location. Hence, this gully seems to be still in a dynamic phase. Gully F is also classified as dynamic; however, the model did not take into account the sedimentation/aggregation along the lower reach of this gully.

The longitudinal profiles show the elevation of the gully beds and adjacent slopes along the gully channel, from upstream to downstream. We made longitudinal profiles for all the gullies. Figure 9 illustrates the profile for gully F showing the two river terraces between 400–800 and 1200–1600 m flow length and the two escarpment zones with steeper slopes at 100–400 and 900–1100 m flow length. The comparison of the gully longitudinal profile (red line) with a profile in the not eroded area located on the undisturbed surface next to the gully (gully shoulder: blue line), demonstrates that the eroded areas are located where the slope is higher and/or where soil material is easily erodible (bigger vertical distance between red and blue line). The latter is confirmed by the substrate analysis in the field. The upper part consists of shallow soils on steeper slopes that are eroded further down exposing carbonatic concretions. Between 400 and 900 m flow length, the soil depth is increasing again. Soils mainly consist in erodible vertisols. Deepest incisions are localized in the area of the tephra outcrops that protect the underlying paleosols and paleolake deposits (900–1000 m flow length). At a distance between 1100 and 1400 m flow length, the gully bed elevation is higher than the surrounding areas indicating deposition and accumulation of transported sediments. This area is also highlighted for gullies B, D and E (see Fig. 7). Particularly, the lower fluvial terrace of the Makuyuni river at 1065–1070 m elevation a.s.l. is composed of fine erodible vertic fluvial deposits. The fluvial terraces are related to raising and lowering phases of a Paleolake Manyara.

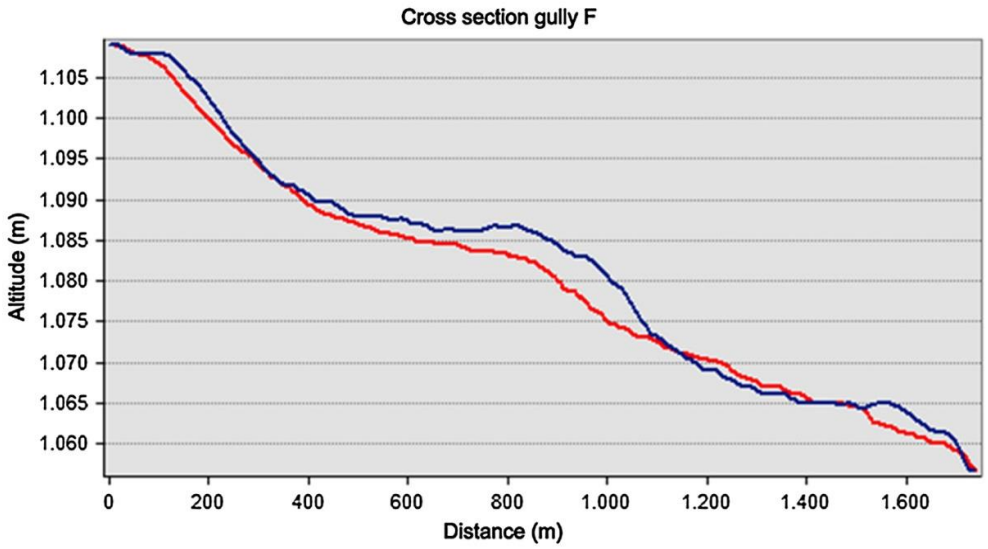

Fig. 9 Longitudinal profile of gully F. In *red gully thalweg* elevation and in *blue gully shoulder* elevation

5 Conclusions

Additional topographic information such as (1) measured *x*-/*y*-GPS gully points, (2) gully depth derived using cross-sectional measurements and (3) gully drainage networks digitized from GeoEye-1 and Ikonos-2 are used to re-interpolate DEMs yielding a higher topographic resolution than the source DEM based on SPOT and SRTM-X data. Generally, the re-interpolated SPOT DEM provides the best results in terms of spatial accuracy, low noise and artifacts. Even though SRTM-X is a SAR-based DEM with low influence of vegetation, the noise in the resulting DEMs was higher than in the SPOT-based DEM. The lowest performance was obtained by the ASTER GDEM due to the fact that ASTER scenes are strongly influenced by the vegetation cover and have a lower spatial resolution compared to the SPOT DEM. Best results for the interpolation of the DEMs were obtained by applying the hydrological forcing option of the ANUDEM algorithm "Topo to Raster." This algorithm guarantees a hydrological correct DEM without sinks. The assessment of the gully erosion processes was subsequently conducted with the best-performing DEM, namely the SPOT ENF10 DEM.

The terrain analysis is mainly based on topographic indices related to slope degree and catchment area. For the latter, we applied the D8 and D∞ algorithms. Generally, the D∞ yield better results and is closer to reality. The calculation of the topographic indices like SPI and TCI finally showed that specific gully features such as head cuts, catchment areas and erosion/deposition zones can be assessed with the improved SPOT ENF10 DEM. The derived results of SPI and LS Factor were also validated in the field confirming the high accuracy and reliability of the improved DEM. The investigated gully systems seem to be very old and belonging to the static gully phase according to Kosov et al. (1978). This is also confirmed by archeological and paleontological evidence in the area.

Additional topographic information can be derived by fieldwork (GPS points and gully cross sections) and GoogleEarth mapping of thalweg systems at high spatial accuracy. This information incorporated in a DEM artificially increases the spatial resolution. The derived DEMs show a good performance in terms of the hydrological and geomorphological process dynamics, which were assessed by terrain analysis. The presented approach is a simple low-cost methodology for gully assessment.

Acknowledgments This study was financed by the The Role of Culture in Early Expansions of Humans (ROCEEH) Research Centre of the Heidelberg Academy of Sciences and Humanities, Germany. We thank the Tanzania Commission for Science and Technology (COSTECH) for their research permission. We would also like to thank the DLR and the German Remote Sensing Data Center (DFS) for providing the SRTM/X-SAR data. ASTER GDEM is a product of the Ministry of Economy, Trade, and Industry (METI) of Japan and the United States National Aeronautics and Space Administration (NASA). The SPOT DEM was acquired from the ISIS Programme, Centre National d'Etudes Spatiales (CNES, France). Finally, we also would like to thank the EU IRSES Project (PIRSES-GA-2012-318969) for support of researcher exchange.

References

Arun PV (2013) A comparative analysis of different DEM interpolation methods. Geod Cartogr 39(4):171–177. doi:10.3846/20296991.2013.859821

ASTER GDEM Validation Team (2011) ASTER global digital elevation model: version 2. Summary of validation results. https://igskmncnwb001.cr.usgs.gov/aster/GDEM/Summary_GDEM2_validation_report_final.pdf. Accessed 5 April 2014

Bachofer F, Quénéhervé G, Märker M (2014) The delineation of paleo-shorelines in the Lake Manyara basin using TerraSAR-X data. Remote Sens 6(3):2195–2212. doi:10.3390/rs6032195

Bergner AGN, Strecker MR, Trauth MH, Deino AL, Gasse F, Blisniuk P, Dühnforth M (2009) Tectonic and climatic control on evolution of rift lakes in the Central Kenya Rift, East Africa. Quat Sci Rev 28(25–26):2804–2816

Brooks AP, Shellberg J, Knight J, Spencer J (2009) Alluvial gully erosion: an example from the Mitchell fluvial megafan, Queensland, Australia. Earth Surf Proc Landforms 34(14):1951–1969. doi:10.1002/esp.1883

Capra A (2013) Ephemeral gully and gully erosion in cultivated land: a review. In: Lannon EC (ed) Drainage basins and catchment management: classification, modelling, and environmental assessment. Nova Science, Hauppauge, pp 109–141

Casanova J, Hillaire-Marcel C (1992) Chronology and paleohydrology of late quaternary high lake levels in the Manyara basin (Tanzania) from isotopic data (18O, 13C, 14C, Th/U) on fossil stromatolites. Quat Res 38(2):205–226. doi:10.1016/0033-5894(92)90057-P

Conoscenti C, Agnesi V, Angileri S, Cappadonia C, Rotigliano E, Märker M (2013) A GIS-based approach for gully erosion susceptibility modelling: a test in Sicily, Italy. Environ Earth Sci 70(3):1–17. doi:10.1007/s12665-012-2205-y

Costanzo D, Cappadonia C, Conoscenti C, Rotigliano E (2012) Exporting a Google Earth™ aided earth-flow susceptibility model: a test in central Sicily. Nat Hazards 61(1):103–114. doi:10.1007/s11069-011-9870-0

D'Agostino V, Vianello A (2005) Identificazione morfodinamica del reticolo idrografico: integrazione fra rilievi di campo e tecniche GIS. Quaderni di Idronomia Montana 24:271–290 **(in Italian)**

Dawson JB (1997) Neogene; recent rifting and volcanism in northern Tanzania; relevance for comparisons between the Gardar Province and the East African Rift valley. Mineral Mag 61(4):543–548

Desmet PJJ, Govers G (1996) A GIS procedure for automatically calculating the USLE LS factor on topographically complex landscape units. J Soil Water Conserv 51(5):427–433

Deus D, Gloaguen R, Krause P (2013) Water balance modeling in a semi-arid environment with limited in situ data using remote sensing in Lake Manyara, East African Rift, Tanzania. Remote Sens 5(4):1651–1680

DLR (2012) SRTM X-SAR digital elevation models: status: 2012-09-28. http://eoweb.dlr.de:8080/eoweb-ng/licenseAgreements/DLR_SRTM_Readme.pdf. Accessed 23 December 2013

El Haj Tahir M, Kääb A, Xu C-Y (2010) Identification and mapping of soil erosion areas in the Blue Nile, Eastern Sudan using multispectral ASTER and MODIS satellite data and the SRTM elevation model. Hydrol Earth Syst Sci 14(7):1167–1178. doi:10.5194/hess-14-1167-2010

Flügel W-A, Märker M, Moretti S, Rodolfi G, Sidorchuk A (2003) Integrating geographical information systems, remote sensing, ground truthing and modelling approaches for regional erosion classification of semi-arid catchments in South Africa. Hydrol Process 17(5):929–942. doi:10.1002/hyp.1171

Frankl A, Poesen J, Haile M, Deckers J, Nyssen J (2013) Quantifying long-term changes in gully networks and volumes in dryland environments: the case of Northern Ethiopia. Geomorphology 201:254–263. doi:10.1016/j.geomorph.2013.06.025

Frost SR, Schwartz HL, Giemsch L, Morgan LE, Renne PR, Wildgoose MM, Sanaane C, Schrenk F, Harvati K (2012) Refined age estimates and Paleoanthropological investigations of the Manyara Beds, Tanzania. JASs 90:151–169

Garbrecht J, Starks P (1995) Note on the use of USGS level 1 7.5-minute DEM coverages for landscape drainage analyses. Photogramm Eng Remote Sens 61(5):519–522

Google (2012) http://www.google.com/intl/en-US/help/terms_maps.html. Accessed 20 February 2014

Gruber S, Peckham SD (2009) Land-surface parameters and objects in hydrology. In: Hengl T, Reuter HI (eds) Geomorphometry: concepts, software, applications. Developments in soil science, vol 33. Elsevier, Amsterdam, pp 171–194

Hancock GR, Evans KG (2010) Gully, channel and hillslope erosion. An assessment for a traditionally managed catchment. Earth Surf Proc Landforms 35(12):1468–1479. doi:10.1002/esp.2043

Hu J, Tan Q, Wang H, Xu X (2014) Accuracy assessment of DEM interpolation algorithms in different landform regions. J Basic Sci Eng 1(1):139–149

Hutchinson MF (1986) Algorithm 642: a fast procedure for calculating minimum cross-validation cubic smoothing splines. ACM Trans Math Softw 12(2):150–153. doi:10.1145/6497.214322

Hutchinson MF (1989) A new procedure for gridding elevation and stream line data with automatic removal of spurious pits. J Hydrol 106(3–4):211–232. doi:10.1016/0022-1694(89)90073-5

Keller CM, Hansen C, Alexander CS (1975) Archaeology and Paleoenvironments in the Manyara and Engaruka Basins, Northern Tanzania. Geogr Rev 65(3):364–376

Kosov BF, Nikol'skaya II, Zorina Y (1978) Eksperimental'nyye issledovaniya ovragoobrazovaniya. In: Makkaveev NI (ed) Eksperimental'naya geomorfologiya, vol 3. Moscow University, Moskva, pp 113–140 (**in Russian**)

Moore ID, Burch GJ, Mackenzie DH (1988) Topographic effects on the distribution of surface soil water and the location of ephemeral gullies. Trans Am Soc Agric Eng 31(4):1098–1107

Mwanukuzi PK (2011) Impact of non-livelihood-based land management on land resources: the case of upland watersheds in Uporoto Mountains, South West Tanzania. Geogr J 177(1):27–34. doi:10.1111/j.1475-4959.2010.00362.x

Nelson A, Reuter HI, Gessler PE (2009) DEM production methods and sources. In: Hengl T, Reuter HI (eds) Geomorphometry: concepts, software, applications. Developments in soil science, vol 33. Elsevier, Amsterdam, pp 65–85

Renard KG, Foster GR, Weesies GA, McCool DK, Yoder DC (1997) Predicting soil erosion by water: a guide to conservation planning with the Revised Universal Soil Loss Equation (RUSLE). Agriculture Handbook, Washington

Rengers FK, Tucker GE (2014) Analysis and modeling of gully headcut dynamics, North American high plains. J Geophys Res Earth Surf 119(5):983–1003. doi:10.1002/2013JF002962

Reuter HI, Nelson A, Jarvis A (2007) An evaluation of void-filling interpolation methods for SRTM data. IJGIS 21(9):983–1008. doi:10.1080/13658810601169899

Reuter HI, Hengl T, Gessler PE, Soille P (2009) Preparation of DEM for geomorphometric analysis. In: Hengl T, Reuter HI (eds) Geomorphometry: concepts, software, applications. Developments in soil science, vol 33. Elsevier, Amsterdam, pp 87–120

Ring U, Schwartz HL, Bromage TG, Sanaane C (2005) Kinematic and sedimentological evolution of the Manyara Rift in northern Tanzania, East Africa. Geol Mag 142(4):355–368. doi:10.1017/s0016756805000841

Schwartz HL, Renne PR, Morgan LE, Wildgoose MM, Lippert PC, Frost SR, Harvati K, Schrenk F, Sanaane C (2012) Geochronology of the Manyara Beds, northern Tanzania: new tephrostratigraphy, magnetostratigraphy and $^{40}Ar/^{39}Ar$ ages. Quat Geochronol 7:48–66. doi:10.1016/j.quageo.2011.09.002

Shellberg JG, Brooks AP, Rose CW (2013) Sediment production and yield from an alluvial gully in northern Queensland, Australia. Earth Surf Proc Landforms 38(15):1765–1778. doi:10.1002/esp.3414

Sidorchuk A (1999) Dynamic and static models of gully erosion. CATENA 37(3–4):401–414. doi:10.1016/S0341-8162(99)00029-6

Sidorchuk A (2006) Stages in gully evolution and self-organized criticality. Earth Surf Proc Landforms 31(11):1329–1344. doi:10.1002/esp.1334

Sidorchuk A, Märker M, Moretti S, Rodolfi G (2003) Gully erosion modelling and landscape response in the Mbuluzi River catchment of Swaziland. CATENA 50(2–4):507–525

Tarboton DG (1997) A new method for the determination of flow directions and upslope areas in grid digital elevation models. Water Resour Res 33(2):309–319. doi:10.1029/96WR03137

Tarboton DG, Bras RL, Rodriguez-Iturbe I (1991) On the extraction of channel networks from digital elevation data. Hydrol Process 5(1):81–100. doi:10.1002/hyp.3360050107

Trauth MH, Deino AL, Bergner AGN, Strecker MR (2003) East African climate change and orbital forcing during the last 175 kyr BP Earth Planet. Sci Lett 206(3–4):297–313

Trauth MH, Larrasoaña JC, Mudelsee M (2009) Trends, rhythms and events in Plio-Pleistocene African climate. Quat Sci Rev 28(5–6):399–411

Vrieling A, Sterk G, Vigiak O (2006) Spatial evaluation of soil erosion risk in the West Usambara Mountains, Tanzania. Land Degrad Dev 17(3):301–319. doi:10.1002/ldr.711

Wilson JP, Gallant JC (eds) (2000) Terrain analysis: principles and applications. Wiley, New York

Wischmeier WH, Smith DD (1978) Predicting rainfall erosion losses—a guide to conservation planning, vol 537. Agriculture Handbook, Washington

Zakerinejad R, Maerker M (2014) Prediction of gully erosion susceptibilities using detailed terrain analysis and maximum entropy modeling: a case study in the Mazayejan plain, southwest Iran. Geogr Fis Dinam Quat 37(1):67–76

V Geomorphology of the Makuyuni Area, Northern Tanzania

Authors

Geraldine Quénéhervé, Felix Bachofer and Michael Maerker

Author contribution:

Geomorphic feature digitizing, maps, figures, photos, interpretation and writing.

Current Status

Submitted to Journal of Maps.

This thesis shows a manuscript version of the submitted paper. The rear end inlet provides a printed version of the map, that is a supplemental material of Journal of Maps.

This version is the submitted version and does not follow the journal layout.

Geomorphology of the Makuyuni Area, Northern Tanzania

Geraldine Quénéhervé[a,*], Felix Bachofer[a] and Michael Maerker[b,c]

[a] University of Tübingen, Department of Geosciences, Institute of Geography, Tübingen, Germany

[b] Pavia University, Department of Earth and Environmental Sciences, Pavia, Italy

[c] Heidelberg Academy of Sciences and Humanities c/o University of Tübingen, Tübingen, Germany

*Corresponding author: Geraldine Quénéhervé (geraldine.queneherve@uni-tuebingen.de). Institute of Geography, Rümelinstr. 19-23, 72070 Tübingen, Germany. Tel: +49 7071 29 72131.

Abstract

In this paper, we present a geomorphologic map of the area around the village of Makuyuni, Monduli district, in Northern Tanzania. This area is known for early hominid occupation dating back 630 ka BP. We applied process detection techniques for semiarid environments with an emphasis on water induced erosion features. The processes and related forms and features were assessed with remote sensing techniques and validated with extensive field surveying. For the geomorphological assessment, we combine information on morphology and morphogenesis with secondary information on sampling and laboratory data. We use Geographic Information Systems (GIS) for the mapping procedure. The GIS is linked with a geomorphologic database. The reference scale allows the in-depth analysis of landforms and geomorphic processes providing important information for related disciplines such as paleoecology, archaeology or palaeontology.

Keywords

Geomorphological Map; Cartography; Tanzania; SRTM; SAR data; Remote Sensing Data

1. Introduction

Geomorphological mapping plays an essential role in understanding surface processes, geochronology, natural resources, natural hazards and landscape evolution (Bishop & Shroder, 2004; Blaszczynski, 1997). A geomorphological map identifies, interprets and represents the morphology (form) and morphogenesis (process) of the landforms. The complexity of mapping comprises information about the composition and structure, chronology (relative and absolute age), environmental system characteristics (land cover, soils, ecology), as well as spatial topological relationships of surface features (landforms) (Bishop, James, Shroder, & Walsh, 2012; Smith & Pain, 2011). The accurate interpretation of specific landforms also depends on complementary data, including topography, geology and sedimentology (Knight, Mitchell, & Rose, 2011). Smith and Pain (2011) state that it is not necessary to combine all elements into a single cartographic document, but to have a clear principal focus that determines the selection of elements.

Modern comprehensive geomorphological map compilation started in the early 20th century. However, until now there is no uniformity among geomorphological legends, as different mapping 'schools' independently developed systems for use at different scales in a variety of landscapes (see Seijmonsbergen, 2013). Gustavsson, Kolstrup, and Seijmonsbergen (2006) published a GIS-based legend for geomorphological mapping that is used widespread through the scientific community (Anders, Seijmonsbergen, & Bouten, 2009; May, 2008; Poppe et al., 2013). Data collection in the field is important for the compilation of geomorphological maps and the issue of scale is substantial (Smith & Pain, 2011); the mapping of a particular area for a specific purpose is usually undertaken at a scale between 1:5000 and 1:50 000 (Doornkamp, 1971). Detailed geomorphological mapping is time consuming (Gustavsson et al., 2006) therefore, in the last decades, many scientists have focused on the elaboration of thematic maps that are immediately applicable and they neglected complex maping with a holistic approaches (Rădoane, Cristea, & Rădoane, 2011).

In the late 1980s, the use of Geographic Information Systems (GIS) became widespread in geomorphology and GIS technologies have become important tools for landform analysis, data management and construction of geomorphological databases (Demek, Kirchner, Mackovčin, & Slavík, 2011; Gustavsson et al., 2006). Digital Elevation Models (DEMs), in particular the increasing availability of high-resolution DEMs with 1 to 20 m spatial resolution within the last decade, have led to quantitative landscape approaches based on terrain analysis (Hengl & Reuter, 2009; Wilson & Gallant, 2000). GIS have become a quantitative technology to

analyse, manage and visualize landforms (Drăguţ & Eisank, 2011; Hengl & MacMillan, 2009; Jasiewicz, Netzel, & Stepinski, 2014; Jasiewicz & Stepinski, 2013; Vannametee et al., 2014) as well as geomorphic processes (Di Crescenzo & Santo, 2007; Maerker, Quénéhervé, Bachofer, & Mori, 2015; Richards, Brasington, & Hughes, 2002). Chronological aspects of landscape dynamics can also be assessed using GIS and quantitative models for the reconstructions of paleo-features (Bachofer, Quénéhervé, & Märker, 2014; Bisson & Bini, 2011; Braun & Sambridge, 1997; Brouwer Burg, 2013; Vogel & Märker, 2010) or with landscape evolution models (see review by Chen, Darbon, & Morel, 2014).

Remotely sensed optical data with a high spatial and spectral resolution like WorldView-2 with a ground resolution of 0.5 m (panchromatic) allow base mapping at scales between 1:25 000 and 1:2500 (Siart, Bubenzer, & Eitel, 2009). Optical satellite imagery and DEMs provide information on surface structure and enables a spectral differentiation and thus, a consistent interpretation. These techniques have been applied to detect geomorphological units and various relief features like glacial landforms (Clark, Knight, & T. Gray, 2000; Jansson, 2005), aeolian landforms (Ewing, McDonald, & Hayes, 2015; Hugenholtz, Levin, Barchyn, & Baddock, 2012), coastal landforms (Devoto et al., 2012; Senthilnathan, Nobi, Thangaradjou, & Kannan, 2012) or for karstic landscapes (Annys et al., 2014; Siart et al., 2009). Radar imagery can assist in the identification of morphological structures (Bachofer, Quénéhervé, Zwiener, Maerker, & Hochschild, 2016; Smith, Rose, & Booth, 2006; Souza, Pedro, & Paradella, 2014).

This study is located in the Lake Manyara rift basin that is part of the East African Rift System (EARS). The area is known for its early hominin remains and artefact during Early and Middle Pleistocene (the majority of the artefacts are dated between 630 000 and 400 000 BP; see Giemsch et al., in press) and are therefore in the interest of (paleo-) environmental studies. Doornkamp (1971) stated in the 1970s that the potential value of geomorphological studies in East Africa ‘has not yet been fully realized and geomorphology has not yet developed beyond its most elementary stage’, nowadays, more than 40 years later, there is no significant change in this statement. Grove (1986) provided a description of the geomorphology of the EARS. A comprehensive geomorphological mapping was carried out at the eastern shorelines of Lake Manyara (Vaidyanadhan, Dixit, & Schlüter, 1993) but does not cover the mapping area of this study.

The aim of this study is to map the morphology and morphogenesis of the landforms in the proximity of Makuyuni village, Monduli district. We follow a multiscale approach with (i) extensive field mapping, (ii) interpretation of multispectral and microwave remote sensing

images (WorldView-2 and TerraSAR-X data) and (iii) the delineation of topographic derivatives (based on SRTM-X). Particular attention was given to the identification and mapping of gully erosion forms and features. Gully erosion is one of the most severe soil erosion processes leading to the loss of fertile topsoil and intensive sediment transport towards the drainage systems. Hence, gully erosion is threading agriculture and pasture as well as the drainage system and related water resources (e.g. Märker, Hochschild, Maca & Vilímek, 2016). In terms of archaeological and paleontological research, linear erosion processes exposing artefacts and/or fossils on the one hand allow to easily assess find locations. On the other hand, downwearing might be also a possible threat in terms of losing finds. The geomorphological map carried out in this study yield valuable information for related disciplines such as paleoecology and geoarchaeology or palaeontology. In particular, the map supports the planning of detailed fieldwork.

2. Regional Setting

The mapped area is located in northern Tanzania and is part of the EARS. The study area consists of approximately 460 km² and is located between S 3° 30’ and S 3° 39’ north-south latitudes and E 36° and E 36° 15’ west-east longitudes. The entire study area is drained by the Makuyuni River with a catchment area of 3084 km², which is running westward into Lake Manyara. Altitudes reach 1358 m a.s.l. in the north-western fault zone located in grid B10 (see Figure 1 for grid reference) whereas the Makuyuni River outlet point, located in grid F1, is the lowest part of the study area with a height of 1002 m a.s.l.

The eastern branch of the EARS runs through Ethiopia and Kenya up to Northern Tanzania, following a N–S trend. As the eastern branch, the so-called Gregory Rift, enters Tanzania, it becomes a half graben system and splays into a 300 km wide zone of block faulting (Dawson, 2008). Many volcanoes are located in this active zone, the closest to the study area, northwest of it, is called Volcano Essimingor. Within the Makuyuni catchment, there are several *en échelon* micro faults, which were active during the late Pleistocene (Dawson, 2008; Ring, Schwartz, Bromage, & Sanaane, 2005). Flores-Prieto, Quénéhervé, Bachofer, Shahzad, and Maerker (2015) stated that gully erosion processes in the Makuyuni catchment might be triggered by local active tectonics. The main lithologies within the study area are proterozoic quartzite and gneiss basements, volcanic and lacustrine deposits as well as recent river bed deposits along commonly with long periods of rare precipitation and short but heavy rains.

The mean annual temperature is 27° C. The main land cover type is shrub and grassland that is used for extensive grazing of goats, cows and sheep, apart from that the main agricultural products in the region are maize and beans.

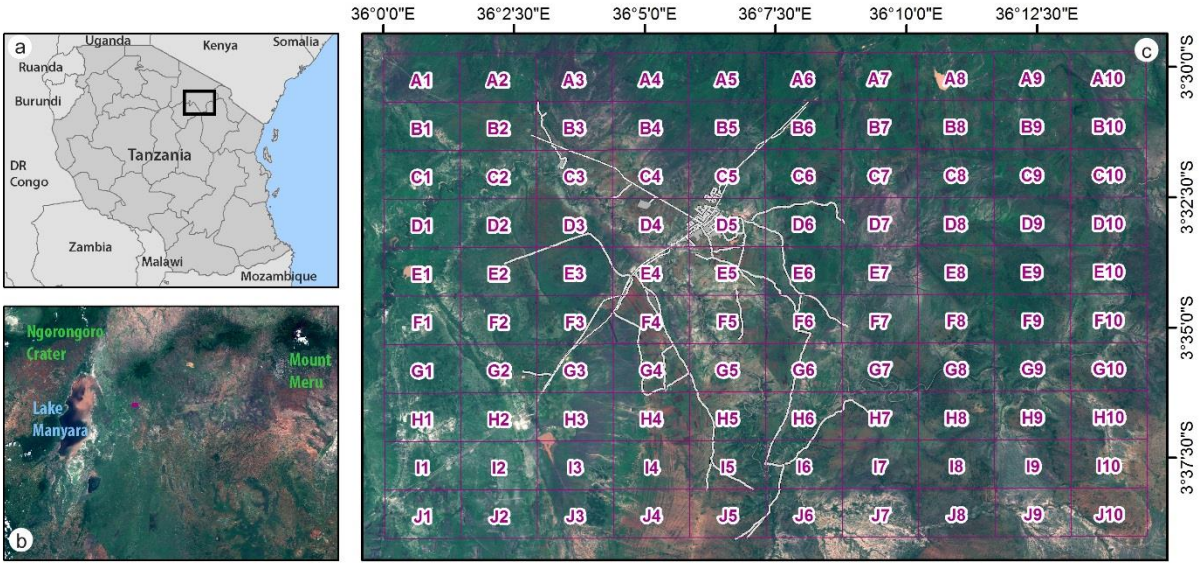

Figure 1: Study Area. a) Overview of Tanzania and bordering countries with extend indicator of b) shown in black. b) Close up of the environmental setting, extend indicator of c) in pink. c) Gridding system for the geomorphologic mapping. Actual mapping was done for grids C to I and 3 to 6. Satellite imagery Sentinel-2, 2016-02-04.

3. Materials and Methods

The GIS mapping is based on extensive fieldwork as well as DEM and remotely sensed information presented in the following chapters.

The geomorphological map is planned to be a guide for fieldwork for other disciplines (e.g. archaeology, palaeontology), therefore, a gridding was generated first for an easy orientation. One grid cell fits into an A4 landscape format with a scale of 1:10 000; the gridding is shown in Figure 1. For this study, the mapped area is shown in a single map with according legend at a scale of 1:25 000 (see Supplemental material).

3.1 Field Mapping

We carried out several campaigns of geomorphological field mapping between March 2012 and February 2014. The field mapping has been performed following the guidelines proposed by Knight et al. (2011). The structure of the mapped features, and hence also the structure of the database, was established prior to field surveying and combines information on morphology and morphogenesis with secondary information on sampling and laboratory data for soil type analysis.

3.2 Remotely Sensed Imagery and GIS Analyses

Multisensoral remote sensing images serve as base data for the geomorphological mapping. The multispectral WorldView-2 sensor was launched in 2009 and provides eight spectral bands (0.40–1.04 μm) with a ground resolution of 1.85 m at nadir and a panchromatic band with 0.46 m ground resolution at nadir (Digital Globe, 2015). The available cloud free scene was acquired on February 21, 2011. The multispectral image gives information on vegetation features as well as on the spectral characteristics such as mineralogical composition of surfaces devoid of vegetation (Bachofer et al., 2015).

the Makuyuni River (Dawson, 2008; Schwartz et al., 2012). Dominating soil types include Cambisols, Vertisols, Calcisols and Luvisols (Bachofer, Quénéhervé, Hochschild, & Maerker, 2015).

The prevailing savannah climate (Aw after Köppen climate system) is characterized by bi-modal rainy seasons (November-January and March-May) with annual rainfall of 651 mm (Bachofer et al., 2015). Nevertheless, the rainfall regime is very irregular and patchy,

In addition, the backscattered signal of Synthetic Aperture Radar (SAR) images is sensitive for the dielectric properties (e.g. moisture), the surface roughness and the orientation of topographic features (Mather & Koch, 2011). To include this supplementary information in the mapping approach, a TerraSAR-X (~9.65 GHz; X-band) StripMap scene was acquired on August 28, 2011 during dry season. The scene was calibrated, radiometrically and geometrically corrected, as well as speckle noise reduced by filtering.

A Shuttle Radar Topographic Mission (SRTM) X-band DEM with a ground resolution of 30 m was used for the topographic analysis. The SRTM provides a high-resolution DEM acquired in the year 2000 (DLR, 2012). The X-band DEM possesses a relative high vertical accuracy

(Hoffmann & Walter, 2006), but results due to its' short wavelength in a noisy surface. Therefore, the DEM was filtered using a multidirectional Lee filter, to preserve the topographic features (Lee, 1980).

The contour lines were derived from the SRTM-X DEM and are plotted in a 5 m elevation interval. After their creation, a smoothing was applied to eliminate pixel artefacts of the SRTM-X raster. Small circle contours were deleted manually to reduce image noise.

Geomorphometry allows for a quantitative analysis of the relief to determine a precise characterisation and to eliminate the researcher's subjectivism (see Hengl & Reuter, 2009). Jenness' (2006) GIS-based script calculates the topographic position index (TPI) based on a DEM. The TPI's 10-class landform classification (a combination of small and large neighborhood TPI) was used in this study to provide additional information in areas, where mapping was not supported by fieldwork. Geomorphons were analysed based on Jasiewicz and Stepinski (2013) in order to derive additional information for validation through a semi-automated manner. Surface classification was done by the authors based on multispectral information, for details see (Bachofer et al., 2015). Further explanations for the classification and according mapping procedures are explained in chapter 4.3.

3.3 Mapped Features and Database Structure

Geomorphological features were mapped in the field and the final product was compiled using GIS software. All mapped features are stored as single layers for flexible data management. Geomorphological features were drawn as polygons, lines or as point symbols within the GIS environment.

Following Schwartz et al. (2012) surface materials are distinguished in (i) lithology: volcanic deposits (nephelinite, volcanic agglomerate/conglomerate; basalt dyke) and basement (Proterozoic quartzite and gneiss). (ii) Consolidated surface formations (terrestrial deposits (Upper Manyara Beds); lacustrine deposits (Lower Manyara Beds)). (iii) Unconsolidated surface formations (recent alluvial/colluvial deposits). According to Bachofer et al. (2015), soils can be differentiated into soils with > 30 cm of soil development, mainly Cambisols on Upper Manyara Beds and Vertisols in (former) plain areas. We distinguish the following fluvial and slope landforms due to surface runoff: (i) gully thalwegs and (ii) head cut areas, (iii) areas affected by rill erosion and (iv) scarp edges. Deposits resulting from gravitational and erosive processes. Hydromorphological data include ephemeral streams and cut off meanders as well as

periodically waterlogged areas. Topographic data are provided as pint elevations for tops and contour lines in a 5 m elevation interval. Anthropogenic landforms include roads (concrete and rough roads), bridges, artificial steps, quarried areas and settlements.

4. Geomorphological Features

4.1 River Channel Morphology

Water is one of the most important agents in forming and shaping of landforms. A channel is defined as a linear feature that shows evidence of erosion and/or deposition by a concentrated water flow (Bull & Kirkby, 1997).

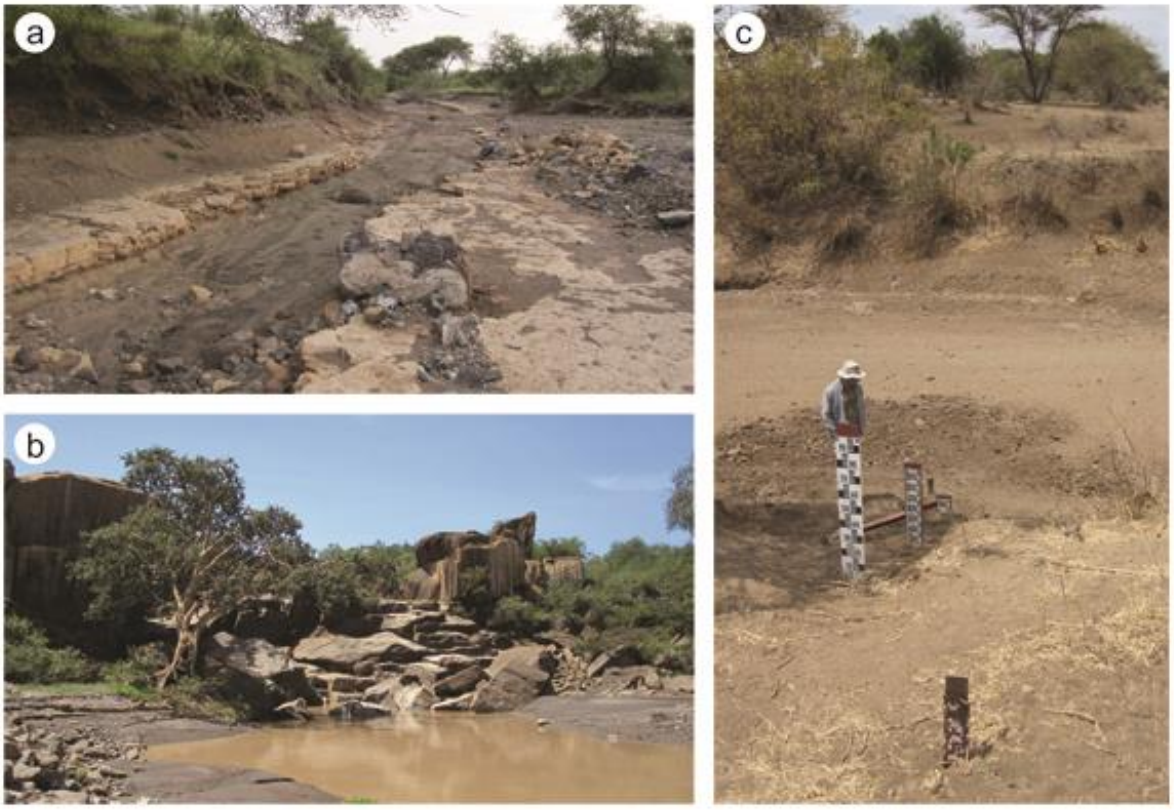

Figure 2: Makuvuni River bed features. a) Tuff incision and pebble point bar, grid C3 (Photo: 03/2012). b) Rapids composed of granite blocks, located ~6 km E of G6 (02/2014). c) Channel incision into the alluvial floodplain, D4 (08/2011). All photos: G. Quénéhervé**.**

River erosion is split into bottom and lateral erosion, causing transport of sediment along the beds (Scheidegger, 1973). Miller and Doyle (2014) stated that rivers are not only affected by resource use within the river channel or in the riparian zone, but instead are affected by activities that take place throughout their catchments. The transition of land to agricultural use is associated with increases in flood magnitudes and therefore increases in erosivity of stream flows that cause channel incision, especially in areas with fine, erodible soils (Fu, 1989).

The Makuyuni River, an ephemeral drainage system, is the major discharge with small tributaries running along its course. For the main channel of the Makuyuni River, the underlying bedrock alternates from granite to cemented tephra deposits. Accumulated alluvial material is dominant over the main distance within the mapped area (Fig. 2).

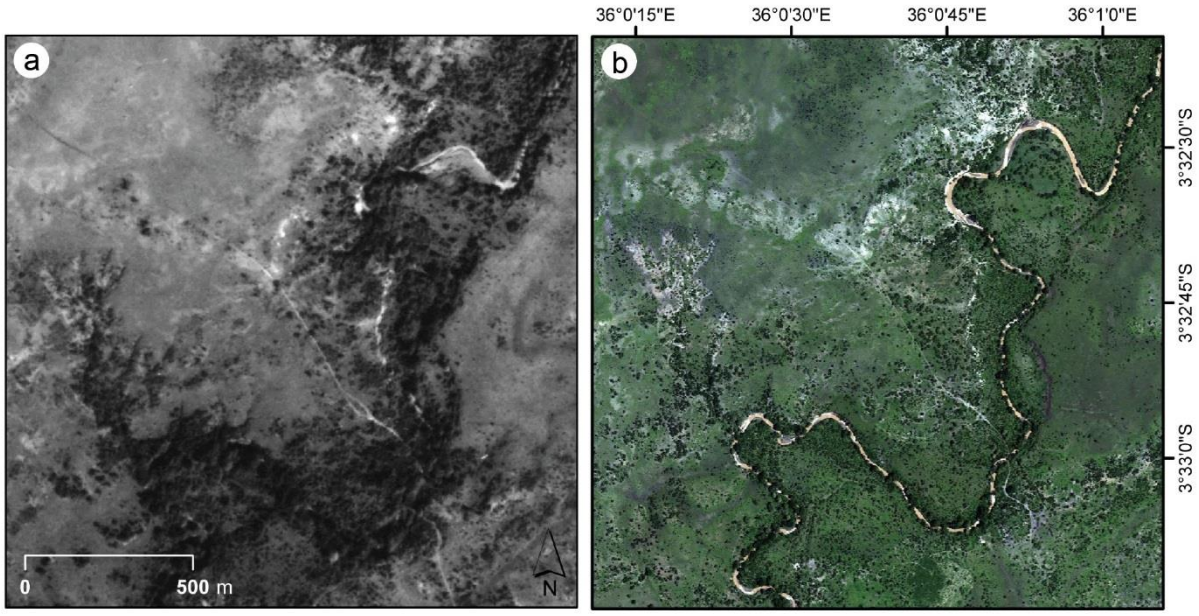

Figure 3: Evolution of the Makuyuni River stream bed over 29 years**,** located ~4 km W of D3. a) Makuyuni River shown by aerial imagery, 1982-12-14. b) Makuyuni River shown by WorldView-2, 2011-02-21.

In many parts of the Makuyuni River changes in channel morphology over time are documented that are related due to changes in stream-flow magnitudes and/or timing, sediment supply and/or size, direct disturbance and vegetation changes (Rosgen, 1994). Such changes can be clearly illustrated during even a short period of 29 years, comparing the aerial photography (1982-12-14) and the WorldView-2 scene (2011-02-21), see Fig. 3.

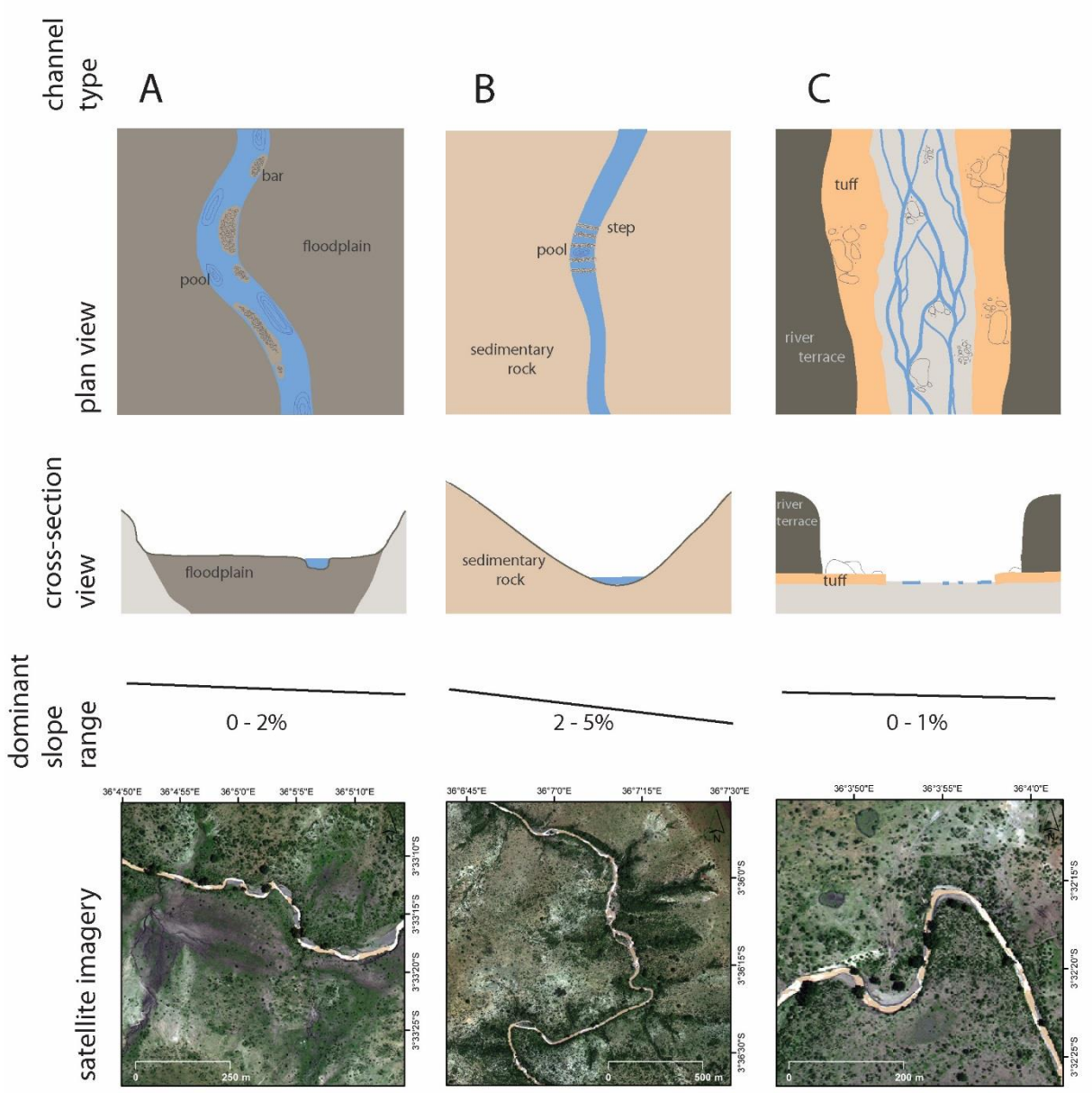

Figure 4: Makuyuni River channel types**.** Type A is a relatively new channel incision into the well-developed floodplain. Type B developed its bed running through sedimentary rocks and follows a narrow river channel of the Lower Manyara Bed section. Type C is running over tephra outcrops as anastomising stream. Satellite imagery: WorldView-2 scene from 2011-02-21

The main tributary shows within the focus area three different kind of channel types (Fig. 4). Type A can be identified as a relatively new channel incision into the well-developed flood-plain. The river bed is characterized by pools and point bars, sorted sands and cobbles that are deposited especially after intense rainfalls in the upper catchment. Type B developed its bed running through sedimentary rocks of the Lower Manyara Bed section. The steeper gradient is expressed by step/pool formation along its course and a narrow river channel. Type C is

dominant where the Manyara River is running over cemented tephra outcrops. This rather horizontal layer is relatively strong compared to the surrounding lithology and therefore its incision is very slow. The channel itself is in the slope range of 0 to 1% and therefore is showing an anastomising stream system bedded into the lower substrates within former alluvial river terraces. On the sidewalls of the terraces, recent material is accumulated on the toes of the terrace.

4.2 Linear Erosion Features

When rainfall exceeds the rate at which water can infiltrate the ground, surface runoff, so-called Hortonian overland flow is produced (Bull & Kirkby, 1997). Overland flow occurs in sparsely vegetated and low inclined surface of this semiarid areas often as laminar sheetflow. In the study area, notable surface runoff is produced when the soil is very dry at the moment precipitations starts (hydrophobicity), especially in homogeneous soils with low activity clays (Quénéhervé, Bachofer, & Maerker, 2015). Rills and gullies may be regarded as different morphological stages of a continuum of incised channels, including microrills, rills, megarills, ephemeral gullies, permanent gullies and arroyos (Poesen, Nachtergaele, Verstraeten, & Valentin, 2003). However, the transition from one stage to another is gradual and no quantitative equation exits to discriminate these classes. When gullies grow into each other, they result in badland formation. Badlands are intensively dissected high relief areas unusable for agriculture (Fig. 5e).

When runoff concentrates and becomes turbulent, sediment detachment is increasing that leads to linear depressions called rills. Rills are ephemeral microchannels on hillslopes that vary in lateral position from year to year (Bull & Kirkby, 1997). A rill is less likely to form in the same position again since drainage is improved and there is a higher resistance to occour than in the neighbouring slope profiles. Rills have a seasonal cycle of development and destruction according to rainfall patterns and are typically 50–300 mm wide and up to 300 mm deep (Knighton, 1998).

Gullies are linear channels (either continuous or discontinuous) formed by removing upland soil and parent materials, they commonly occur in areas with increased concentrated runoff like in swales and at the valley bottom. Discontinuous gullies are isolated from the rest of the draining network. Continuous gullies discharge into streams at the bottom of the slope and hence form part of a drainage network (Poesen et al., 2002).

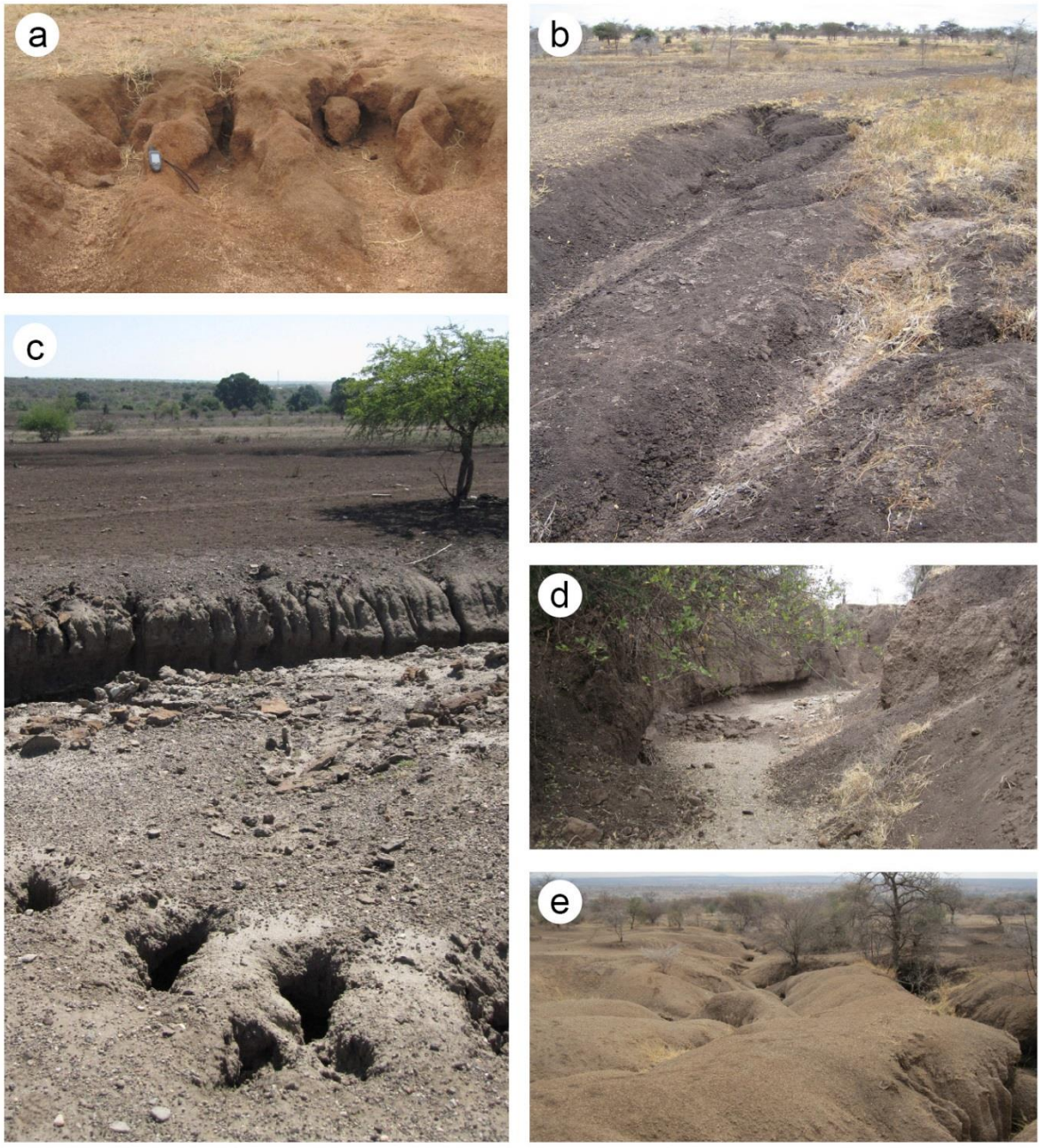

Figure 5: Gully Morphology and Processes**.** a) Gully Headcut, E3 (Photo: 06/2013). b) Ephemeral Gully with headcut, F4 (09/2010). c) Gully (background) and Piping (foreground), F4 (03/2014). d) Permanent Gully with mass failure, F5 (08/2011). e) Badland formation, F5 (08/2011). All photos: G. Quénéhervé.

They differ from stable river channels in having steep sides, step/pool profiles, characteristically with a headcut at the upslope end (Knighton, 1998). They are typically more than 0.3 m wide and range from 0.5 to 30 m in depth (Poesen et al., 2002). Gullies retreat upslope by seepage (Fig. 5a) and tunnel/pipe erosion at the face of the headcut. Piping (Fig. 5c) is an

erosional process caused by subsurface flow within the bulk soil and has often a preparative function for gully processes. Gullies show very high erosion rates in the first part of their lifetime (Kosov, Nikol'skaya, & Zorina, 1978) and are characterized by a high sediment supply, resulting in high bedloads and suspended sediment transport rates. Channel degradation and sideslope rejuvenation processes are typical. Two main processes initiate permanent gully formation in the study area: surface flow and piping.

Poesen et al. (2002) distinguish gullies on a physically-based classification in ephemeral and permanent systems. Ephemeral gullies (Fig. 5b) have small, linear channels formed during one rainfall event but may be filled in subsequent events or artificially. They are impermanent channels but small enough to be obliterated by farming operations (e.g deep tillage or land-levelling practices) (Grissinger, 1995). Their infilling generally leaves depressions, new gullies develop subsequently as they tend to return to the same position.

Permanent gullies (Fig. 5d) are larger systems that typically develop on abandoned fields or rangeland, they occur as (i) valley-floor, or as (ii) valley-head and valley-side gullies (Higgins, Hill, & Lehre, 1990). Valley-side gullies have a distinctive steep head from which they become shallower downslope until they end in a small fan. Valley-head gullies differ from valleyside gullies only in their location and orientation in respect to the valley axis (Higgins et al., 1990). If gullies occur on valley floors or river banks, a section of a discontinuous gully is characterized by a vertical headcut, a channel immediately below the headcut with depth greater than its width, a bed gradient slightly bigger than that of the original valley floor, and a decreasing depth of the channel downstream. Where the gully floor intersects the valley floor, the gully depth becomes zero and a small gully fan occurs (Bocco, 1991). The distinction between valley-floor gullies and stream channels is subjective, typically, valley-floor gullies are strongly modified by mass failure processes (Grissinger, 1995).

4.3 Surface Cover

Surface characteristics of the study area was conducted by a description of field reference points, laboratory analyses from 27 locations and remote sensing image classification (Bachofer et al., 2015). This resulted in seven topsoil classes, two lithological classes and a class for surface water. In order to validate and interpret the results of the classification process, three soil catenae were analyzed, consisting of 24 soil profiles with detailed profile descriptions

(Bachofer et al., 2015) according to the World Reference Base for Soil Resources (FAO, 2014). This classification supported the geomorphological mapping processes.

In this work, we distinguish ten non-artificial surface classes: a water surface classes: 'periodically water logged areas'; three unconsolidated surface classes: 'surface wash of upslope material', 'alluvial deposits' as well as 'recent river bed deposits'; one consolidated surface class: 'lacustrine deposits'; two soil cover types: 'soils on Upper Manyara Beds' and 'Vertisol in (former) plain areas'; and three lithology classes: 'Nephelinite, volcanic agglomerate/conglomerate', 'basalt dyke' and ' Proterozoic quartzite and gneiss'.

5. Conclusions

The results of the geomorphological surveys carried out in the Lake Manyara basin from 2012 to 2014 led to a composed geomorphological map. The mapping based on GIS procedures was supported by remotely sensed image classification and high-resolution panchromatic as well as true color imagery. The multispectral WorldView-2 image and the TerraSAR-X scene contributed to the delineation of lithological units and surface substrates, as well as geomorphological features. Those underlying data layers proved to be very helpful and should be considered to be included in any mapping work. Field mapping and ground truthing must remain an important part to calibrate and validate RS and GIS techniques.

The geomorphological map product, due to its detail, provides a reliable base document, which yield valuable information to identify areas that are recently exposed for archaeologists and palaeontologists and for the recognition of features of interests for physical geographers and related disciplines, e.g. soil scientists, geologists. In semiarid regions, where irrigation farming is necessary, a knowledge of land and drainage conditions contributes to water conservation and land use planning processes, especially in agricultural areas.

Acknowledgments

We would like to thank the Heidelberg Academy of Sciences and Humanities' research centre 'The Role of Culture in Early Expansions of Humans' personnel and financial support. Moreover, we thank the Tanzania Commission for Science and Technology (COSTECH) for permits and clearance. We would like to thank the DLR and the German Remote Sensing Data Center (DFS) for providing the TerraSAR-X and SRTM/X-SAR data. The WorldView-2 scene is courtesy of the DigitalGlobe Foundation. We acknowledge support by Deutsche Forschungsgemeinschaft and Open Access Publishing Fund of University of Tübingen.

References

Anders, N.S., Seijmonsbergen, A.C., & Bouten, W. (2009). Modelling channel incision and alpine hillslope development using laser altimetry data. *Geomorphology, 113*(1-2), 35–46. doi:10.1016/j.geomorph.2009.03.022

Annys, K., Frankl, A., Spalević, V., Čurović, M., Borota, D., & Nyssen, J. (2014). Geomorphology of the Durmitor Mountains and surrounding plateau Jezerska Površ (Montenegro). *Journal of Maps, 10*(4), 600–611. doi:10.1080/17445647.2014.909338

Bachofer, F., Quénéhervé, G., Hochschild, V., & Maerker, M. (2015). Multisensoral Topsoil Mapping in the Semiarid Lake Manyara Region, Northern Tanzania. *Remote Sensing, 7*(8), 9563–9586. doi:10.3390/rs70809563

Bachofer, F., Quénéhervé, G., & Märker, M. (2014). The Delineation of Paleo-Shorelines in the Lake Manyara Basin Using TerraSAR-X Data. *Remote Sensing, 6*(3), 2195–2212. doi:10.3390/rs6032195

Bachofer, F., Quénéhervé, G., Zwiener, T., Maerker, M., & Hochschild, V. (2016). Comparative analysis of Edge Detection techniques for SAR images. *European Journal of Remote Sensing, 49*(1), 205–224. doi:10.5721/EuJRS20164912

Bishop, M.P., James, L.A., Shroder, J.F., Jr., & Walsh, S.J. (2012). Geospatial technologies and digital geomorphological mapping: Concepts, issues and research. *Geomorphology, 137*(1), 5–26. doi:10.1016/j.geomorph.2011.06.027

Bishop, M.P., & Shroder, J.F. (Eds.). (2004). *Geographic Information Science and Mountain Geomorphology*. Berlin: Springer.

Bisson, M., & Bini, M. (2011). A multidisciplinary approach to reveal palaeo-hydrographic features: the case study of Luna archaeological site surroundings. *International Journal of Geographical Information Science, 26*(2), 327–343. doi:10.1080/13658816.2011.592647

Blaszczynski, J.S. (1997). Landform Characterization with Geographic Information Systems. *Photogrammetric Engineering and Remote Sensing, 63*(2), 183–191.

Bocco, G. (1991). Gully erosion: processes and models. *Progress in Physical Geography, 15*(4), 392–406. doi:10.1177/030913339101500403

Braun, J., & Sambridge, M. (1997). Modelling landscape evolution on geological time scales: A new method based on irregular spatial discretization. *Basin Research, 9*(1), 27–52. doi:10.1046/j.1365-2117.1997.00030.x

Brouwer Burg, M. (2013). Reconstructing "total" paleo-landscapes for archaeological investigation: an example from the central Netherlands. *Journal of Archaeological Science, 40*(5), 2308–2320. doi:10.1016/j.jas.2013.01.008

Bull, L.J., & Kirkby, M.J. (1997). Gully processes and modelling. *Progress in Physical Geography, 21*(3), 354–374. doi:10.1177/030913339702100302

Chen, A., Darbon, J., & Morel, J.-M. (2014). Landscape evolution models: A review of their fundamental equations. *Geomorphology*, *219*(0), 68–86. doi:10.1016/j.geomorph.2014.04.037

Clark, C.D., Knight, J.K., & T. Gray, J. (2000). Geomorphological reconstruction of the Labrador Sector of the Laurentide Ice Sheet. *Quaternary Science Reviews*, *19*(13), 1343–1366. doi:10.1016/S0277-3791(99)00098-0

Dawson, J.B. (2008). *Geological Society Memoir: Vol. 33. The Gregory Rift Valley and neogene-recent-volcanoes of Northern Tanzania*. London: Geological Society. http://swb2.bsz-bw.de/DB=2.106/PPN?PPN=306264471

Demek, J., Kirchner, K., Mackovčin, P., & Slavík, P. (2011). Geomorphodiversity derived by a GIS-based geomorphological map: case study the Czech Republic. *Zeitschrift für Geomorphologie*, *55*(4), 415–435. doi:10.1127/0372-8854/2011/0058

Devoto, S., Biolchi, S., Bruschi, V.M., Furlani, S., Mantovani, M., Piacentini, D., . . . Soldati, M. (2012). Geomorphological map of the NW Coast of the Island of Malta (Mediterranean Sea). *Journal of Maps*, *8*(1), 33–40. doi:10.1080/17445647.2012.668425

Di Crescenzo, G., & Santo, A. (2007). High-resolution mapping of rock fall instability through the integration of photogrammetric, geomorphological and engineering–geological surveys: Natural hazards related to recent geological processes and regional evolution: 14th MAEGS, Torino, Italy. *Quaternary International*, *171–172*, 118–130. doi:10.1016/j.quaint.2007.03.025

Digital Globe. (2015). WorldView-2: Status: 2015-01-20. Retrieved from http://global.digitalglobe.com/sites/default/files/DG_WorldView2_DS_PROD.pdf

DLR. (2012). SRTM X-SAR Digital Elevation Models: Status: 2015-10-21. Retrieved from http://eoweb.dlr.de:8080/eoweb-ng/licenseAgreements/DLR_SRTM_Readme.pdf

Doornkamp, J.C. (1971). Geomorphological Mapping. In S.H. Ominde (Ed.), *Studies in East African Geography and Development* (pp. 9–28). Berkeley: Heinemann.

Drăguţ, L., & Eisank, C. (2011). Object representations at multiple scales from digital elevation models. *Geomorphology*, *129*(3–4), 183–189. doi:10.1016/j.geomorph.2011.03.003

Ewing, R.C., McDonald, G.D., & Hayes, A.G. (2015). Multi-spatial analysis of aeolian dune-field patterns: Planetary Geomorphology: Proceedings of the 45th Annual Binghamton Geomorphology Symposium, held 12-14 September 2014 in Knoxville, Tennessee, USA. *Geomorphology*, *240*, 44–53. doi:10.1016/j.geomorph.2014.11.023

FAO. (2014). *World Soil Resources Report: Vol. 106. World reference base for soil resources: International soil classification system for naming soils and creating legends for soil maps.* http://www.fao.org/soils-portal/soil-survey/soil-classification/world-reference-base/en/

Flores-Prieto, E., Quénéhervé, G., Bachofer, F., Shahzad, F., & Maerker, M. (2015). Morphotectonic Interpretation of the Makuyuni Catchment in Northern Tanzania using DEM and SAR data. *Geomorphology*, *248*, 427–439. doi:10.1016/j.geomorph.2015.07.049

Fu, B. (1989). Soil erosion and its control in the loess plateau of China. *Soil Use and Management, 5*(2), 76–82. doi:10.1111/j.1475-2743.1989.tb00765.x

Giemsch, L., Hertler, C., Märker, M., Quénéhervé, G., Saanane, C., & Schrenk, F. (in press). Acheulean Chronology and Technology at Makuyuni (Lake Manyara, Tanzania): Results of archaeological fieldwork and classification of the lithic assemblages.

Grissinger, E.H. (1995). Rills and Gullies. In M. Agassi (Ed.), *Soil Erosion, Conservation, and Rehabilitation* (153-167). CRC Press.

Grove, A.T. (1986). Geomorphology of the African Rift System. In L.E. Frostick, R.W. Renaut, I. Reid, & J.-J. Tiercelin (Eds.), Sedimentation in the African Rifts. *Geological Society Special Publications, 25,* 9–16.

Gustavsson, M., Kolstrup, E., & Seijmonsbergen, A.C. (2006). A new symbol-and-GIS based detailed geomorphological mapping system: Renewal of a scientific discipline for understanding landscape development. *Geomorphology, 77*(1–2), 90–111. doi:10.1016/j.geomorph.2006.01.026

Hengl, T., & MacMillan, R.A. (2009). Geomorphometry: A key to landscape mapping and modelling. In T. Hengl & H.I. Reuter (Eds.), *Developments in Soil Science: Vol. 33. Geomorphometry: Concepts, Software, Applications* (pp. 433–460). Amsterdam: Elsevier.

Hengl, T., & Reuter, H.I. (Eds.) (2009). Developments in Soil Science. *Vol. 33*. *Geomorphometry: Concepts, Software, Applications*. Amsterdam: Elsevier.

Higgins, C.G., Hill, B.R., & Lehre, A.K. (1990). Gully development. In C.G. Higgins & D.R. Coates (Eds.), *Special paper. The Geological Society of America: Vol. 252. Groundwater Geomorphology: The Role of Subsurface Water in Earth-Surface Processes and Landforms* (pp. 139–155).

Hoffmann, J., & Walter, D. (2006). How Complementary are SRTM-X and -C Band Digital Elevation Models? *Photogrammetric Engineering & Remote Sensing, 72*(3), 261–268. doi:10.14358/PERS.72.3.261

Hugenholtz, C.H., Levin, N., Barchyn, T.E., & Baddock, M.C. (2012). Remote sensing and spatial analysis of aeolian sand dunes: A review and outlook. *Earth-Science Reviews, 111*(3–4), 319–334. doi:10.1016/j.earscirev.2011.11.006

Jansson, K.N. (2005). Map of the glacial geomorphology of north-central Québec-Labrador, Canada. *Journal of Maps, 1*(1), 46–55. doi:10.4113/jom.2005.33

Jasiewicz, J., Netzel, P., & Stepinski, T.F. (2014). Landscape similarity, retrieval, and machine mapping of physiographic units. *Geomorphology, 221,* 104–112. doi:10.1016/j.geomorph.2014.06.011

Jasiewicz, J., & Stepinski, T.F. (2013). Geomorphons — a pattern recognition approach to classification and mapping of landforms. *Geomorphology, 182,* 147–156. doi:10.1016/j.geomorph.2012.11.005

Jenness, J. (2006). *Topographic Position Index (tpi jen.avx) extension for ArcView 3.x, v. 1.3a.* (Technical Report). Jenness Enterprises.

Knight, J., Mitchell, W.A., & Rose, J. (2011). Geomorphological Field Mapping. In M.J. Smith, P. Paron, & J.S. Griffiths (Eds.), *Geomorphological mapping: Methods and applications* (pp. 151–188). Amsterdam: Elsevier.

Knighton, D. (1998). *Fluvial Forms and Processes: a New Perspective*. London, New York: Routledge.

Kosov, B.F., Nikol'skaya, I.I., & Zorina, Y.F. (1978). Eksperimental'nyye issledovaniya ovragoobrazovaniya. In N.I. Makkaveev (Ed.), *Eksperimental'naya Geomorfologiya*. Moskva: Izd Moskva Univ., Vol. 3, pp. 113–140 [in Russian].

Lee, J.S. (1980). Digital image enhancement and noise filtering by use of local statistics. *IEEE Trans Pattern Anal Mach Intell, 2*(2), 165–168.

Märker, M., Hochschild, V., Maca, V., & Vilímek, V. (2016). Stochastic Assessment of Landslides and Debris Flows in the Jemma Basin, Blue Nile, Central Ethiopia. *Geografia Fisica e Dinamica Quaternaria*, 39, 51–58. doi:10.1007/s11069-015-1855-y

Maerker, M., Quénéhervé, G., Bachofer, F., & Mori, S. (2015). A simple DEM assessment procedure for gully system analysis in the Lake Manyara area, northern Tanzania. *Natural Hazards, 79*(1), 235–253. doi:10.1007/s11069-015-1855-y

Mather, P.M., & Koch, M. (2011). *Computer processing of remotely-sensed images: An introduction* (4th ed.). Chichester: Wiley-Blackwell.

May, J.-H. (2008). A geomorphological map of the Quebrada de Purmamarca, Jujuy, NW Argentina. *Journal of Maps, 4*(1), 211–224. doi:10.4113/jom.2008.1019

Miller, B.W., & Doyle, M.W. (2014). Rangeland management and fluvial geomorphology in northern Tanzania. *Geomorphology, 214*(0), 366–377. doi:10.1016/j.geomorph.2014.02.018

Poesen, J., Nachtergaele, J., Verstraeten, G., & Valentin, C. (2003). Gully erosion and environmental change: importance and research needs. *CATENA, 50*(2-4), 91–133. http://www.sciencedirect.com/science/article/B6VCG-473W23Y-1/2/027a1755ac75021c97520eaa2ad8fc3a

Poesen, J., Vandekerckhove, L., Nachtergaele, J., Oostwoud Wijdenes, D., Verstraeten, G., & van Wesemael, B. (2002). Gully erosion in dryland environments. In L.J. Bull (Ed.), *Dryland rivers: Hydrology and geomorphology of Semi-arid channels* (pp. 229–262). Chichester: Wiley.

Poppe, L., Frankl, A., Poesen, J., Admasu, T., Dessie, M., Adgo, E., . . . Nyssen, J. (2013). Geomorphology of the Lake Tana basin, Ethiopia. *Journal of Maps, 9*(3), 431–437. doi:10.1080/17445647.2013.801000

Quénéhervé, G., Bachofer, F., & Maerker, M. (2015). Experimental Assessment of Runoff Generation Processes on Hillslope Scale in a Semiarid Region in Northern Tanzania. *Geografia Fisica e Dinamica Quaternaria, 38*(1), 55–66. doi:10.4461/GFDQ.2015.38.06

Rădoane, M., Cristea, I., & Rădoane, N. (2011). Geomorphological Mapping. Evolution and Trends. *Revista de geomorfologie, 13*, 19–39.

Richards, K., Brasington, J., & Hughes, F. (2002). Geomorphic dynamics of floodplains: ecological implications and a potential modelling strategy. *Freshwater Biology, 47*(4), 559–579. doi:10.1046/j.1365-2427.2002.00920.x

Ring, U., Schwartz, H.L., Bromage, T.G., & Sanaane, C. (2005). Kinematic and sedimentological evolution of the Manyara Rift in northern Tanzania, East Africa. *Geological Magazine, 142*(4), 355–368. doi:10.1017/s0016756805000841

Rosgen, D.L. (1994). A classification of natural rivers. *CATENA, 22*(3), 169–199. doi:10.1016/0341-8162(94)90001-9

Scheidegger, A.E. (1973). Hydrogeomorphology. *Journal of Hydrology, 20*(3), 193–215. doi:10.1016/0022-1694(73)90061-9

Schwartz, H.L., Renne, P.R., Morgan, L.E., Wildgoose, M.M., Lippert, P.C., Frost, S.R., . . . Sanaane, C. (2012). Geochronology of the Manyara Beds, northern Tanzania: New tephrostratigraphy, magnetostratigraphy and 40Ar/39Ar ages. *Quaternary Geochronology, 7*(0), 48–66. doi:10.1016/j.quageo.2011.09.002

Seijmonsbergen, A.C. (2013). 14.4 The Modern Geomorphological Map. In J.F. Shroder, Jr., A.D. Switzer, & D.M. Kennedy (Eds.), *Treatise on Geomorphology* (Vol. 14, Methods in Geomorphology, pp. 35–52). San Diego, CA: Academic Press. doi:10.1016/B978-0-12-374739-6.00371-7

Senthilnathan, L., Nobi, E.P., Thangaradjou, T., & Kannan, L. (2012). Long-time shoreline monitoring of the vellar estuarine complex, southeast coast of India: Using multispectral satellite data: Journal of Earth Science. *J. Earth Sci., 23*(6), 900–907. doi:10.1007/s12583-012-0304-z

Siart, C., Bubenzer, O., & Eitel, B. (2009). Combining digital elevation data (SRTM/ASTER), high resolution satellite imagery (Quickbird) and GIS for geomorphological mapping: A multi-component case study on Mediterranean karst in Central Crete. *Geomorphology, 112*(1–2), 106–121. doi:10.1016/j.geomorph.2009.05.010

Smith, M.J., Rose, J., & Booth, S. (2006). Geomorphological mapping of glacial landforms from remotely sensed data: An evaluation of the principal data sources and an assessment of their quality. *Geomorphology, 76*(1-2), 148–165. doi:10.1016/j.geomorph.2005.11.001

Smith, M.J., & Pain, C.F. (2011). Geomorphological Mapping. In K.J. Gregory & A.S. Goudie (Eds.), *The SAGE handbook of geomorphology* (pp. 142–153). SAGE Publications Ltd.

Souza, F., Pedro, W.M., & Paradella, W.R. (2014). Use of RADARSAT-1 fine mode and Landsat-5 TM selective principal component analysis for geomorphological mapping in a macrotidal mangrove coast in the Amazon Region. *Canadian Journal of Remote Sensing, 31*(3), 214–224. doi:10.5589/m05-009

Vaidyanadhan, R., Dixit, P.C., & Schlüter, T. (1993). Geomorphology and Sedimentology of Lake Manyara Environs, Tanzania, East Africa. *Documenta naturae, 77*, 41–62.

Vannametee, E., Babel, L.V., Hendriks, M.R., Schuur, J., Jong, S.M. de, Bierkens, M.F.P., & Karssenberg, D. (2014). Semi-automated mapping of landforms using multiple point geostatistics. *Geomorphology, 221*, 298–319. doi:10.1016/j.geomorph.2014.05.032

Vogel, S., & Märker, M. (2010). Reconstructing the Roman topography and environmental features of the Sarno River Plain (Italy) before the AD 79 eruption of Somma-Vesuvius. *Geomorphology, 115*(1-2), 67–77. doi:10.1016/j.geomorph.2009.09.031

Wilson, J.P., & Gallant, J.C. (Eds.) (2000). Terrain analysis: Principles and applications. New York: Wiley.

Geomorphology of the Makuyuni Area
(Monduli District, Northern Tanzania)

Geraldine QUÉNÉHERVÉ [1] - Felix BACHOFER [1] - Michael MAERKER [2,3]

1 - Institute of Geography, University of Tuebingen, Germany; Email: geraldine.queneherve@uni-tuebingen.de
2 - Earth and Environmental Department, University of Pavia, Italy
3 - Heidelberg Academy of Sciences and Humanities c/o University of Tübingen, Tübingen, Germany

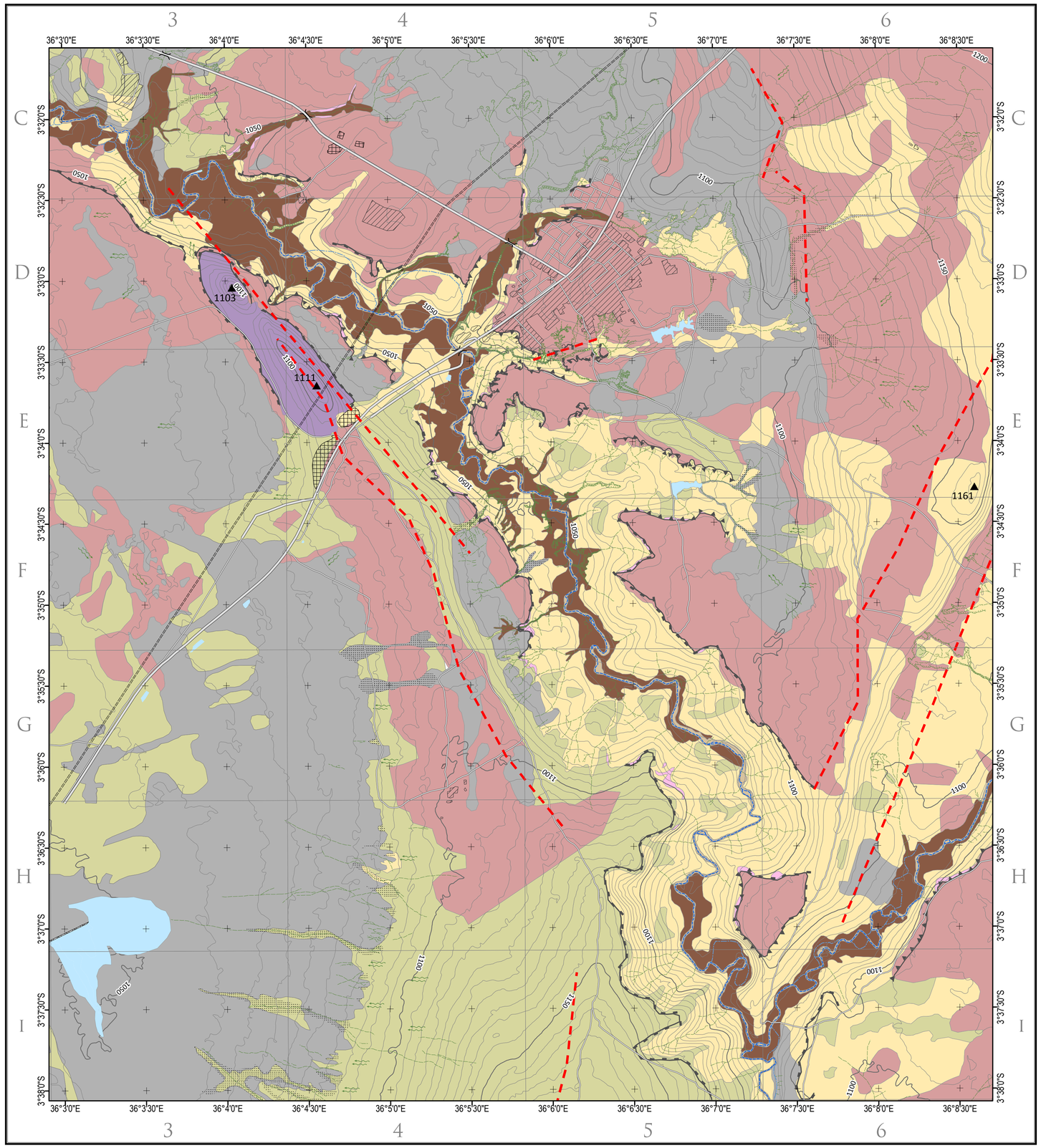

Contour lines derived from SRTM-X DEM (see Bachofer et al. (2014).
Geology based on Schwartz et al. (2012).
Tectonics based on Dawson (2008).
Mapping based on field work and WorldView-2 satellite iamge (2011-02-21).

Scale 1:25.000
0 1 km

Coordinate System: WGS 1984 UTM Zone 37S
Projection: Transverse Mercator
Datum: WGS 1984

LITHOLOGY

Volcanic Deposits

- Nephelinite, volcanic agglomerate/conglomerate
- Basalt dyke

Basement

- Proterozoic quartzite and gneiss

CONSOLIDATED SURFACE FORMATIONS

- Lacustrine deposits (Lower Manyara Beds)

UNCONSOLIDATED SURFACE FORMATIONS

- Surface wash of uplsope material
- Alluvial deposits
- Recent river bed deposits

SOIL COVER TYPES

- Soils on Upper Manyara Beds
- Vertisol in (former) plain areas

STRUCTURAL LANDFORMS

- Scarp edge: a = > 5 m, b = < 5 m
- Tectonics

SLOPE LANDFORMS

- Gully thalweg
- Gully scarps
- Gully headcut
- Rill erosion

HYDROLOGY

- Ephemeral stream
- Abandoned loop
- Periodically waterlogged area

TOPOGRAPHY

- Top (elevation, in m a.s.l.)
- Contour line (5 m interval)
- —1050— Index contour line (50 m interval, in m a.s.l.)

ANTHROPOGENIC LANDFORMS

- Road (concrete)
- Road (rough)
- Bridge
- Power line
- Settlements
- Artificially altered areas

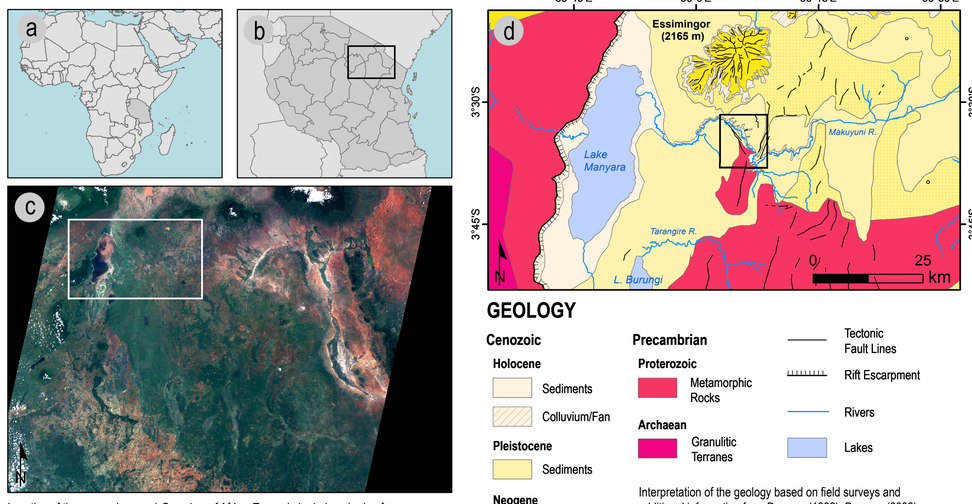

Location of the mapped area. a) Overview of Africa, Tanzania in darker shade of grey. b) Tanzania with district boundaries, black box shows extent of c. c) SENTINEL-2 scene (2016-02-04) of the greater Makuyuni area, Lake Manyara and the East African Rift shoulder in the west, Kilimanjaro in the northeast.White box shows extent of the geology overview d. d) Geology of the greater Makyuni area, black box shows extent of the mapped area.

GEOLOGY

Cenozoic

Holocene
- Sediments
- Colluvium/Fan

Pleistocene
- Sediments

Neogene
- Lava Hills
- Lava Plains

Precambrian

Proterozoic
- Metamorphic Rocks

Archaean
- Granulitic Terranes

- Tectonic Fault Lines
- Rift Escarpment
- Rivers
- Lakes

Interpretation of the geology based on field surveys and additional information from Dawson (1992), Dawson (2008), Vaidyanadhan et al. (1993) and Schlüter (2008).

Date of Compilation: 2018-02-08